

# Alma Mater Studiorum – Università di Bologna

---

---

FACOLTÀ DI CHIMICA INDUSTRIALE  
DIPARTIMENTO DI CHIMICA INDUSTRIALE E DEI MATERIALI

DOTTORATO DI RICERCA IN CHIMICA INDUSTRIALE

## ***Catalysts for H<sub>2</sub> production***

Tesi di Dottorato di Ricerca di  
Dott. Rosetti Valentina

Coordinatore:  
Chiar.mo Prof. Luigi Angiolini

Relatore:  
Dr. Francesco Basile

Correlatori:  
Prof. G. Fornasari  
Prof. A. Vaccari

---

XIX CICLO

Settore CHIM/04

## **KEY WORDS**

*CATALYTIC PARTIAL OXIDATION OF METHANE*

*STEAM REFORMING OF METHANE*

*NI AND/OR RH ACTIVE PHASE*

*HYDROTALCITE-TYPE CATALYST PRECURSORS*

*PEROVSKITE –TYPE CATALYSTS*

*STRUCTURED CATALYSTS (SIC, FECRALY ALLOY)*

The research of new catalysts for the hydrogen production described in this thesis was inserted within a collaboration of Department of Industrial Chemistry and Materials of University of Bologna and Air Liquide (Centre de Recherche Claude-Delorme, Paris).

The aim of the work was focused on the study of new materials, active and stable in the hydrogen production from methane, using either a new process, the catalytic partial oxidation (CPO), or a enhanced well-established process, the steam methane reforming (SMR).

Two types of catalytic materials were examined:

- 1) Bulk catalysts, i.e. non-supported materials, in which the active metals (Ni and/or Rh) are stabilized inside oxidic matrix, obtained from perovskite type compounds (PVK) and from hydrotalcite type precursors (HT);
- 2) Structured catalysts, i.e. catalysts supported on materials having high thermal conductivity (SiC and metallic foams).

As regards the catalytic partial oxidation, the effect of the metal (Ni and/or Rh), the role of the metal/matrix ratio and the matrix formulation of innovative catalysts obtained from hydrotalcite type precursors and from perovskites were examined.

In addition, about steam reforming process, the study was carried out first on commercial type catalysts, examining the deactivation in industrial conditions, the role of the operating conditions and the activity of different type of catalysts. Then, innovative materials bulk (PVK and HT) and structured catalysts (SiC and metallic foam) were studied and a new preparation method was developed.

# INDEX

<b>INTRODUCTION</b>	1
<b>1. H<sub>2</sub> relevance and applications</b>	3
1.1. Ammonia synthesis	5
1.1.1. Reaction mechanism	6
1.1.2. Ammonia synthesis catalysts	7
1.1.3. Ammonia plants	11
1.2. Direct Reduction of iron ore (DRI)	15
1.3. Methanol synthesis	17
1.3.1. Methanol synthesis catalysts	18
1.3.2. Reaction mechanism	24
1.3.3. Methanol plants	26
1.4. Dimethyl ether synthesis	28
1.5. Fischer-Tropsch synthesis	31
1.5.1. FT synthesis catalysts	35
1.5.2. Thermodynamics and reaction mechanism	37
1.5.3. FT synthesis plants	42
1.6. Fuel cells	47
<b>2. Processes for H<sub>2</sub> and/or syngas production</b>	53
2.1. Steam reforming process	54
2.1.1. Chemistry of steam reforming: Thermodynamics	55
2.1.2. Kinetics and reaction mechanism	62
2.1.3. Steam reforming catalysts	68
2.1.4. Carbon formation on reforming catalyst	86
2.1.5. Sintering of reforming catalysts	96
2.1.6. Catalyst shape and dimensions	102
2.1.7. Practical aspects of steam reformers	104
2.1.8. Water gas shift reaction (WGS)	110
2.2. Partial oxidation of fossil fuels (POX)	115
2.3. Autothermal reforming (ATR)	117
2.4. Catalytic partial oxidation of methane (CPO)	119

<b>EXPERIMENTAL SESSION</b>	126
<b>1. Catalysts preparation</b>	126
1.1. Perovskite type catalysts (PVK)	126
1.2. Catalysts obtained from hydrotalcite type precursors	127
<b>2. Characterization of the catalysts</b>	128
2.1. X-Ray diffraction analysis (XRD)	128
2.2. Surface area and porosimetry analyses	129
2.3. Temperature programmed reduction (TPR) and oxidation (TPO)	129
2.4. H <sub>2</sub> Chemisorption analysis	129
2.5. Shaping in form of the catalysts	131
2.6. CPO laboratory plant	131
2.7. SMR laboratory plant	134
<b>RESULTS AND DISCUSSION</b>	139
<b>1. Aim of the work</b>	139
<b>2. Catalytic partial oxidation of methane</b>	140
2.1. Perovskite (PVK) type catalysts	140
2.1.1. Effect of Rh amount (La <sub>1</sub> Fe <sub>(0.7-z)</sub> Ni <sub>0.3</sub> Rh <sub>z</sub> )	142
2.1.2. Effect of Ce amount (La <sub>(1-x)</sub> Ce <sub>x</sub> Fe <sub>0.69</sub> Ni <sub>0.3</sub> Rh <sub>0.01</sub> )	145
2.1.3. Effect of Ni amount (La <sub>0.8</sub> Ce <sub>0.2</sub> Fe <sub>(0.98-y)</sub> Ni <sub>y</sub> Rh <sub>0.02</sub> )	149
2.1.4. Effect of calcination temperature: 900 or 1100°C (La <sub>0.8</sub> Ce <sub>0.2</sub> Fe <sub>0.7</sub> Ni <sub>0.25</sub> Rh <sub>0.05</sub> )	155
2.2. Catalysts obtained from hydrotalcite (HT) type precursor	159
2.2.1. Role of the M <sup>2+</sup> /M <sup>3+</sup> ratio and role of the active metal	163
2.2.2. Role of the hydrotalcite type matrix as support	175
<b>3. Steam reforming of methane</b>	185
3.1. Characterization of spent industrial catalysts	185
3.1.1. Characterization of Portugal used samples	186
3.1.2. Characterization of USA used samples	194
3.1.3. Activity of industrial spent samples	202
3.2. Comparison of different commercial catalyst	216
3.2.1. Characterization of commercial catalysts	216

---

3.2.2. Effect of the operative parameter on the steam reforming reaction carried out in the laboratory plant	221
3.2.3. Activity of commercial catalysts	229
3.2.4. Characterization of used commercial catalysts	234
3.3. Catalyst obtained from hydrotalcite (HT) type precursor	238
3.4. Catalyst obtained from perovskite (PVK)	255
3.5. Comparison among ex-HT sil, PKV and commercial catalysts	261
3.6. Structured catalysts: support with high thermal conductivity	263
3.6.1. Ni/SiC catalysts	263
3.6.2. Electrochemical deposition of hydrotalcite type precursors on metallic foams	269
<b>CONCLUSIONS</b>	276
<b>REFERENCES</b>	281

## INTRODUCTION

Hydrogen is a “building block” product of remarkable industrial interest and it is indicated as energy carrier of increasing relevance. Hydrogen is found naturally in hydrogen-rich compounds; it cannot be extracted like natural gas or oil, but needs to be released by applying energy. On the one hand, this represents a drawback because the process requires the input of primary energy carriers like coal, natural gas or biomass, of electricity or high temperatures. The advantage is that a wide range of different feedstocks and energy sources can be used for hydrogen production. It can be manufactured from a wide range of energy sources and in particular from fossil fuels, biofuels by thermochemical way and from water by electrolytic way. Currently, the main sources for the next two or three decades will remain fossil fuels and in particular the natural gas<sup>1</sup>.

The synthesis gas is a mixture of hydrogen and carbon monoxide; it may contain carbon dioxide together with some nitrogen and other inert gases, depending from the used source and the production process. Synthesis gas may be manufactured by coke and biomass gasification, by steam reforming or partial oxidation of hydrocarbons, usually natural gas.

Today, “hydrogen economy” is high on the political agenda and on the priorities of agencies funding research. Hydrogen is claimed to replace hydrocarbons and to provide a clean fuel with no carbon emissions for use in stationary and mobile applications as well. Fuel cells will play a key role for both applications. However, hydrogen is an energy carrier, not a fuel<sup>2</sup>.

The world energy production is dominated by fossil fuels as energy sources. It amounted to 88 % in 2003 with oil responsible for 37 %. The energy consumption is growing fast in Asia (7 % in 2003), and China has become the world’s second largest consumer of oil behind the United States. The proven reserves of oil are concentrated in the Middle East (63 %) and those of natural gas in the Middle East (41 %) followed by Russia. Coal is more evenly distributed between Asia, Europe and North America.

With the present world production, the oil reserves known today would be used up within about 40 years. This figure should be considered with care. It does not include reserves still to be discovered and it does not include the changes in consumption (for instance the growth in Asia). It has been emphasized the need for flexibility in the energy network and the need for alternative fuels. Oil is the most versatile of the fossil fuels with high energy density and ease of transportation.

The power industry is very flexible to feedstocks. Coal can be transported over long distances to big centralized power plants close to deep water harbors. Natural gas in large quantities is provided by pipeline or as liquefied natural gas (LNG). The automotive sector represents a special challenge as the energy conversion is strongly decentralized. So far oil derived products have been the solution, but in view of the limited reserves, a number of alternative fuels are being considered, such as LPG (liquefied petroleum gas), natural gas, methanol, DME (dimethyl ether), ethanol, bio-diesel, Fischer-Tropsch synthetic fuels, and hydrogen.

Biofuels represent a “sustainable” response for liquid fuels. It may be based on ethanol and bio-diesel derived from conventional agricultural products or from synfuels via gasification of biomass.

As an example, the manufacture of ethanol from biomass requires the use of fossil energy that for methanol from corn, the ratio of the energy from ethanol divided by the amount of no renewable energy to produce it is only slightly above one if no other waste of the process are used to recover energy. This energy is used for fertilizer, harvesting, transportation, and processing. Ethanol may be produced more efficiently from sugar cane when the bagasse is also used to produce heat, as in Brazil, but it remains a challenge to find routes converting cellulose into ethanol.

Comparing the alternative fuels with conventional oil-derived fuels is a comparison against a moving target, since technologies for making and using conventional fuels are developing as well<sup>2</sup>.

In locations with high natural gas prices, the energy efficiency becomes critical and the feedstock costs may amount to 2/3 of the total production costs. This means that the potential for reduction in hydrogen production costs are limited if energy costs are high.

## 1. H<sub>2</sub> relevance and applications

The development of hydrogen production technologies requires identification of potential markets and the constraints associated with those markets.

For non-carbon-dioxide-emitting hydrogen production technologies (nuclear, renewable, and fossil fuels with carbon dioxide sequestration), restrictions on carbon dioxide emissions to the atmosphere are an important factor in the increasing potential size of a future markets<sup>3</sup>. Existing and potential hydrogen markets were identified as follows<sup>3</sup>:

- **Industrial**. The two major industrial markets for hydrogen are fertilizer production (ammonia), steel, methanol and H<sub>2</sub> for cracking and hydrodesulphurization. All nitrate fertilizers require hydrogen in their production processes. Some but not all steel production processes require hydrogen. These are large-scale facilities that match large-scale hydrogen production systems.
- **Vehicle**. Transportation requirements can be met with different fuels (methanol, dimethyl ether, Fischer-Tropsch fuels or gasoline, diesel, jet fuel and in the future H<sub>2</sub> itself). Each fuel requires different amounts of hydrogen in the production process and has different economics of scale.
- **Power**. Hydrogen is a candidate for power production, particularly as a vector for storage and use for production when necessary.
- **Commercial**. Hydrogen is being considered for commercial applications in buildings with the co-generation of power and heat.

With interest in its practical applications dating back almost 200 years, hydrogen energy use is hardly a novel idea. What is new is the confluence of factors since the mid-1990s that increase the attractiveness of hydrogen energy economy. Those factors include persistent urban air pollution, demand for low or zero-emission vehicles, the need to reduce foreign oil imports, carbon dioxide emissions and global climate change, and the need to store renewable electricity supplies. These considerations are not confined to a single nation or region, and make hydrogen a virtually ideal energy carrier that is abundantly and equitably available to humanity<sup>4</sup>.

The interest on hydrogen-based energy systems surged in response to the first oil crisis and the growing concerns about environmental issues. The advantages are the hydrogen nearly zero emissions, its potential role in reducing greenhouse gases (improving air quality), reducing climate changes and the possibility of local

production on the basis of a variety of fuels (decreasing dependence on imported oil). In fact, the high end-use efficiency in fuel cells and the possibility to produce hydrogen from non-fossil sources or clean fossil fuels (fossil fuel combustion in combination with coke capture and storage – CCS) could reduce greenhouse gas emissions from the energy system<sup>5</sup>. Currently, most hydrogen production technologies for energy purposes (large-scale and low cost) are currently still in the laboratory phase or at best in the demonstration phase. Natural gas plays an important role, almost all transition scenarios start with small-scale production of hydrogen from natural gas via steam reforming (SR), possibly in combination with electrolysis. In long term, literature shows three different possible configurations of the large-scale hydrogen energy system:

- large scale production of hydrogen from fossil sources, mainly coal and natural gas;
- a situation with climate constraints, when a fossil based hydrogen system can be combined with CCS (coke capture and storage);
- renewable hydrogen production, based on biomass gasification, direct solar thermal hydrogen production and electrolysis from solar or wind electricity.

These configurations do not necessarily exclude each other. The costs of producing hydrogen consist largely of feedstock and investment costs. Future hydrogen production costs are generally assumed to be lower than current values as a result of technology development. For small-scale, steam reforming (SR) costs are generally significantly higher than that of large scale, but some authors expect cost declines down to the level of large scale reformers<sup>5</sup>.

## 1.1. Ammonia synthesis

Ammonia is used in various applications, such as textile processing, water purification, and manufacturing explosives. The main part, however, is used as fertilizer<sup>6</sup>. Ammonia production consumes about half the hydrogen produced today and is the primary chemical industry use of hydrogen. Ammonia is currently made where there is inexpensive natural gas that provides economical hydrogen and shipped to the customer. The low cost of shipping ammonia favors very large ammonia production plants with very large demands for hydrogen<sup>3</sup>.

At the beginning of the 20<sup>th</sup> century, the use of nitrogenous fertilizers was already well established. Haber and Bosch developed the direct synthesis of ammonia from hydrogen and nitrogen<sup>7</sup>.

The synthesis of ammonia from nitrogen and hydrogen is a clean reaction, in that it is not complicated by the formation of byproducts, such as hydrazine, and the thermodynamics are seemingly straightforward.



The reaction is exothermic and is accompanied by a decrease in volume at constant pressure. The value of the equilibrium constant (K<sub>p</sub>) therefore increases as the temperature is lowered, and the equilibrium ammonia concentration increases with increasing pressure.

The formation of ammonia is favored by operation at high pressure and low temperature. The optimum pressure for economic operation with the available catalysts has been in the range 150 - 350 bar. Normally, the advantages of the higher equilibrium concentration of ammonia at very high pressure are more than offset by the higher costs of both gas compression and additional plant capital.

The temperature at which the synthesis process is operated is determined by the activity characteristics of the catalyst. Thermodynamically, low temperature is advantageous, but for kinetic reasons high temperatures have to be used. The most effective catalyst is clearly the one that will give the highest rate of conversion of ammonia at the lowest temperature.

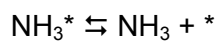
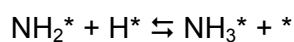
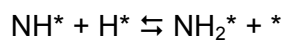
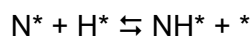
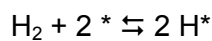
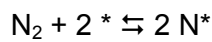
As the synthesis reaction proceeds, the heat of reaction causes the temperature to rise down the bed, so making the specific rate of reaction faster. Since the equilibrium becomes less favorable at higher temperatures, the rate of the

reverse reaction is progressively increased and the overall conversion becomes equilibrium-controlled. Careful control of the temperature profile is therefore necessary for the equilibrium balance to be obtained between the limit set by the thermodynamic equilibria, and by the kinetics of the catalyzed reactions in both forward (synthesis) and reverse (ammonia decomposition) directions.

### 1.1.1. Reaction mechanism

The ammonia synthesis reaction from  $N_2$  and  $H_2$  is composed of several steps: dissociation of  $N_2$ , dissociation of  $H_2$ , and formation of N-H bonds.

On the best elementary metal catalyst (Ru, Fe) the branchless  $NH_3$  synthesis proceeds along a well-defined Langmuir–Hinshelwood reaction path. Hence, the stepwise addition of adsorbed H to the N-compounds can be written as:



where \* and  $X^*$  correspond to an empty site and an adsorbed X chemical compound, respectively.

The main role of the ammonia catalyst is to dissociate the  $N_2$  bond. Under industrial conditions, this is the rate-determining step (RDS) for  $NH_3$  synthesis on Ru, due to the high bond energy (Fig. 1. 1). The dissociation takes place at defects and steps, rendering the  $NH_3$  synthesis extremely structure sensitive<sup>6</sup>.

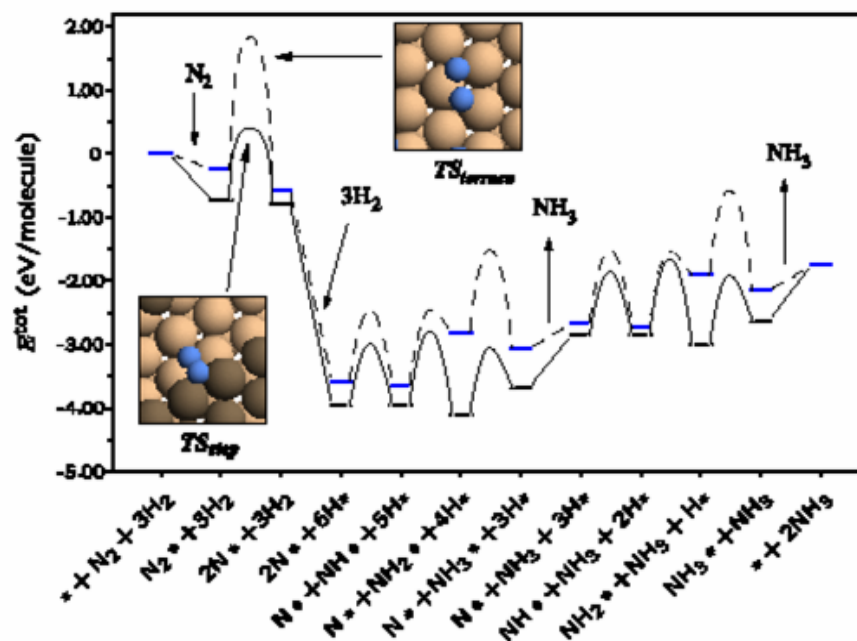


Fig. 1. 1 - The reaction pathway for NH<sub>3</sub> synthesis on the flat (dashed line) and stepped (solid line) Ru surface. The transition state (TS) configurations of the N<sub>2</sub> dissociation over the terrace and step sites are shown in the inserts<sup>6</sup>.

### 1.1.2. Ammonia synthesis catalysts

All commercial ammonia synthesis catalysts are currently based on metallic iron promoted with alkali (K), and various metal oxides, such as those of aluminum, calcium or magnesium. The principal material used to make these catalysts is usually magnetite (Fe<sub>3</sub>O<sub>4</sub>), with some of the components in the catalyst originating as impurities in the magnetite. A typical catalyst contains approximately 0,8 % K<sub>2</sub>O, 2.0 % CaO, 0.3 % MgO, 2.5 % Al<sub>2</sub>O<sub>3</sub> and 0.4 % SiO<sub>2</sub>, as well as traces of TiO<sub>2</sub>, ZrO<sub>2</sub> and V<sub>2</sub>O<sub>5</sub>. In developing the process to manufacture catalysts of this sort, it was recognized that these minor components could have a large effect on the performance of the final catalyst, since they may also interact with each other, giving rise to both harmful and beneficial effects. In modern catalysts, these factors have been taken onto account, resulting in optimized performance in terms of high activity and long life.

The main component of the catalyst, iron, has remained unchanged since the catalyst was first introduced in 1913, despite a large amount of research into alternative formulations. Magnetite has a spinel structure (similar to that of

MgAl<sub>2</sub>O<sub>4</sub>) consisting of a cubic packing of oxygen ions, in the interstices of which Fe<sup>2+</sup> and Fe<sup>3+</sup> ions are distributed. During reduction, oxygen is removed from the crystal lattice without shrinkage, so the metallic iron is obtained as a pseudomorph of the original magnetite. Metallic iron produced in this way is therefore extremely porous, and the way in which porosity is developed is an important factor affecting the activity of the final catalyst. Another major factor is the size of the individual crystals of iron produced during reduction. This is largely determined by the nature and amounts of promoters present and of course of the actual conditions during reduction.

The most important promoters are alumina and potash, which generate the so-called "doubly promoted" catalyst, but several other oxides may also be added.

Promoters as calcium oxide, silica, magnesia and the oxide of manganese, chromium, zirconium and vanadium, are conveniently classified as structural or electronic, depending on their accepted mode of action.

The production and preservation of a porous structure during the reduction of the catalyst is of fundamental importance in obtaining high activity, and the prime role of structural promoters (Al<sub>2</sub>O<sub>3</sub>, MgO and Cr<sub>2</sub>O<sub>3</sub>) is to facilitate the formation of porous, high area, metallic iron.

Silica and other acidic components are common impurities in natural magnetite used for catalysts production, and consequently they become incorporated into the structure of the final catalyst. They have the effect of neutralizing the electronic promotional effect of basic components such as K<sub>2</sub>O and CaO, and their presence in excess can result in lower catalyst activities. However, silica also has a stabilizing effect like alumina, and high-silica catalysts tend to be more resistant to both water poisoning and sintering.

The presence of alkali-metal species in the ammonia synthesis catalyst is essential to obtain high activity. Although all of the alkali metals are effective to some extent, the best are potassium, rubidium and cesium, with potassium being the most cost effective. On reduction of the catalyst, much of the potash remains associated with the somewhat acidic support phase, though some interacts with the iron particles and greatly increases their activity.

In the early 1970s, an alkali-metal-promoted carbon-supported Ru catalyst was introduced, it exhibited a 10-fold increase in activity over the conventional iron-based catalyst under similar conditions. In 1992 using this kind of graphite-supported ruthenium catalyst, a 600 tonn NH<sub>3</sub> per day plant has begun to

produce ammonia under milder condition compared with the plants using iron-based catalysts. Thus, it is believed that Ru-based catalyst could become the second-generation catalyst for ammonia synthesis. However, the ruthenium-based catalysts are not widely employed in industrial ammonia synthesis because they are expensive<sup>8</sup>.

Because of the advance in the ruthenium-based catalyst for ammonia synthesis, a number of research groups have investigated the roles of support and promoter of the catalyst played in the catalytic reaction. Various supports, such as active carbon and graphite, alumina, carbon-coated alumina, magnesia, a series of zeolites and even rare-earth metal oxides were used in Ru-based catalysts for the ammonia synthesis. The promoters used are mainly alkali metal, alkaline earth metal, rare earth metal and their oxides or hydroxides. However, it seems that the ruthenium supported on carbon material with promoters is the most promising catalyst for commercial applications. This is due to the many attributes linked with carbon materials, such as specific electronic properties, variable surface functional groups, and easy metal recovery by the burning of the support. For the above-mentioned reason, Li and coworkers<sup>9</sup> carried out studies to investigate in detail the ammonia synthesis on the ruthenium catalysts supported on different carbon materials promoted with K and Ba compounds under moderate pressure. They found that the Ba and K promoters change Ru dispersion, modify electron properties on Ru surface, and neutralize the surface groups of carbon supports; as a result, these promoters significantly enhance the ammonia synthesis activity of Ru/C catalysts. The Ba-promoted Ru/AC (active carbon) catalyst gives the highest ammonia concentration, because Ru metal is well dispersed on the support, while Ru-Ba/ACF (active carbon fiber) gives the highest TOF value (turnover frequency). This is due to the high purity and electronic conductivity of ACF. The low activity on the CMS (carbon molecular sieve) support can be attributed to the low surface area and the lower graphitization. Therefore, the carbon supports with high purity, high electronic conductivity and high surface area favor the high activity of Ru-based catalysts for ammonia synthesis. The ammonia synthesis on Ru/C catalyst is structure sensitive and exhibits higher activity, but the TOF becomes constant when Ru particle size is beyond about 5nm<sup>9</sup>.

To avoid methanation and the easy loss of the carbon support, Liao and coworkers<sup>8</sup> studied bimetallic catalysts (Ru-M, M = Fe, Co, Ni, Mo) with low

ruthenium loadings and without a carbon support, but  $\text{MgAl}_2\text{O}_4$ ,  $\text{MgO}$  and a Mg-Al complex oxide obtained by calcining hydrotalcite type precursors at  $800^\circ\text{C}$ . It was shown that the bimetallic Ru-Co/MgO exhibited good ammonia synthesis activity<sup>8</sup>.

Ru-based catalysts are known to be active for  $\text{NH}_3$  synthesis at atmospheric pressure and low temperature<sup>10, 11</sup>. The most stable and commercially available Ru precursor used for ammonia synthesis is  $\text{RuCl}_3$ . The main advantage of this metal precursor is its low cost in comparison to other metal precursors, but the main disadvantage of using  $\text{RuCl}_3$  is the strong binding of chlorine atom with the metal surface even after reduction. Alkali metal nitrate used as a promoter is thought to have two effects: one is to remove chlorine ions from the catalyst and the other is to donate electrons to ruthenium. The promoting effect of alkali metal to Ru on  $\text{NH}_3$  synthesis activity is found to be inversely proportional to the electronegativity of the alkali metal in the order of  $\text{Cs} > \text{Ba} > \text{K} > \text{Na}$ .

It has been observed that the high activity of the active carbon supported promoted ruthenium catalysts are attributed to the electron deficient graphite lattice of active carbon. The  $\text{MgO}$  support shows less activity because of strong interaction with chlorine in  $\text{RuCl}_3$ . The strong chemisorption of product ammonia on the acid centers of alumina makes it a less attractive support for ruthenium. Hydrotalcite-like compounds are a class of precursors useful for the preparation of catalytically active oxides showing basic properties. Rama Rao et al<sup>11</sup> shows in a recent work the comparison of activity studies of ammonia synthesis over Ru supported on mixed oxide support obtained from Mg-Al HT precursor (with Mg/Al ratio of 2) with the Ru catalysts supported on simple oxides  $\text{MgO}$  and  $\text{Al}_2\text{O}_3$  under atmospheric pressure. They found that calcined hydrotalcite precursor is the promising support for the ammonia synthesis, because it is highly basic, thermally stable, and is resistant to  $\text{Cl}^-$  when compared to  $\text{MgO}$  support. Ruthenium with cesium promoter over novel Mg-Al HT support is found to be very efficient for the synthesis of ammonia at atmospheric pressure compared to Cs-Ru catalysts on  $\text{MgO}$  and  $\text{Al}_2\text{O}_3$  supports. The higher activity of the Cs-Ru/HT catalyst has been attributed to the presence of easily reducible Ru species and nano-particles of Ru in highly dispersed form over calcined Mg-Al HT support<sup>11</sup>.

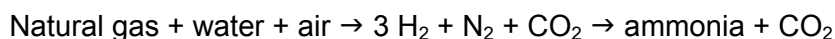
In a recent work, Liao et al<sup>12</sup> studied new supported catalysts to develop catalysts with high stabilization ( $\text{MgO}$ ) and high activity (CNTs = carbon nanotubes). They

studied K-Ru/MgO and K-Ru/CNTs separately and then combined at different weight ratio to obtain a combination-type catalyst. For the as-prepared combination-type ruthenium catalysts, ruthenium particles well disperse on the surfaces of MgO and CNTs relatively. The optimal weight ratio of K-Ru/MgO to K-Ru/CNTs for the preparation of the combination-type ruthenium catalysts is 1/1, that is because the combination between MgO and CNTs is strong and the interactional effects are prominent at this weight ratio. A complementary interaction between two supports is suggested, which promotes electron transfer from alkali metallic atoms to the B5-sites of ruthenium more easily. Due to the high catalytic activity and high thermal stability under operating conditions, the combination-type ruthenium catalyst of K-Ru/MgO and K-Ru/CNTs may be a good catalyst for ammonia synthesis.

### 1.1.3. Ammonia plants

The principle of circulating gases over the catalyst, which was first appreciated by Haber in 1908, is still an important feature of modern ammonia plants. Synthesis gas of the appropriate composition passes through the catalyst beds, and the ammonia produced is condensed and recovered. Unreacted gas, to which fresh make-up gas is added, is then recirculated through the catalyst. Using heater exchangers the temperature of the recirculating gas is raised in two stages to a reaction temperature of about 400°C and, at the same time, the temperature of the converter effluent gas is reduced. To prevent accumulation of inert gases generally present in the synthesis gas, part of the circulating gas is purged. The residual ammonia in the purge gas is usually recovered, and the hydrogen content is either used as fuel in the primary reformer or recovered and recirculated<sup>7</sup>.

In modern ammonia plants, it takes 28-30 GJ/te to produce ammonia from natural gas by the overall reaction:



The exergy consumption for ammonia production depends strongly on the ammonia synthesis loop design. In general, even at high pressure up to 300 bar, not more than the 20-25 % of the synthesis gas is converted to ammonia per pass<sup>13</sup>. After the removal of ammonia by its condensation at low temperatures, the unreacted hydrogen – nitrogen mixture is returned to the reactor. Therefore,

since its first development in 1913 by Haber and Bosch, industrial ammonia synthesis always has been implemented as a recycle process. Thus, to produce 1 Kg ammonia, 4-6 Kg synthesis gas must be recycled through the reactor.

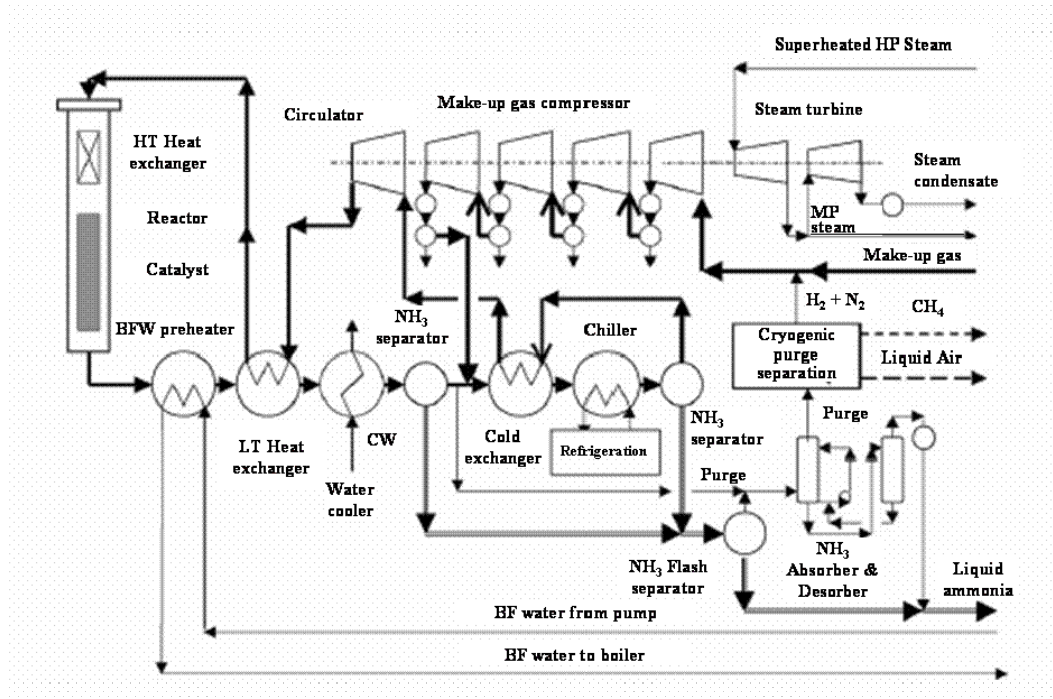


Fig. 1. 2 - Flowsheet of typical ammonia synthesis loop.

The energy efficiency of an industrial ammonia synthesis process depends on two types of parameters:

- Parameters defined by external systems: pressure and inerts ( $\text{CH}_4 + \text{Ar}$ ) content of the make-up gas, refrigeration plant and purge recovery.
- Internal parameters defined by the loop design: degree of conversion (or recycle ratio), reaction approach to equilibrium, inerts ( $\text{CH}_4 + \text{Ar}$ ) content in the circulating gas and reaction heat- and cold recovery system parameters.

The exergy efficiency of an ammonia synthesis loop depends strongly on the degree of conversion, respectively, on the recycle ratio. The higher the conversion is (respectively the lower the recycled/fresh gas ratio), the better the heat utilization and the less the exergy consumption for gas recycling and for ammonia condensation. However, exergy efficiency increases when the reaction approaches equilibrium, because exergy consumption for ammonia condensation decreases.

The equilibrium concentrations of components in the ammonia synthesis reaction depend on the pressure and the temperature, and, to a lesser extent, on the concentration of inerts. Since catalysts are active over the narrow temperature range of 380–500°C and unable to approach more than 80 % of the equilibrium, the maximum ammonia concentration in the recycling gas at the reactor outlet depends in fact only on the pressure.

Actually, outlet ammonia concentration is being chosen somewhat lower in order to reduce the catalyst volume, and the reactor costs. In most cases, the inlet and outlet ammonia concentrations are connected depending on the reactor design. The oldest “quench” and “cooling tube” reactors afford a degree of conversion of no more than 10–11 %. Modern reactor designs with intercoolers between catalyst beds provide a degree of conversion as high as 15 %. With maximum outlet ammonia concentration of 20 %, a degree of conversion of more than 16 % may be reached only in the case of full removal of ammonia from recycling gas mixture, e.g. by water absorption. However, water absorption is not used in industrial ammonia plants and ammonia condensation is still the only way to separate ammonia from the unreacted gas mixture.

The inlet ammonia concentration depends on the vapor–liquid equilibrium (VLE) in the system NH<sub>3</sub>–N<sub>2</sub>–H<sub>2</sub>–CH<sub>4</sub>–Ar. Ammonia is the only component of this system, which might be condensed at non-cryogenic temperatures. However, the VLE position of ammonia in the presence of non-condensable gases at high pressures (80–300 bar) is very unfavorable. The real vapor pressure of ammonia in this system is up to twice as high as the equilibrium pressure of pure ammonia at the same temperature. Thus, the partial condensation of ammonia from the outlet gas mixture, containing 20 % ammonia at 300 bar, begins at relatively low temperature (65 – 70°C). To obtain ammonia content as low as 2%, the gas mixture must be cooled down to temperatures such as – 20°C. Therefore, the first stage of condensation is carried out in water-cooled or air-cooled condensers. But the ammonia content at temperatures 25–30 °C is still high (7 – 8 %) and in most modern ammonia plants an ammonia refrigeration unit is used to cool the recycling gas down to – 20 / + 10°C in order to decrease the converter inlet ammonia concentration down to 2 – 5 %.

In the first stage, the ammonia condensation heat is released to the environment and some power is consumed in the air coolers or in the cooling water system. In the second stage, cold recovery could not be complete because the heat

capacity flow rate of the warm gas, in which the ammonia condensation occurs, is much greater than the heat capacity flow rate of the cold gas exiting the ammonia separator. In most ammonia plants, a simple vapor-compression refrigeration cycle is used to reject the condensation heat at low temperatures. In this case, all this heat is rejected from the recycle gas at the lowest temperature in the synthesis loop and the irreversible losses are too large. If the ammonia content at the reactor inlet is given, the minimum temperature approaches in the cold exchanger and in the chiller are the only independent parameters of the second-stage ammonia condensation subsystem.

The exergy efficiency of modern ammonia synthesis plants is improved by the use of well-developed heat- and cold recovery. In most ammonia plants, the reaction heat is utilized at a relatively low temperature, e.g. for boiler feed water (BFW) preheating. The temperature approach in high temperature (HT) heat exchanger depends only on the degree of conversion. A small temperature approach (about 10 – 20°C) along the low temperature (LT) heat exchanger is possible and then a substantial (90 – 95 %) part of the reaction heat could be utilized. However, the temperature level of heat utilization is low and the exergy efficiency of the entire heat utilization system is small. If the degree of conversion is given, the minimum temperature approach in the low temperature heat exchanger and the hot gas BFW preheater input temperature are the only independent parameters of heat recovery and utilization subsystem.

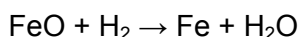
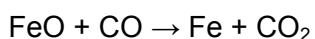
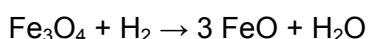
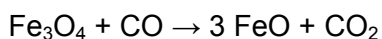


**Fig. 1. 3 - Ammonia plant.**

## 1.2. Direct Reduction of iron ore (DRI)

Direct reduction of iron ore is today's major process for generating metallic iron, necessary in the iron and steel industry. World production of direct reduce iron (DRI) has grown from near zero in 1970 to 45.1 Mt in 2002<sup>3,14</sup>.

In the production processes for converting iron ores into iron and steel, carbon, primarily in the form of coke, has been traditionally used to reduce the iron oxides to iron metal. However, in the last several decades, there has been increasing production of iron using the direct reduction iron (DRI) process. In 1998, about 4 % of the primary iron in the world was produced by the DRI process with rapid growth in iron production. In the DRI process, syngas (a mixture of hydrogen and carbon monoxide) made from natural gas is used to reduce iron ores to iron. The major chemical reactions are as follows:



The DRI process has lower capital costs than alternative methods used to produce iron, but requires a low-cost source of hydrogen. The primary market for DRI is to provide a purified iron feed for electric arc furnaces (EAFs) that produce various steel products. EAFs have lower capital costs than traditional steel mills and are environmentally cleaner operations than blast furnaces. Over a third of the world's steel production uses this process. It is predicted that by 2010 up to 45 % of the world's steel may be made with EAFs. Historically, scrap metal has been the traditional feed for EAFs. However, there are two constraints: the availability of scrap metal and the various difficult-to-remove impurities (copper, nickel, chrome, molybdenum, etc.) that are present in the lower-grade scrap metal. Blending clean DRI-process iron with scrap metal dilutes the impurities below the level that affect product quality. Traditional steel-making processes using coke result in iron with a high carbon content and various other impurities from the coke.

Iron production is potentially a significant existing market for hydrogen. If low-cost hydrogen is available, the DRI process would replace other methods of iron production. The economics of DRI relative to other processes (and the potential demand for hydrogen) depend upon three factors.

- Technological developments: The continuing improvements in EAF technology in terms of reduced production costs and increased capabilities to produce higher-quality steel have expanded the market share of this technology. That, in turn, creates the demand for more high-purity iron by the DRI process as traditional sources of scrap metal are exhausted.
- Environmental protection: Traditional steel processes use coal and generate large quantities of pollutants. Clean air requirements strongly affect the economics of these competing processes.
- Hydrogen costs: The process is used where there is low-cost natural gas for hydrogen production near iron deposits.

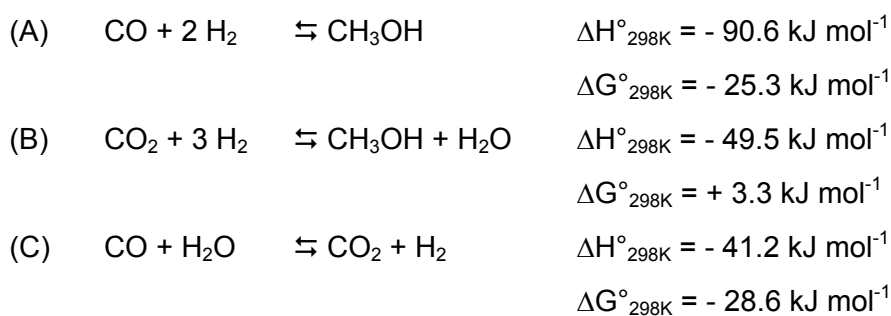
### 1.3. Methanol synthesis

Methanol is inside the top 10 produced molecules. Methanol has been a common chemical feedstock for several important chemicals such as acetic acid, methyl ter-butyl ether (MTBE), formaldehyde and chloromethane. Moreover, methanol being a clean liquid fuel could provide convenient storage of energy for fuel cell applications, particularly in transportation and mobile devices<sup>15</sup>. In additions, over the last few decades, methanol-to-hydrocarbons (MTHC) technologies, in particular methanol-to-olefin (MTO) and methanol-to-gasoline (MTG), have been the focus for a large number of researcher dealing with the upgrading of natural resources beneficial both for the petrolchemistry and fuel industries<sup>16, 17, 18</sup>.

The process to synthesize methanol from carbon monoxide and hydrogen was introduced by BASF in 1923 and it was the second large-scale application of catalysis (after ammonia synthesis) and high-pressure technology (100-300 bar) to the chemical industry<sup>7</sup>.

Like the ammonia process, methanol synthesis was dependent on the development of an effective catalyst, but unlike the ammonia synthesis catalyst, the methanol catalyst had to be selective as well as active.

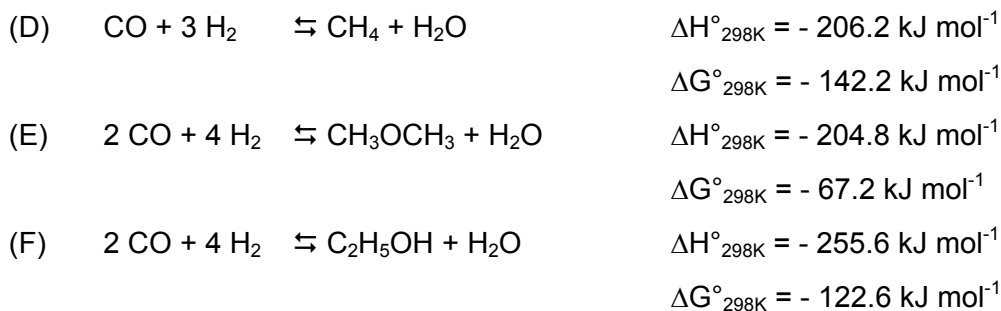
The reactions involved in the methanol synthesis are:



Reaction (B) and (C) combined are equivalent to reaction (A), so that either, or both, of the carbon oxides can be the starting point for methanol synthesis.

Reactions (A) – (C) are exothermic; reactions (A) and (B) are accompanied by a decrease in volume. Hence, the value of the equilibrium constant decreases with temperature and increases with pressure ( $K_p = p_{\text{CH}_3\text{OH}} / p_{\text{CO}} p_{\text{H}_2}^2$ ). Thus, high conversions to methanol, given a sufficiently active catalyst, will be obtained at high pressures and low temperatures.

In addition to the synthesis of methanol, both carbon monoxide and carbon dioxide can take part in other hydrogenation reactions, producing by-products such as hydrocarbons, ethers and higher alcohols:



These reactions are much more exothermic than the methanol synthesis reactions and methanol is thermodynamically less stable and less likely to be formed from carbon monoxide and hydrogen than the other possible products, such as methane. Which of the products is formed is controlled by kinetics factors; that is, by the catalyst being selective in favoring a reaction path leading to the desired product.

The catalytic synthesis of methanol from syngas has been conventionally carried out in two-phase reactors with the syngas and products in the vapor phase and the catalyst as solid phase. The large exothermic heat of reaction in addition to the low heat capacity of the vapor increases the potential for thermal runaway and damage to the catalyst in the vapor phase, thus limiting the maximum operable reaction temperature<sup>19</sup>.

### 1.3.1. Methanol synthesis catalysts

There are two class of catalysts studied and used for methanol synthesis: high-pressure and low-pressure catalysts (Tab. 1. 1).

#### High-pressure catalysts

The catalyst used in the original process was derived by empirical methods. It contains zinc oxide and chromia and was used in the high-pressure process for 40 years. Zinc oxide alone was a good catalyst for methanol synthesis at high pressure and temperature above 350°C, but it was not stable and quickly lost its activity. It was found that die-off could be retarded by the incorporation of chromia, which acted as a stabilizer preventing the growth of the zinc oxide crystals.

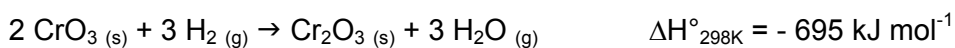
Catalyst composition	Active phase in methanol synthesis	Properties and use
ZnO	ZnO	Original synthesis catalyst, short life
ZnO/Cr <sub>2</sub> O <sub>3</sub> (ICI catalyst)	ZnO	Standard high pressure catalyst
ZnO/MnO/Cr <sub>2</sub> O <sub>3</sub> + alkali	Alkalized ZnO (+MnO)	Standard high pressure catalyst for methanol and higher alcohol mixtures
Cu/ZnO Cu/ZnO/Cr <sub>2</sub> O <sub>3</sub>	Cu	Early low pressure catalysts, short life
Cu/ZnO/Al <sub>2</sub> O <sub>3</sub> (ICI catalyst)	Cu	Industrial low-pressure catalyst
Pd/SiO <sub>2</sub> Pd/basic oxides	Pd	Active; poorer selectivity than copper catalysts (by-products: hydrocarbons)
Rh/SiO <sub>2</sub> Rh/basic oxides	Rh	Active; poorer selectivity than copper catalysts (by-products: hydrocarbons)
Rh complex	Rh complex	Low activity; poorer selectivity (homogeneous catalyst; co-product: ethylene glycol)

**Tab. 1. 1 - Catalysts proposed or used for industrial methanol synthesis<sup>7</sup>.**

Today zinc oxide, still a major component in synthesis catalysts, is known to have a defect structure with a non stoichiometric oxide lattice which is probably responsible for its catalytic activity. Stabilizers such as chromia probably prevent recrystallization of the zinc oxide and preserve the defect structure, as well as preventing crystal growth and loss of surface area. The most active zinc oxide was obtained from the zinc carbonate mineral smithsonite, containing traces of various impurities, which acted as “promoters”, probably by forming solid solutions. The promoters may have both increased the specific activity of the zinc oxide by inducing lattice defects, and stabilized the zinc oxide by the inhibition of sintering.

The zinc oxide/chromia catalyst was tolerant of the impure synthesis gas, and could have a plant life of several years. It was not very selective and depending on synthesis conditions, as much as 2 % of the inlet carbon oxide could be converted to methane, with a similar proportion to dimethyl ether. Because these side reactions are very exothermic, careful control of catalyst temperature was necessary. The catalyst was made by precipitation from zinc and chromium solutions or by impregnation of, for example, zinc carbonate with chromic acid or dichromate solution. In the catalyst produced by impregnation, the chromium was present in the hexavalent form, as CrO<sub>3</sub> rather than Cr<sub>2</sub>O<sub>3</sub> as in the precipitated

catalyst. Cr(VI) is particularly toxic and present a health hazard in the handling of the catalyst. The chromate also has to be reduced with great care to avoid a temperature runaway, because the reduction of  $\text{CrO}_3$  to  $\text{Cr}_2\text{O}_3$  with hydrogen is extremely exothermic:



Although the low pressure process based on high-activity catalysts has almost entirely taken the place of the high pressure process, there have been occasions when high pressure plant being supplied with pure synthesis gas could, to advantage, use a catalyst of higher activity. The copper/zinc oxide/alumina type was found to be very satisfactory, although at the synthesis pressure of 350 bar, with high partial pressure of water, sintering processes are accelerated.

### Low-pressure catalysts

The methanol synthesis process has been operated at high pressure since its invention by BASF in 1920s. With the development of newer catalysts, the operating pressure was obviously decreased<sup>15</sup>. Among those catalysts copper oxide appeared to have little activity itself, but was very effective when added to zinc oxide. This was also the case when copper was added to the zinc oxide/chromia catalyst, so it could be used at temperature as low as 300°C. However, the catalysts containing copper were not stable and lost activity. For example, a Zn/Cu/Cr catalyst in atomic proportions of 6/3/1 lost 40 % of its activity in 72 hours. However, as a result of the ICI work on methanol catalysts, stable copper catalysts were produced. The loss of activity of the early copper catalysts in use was almost certainly due to loss of copper surface area and sintering, despite the presence of zinc oxide and other stabilizers. Although ZnO has activity for methanol synthesis, this is so much less than that of copper that acts as an inert diluent in copper/zinc oxide catalysts.

In an oversimplified model, the catalyst can be considered as particles of copper metal, surrounded and kept apart by stabilizer particles. The smaller the diameter of the refractory spacers, the higher is the practical copper loading and the higher the activity. High metal concentrations are used in industrial catalysts: in use, both metal and spacer dimensions increase and the rough relationship still holds. In the copper/zinc oxide/alumina, synthesis catalysts high activity and stability are obtained by optimizing the compositions and producing very small particles of the components in a very intimate mixture. By precipitation at a controlled pH, in

which the acidic and alkaline solutions were mixed continuously, a catalyst of optimum composition and particle size is obtained. Although chromia had been effective as a stabilizer in the high pressure catalyst, alumina is superior to it as the third component in the low pressure catalyst. The alumina, present as a high surface area, poorly crystalline phase, is more effective than zinc oxide in preventing the sintering of copper crystallites. It might then be thought that a copper/alumina catalyst would be superior to the ternary catalysts, but there are several reasons why this is not so.

High area aluminas have acidic sites on the surface, which catalyze the parasitic reaction of methanol to dimethyl ether, so Cu/Al<sub>2</sub>O<sub>3</sub> catalysts have poor selectivity. In the ternary catalysts, formation of dimethyl ether is very low, showing that the acidic sites are neutralized by the basic zinc oxide (either as a surface reaction only or in bulk reaction to zinc spinel).

The chemistry of the metal and support precursors, formed in the precipitation process, gives smaller copper crystallites with zinc oxide support than with alumina. Hence, the optimum combination of high initial activity and catalyst stability is obtained with the ternary Cu/ZnO/Al<sub>2</sub>O<sub>3</sub> catalyst.

Although poisoning is not usually a significant problem in well-run methanol plants, the presence of a "poison-soak" in the support phase can be useful. Zinc oxide is much more effective than alumina in picking up and holding typical poisons, such as sulphur and chlorine compounds.

Cu/ZnO/Al<sub>2</sub>O<sub>3</sub> catalysts are still widely used and studied for the industrial synthesis of methanol. Various methods have been developed for the preparation of these kinds of catalysts. The difference in preparation methods, synthesis conditions, and pre-treatment have a considerable influence on the structure of the catalysts, which finally leads to disparities in the catalytic performance. It is generally accepted that a large specific Cu surface area leads to an active methanol synthesis catalyst. In addition, the metal-support interaction plays a key role in this catalytic reaction<sup>20</sup>.

Hydrocarbons and higher alcohol are thermodynamically more stable than methanol and could be formed. The extent to which this occurs is controlled by the selectivity of the catalyst. In this respect, the Cu catalysts are superior to the ZnO/Cr<sub>2</sub>O<sub>3</sub> catalyst. Methanation needs to be minimized, both because it is a loss of feedstock and, as a highly exothermic reaction, it can cause temperature runaways. As the by-products are formed in parasitic (parallel) reactions and not by any intrinsic inefficiency of the synthesis reaction itself, improved activity for methanol synthesis alone, also give improved selectivity. Thus, the copper catalysts are more selective than ZnO catalysts under the same process conditions, but there is a further benefit. The higher activity allows the use of lower process temperatures, so by-products formation is further decreased relative to methanol synthesis, because most of the parasitic reactions have higher activation energies. The formation of by products is influenced markedly by any impurities in the catalyst, either left in the catalyst during its manufacture or introduced during use. Thus, alkaline impurities can result in the production of higher alcohols and, in addition, cause some decrease in activity. Similarly, acidic impurities (for example silica) can lead to the formation of high molecular weight waxes on the catalyst, which can cause loss of activity by blocking some of the smaller pores. The weaker acidity found on the surface of high area aluminas does not give waxes, but it catalyses the dehydration of methanol to dimethyl ether. These potential problems are eliminated by careful design and manufacture of the catalyst.

The presence of VIII group metals, such as iron, is particularly undesirable, as they increase hydrogenation activity and promote the dissociation of carbon monoxide and dioxide, leading to formation of methane and long-chain paraffins and/or waxes by Fischer-Tropsch type reaction. Methanation was always a problem with the high-pressure catalyst, and it is thought that this was mainly caused by iron impurities. Other VIII group metals, as cobalt or nickel, can also catalyze methanation but they have been found to have a further deleterious effect. Methanol synthesis itself is inhibited, probably by surface coverage of copper crystallites with support oxide. Thus, alkali, acidic species and VIII group metals can be regarded as poisons for synthesis catalysts. In addition, traces of sulphur and chlorine can reduce the activity of the copper catalyst by reacting with the active surface. Chlorine is particularly undesirable because, in addition to poisoning of copper surface, the copper chloride produced is mobile and cause

rapid sintering of the metal. Chlorine and sulphur also react with the free zinc oxide in the catalyst, so that much of the uptake occurs on the catalyst near the inlet to the bed, which therefore acts as a guard for the rest of the bed. Poisoning of synthesis catalyst is not normally a problem except as a result of maloperation. Although extensive studies have been carried out, controversies remain concerning the role of active sites involved in the catalysts, the effect of the additions of various promoters and the reaction mechanism<sup>15</sup>. The active sites in Cu/ZnO catalysts have long been studied. On this issue, researchers are roughly divided in two groups: one insists that metallic Cu atoms are homogeneously active for the methanol synthesis, and the other claims that special sites (or active sites) exist in addition to metallic Cu atoms<sup>21</sup>.

Also for ZnO the model proposed are divided in four groups (i) ZnO increases the dispersion of Cu; (ii) ZnO acts as a reservoir for atomic hydrogen spilling over onto the Cu surface to promote hydrogenation process; (iii) ZnO stabilizes some active planes of Cu or the morphology of Cu particles and (iv) ZnO creates active sites on the Cu surface<sup>21</sup>.

Several non-conventional catalyst types have attracted attention because of their high activity for methanol synthesis<sup>23</sup>. These include:

- Alloys: Raney - The Raney method has been utilized for catalyst preparation, dissolving aluminum from CuAl<sub>2</sub> alloys with or without the presence of dissolved zinc. Catalysts so prepared have high activity and selectivity. Properties depended on leaching conditions, and it was found that greatly improved catalysts could be obtained by low temperature leaching in caustic solutions that contain near-saturation levels of sodium zincate.
- Alloys: Cu- rare earths – Binary copper-thorium alloys were prepared, followed by oxidation of the thorium to thoria, then reducing the copper oxide formed to copper metal. This catalyst was active for methanol synthesis over a range of conditions. Catalysts derived from rare earth-copper intermetallic alloy precursors have been found to exhibit extraordinarily high activity for CO hydrogenation to methanol. Typical precursor alloys were prepared by melting Cu with Ce or La. Methanol synthesis over Cu-La catalysts was observed at temperatures as low as 100°C.
- Supported platinum group VIII metals – Catalysts containing Pd can produce sizeable amounts of methanol when operated under conditions where methanol is thermodynamically stable. Of the platinum group metals, rhodium

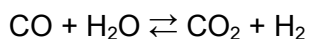
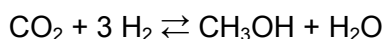
catalysts have received most attention. Supported rhodium catalysts containing large amounts of molybdenum are particularly active. While selectivity towards alcohols is enhanced by molybdenum additions to about 60 % alcohols and 40 % hydrocarbons at 250°C such selectivity is not attractive commercially.

### 1.3.2. Reaction mechanism

The methanol synthesis reaction has been the subject of many mechanistic studies since the process was first introduced. Bridger and Spencer in a detailed analysis, reported in the Catalyst Handbook<sup>7</sup>, show how the results of many studies are often conflicting due to the properties of different type of catalysts (which often depend on details of preparation), to the different bulk phases present in the operating catalyst (varying with process conditions), to the reaction conditions and poisons.

All industrial plants operate with CO/CO<sub>2</sub>/H<sub>2</sub> mixtures and it is not obvious which carbon oxide is the source of methanol. In most studies, it was concluded or assumed that adsorption of carbon monoxide is the starting point, but also evidence has been obtained indicating that methanol is synthesized directly from carbon dioxide. Certainly, the presence of CO<sub>2</sub> in the reacting gas has a marked effect in increasing reaction rate, and the effect is reversible, even if it was found also that using a zinc/chromia catalyst the carbon dioxide decrease the synthesis rate.

On Cu/Zn/Al<sub>2</sub>O<sub>3</sub> catalysts, the role of carbon dioxide on the methanol synthesis reaction is very important<sup>19, 22</sup>. It was observed that the optimal loading of carbon dioxide depends upon the operating temperature. The reactions describing the methanol synthesis over Cu/Zn/Al<sub>2</sub>O<sub>3</sub> catalyst primarily involve the CO<sub>2</sub> hydrogenation reaction and the forward water gas shift reaction:



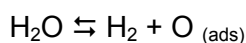
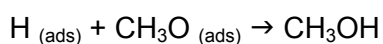
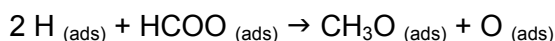
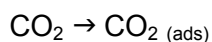
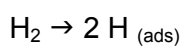
The CO<sub>2</sub> concentration in the syngas feedstock is very important to the right balance of the two reactions. If the CO<sub>2</sub> concentration is too high, the direction of the WGS reaction is reversed and carbon dioxide is competitively consumed in both the reactions. If the CO<sub>2</sub> concentration is too low, the potential for carbon

deposition and the reduction of catalyst oxides is increased, thereby increasing the catalyst deactivation. The catalytic activity drops significantly and progressively when it is exposed to a CO<sub>2</sub>-free syngas feed. The catalyst deactivates in absence of carbon dioxide<sup>19, 15</sup>.

For what concern the state of the active metals in a working catalyst, it was demonstrated that the catalyst surface is in a dynamic state.

The support oxides play a minor role in the reaction mechanism, but it has been observed that the coverage of adsorbed oxygen varies with different support oxides.

A surface formate is the pivotal intermediate over both zinc oxide and supported copper catalysts. Surface formate is made by the hydrogenation of adsorbed carbon dioxide, and the rate determining step in methanol synthesis appears to be hydrogenolysis of the formate intermediate first to methoxy and then to methanol. The remaining adsorbed oxygen is removed by carbon monoxide or hydrogen, depending on the reaction conditions, to give CO<sub>2</sub> or H<sub>2</sub>O. The concurrent water gas shift reaction probably occurs via adsorbed oxygen rather than formate intermediate:



The active sites are on the surface of the copper metal crystallites. The surface of copper is mobile under reaction conditions and it is partially covered by a mobile layer of adsorbed oxygen. Adsorbed hydrogen mostly is present on the uncovered copper metal (even if requiring O<sub>(ads)</sub> for adsorption), whereas carbon dioxide adsorbs on the oxidized surface. Thus, the site of reaction consists of bare copper metal atoms next to an oxide surface site, i.e. a Cu(0)/Cu(I) site, but this occur in different parts of the surface as the reaction proceeds.

The mechanism of the synthesis of methanol on copper catalysts from CO<sub>2</sub>-free gas mixtures is not well understood. Formate intermediates, made from residual O<sub>(ads)</sub>, may be involved again or successive additions of H<sub>(ads)</sub> to adsorbed carbon monoxide may give first adsorbed methoxy and then methanol.

### 1.3.3. Methanol plants

Although the chemistry of methanol manufacture is simple,  $\text{CO} + 2 \text{H}_2 \rightarrow \text{CH}_3\text{OH}$ , several process steps are required for a modern plant for methanol production<sup>23</sup>. Conversion of syngas to methanol per pass in present commercial operation is limited to 25 vol. % or less by thermodynamic restrictions, even with modern catalysts and plant design, costly recycle is required<sup>23</sup>.

Synthesis gas of an appropriate composition (ideally:  $p_{\text{H}_2} = 2 p_{\text{CO}} + 3 p_{\text{CO}_2}$ ) is supplied to the loop and circulated continuously, so that unreacted gas is recycled over the catalyst. From the converter the gas passes to a condenser, which removes the crude methanol liquor, and then to the circulator, which takes the gas back to the converter. Fresh "make-up gas" is supplied continuously to maintain the pressure in the loop as the synthesis proceeds. This gas always departs from the ideal composition to some degree: methane and other inert gases are present and frequently there is excess hydrogen, depending on the feedstock and processes used to manufacture the make-up gas. To prevent these gases from building up in the loop and diluting the reactants, a continuous purge is taken off. Depending on process economics, the purge may be used as fuel for the reformer or it gives a supply of hydrogen after passage through a pressure swing adsorption unit.

The crude methanol is distilled to separate the methanol from water and impurities such as higher alcohols, ethers, etc., that are present in low concentrations.

The use of low conversion per pass together with the recycling of the unreacted gas around the loop facilitates the control of temperature in the catalyst bed. Nevertheless, the highly exothermic nature of the reaction requires the use of special reactor designs.

Part of the circulating gas is preheated and fed to the inlet of the reactor. The remainder is used as quench gas and is admitted to the catalyst bed through lozenge distributors in order to control bed temperatures. Temperature control within the catalyst bed can also be achieved using tube-cooled or steam raising reactor designs. The tube-cooled reactor combines a lower capital cost than the quench reactor with simplicity of operation and very flexible design. Circulating gas is pre-heated by passing it through tubes in the catalyst bed. This removes the heat of reaction from the catalyst bed. Temperature control is achieved by

using a gas bypass around the catalyst bed and by controlling heat recovery in a feed-effluent heat exchanger immediately downstream. Two configurations are possible with the steam-raising type of reactor. The catalyst may be contained within the tubes of a shell-and-tube heat exchanger, with boiling water acting as coolant on the shell side. Alternatively, the catalyst may be contained within the shell with boiling water in the tubes, and this arrangement is similar to that used in the tube-cooled reactor design, as in both reactors the catalyst bed is cooled by fluid flow through tubes in the bed. Since the design with catalyst on the shell side allows the heat transfer surface area to be reduced to as little as one-seventh that of the design with catalyst in the tubes, the former is the preferred configuration.

In the ICI steam-raising reactor design, circulating gas enters through a vertical distribution plate and flows transversely across the catalyst bed. This allows the steam coils to be placed asymmetrically within the catalyst bed, so optimizing heat removal, and giving a small pressure drop. In plants based on natural gas, steam-raising reactors are less efficient at recovering the heat of reaction than quench or tube-cooled designs. This is because heat can be recovered into boiler feed water from the quench or tube-cooled designs, which can then be used to generate high pressure rather than intermediate-pressure steam<sup>7</sup>.

Chem Systems first developed the liquid phase methanol synthesis process (LPMeOH<sup>TM</sup>) in the late 1970s<sup>19,23</sup>. The novel feature of this technology is that methanol is derived from synthesis gas over a finely powdered commercial Cu/Zn/Al<sub>2</sub>O<sub>3</sub> catalyst dispersed in an inert liquid. The slurry phase operation facilitates easy heat removal, thus enabling isothermal conditions in the reactor system. High agitation rates in the reactor provide for a reaction environment without temperature and concentration gradients. The salient features of the liquid phase process are:

- (i) use of CO rich gas;
- (ii) enhanced heat transfer of exothermic heat;
- (iii) high once-through conversion of syngas.

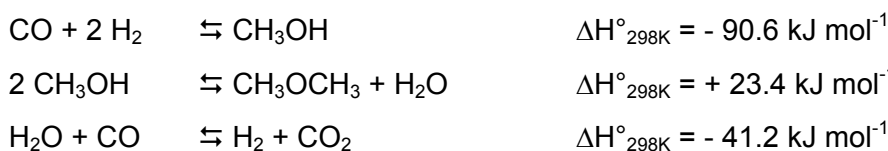
The liquid acts as a heat sink and, by making possible efficient heat exchange, limits temperature increase. The catalyst size must be 1-10 μm and need in situ activation.

### 1.4. Dimethyl ether synthesis

Dimethyl ether (DME) is an alternative fuel that could potentially replace petroleum-based fuels<sup>24</sup>. Dimethyl ether is the simplest ether (CH<sub>3</sub>OCH<sub>3</sub>). The physical properties of DME are similar to those of liquefied petroleum gases (propane and butane). It burns with a visible blue flame and is non-peroxide forming in the pure state or in aerosol formulations. Unlike methane, DME does not require an odorant because it has a sweet ether-like odor. It is a volatile organic compound, but is non-carcinogenic, non-teratogenic, non-mutagenic and non-toxic<sup>24</sup>.

Currently, the major usage of DME is as a propellant in the aerosols industry. In addition, it can be used as a clean-burning fuel in diesel engines, as a household fuel (LPG alternative) for heating and cooking, as a fuel for gas and turbines in power generation, as a fuel for fuel cells, and as a chemical feedstock for higher ethers and oxygenates<sup>19, 25</sup>.

Traditionally, DME has been produced in a two steps process where syngas is first converted to methanol, followed by methanol dehydration to dimethyl ether.



Net reaction:



Natural gas is not the only resource that can be used to generate syngas, coal and biomass can also be used. Hence, DME production is not limited to one feedstock and the price of DME synthesis process is directly related to the price of the feedstock. New processes are being commercialized to produce DME in a single step via autothermal reactors and slurry phase reactors.

DME can be introduced and exploited with existing technologies, and enable the eventual implementation of advanced technologies, such as fuel cells. Because DME is produced from natural gas, coal or biomass, it can increase the energy security by displacing petroleum derived fuels.

The prominent advantages of DME as a fuel and energy carrier are<sup>24</sup>:

- DME, due to its high cetane number<sup>26</sup>, can be used in the most efficient engine technology currently produced. DME demonstrated lower NO<sub>x</sub> and SO<sub>x</sub> than conventional diesel, is sootless<sup>27</sup>.
- Using existing engine technology, DME produces the least amount of well-to-wheel greenhouse gas emissions compared to FT diesel, FT naphtha, bio-diesel, bio-naphtha, methanol, methane and ethanol.
- Excluding natural gas, DME has the highest well-to-wheel efficiency of all non-petroleum based fuels using conventional, hybrid and fuel processor fuel cell vehicle technologies.
- DME can be used as a residential fuel for heating and cooking.
- On-board automotive fuel processors using methanol and DME exhibit the lowest start-up energies and the lowest fuel processor volumes – correlating to higher overall efficiencies as compared to ethanol, methane and gasoline fuel processor fuel cell vehicles.
- The infrastructure of DME is less cost intensive than that for hydrogen because DME can use the existing LPG and natural gas infrastructures for transport and storage.

Synthesis of DME from syngas in a single step is more favorable in thermodynamic and economical<sup>26, 25</sup>.

Single-stage DME synthesis in the vapor phase suffers from low per pass conversions<sup>23</sup>, due, in part, by the effects of high temperature on the catalysts. Gas-phase DME synthesis processes, in general, suffer from the drawbacks of low hydrogen and CO conversions per pass, along with low yield and selectivity of DME, coupled with a high yield of carbon dioxide. These processes are typically expensive due to high capital costs for reactors and heat exchangers, and high operating costs due to inefficient CO utilization and high recycle rates. Using an inert liquid as a heat sink for highly exothermic reactions offers a number opportunities in syngas processing. Heat generated by the exothermic reactions is readily accommodated by the inert liquid medium. This enables the reaction to be run isothermally; minimizing catalyst deactivation commonly associated with the more adiabatic gas phase technologies<sup>19</sup>.

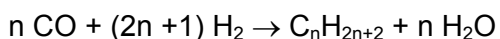
The single stage, liquid phase DME synthesis process, investigated in detail, incorporates the sequential reaction of methanol synthesis and methanol

dehydration in a slurry phase reactor system. Combining these reversible reactions in a single step makes each reaction thermodynamically more favorable by utilizing its inhibiting products as reactants in the subsequent reaction. In addition to the superior heat management allowed by the liquid phase operation, the synergistic effect of these reactions occurring together yields higher quantities of DME than that could be obtained from sequential processing.

The process is based on dual-catalytic synthesis in a single reactor stage, and based on a combination of an equilibrium limited reaction (methanol synthesis) and an equilibrium unlimited reaction (methanol dehydration). The methanol synthesis and the water gas shift reaction take place over the coprecipitated Cu/Zn/Al<sub>2</sub>O<sub>3</sub> catalyst and the methanol dehydration takes place over  $\gamma$ -Al<sub>2</sub>O<sub>3</sub> or zeolite<sup>26, 25, 27</sup> catalysts. Moreover, by varying the mass ratios of methanol synthesis catalyst, it is possible to co-produce DME and methanol in any fixed proportion, from 5 % DME to 95 % DME<sup>19</sup>.

## 1.5. Fischer-Tropsch synthesis

The growing reliance on imported oil gave the synthetic fuels a fresh impetus in the 1980s<sup>28, 23</sup>. The Fischer-Tropsch synthesis (FTS) is the exothermic reaction of carbon monoxide and hydrogen to mainly hydrocarbons together with water and carbon dioxide. It can be represented by the following reaction equation:



Sabatier was the first to react carbon monoxide and hydrogen over a nickel catalyst in 1902. The result was the production of methane and water. Then, in 1923 Franz Fischer and Hans Tropsch of the Kaiser Wilhelm Institute (Germany) developed the Fischer-Tropsch process (i.e. Synthol process), in which a carbon monoxide and hydrogen flow, in the presence of iron, cobalt or nickel catalyst at 180-250°C and at pressures from atmospheric to 150 bar, produced a mixture of straight hydrocarbons and smaller amounts of oxygenates. The initial objective of this process was gasoline production. Experience at high and medium reactor pressures was disappointing from an unacceptably high oxygenate product content point of view. Hence, it was adopted an atmospheric reactor pressure. Cobalt became strongly favored as catalytic element, since iron was less active and deactivated rapidly at atmospheric pressure synthesis operation, while nickel gave high methane selectivity and was affected by its loss due to volatile nickel tetracarbonyls production<sup>29, 30</sup>.

The best catalyst was found to be based on cobalt, supported on Kieselguhr with thoria and magnesium oxide as promoters (100g Co / 5g ThO / 8g MgO / 200g Kieselguhr).

In recent years, we assist to a second renewal of interest in the F-T process for producing liquid hydrocarbons. This new interest centers on making synthetic fuels from natural gas instead of coal.

The process of converting natural gas or coal into marketable liquid hydrocarbons comprises three main elements: 1) synthesis gas production, 2) hydrocarbon synthesis via the F-T conversion process, 3) products work-up (Fig. 1. 4).

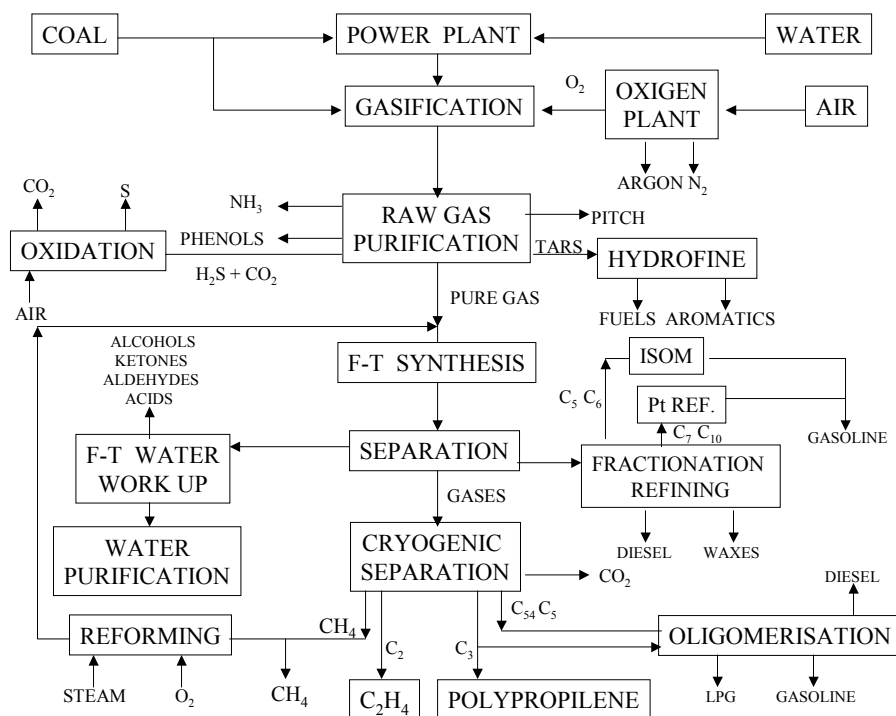


**Fig. 1. 4 - Scheme of the overall FT process.**

In the first step, natural gas is converted to synthesis gas (syngas), a mixture of hydrogen and carbon monoxide, through the commercially known methods (steam-reforming, partial oxidation, or autothermal reforming). The syngas in the second step is converted to hydrocarbons via the F-T synthesis process. In the third step, the primary hydrocarbons in the form of syncrude are worked up to final products consisting mainly of naphtha, diesel fuel and kerosene (middle distillates).

As far as syngas production is concerned, other feedstocks such as coal, heavy residue or shale oil can be used, but the process becomes less economical.

Sasol is the largest producer of synfuels and chemicals made by coal gasification (Lurgi's technology is employed). Besides coal plants, since 1993 Sasol has also operated natural gas-based plants at Moss gas, South Africa, with a capacity of 44.000 BPD of fuels. The company is by far the most experienced player in the syngas-based chemical business, as far as reactors design, catalytic formulations, process technology are concerned.

Sasol has been opting for iron-based catalyst since 1955. Only in recent years the advantages of cobalt based catalyst for use in slurry phase reactor have been recognized.

For the preparation of Synthol catalyst, Sasol uses iron oxides: the suitable iron oxide is fused together with the required chemical and structural promoters. The fused ingots are milled to a specified particle size range (for optimum fluidization properties). The catalyst is pre-reduced with H<sub>2</sub> at about 400°C and then loaded in the F-T reactors. Because of the simplicity of the preparation and the low cost of the raw materials, the cost of Synthol catalyst is a minor part of the overall process<sup>31</sup>.

The catalyst used in the fixed bed process is more expensive as it is prepared by wet chemical means. Iron oxide is precipitated by adding an alkaline solution to an iron nitrate solution. The precipitate is washed, re-slurried, silica based support and promoters added and the gel is then extruded. The surface area and pore size distribution of this catalyst is largely determined by the conditions used in the initial iron oxide precipitation step, these effects, such as precipitation time, temperature, order of addition etc., have been quantified. Because of the high surface area and the presence of reduction promoters (i.e. Cu), the catalyst is pre-reduced under mild condition and then coated with wax to prevent re-oxidation<sup>30, 31</sup>.

The advantages of iron are the following:

1. it is the cheapest metal to use,
2. it has a higher selectivity to olefins,
3. it is an active water-gas shift catalyst.

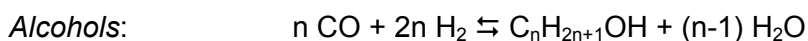
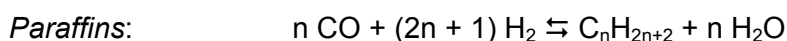
The latter is important since feed gases with H<sub>2</sub>/CO ratio below 2 can be utilized directly. A disadvantage of iron is that it deactivates faster than cobalt due to oxidation and coke deposition.

Studies performed at Sasol on the commercial spray dried precipitated iron catalyst and Co/Al<sub>2</sub>O<sub>3</sub> slurry phase FTS catalyst, resulted in the following conclusions:

1. the cobalt does not show any significant water-gas-shift activity and no water inhibition of the F-T reaction rate,
2. the cobalt catalyst is the preferred option if high per pass conversions are required,
3. desired stabilized intrinsic activity levels can be achieved with cobalt catalyst, implying that extended slurry phase synthesis runs can be realized,
4. cobalt derived hydrocarbon product selectivities show greater sensitivity towards process conditions (i.e. reactor pressure) than that of iron. Iron catalyst,

on the other hand, shows marked sensitivity towards chemical promotion. Indeed, the geometric tailoring of pre-shaped support materials can be an optimization tool for effecting increased wax selectivities with cobalt based catalyst, an approach also suggested by others (Exxon, Shell).

The conversion of synthesis gas to hydrocarbons (Fischer-Tropsch synthesis) has been widely studied and extensively described. A number of synthesis reactions can occur and the whole are quite exothermic,  $\Delta H = -170 \text{ kJ (C atom}^{-1}\text{)}$ :



Some other reactions, such as the water-gas shift or Boudouard reaction also occur:



The free energy changes ( $\Delta G^\circ$ ) in the above reactions are such that the hydrocarbon synthesis is normally favored below about  $400^\circ\text{C}$ . Over the temperature range of  $200\text{--}400^\circ\text{C}$ , the formation of methane is favored. However, since the thermodynamic equilibrium is reached slowly in FT synthesis, it is possible to take advantage of kinetic factors by using suitable catalysts, so that heavier hydrocarbons or alcohols are produced in suitable quantity<sup>28</sup>.

The production of hydrocarbons using traditional FT catalysts, such as Fe or Co, is governed by chain growth or polymerization kinetics. The so-called “surface carbide” mechanism is a plausible one for the interaction of CO and H<sub>2</sub> with the catalytic surface and the subsequent synthesis of hydrocarbons. Ample evidence shows that this is the prevalent mode of activation of CO at elevated temperatures on the Group VIII metal catalysts Fe, Co, Ni and Ru<sup>23, 28</sup>. The model can be used as a starting point for understanding the formation of various molecular species during FT synthesis and also for examining hydrocarbon chain growth<sup>28</sup>.

The process is only provided to indicate how chain growth can occur. Several models of chain growth have been discussed in the literature: repeated carbon insertion as indicated above results in chain growth. As a certain stage of chain growth, the hydrocarbon species is desorbed. If an unsaturated surface species is

desorbed, one obtains an olefinic product. Desorption after hydrogenation results in paraffin species. In some instances, CO insertion into the metal-alkyl bond and subsequent desorption results in an oxygenated species, such as an alcohol. The nature of the product and the product distribution among the carbon numbers will depend upon the catalyst surface, composition (H<sub>2</sub>/CO ratio) and the rate of flow feed gas, reaction pressure and the temperature at which FT synthesis is performed. The above parameters will affect the rate of hydrogen and CO dissociation, hydrogenation, degree of polymerization and desorption of the product species<sup>28</sup>.

At low temperatures, the main primary products are linear 1-alkenes, alkanes, alcohols and aldehydes. The linearity of the product is important for many of their applications. It gives the waxes with high melting point and low viscosity.

The C<sub>9</sub> to C<sub>15</sub> olefins are ideal for the manufacture of biodegradable detergents. The C<sub>10</sub> to C<sub>18</sub> cut is an excellent diesel fuel (with the high cetane number of 75 and zero aromatics). On the other hand, the product linearity is a disadvantage for gasoline production, since a high octane number requires branched alkane and aromatics. Hence, the gasoline requires extensive isomerization and aromatization.

At higher synthesis temperatures secondary reactions occur, i.e branched hydrocarbons and aromatics are formed. In that way, the diesel cetane number decreases, while the gasoline octane number increases. Olefins in the hydrocarbons reach a maximum at C<sub>3</sub> or C<sub>4</sub> (up to 90 %), to then decrease continuously, the waxes being essentially paraffinic<sup>30</sup>.

### 1.5.1. FT synthesis catalysts

Most Group VIII metals have significant CO hydrogenation activity, being the product distribution the distinguishing feature. The specific activity of various Group VIII metals was determined: Ru > Fe > Ni > Co > Rh > Pd > Pt, while the average hydrocarbon molecular weight decreased in the order: Ru > Fe > Co > Rh > Ni > Ir > Pt > Pd.

The catalysts that were active for F-T synthesis were compared in order to identify common properties<sup>32</sup>. It was found that:

- they are active for hydrogenation reactions
- they are capable for metal carbonyl formation

- the F-T reaction conditions (T, P) are not far from those where thermodynamics would allow the metals to be converted into metal carbonyl.

From the latter observation, it was suggested that 'surface carbonyls' play an essential mechanistic role in the formation of hydrocarbons.

Iron and cobalt are the only metals used until now for industrial application. Nickel tends to form volatile nickel carbonyl at elevated pressure and is most selective for methane relative to Co, Fe and Ru catalysts. Ruthenium is the most active F-T catalyst, working at the lowest reaction temperature of about 150°C, and it is selective towards high molecular weight products. However, it is most active in the pure form, i. e. supports and/or promoters appear to have no beneficial effect. Even under conditions favorable for high wax yields, Ru tends to have high methane selectivity. Ruthenium has a high potential as catalyst for converting synthesis gas to a variety of hydrocarbons, but its high price and limited world resources exclude possible industrial application.

Other Group VIII metals, namely Rh, Re, Os, Pd, Pt and Ir, yield mostly oxygenated compounds partly because CO does not chemisorb dissociatively on these metals. Mo is not a Group VIII metal, but it exhibits moderate F-T activity and its nitride and carbide show excellent alkene synthesis rate. It is attractive because of its sulphur-resistant characteristics<sup>33, 30</sup>.

Iron catalysts are commonly used because of their low costs. They have a high selectivity to olefins and a high water-gas shift activity. The latter aspect is important since it means that CO<sub>2</sub> can also be hydrogenated to hydrocarbons and that feed gases with H<sub>2</sub>/CO ratios below 2 can be utilized directly. A disadvantage of Fe is that it deactivates faster due to oxidation and coke deposition. In fact, metallic iron is extremely active for the F-T reaction but it is not thermodynamically stable under F-T conditions and is rapidly converted to more stable, but less active, iron carbides. With time, the carbides are also slowly oxidized by water vapor to inert magnetite. Another factor that contributes to deactivation is poisoning by S-containing compounds such as H<sub>2</sub>S. Poisoning by chemisorbed S is permanent. Chlorine, although to a lesser extent, also deactivates iron catalysts.

Cobalt catalysts do not oxidize or carburize under normal F-T conditions and because of this should deactivate less rapidly than iron catalysts. Co catalysts can give high yields of liquid hydrocarbons and waxes but under similar conditions the methane yields are usually higher and the olefin yields are lower

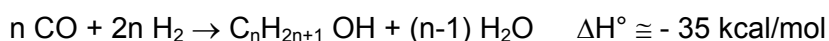
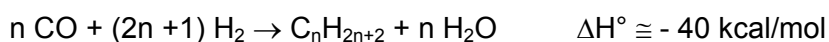
than for iron catalysts, i.e. they are more hydrogenating. The yields of oxygenated compounds are lower for cobalt catalysts and this can be an advantage if they are not desired.

The relatively high cost of Co makes of fundamental importance its distribution on suitable supports (i.e. Al<sub>2</sub>O<sub>3</sub>, TiO<sub>2</sub>, SiO<sub>2</sub>). The activity of supported Co catalysts increases linearly with loading in the range 5 to 30 mass % Co and so a compromise between cost and activity has to be made. Under F-T conditions, Co is a poor water gas shift catalyst and so the feed gas needs to be adjusted to about 2, as required by the stoichiometry of the F-T reaction. Poisoning by S-containing compounds causes the permanent deactivation of cobalt-based catalysts. Cobalt is the most widely Group VIII used in natural gas-to-liquids research project.

F-T catalysts are often prepared by precipitation, impregnation, ion exchange, and synthesis from organometallic compounds and vapor phase deposition in which the metal precursor is loaded onto the support surface. This is then followed by drying, calcination and catalyst activation (via reduction of the metal precursor to generate the metallic phase). The interplay of catalyst composition and preparation conditions determines the activity and selectivity behavior for a given set of process parameters. The selection of the 'best' catalyst is the most crucial step in F-T technology.

### 1.5.2. Thermodynamics and reaction mechanism

The Fischer-Tropsch synthesis is a highly exothermic reaction:



Thermodynamically, the formation of methane and other hydrocarbons is energetically favorable, that means negative Gibbs energy. For example,  $\Delta G^\circ$  values at 227°C for the formation of ethane and propane are -29.2 and -37.3 kcal/mol respectively, while at 200°C  $\Delta H^\circ$  values for the formation of methane, ethane and propane are about -50, -42, and -29 kcal/mol, so confirming the exothermic nature of the process.

In Fig. 1. 5 standard Gibbs energy variation for the production of hydrocarbons and alcohols is reported as a function of temperature.

From the diagram reported in figure 4, it can be deduced that methane formation is highly favored over that of the alcohols, olefins and hydrocarbons of heavier molecular weight. Moreover, hydrocarbons are favored over olefins and alcohols. Finally, as far as olefins are concerned, ethylene is less favored at temperature below 430°C.

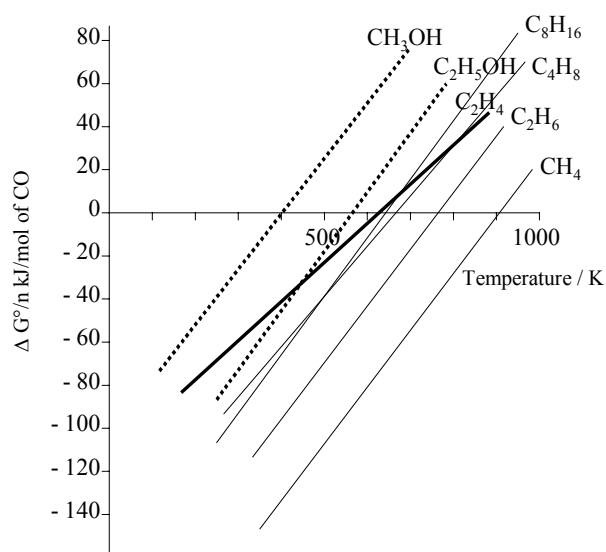
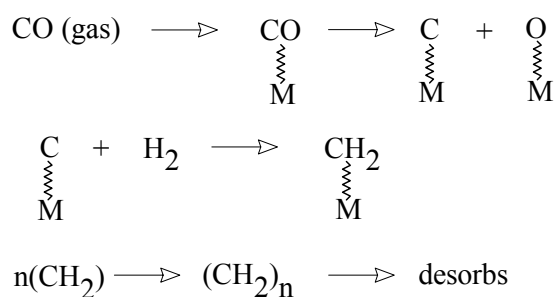


Fig. 1. 5 - Standard Gibbs energy of some FTS products.



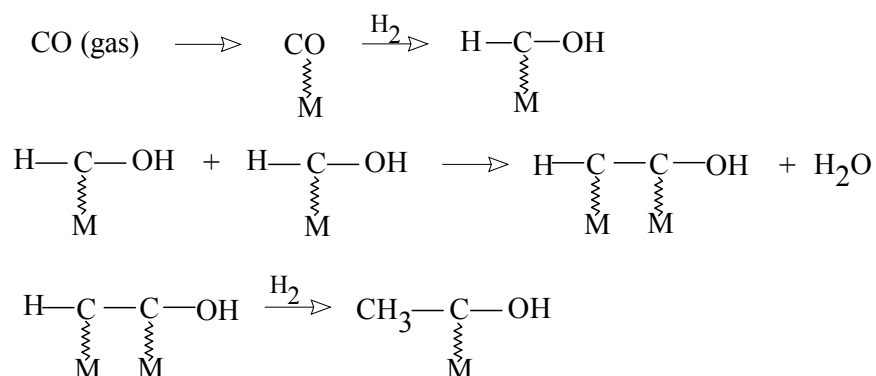
**Scheme 1 - CO dissociative chemisorption**

Fischer-Tropsch synthesis has long been recognized as a non-trivial polymerization reaction with the following steps as the key sequence:

1. reactants adsorption
2. chain initiation
3. chain growth
4. chain termination
5. products desorption
6. re-adsorption and further reaction

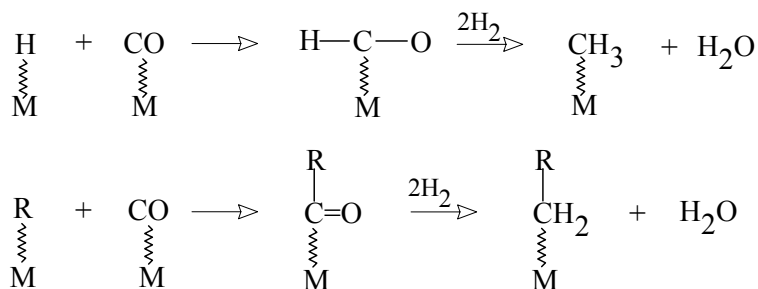
Since its discovery, many efforts have been made to identify the surface species that lead to chain initiation and chain growth. Fischer and Tropsch proposed the earliest ideas in 1926. They hypothesized CO reaction with the metal of the catalyst to form bulk carbide (CO dissociative chemisorption), which subsequently undergoes hydrogenation to form methylene groups (see Scheme 1). These species were assumed to polymerize to form hydrocarbon chains that then desorb from the surface as saturated and unsaturated hydrocarbons (see Scheme 4).

Molecularly adsorbed CO (associative adsorption) was hydrogenated to form a hydroxycarbene or enol,  $M = CH(OH)$ , which then underwent further hydrogenation to produce a methylene group. The growth of hydrocarbons occurs by polymerization of these latter species. The formation of enol intermediates was suggested that chain growth takes place by the condensation of enol groups with the concurrent elimination of water (see Scheme 2).



**Scheme 2 - CO associative adsorption**

Another mechanism for chain growth was proposed: molecular CO was postulated to insert into the metal-carbon bond of an adsorbed alkyl species. Hydrogenation of the resulting acyl group was assumed to produce water and a new alkyl group containing an additional methylene unit. The chain is initiated by methyl groups formed by stepwise hydrogenation of molecularly adsorbed CO (see Scheme 3).



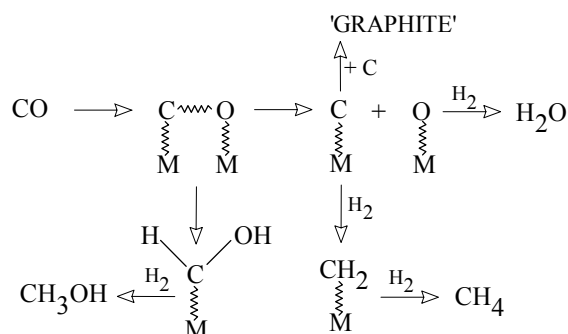
**Scheme 3 - Undissociated CO insertion**

In Scheme 4 the three different proposals are resumed and a global view of chain growth and chain termination to various types of products is given.

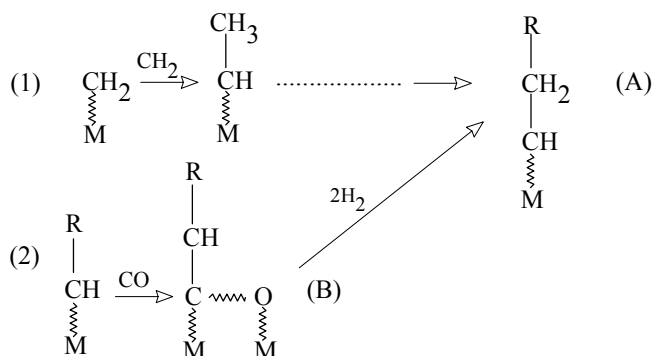
The mechanism proposed by Fischer ('carbide' theory) did not explain the production of relatively large amounts of oxygenated products, i.e. alcohols. Mechanisms described by the Schemes 2 and 3, explained the formation of oxygenated products, nevertheless recent experimental evidence indicated the mechanism of Scheme 1 is possible.

In drawing Scheme 4, it was suggested that non-oxygenated, rather than oxygenated, intermediates play a dominant role in the synthesis of hydrocarbons from CO and H<sub>2</sub>. Moreover, results obtained from the fields of surface science, organometallic chemistry, and catalysis strongly support that hydrocarbon synthesis is initiated by the dissociation of CO<sup>30</sup>.

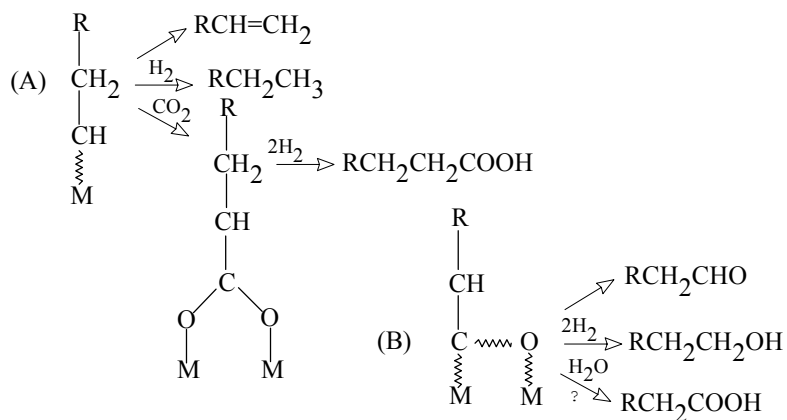
INITIATION AND C<sub>1</sub> COMPOUNDS



CHAIN GROWTH



CHAIN TERMINATIONS



**Scheme 4 – Summary of different proposals and a global view of chain growth and chain termination to various types of products**

### 1.5.3. FT synthesis plants

Sasol is the largest producer of syngas and chemicals made by coal gasification. Besides coal plants, since 1993 Sasol has also operated natural gas-based plants at Moss gas, South Africa. The company is by far the most experienced player in the syngas-based chemical business, as far as reactors design, catalytic formulations, process technology are concerned.

Since 1955, Sasol has operated with the Fischer-Tropsch synthesis at either low temperatures (LTFT) to produce a syncrude with a large fraction of heavy, waxy hydrocarbons, or at high temperatures (HTFT) to produce a light syncrude and olefins. Until the nineties, two types of F-T reactors have been used, the tubular fixed bed (TFB) reactor for LTFT and the circulating fluidized bed (CFB) reactor for HTFT.

The TFB, also known as Arge reactor, has been in use at its Sasolburg plants in South Africa for the production of wax since 1955. This type of reactor consists of a shell containing 2050 tubes, 12 m long, 5 cm in internal diameter and operates at a shell side temperature range of 220-250°C and a reactor pressure of 25 bar for the earlier reactors and 45 bar for a reactor commissioned in 1987. It produces heavy waxy hydrocarbons that are subsequently hydrocracked and/or isomerized for diesel production (Fig. 1. 6-A).

The TFB reactor makes use of extruded on silica precipitated iron-based catalyst, promoted with a small amount of potassium and packed into the tubes.

Syngas is passed downward through the catalyst bed and is converted to hydrocarbons. The exothermic heat of the F-T reaction is removed through the tube wall to produce steam on the shell side of the reactor. That gives rise to axial and radial temperature profiles. For maximum reaction rates, a maximum average temperature is required. This is limited however by the maximum allowable temperature peak, which cannot be exceeded in order to prevent catalyst deactivation and carbon formation on the catalyst. Carbon formation causes break up of the catalyst with a consequent loss in conversion efficiency and necessity to catalyst replacement.

Product selectivities are temperature dependent and flexibility with respect to temperature control would be advantageous. The choice of temperature level is however limited by the need to not exceed the maximum peak temperature.

Pressures drop across TFB reactor are high, from 3 to 7 bar; that gives rise to considerable compression cost.

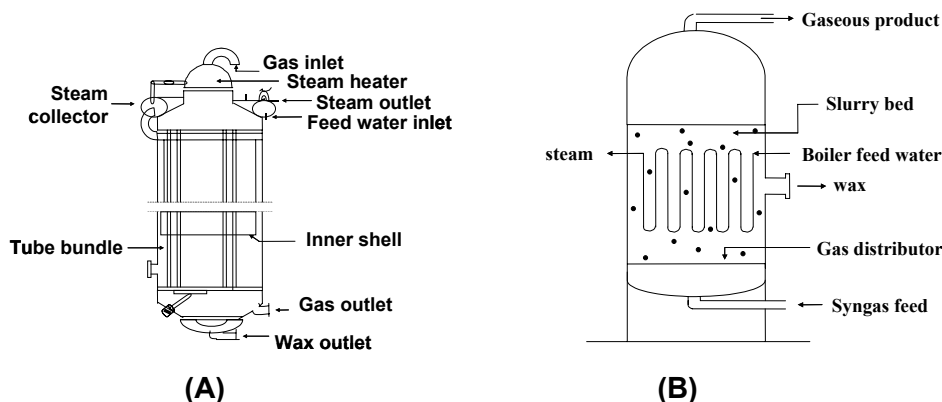


**Fig. 1. 6 - (A) Sasol fixed bed reactor. Only a few of the 5-cm ID reactor tubes are shown. (B) Slurry bed reactor**

An advantage of the TFB reactor is that there are no problems in separating the wax product from the catalyst, on the other hand, the reactor is complex and has a high capital cost. At the prevailing reactor conditions, scale up is mechanically difficult, the tube sheets become very heavy. In addition to this, special removable grids are required for the removal and replacement of the catalyst, making the reactor design more complex and costly. The catalyst replacement itself is cumbersome and maintenance and labor intensive, and it causes down time and disturbances in plant operations.

For all the reasons mentioned above TFB reactors are now being replaced by another type of reactor concept: multiphase slurry bed reactor. The process is still based on the low temperature Fischer-Tropsch synthesis (LTFT), namely Sasol's Slurry-Phase Distillate (SSPD) process, and it has been developed to convert natural gas to liquid fuels using the slurry-phase F-T reactor (Fig. 1. 6-B). The SSPD reactor, commercially operated by Sasol since 1993, is much simpler than a TFB reactor. It consists of a vessel fitted with cooling coils in which steam is generated. The vessel contains slurry of the process-derived wax with the catalyst particles. Syngas is distributed at the bottom and it rises through the slurry, the reagent gases diffuse from the gas bubbles through the liquid phase to the suspended catalyst where they react to produce hydrocarbons and water. The heavier hydrocarbons form part of the slurry phase, whereas the lighter gaseous products and water diffuse through the liquid to the gas bubbles.

Gaseous products together with unreacted syngas pass through the slurry bed to the freeboard above the bed and then to the gas outlet.

The main difficulty with the commercial application of the SSPD is the separation of the wax product from the catalyst. This is especially true for the relatively friable precipitated iron catalysts. Sasol has developed a proprietary solid-separation technique. The catalyst particles are removed from the product liquid hydrocarbons and returned into the process after reactivation. The heavy hydrocarbons from SSPD reactor are hydrogenated and converted to specialty waxes. These waxy hydrocarbons can easily be hydrocracked to excellent diesel with a cetane number of more than 70. The products have a negligible aromatic and a zero sulphur content. The waxy hydrocarbons, upon hydroisomerization, give lube oils. In addition, the olefins obtained in the reactor are mainly straight-chain  $\alpha$ -olefin. These are commercially valuable products and can be used in the manufacture of oxo-alcohols, lubricants, and detergents or easily hydrogenated to straight-chain paraffin. According to Sasol, the SSPD reactor is much simpler in construction than the TFB reactor. The suspended cooling coils and the gas distributor are cheaper than the tube and the tube-sheet arrangement. Scale-up of a TFB reactor is difficult and is achieved by increasing the shell diameter and the number of tubes. In the case of SSPD reactor, capacity can be increased by increasing both diameter and height of the reactor, resulting in a significant advantage in terms of economy of scale. In fact, the largest Arge TBF reactor has been designed for about 1.500 BPD, while the present SSPD commercial reactor has been designed for a capacity of about 2.500 BPD. A single SSPD reactor with a capacity of at least 10.000 bbl is planned to be built.

What is more, the SSPD reactor gives much greater flexibility towards temperature control, because the slurry phase is well mixed favoring isothermal operation. Temperatures, on average, can be much higher than in a TFB reactor without the danger of catalyst deactivation, carbon formation and break-up of catalyst. A much better control of product selectivities becomes possible at higher average conversions. This also makes the reactor ideal for higher activity catalysts that, in the case of TFB reactor, add to problems of temperature gradients and peaks.

The pressure drop across the bed is practically that of the static hydraulic head and is much lower than the pressure drop for the TFB reactor. That implies considerable savings in recompression costs where recycle is required.

On-line catalyst removal and addition can be done without difficulty; losses to down time and labor intensive turn-around are eliminated. The reactor uses iron based catalyst, but in recent years, the advantages of cobalt based catalysts for use in slurry phase reactors has been recognized, and subsequent work has led to the development of a superior cobalt based catalyst<sup>34</sup>.

CFB reactors (Fig. 1. 7-A), whose commercial name is Synthol reactors, differ from TBR and SSPDR for operating at a higher temperature range (330-350°C), HTFT. Sasol uses them for the production of gasoline and olefins. The Synthol reactor system is complex and consists of a fluidized bed of catalyst (fused iron) circulating through the reactor via an external catalyst-recovery loop.

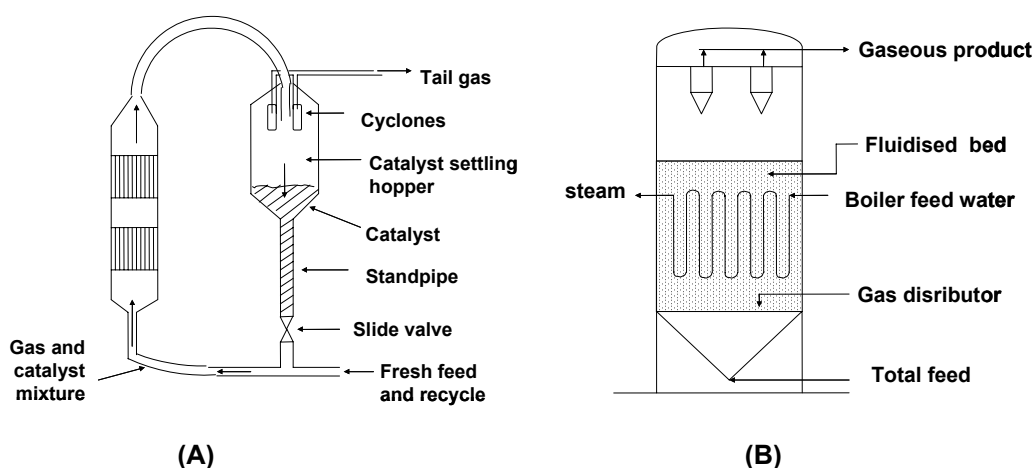


Fig. 1. 7 - (A) The CFB reactor. (B) The SAS reactor.

The iron catalyst powder flows down the standpipe as a dense phase aerated powder with a void age similar to that in the loosely packed settled state. Pressure builds up on going down the standpipe to give the highest pressure in the system just above the slide valve. The catalyst flows through the slide valve, is picked up by the high velocity syngas stream, and is carried round the lower transfer bend into the vertical reactor section. The heat of reaction is removed from the reactor section by steam generating cooling coils producing 40 bar steam. Pressure decreases continually on this side of the loop. On leaving the reactor section, the catalyst passes through the upper transfer bend or gooseneck into the hopper and flows down the standpipe. Catalyst entrained with the gas is separated by means of cyclones before the gas exits the hopper.

The large tonnage of circulating catalyst results in high-pressure drop across the reactor system. Moreover, because of increased erosion, system downtime is high, as are maintenance costs.

The SAS reactor is a vessel containing a fluidized bed consisting of fused and reduced iron catalyst (similar to that used for the Synthol CFB reactor) (Fig. 1. 7-B)

Syngas is bubbled by means of a gas distributor through the bed where it is catalytically converted to hydrocarbons. The reactor is designed to operate at pressures ranging from 20 to 40 bars. It typically operates at a temperature of around 340°C. Cooling coils are in the bed, and cyclones retain all the catalyst particles within the reactor, hence eliminating the requirement of an external catalyst recovery system. The catalyst/gas ratio in the reaction zone for the SAS reactor is about twice that for the CFB reactor. That is because less than a half of the catalyst in the CFB reactor is in the reaction zone, although the same quantity of catalyst is overall contained. In the SAS reactor, the whole of the catalyst inventory is always in the reaction zone. That strongly affects the relative conversion performance of the two types of Synthol reactors.

The higher gas velocities needed to transport the catalyst through the CFB reactor results in a narrower diameter reactor section compared to the SAS reactor. The CFB reactor design is strictly constrained, while constraints are no longer relevant for the simple cylindrical configuration of the SAS reactor. A SAS reactor has a larger capacity than a CFB reactor, so that a plant can achieve the benefits of economy of scale. For an SAS reactor, the capacity can be increased to 20.000 BPD, while for a CFB reactor the capacity is of about 8000 BPD. The scale-up of a CFB reactor is complex and problematic unlike the SAS reactor scale-up where only the reactor diameter must be increased. Finally, the SAS reactor is characterized by a reduced pressure drop (half than that of a CFB reactor) and a decreased recycle ratio, leading to a much lower cost for the compression of the recycled tail gas.

## 1.6. Fuel cells

Sir William R. Grove, who used hydrogen and oxygen as fuels catalyzed on platinum electrodes, first discovered the principle of fuel cell in 1939.

A fuel cell is defined as an electrochemical device in which the chemical energy stored in a fuel is converted directly into electricity.

Fuel cells operate without combusting fuel and with few moving parts, and thus they are very attractive from both energy and environmental standpoints<sup>35</sup>. A fuel cell can be two or three times more efficient than an internal combustion engine in converting fuel to electricity.

A fuel cell consists of an electrolyte material, which is sandwiched between two thin electrodes (porous anode and cathode). Specifically a fuel cell consists of an anode – to which a fuel, commonly hydrogen, is supplied – and a cathode – to which an oxidant, commonly oxygen, is supplied. The oxygen needed by a fuel cell is generally supplied by feeding air. The two electrodes of a fuel cell are separated by an ion-conducting electrolyte.

All fuel cells have the same basic operating principle. An input fuel is catalytically reacted (electrons removed from the fuel elements) in the fuel cell to create an electric current. The input fuel passes over the anode (negatively charged electrode) where it catalytically splits into electrons and ions, and oxygen passes over the cathode (positively charged electrode). The electrons go through an external circuit to serve an electric load, while the ions move through the electrolyte toward the oppositely charged electrode. At the electrode, ions combine to create by-products, primarily water and CO<sub>2</sub>. Depending on the input fuel and electrolyte, different chemical reactions will occur.

The main product of fuel cell operation is the DC electricity produced from the flow of electrons from the anode to the cathode. The amount of current available to the external circuit depends on the chemical activity and amount of the substances supplied as fuel and the loss of power inside the fuel cell stack. The current producing process continues for as long as there is a supply of reactants because the electrode and electrolyte of a fuel cell are designed to remain unchanged by the chemical reactions.

Most individual fuel cells are small in size and produce between 0.5 and 0.9 V of DC electricity. Combination of several or many individual cells in a “stack” configuration is necessary for producing the higher voltages more commonly

found in low and medium voltage distribution systems. The stack is the main component of the power section in a fuel cell power plant. The by-products of fuel cell operation are heat, water in the form of steam or liquid water, and  $\text{CO}_2$  in the case of hydrocarbon fuel<sup>35</sup>.

Because a fuel cell transforms chemical energy directly into electrical energy, its theoretical efficiency is not limited by the Carnot inefficiency problem for heat-to-work conversion, unlike conventional power generation plants and the internal combustion engine<sup>36</sup>. Therefore, a fuel cell system can exhibit a higher fuel-to-electricity efficiency than almost all the other energy conversion systems.

The operating mode of fuel cells differs dramatically from that of larger fuel cell systems designed for utility power generation, which tend to operate at relatively constant power output with infrequent shutoff and restart. The small systems will operate over a wide load range, with only brief periods at full power, considerable time at 30-50 % of the rated power and relatively frequent shutoff and restart<sup>36</sup>.

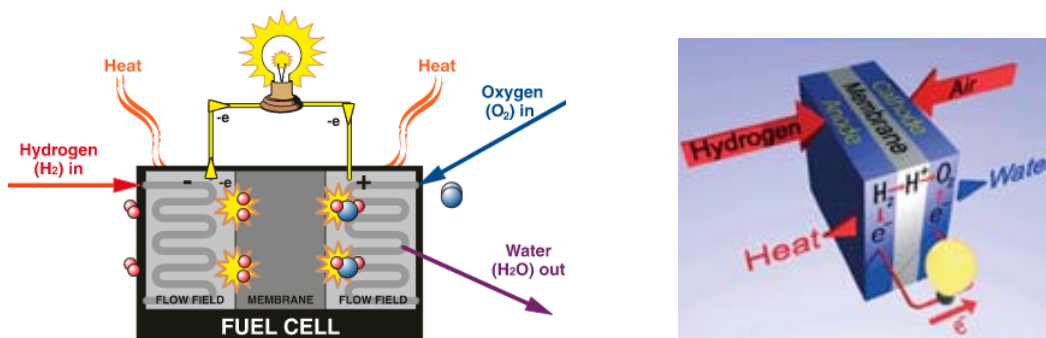


Fig. 1. 8 - Images of fuel cell system.

On the basis of the electrolyte employed, there are five types of fuel cells. They differ in the composition of the electrolyte and are in different stages of development. In all types, there are separate reactions at the anode and the cathode, and charged ions move through the electrolyte, while electrons move round an external circuit. Another common feature is that electrodes must be porous, because the gases must be in contact with the electrode and the electrolyte at the same time.

The five types of fuel cells are:

1. Proton-exchange membrane fuel cell (PEMFC) - PEMFC uses a solid polymer membrane as electrolyte. This membrane is an electronic insulator, but an excellent conductor of protons (hydrogen cations). The

ion-exchange membrane used is fluorinated sulfonic acid polymer. The acid molecules are fixed to the polymer and cannot leak out, but the protons on these acid groups are free to migrate through the membrane. The solid electrolyte exhibits excellent resistance to gas crossover. Typically, the anode and cathode catalysts consist of one or more precious metals, particularly platinum supported on carbon. Because of the limitation on the temperature imposed by the polymer and water balance, the operating temperature of PEMFC is less than 120°C, usually between 70 and 90°C. The PEMFC technology is primarily suited for residential/commercial (business) and transportation applications. The use of a solid polymer electrolyte eliminates the corrosion and safety concerns associated with liquid electrolyte fuel cells.

In addition to pure hydrogen, the PEMFC can also operate on reformed hydrocarbon fuels without removal of the by-product CO<sub>2</sub>. However, the anode catalyst is sensitive to CO, so the traces of carbon monoxide produced during the reforming process must be converted to carbon dioxide by selective oxidation.

Water management is critical: the fuel cell must operate under conditions where the by-product water does not evaporate faster than it is produced because the membrane must be hydrated<sup>35</sup>.

2. Phosphoric acid fuel cell (PAFC) – The PAFC uses liquid, concentrated phosphoric acid as the electrolyte. The phosphoric acid is usually contained in a Teflon bonded silicon carbide matrix. The small pore structure of this matrix preferentially keeps the acid in place through capillary action. Some acid may be entrained in the fuel or oxidant streams and addition of acid may be required after many hours of operation.

Platinum supported on porous carbon is used on both anode and cathode sides of the electrolyte. PAFC operates at 180-220°C, typically around 200°C, so PAFC plant also produces heat for domestic hot water and space heating<sup>35</sup>.

3. Alkaline fuel cell (AFC) – The AFC uses aqueous solution of potassium hydroxide (KOH) as electrolyte, which is retained in a solid matrix (usually asbestos), and a wide range of electro-catalysts can be used, including nickel, metal oxides, spinels and noble metals electrode.

The operating range of temperatures can be higher than PAFC: they can work up to 250°C by using concentrated KOH (85%), or at temperature lower than 120°C by using less concentrated KOH (35-50%).

The fuel supply is limited to hydrogen, CO is a poison and CO<sub>2</sub> reacts with KOH to form K<sub>2</sub>CO<sub>3</sub>, thus changing the electrolyte<sup>35</sup>.

4. Molten carbonate fuel cell (MCFC) – the MCFC uses a molten carbonates salt mixture as electrolyte. The composition of the electrolyte varies, but usually consist of lithium carbonate and potassium carbonate (Li<sub>2</sub>CO<sub>3</sub>-K<sub>2</sub>CO<sub>3</sub>). At the operating temperature of about 650°C, the salt mixture is liquid and a good ionic conductor. The electrolyte is suspended in a porous, insulating and chemically inert ceramic (LiAl<sub>2</sub>O) matrix. At the high operating temperature, noble metals are not required for electrodes, nickel or its alloy with chromium or aluminum can be used as anode, and nickel oxide as cathode. The cell performance is sensitive to operating temperature; a change in cell temperature from 650 to 600°C results in a drop in cell voltage of almost 15 %. The reduction in cell voltage is due to increase ionic and electrical resistance and a reduction in electrode kinetics. The disadvantages of MCFC are that the electrolytes is corrosive and mobile, and a source of CO<sub>2</sub> is requires at the cathode to form the carbonate ion<sup>35</sup>.
5. Solid oxide fuel cell (SOFC) – SOFC uses a ceramic, solid phase electrolyte, which reduces corrosion considerations and eliminates the electrolyte management problems associated with the liquid electrolyte fuel cells. To achieve adequate ionic conductivity in such a ceramic, however, the system must operate at high temperatures in the range of 650-1000°C, typically 800-1000°C in the current technology. The preferred electrolytes material, dense yttria (Y<sub>2</sub>O<sub>3</sub>) - stabilized zirconia (ZrO<sub>2</sub>), is an excellent conductor of negatively charged oxygen (oxide) ions at high temperatures. The SOFC is a solid-state device and shares certain properties and fabrication techniques with semiconductor devices. The anode is typically a porous nickel-zirconia (Ni-ZrO<sub>2</sub>) cermet (ceramic-metal composite) or cobalt zirconia (Co-ZrO<sub>2</sub>) cermet, while the cathode is typically magnesium-doped lanthanum manganate or strontium-doped lanthanum manganate (LaMnO<sub>3</sub>).

At the operating temperature, internal reforming of most hydrocarbon fuels should be possible, and the waste heat from such a device would be easily utilized by conventional thermal electricity generating plants to yield excellent fuel efficiency. On the other hand, the high operating temperature has its own drawbacks due to the demand and thermal stressing on the materials including the sealants and the longer start up time. Because the electrolyte is solid, the cell can be cast into various shapes such as tubular, planar, or monolithic. Operation up to 1000°C allows more flexibility in the choice of fuels and can produce better performance in combined-cycle applications<sup>35</sup>.

The general advantages of fuel cells are reflected by the following desirable characteristic:

- (i) High energy conversion efficiency;
- (ii) Extremely low emissions of pollutants;
- (iii) Extremely low noise or acoustical pollutions;
- (iv) Effective reduction of greenhouse gas (CO<sub>2</sub>) formation at the source compared to low-efficiency devices;
- (v) Process simplicity for conversion of chemical energy to electrical energy<sup>35</sup>.

Depending on the specific types of fuel cells, other advantages may include fuel flexibility and existing infrastructure of hydrocarbon fuel supplies, co-generation capability, modular design for mass production and relatively rapid load response. Therefore, fuel cells have great potential to penetrate into markets for both stationary power plants (for industrial, commercial and residential home applications) and mobile power plants for transportation by cars, buses, trucks, trains and ship, as well as man-portable micro-generators<sup>35</sup>.

Unlike power plants that use combustion technologies, fuel cells plants that generate electricity and usable heat can be built in a wide range of sizes – from 200 kW units suitable for powering commercial buildings, to 100MW plants that can add base-load capacity to utility power plants<sup>35</sup>.

The disadvantages or challenges to be overcome include the costs of fuel cells and that the hydrogen fuel is not readily available and thus on-site or on-board H<sub>2</sub> production via reforming is necessary. There are no readily and affordable ways for on-board or on-site desulphurization of hydrocarbon fuels and this presents a

challenge for using hydrocarbon fuels. The efficiency of fuel processing affects the over system efficiency<sup>35</sup>.

For a conventional combustion system, a wide range of gaseous, liquid and solid fuels may be used, while hydrogen, reformat (hydrogen rich gas from fuel reforming) and methanol are the primary fuels available for current fuel cells (Fig. 1. 9). The sulphur compounds, in hydrocarbon fuels, poison the catalysts in the fuel processor and fuel cells and must be removed. Syngas can be generated from reforming. Reformat can be used as the fuel for high-temperature fuel cells such as SOCF and MCFC, for which the solid or liquid or gaseous fuels need to be reformulated. Hydrogen is the real fuel for low-temperature fuel cells such as PEMFC and PAFC, which can be obtained by fuel reformulation on-site for stationary applications or on-board for automotive applications. When natural gas or other hydrocarbon fuel is used in a PAFC system, the reformat must be processed by water gas shift reaction. A PAFC can tolerate about 1-2 % of CO. When used in a PEMFC, the product gas from WGS must be further processed to reduce CO to < 10 ppm. Synthetic ultra-clean fuels can be made by Fischer-Tropsch synthesis or methanol synthesis using the synthesis gas produced from natural gas or from coal gasification, but the synthetic cleanness is obtained at the expense of extra cost for the extra conversion and processing steps<sup>35</sup>.

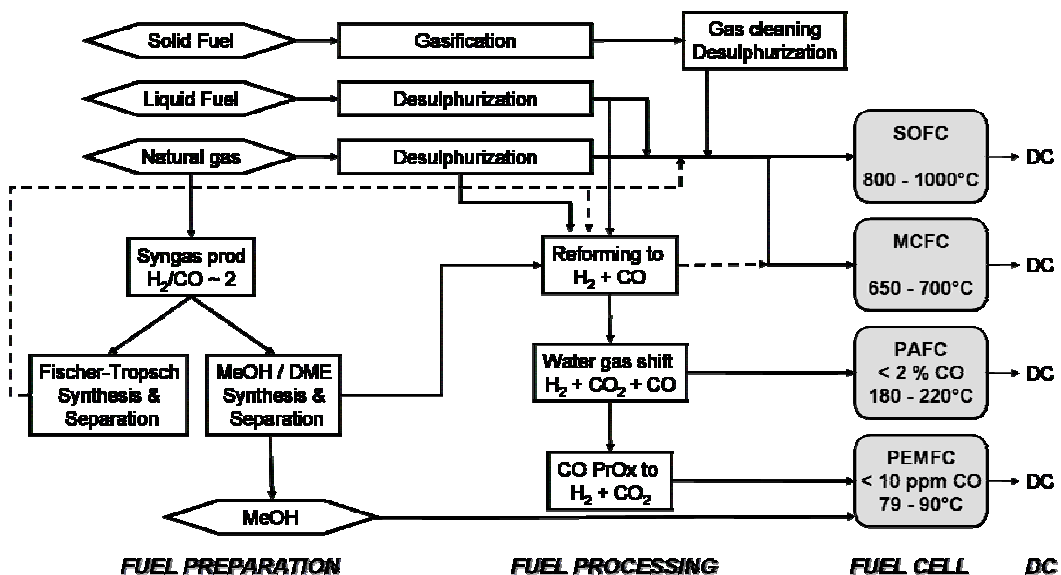


Fig. 1. 9 - The concept and the steps for fuel processing of gaseous, liquid and solid fuels for high and low temperature fuel cell applications.

## 2. Processes for H<sub>2</sub> and/or syngas production

Although hydrogen can be produced from a large variety of sources by using different methods, up to now the most extensively used process is the steam reforming of hydrocarbons. Biomass can be also used to produce H<sub>2</sub> by thermochemical or biological processes. Metabolic processing appears as an interesting alternative for the treatment of wastes while generating H<sub>2</sub> as product. Some other approaches for hydrogen production from water or other hydrogen-containing materials such as photodecomposition or thermochemical processes are also in development. Solar photodecomposition of water still has many technical hurdles remaining that suggest it is decades away from large scale, cost-effective implementation<sup>37</sup>.

The conversion of hydrocarbons to hydrogen and syngas will play an important role in the 21<sup>st</sup> century ranging from large gas to liquid plants and hydrogen plants for refineries to small units providing hydrogen for fuel cells. The choice of technology for manufacture of syngas depends on the scale of operation<sup>38</sup>.

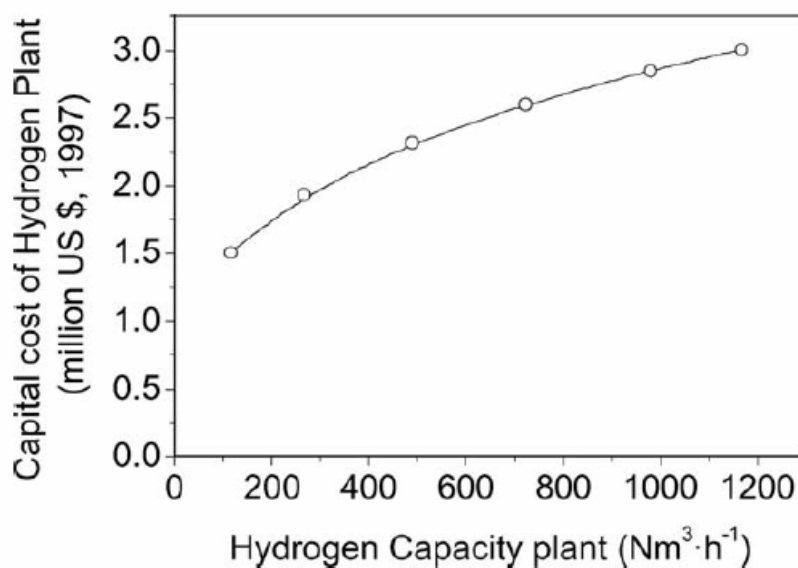


Fig. 1. 10 - Capital cost of a hydrogen plant as a function of capacity<sup>37</sup>.

Currently, steam reforming of hydrocarbons (SR) especially steam methane reforming (SMR) is the largest and generally the most economical way to make H<sub>2</sub>. Alternative non-catalytic, industrial chemical approaches include partial oxidation (POX) of heavy oil or coal. When electricity is available and relatively inexpensive, electrolysis of water offers an alternative commercial approach<sup>39,40</sup>.

Industrially, two main reactions are important in the conversion of natural gas to syngas<sup>41</sup>:

- (i) Steam reforming (SR),
- (ii) Non-catalytic partial oxidation (POX).

While most syngas is produced by steam reforming, two other processes may be more attractive, depending on factors such as H<sub>2</sub>:CO ratio, downstream use, product purity, the presence of CO<sub>2</sub>, N<sub>2</sub>, H<sub>2</sub>O and CH<sub>4</sub>, plant capacity, feedstock availability, purity and cost, including O<sub>2</sub>. These processes are:

- (i) Autothermal catalytic reforming (ATR),
- (ii) Catalytic partial oxidation (CPO).

## **2.1. Steam reforming process**

In areas where natural gas is available in large quantities, interest is centered on steam reforming of methane as hydrogen source<sup>7</sup>. The process is more economic than that based on coal. The hydrogen content of the hydrocarbon improved the yield of hydrogen per unit of carbon in the feedstock compared with coal, and there were also fewer unwanted by-products. The methane steam technology was pioneered in the first quarter of 20<sup>th</sup> century by BASF who established the essential configuration of the primary steam reformer, and the technology was used in 1931 by Standard Oil of New Jersey to produce hydrogen from off-gases at its Baton Rouge and Bayway refineries.

The methane reforming process was adopted mainly in the US where natural gas was easily available as feedstock, whereas reformers in Europe were initially reduced to operate on propane and LPG<sup>42</sup>.

The steam reforming reaction took place over catalyst in vertical tubes, which were supported in parallel rows in a radiant furnace. The endothermic heat of reaction was supplied by burning fuel in the furnace. The process was considerably improved by ICI, who developed the fundamental engineering data for the design of the furnace, improved the catalyst formulation and introduced the desulphurization step using zinc oxide. The process was used to produce hydrogen from off-gases for coal hydrogenation plants, which ICI built in 1936 and 1940. The ICI technology was subsequently used in the development of the North American ammonia industry when plants were constructed at El Dorado,

Baxter Springs, Ethers, Sterlington and Calgary. The plants used natural gas, which contained mainly methane with low concentrations of higher hydrocarbons, and nearly all used catalyst developed by ICI. Natural gas was not a readily available feedstock in the UK before the discovery in the North Sea, but as more refineries were built other hydrocarbons, such as naphthas, became increasingly available. It was apparent in the 1950s that if naphthas could be steam reformed economically they would provide a cheap source of hydrogen for the manufacture of ammonia. Work by ICI at this time led to the development of a catalyst, which would reform naphthas at economic steam ratios without carbon formation. The catalyst was stable, resistant to poisons and had an economical life.

In the 1959 ICI started up the first large scale pressure steam reformer using naphtha as a feedstock, and this became the precursor of over 400 plants subsequently licensed around the world in areas where natural gas was not available. From 1959 to date development of the catalyst continued in order to allow plants to be run at higher pressure and temperature, and with feedstocks containing quantities of unsaturated and aromatics compounds to be reformed. In more recent years the increasing availability of natural gas has resulted in its use as a major source of reformer feedstock, and this is likely to remain so for some time. Development of catalyst for natural gas reforming has concentrated on extending catalyst life, improving activity, inhibiting carbon-forming reactions, and by improving the physical properties.

### 2.1.1. Chemistry of steam reforming: Thermodynamics

The objective of the catalytic steam reforming process is to extract the maximum quantity of hydrogen/syngas held in water and in the hydrocarbon feedstock. Thereafter the subsequent manipulation of the gas stream depends on the purpose for which the gas is intended.

The reforming of natural gas utilizes two simple reversible reactions:



The reforming reaction (A) is strongly endothermic, so the reaction is favored by high temperature as well as by low pressure, while the shift reaction (B) is exothermic and is favored by low temperature but is largely unaffected by changes in pressure. To minimize the overall efficiency (and hence economics) of

the conversion of carbon to carbon dioxide and the production of hydrogen, reformers are operated at relative high temperature and pressure. This is followed by the shift process that, by using two different catalysts, permits the shift reaction to be brought to equilibrium at as low temperature as possible. It can be seen that with methane the stoichiometric requirement for steam per carbon atom is 1.0. However, it has been demonstrated that this is not reliable because all catalysts so far developed tend to promote carbon formation under steam reforming conditions. These reactions can be suppressed by using an excess of steam, with the results that the minimum ratio is in the region of 1.7. However, the reforming reaction itself is also promoted by an excess of steam and hence some advantage is derived from this. In practice ratio of 3.0 - 3.5 are commonly used, but in some cases, there can be economic attractions in using lower steams ratios and there is a trend in this direction.

Knowledge of the thermodynamic data associated with the reforming reaction allows graphs to be constructed from which equilibrium concentrations of reactant gases leaving a reformer can be determined for specified feed gas and reforming conditions (Fig. 1. 11).

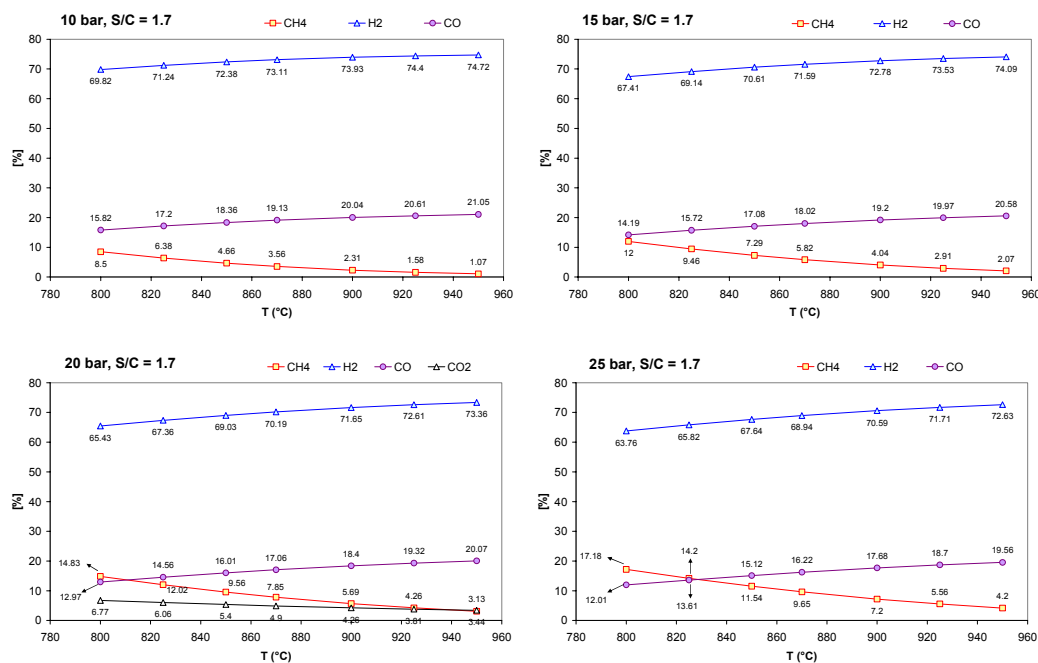


Fig. 1. 11 - Equilibrium composition vs temperature at different pressure.

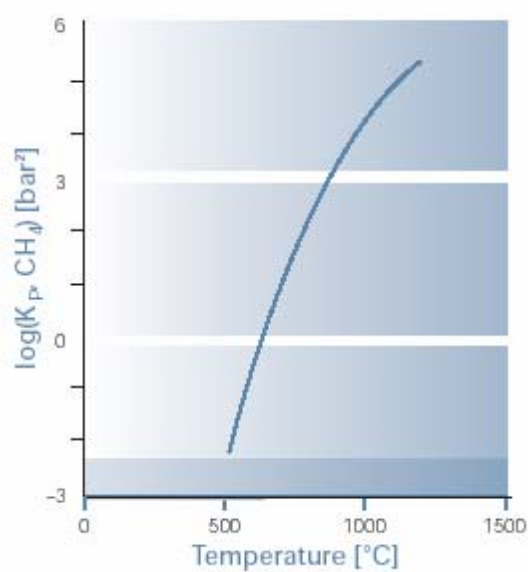


Fig. 1. 12 - Steam reforming reaction: equilibrium constant.

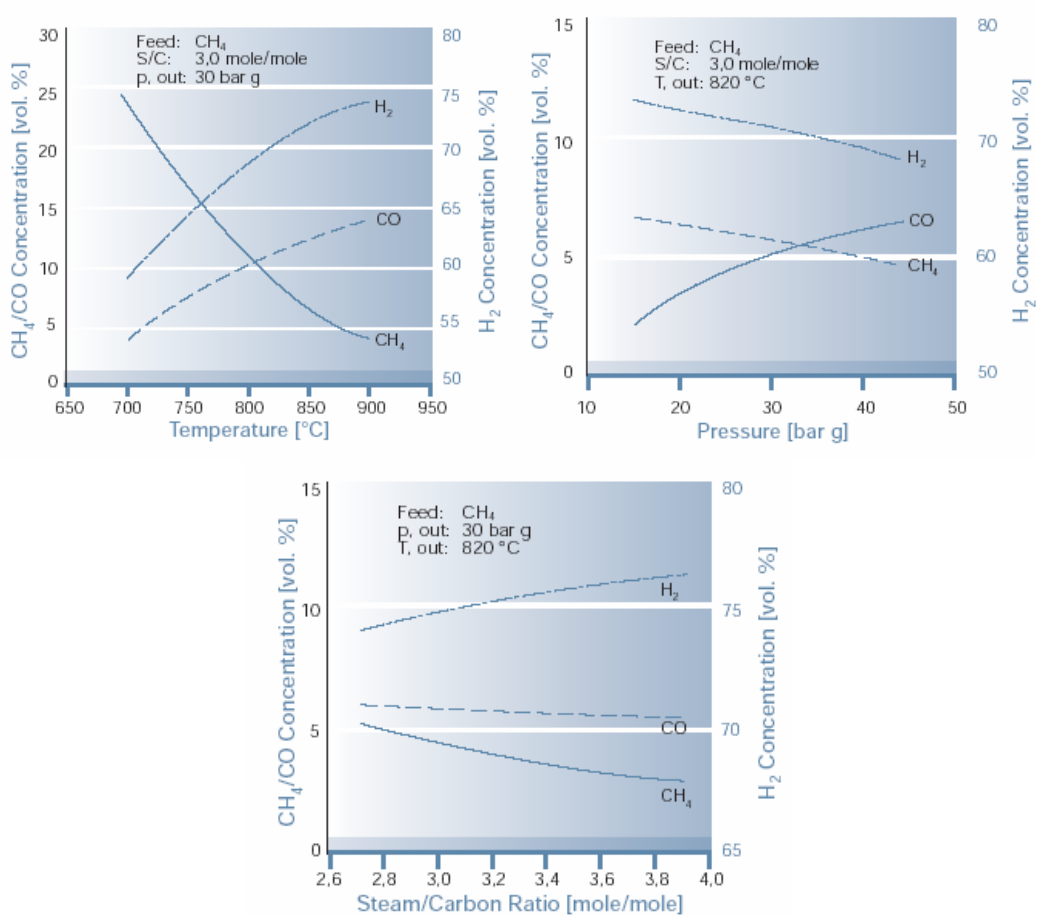


Fig. 1. 13 - Variation of the reformed gas depending on: (a) outlet temperature; (b) outlet pressure; and (c) inlet S/C ratio.

The reforming of saturated naphthas of general formula  $C_nH_{2n+2}$  is based on the following reaction:

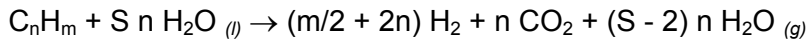


Reaction (C) is strongly endothermic, absorbing more heat than the following methanation reaction (D) and shift reaction (B) evolve, thus making the overall process normally an endothermic one.

Analogously to methane, the naphtha reforming reaction is favored by high temperature and low pressure, while the shift reaction is inhibited by high temperature but largely unaffected by pressure. The tendency towards carbon formation on catalysts when stoichiometric ratios of carbon and steam are used is greater with naphtha than with methane, and the minimum practical ratio is about 2.2. As with methane, the excess steam favors the reforming reaction, and in practice steam/carbon ratios of 3.5 - 4.5 are common. At low steam/carbon ratio the methanation reaction begins to dominate, and under certain conditions of pressure and temperature can cause the overall reaction to be exothermic. As with methane reforming, it is possible to calculate the equilibrium methane, carbon monoxide, carbon dioxide, hydrogen and water concentrations from inlet steam/carbon ratios and the operating conditions of a reformer<sup>7</sup>.

Lutz and co-workers<sup>43</sup> examined the thermodynamics of the steam reforming process. SR is achieved by reaction over a catalyst at high temperature. In addition to the energy required to provide the steam, the overall reaction is endothermic, so energy must be added to drive it. The process must burn either a second fuel, a fraction of the primary fuel, or the residual fuels that remain in the reformat stream. This last option is often done in practice to recover heating value that would otherwise be wasted. The analysis presented by Lutz considers two levels of sophistication in treating the chemistry. The first uses a global species balance that assumes that the reforming reaction goes to completion. An energy balance for the reaction allows to examine the definition of thermal efficiency. This analysis provides a theoretical upper limit on the thermal efficiency that is independent of temperature or other influences on the reaction kinetics. The second analysis replaces the global reaction step with a calculation of chemical equilibrium for the reforming reaction. The equilibrium computation brings in temperature dependence, without requiring detailed information regarding the specific reactions or catalyst performance.

To study the thermodynamics of steam reforming of hydrocarbon fuel at a basic level, a global reaction balance was examined:



where  $n$  and  $m$  define the composition of the fuel, and  $S$  is the steam-to-carbon ratio for the mixture. The term “global reaction” recognizes that the reaction is actually the net result of a series of elementary reactions, some of which include catalytic interaction with surfaces. This balance conserves elements with two assumptions: there is sufficient steam to react with the fuel ( $S \geq 2$ ), and the reaction goes to completion. Using this reaction, the formation enthalpies of the species can be added to determine the net enthalpy change:

$$\Delta H_R = n h_{CO_2}^f + (S - 2) n h_{H_2O(g)}^f - (h_{C_nH_m}^f + S n h_{H_2O(l)}^f)$$

where  $h_k^f$  is the formation enthalpy per mol of species  $k$  at standard temperature and pressure. Note that  $h_{H_2}^f = 0$ , by definition (was dropped from the equation).

Since water is liquid at room temperature it was considered that as the state for the reactant ( $H_2O_{(l)}$ ). Since the reactants must be raised to higher temperatures to make the reaction proceed, Lutz et al<sup>43</sup> took the water in the products to be vapor,  $H_2O_{(g)}$ .

Using methane as example, with  $S = 2$ , the net enthalpy change for the reaction is  $\Delta H_R = + 60$  kcal/mol of fuel, thus the process requires energy input. For heptane ( $C_7H_{16}$ ) the net enthalpy is  $\Delta H_R = + 339$  kcal/mol of fuel. It appears that reforming heptane requires more energy than methane, but to put the comparison in perspective, note that these enthalpies changes are based on 1 mol of fuel. A more level comparison would be the energy cost per mol of hydrogen produced. Methane takes 15 kcal/mol of  $H_2$  produced, compared to 15.4 kcal/mol of  $H_2$  for reforming heptane and cetane ( $C_{16}H_{34}$ ) requires 15.9 kcal/mol of  $H_2$ . Therefore, the energy necessary to produce  $H_2$  is roughly constant, at least for these saturated hydrocarbons. However, in the analyses Lutz et al<sup>43</sup> showed that the thermal efficiency of the process is not constant, but depends on the fuel.

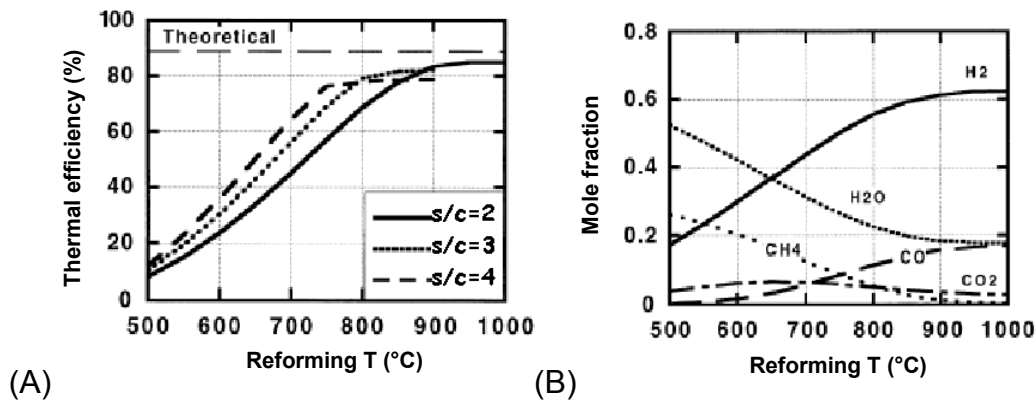


Fig. 1. 14 - (A) Efficiency of methane steam reforming computed in equilibrium model versus reformer temperature at pressure of 10 atm at different S/C ratios. (B) Equilibrium composition leaving the methane steam reformer for S/C = 2 and pressure 10 atm<sup>43</sup>.

The equilibrium model solutions show the effects of two parameters: the steam/carbon (S/C) ratio and the temperature (Fig. 1. 14 - A). Focusing on the solid curve (Fig. 1. 14 - A), for steam to carbon ratio of 2, the effect of temperature is to increase the efficiency of the equilibrium reformer. This is simply due to the fact that at lower temperatures the equilibrium composition leaving the reformer (Fig. 1. 14 - B) contains more unreacted methane and water. As the temperature increases, the equilibrium composition approaches the product stream expected from the global balance, except that there is still an excess of steam, and the CO concentration is 20 % of the mixture.

The equilibrium solutions suggest that the reformer must operate at higher temperatures. There is, however, a limit to which higher temperature improves performance. The equilibrium does not shift much farther towards reaction completion as the temperature goes above 900°C. A secondary effect is that the reformat stream contains insufficient heating value, so supplemental fuel must be added prior to the burner. The effect of S/C ratio is complicated by the fact that its influence depends on the temperature. The three curves (Fig. 1. 14 - A) at steam to carbon ratios of 2, 3 and 4 show that at low temperature, where the reaction is far from completion, the efficiency increase with excess of steam. At high temperature, where maximum H<sub>2</sub> is obtained, the equilibrium model behaves like global analysis. In this limit, the excess of water does reduce the efficiency. The observation that the thermal efficiency intersect at some temperature means

that there is a point where the chemical benefit of extra steam is offset by the energy required to generate it.

Fig. 1. 15 shows that a higher exhaust temperature reduces the thermal efficiency.

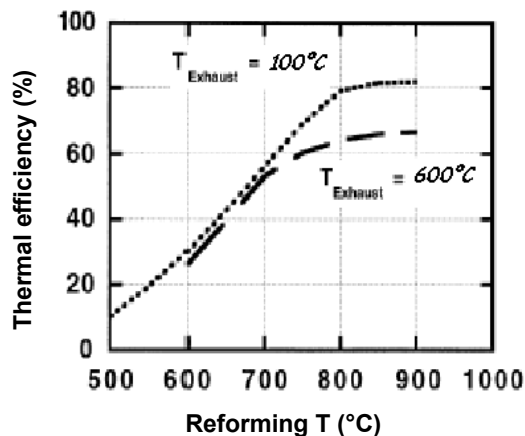


Fig. 1. 15 - Thermal efficiency versus equilibrium reformer temperature for steam reforming of methane at S/C = 3 and two exhaust temperatures<sup>43</sup>.

From thermal efficiency analysis, Lutz and co-workers concluded that definitions of thermal efficiency can be misleading. The definition should be accompanied by identification of the system boundary and the heat flows across it. The definition should include external heat addition. Comparisons of the equilibrium model for steam reforming to experimental data showed that the chemical equilibrium is appropriate for understanding the effect of temperature. Experimental thermal efficiencies for steam reforming were significantly lower than the thermodynamic limit predicted by the equilibrium model. Species measurements showed the deficiency was partly due to non-equilibrium composition, but other heat transfer losses are a dominant effect, especially for compact steam reformers. The effect of extra steam suggested by the equilibrium analysis is to increase the H<sub>2</sub> conversion and thermal efficiency, at least until a high temperature limit is reached where the H<sub>2</sub> conversion is maximized. Only in this limit is the global analysis valid. The global and equilibrium analyses both show a decrease in thermal efficiency for reforming larger hydrocarbons compared to methane. Expect the efficiency of reforming diesel fuel to be at least 15 % lower than that of natural gas, from thermodynamic alone.

### 2.1.2. Kinetics and reaction mechanism

The results of a number of studies on the kinetics of the methane steam reforming have been published. There is general agreement that the reaction is first order in methane, but there is less agreement with other kinetic parameters. In part, this is due to the use of different catalysts and experimental conditions, but often it has resulted from a lack of consideration of diffusion and heat transfer limitations. Thus, reported activation energies are spread in a wide range of values due to different degrees of diffusion limitation, and these can also cause misleading total pressure effect. Indeed, with the relatively large catalyst particle sizes used in industrial steam reformers, these effects results in very low effectiveness of the catalyst. Effectiveness factors ( $\eta$ ) may, depending on conditions, only be as high as 0.3 at the inlet region, and perhaps as low as 0.01 at the exit. Because of this, apparent activity increases as the particle size is made smaller, but the increased pressure drop, which arises across the reformer, restricts the size of the catalyst that can be used in practice<sup>7</sup>.

There has been some debate about the first formed products of the steam reforming reactions, and it appears that the relative concentrations of carbon monoxide and carbon dioxide leaving the catalyst surface depend on the efficiency of the catalyst in the water gas shift reaction. With rhodium-based catalysts the CO/CO<sub>2</sub> ratio of the initially formed carbon oxides is relatively high (in keeping with poor shift activity), whereas with nickel catalysts the amount of carbon monoxide is lower<sup>7</sup>.

A wide variety of rate expressions for the steam reforming of methane have been proposed. These models range in complexity from simple first order dependency on methane, involving two parameters, to complex Langmuir–Hinshelwood models with over ten parameters<sup>44</sup>. It is generally agreed that the rate of methane reforming has a first order dependency on methane. Furthermore, it is also agreed that the rate-determining step in the reforming process is the formation of adsorbed carbon species:  $\text{CH}_4 + * \text{--- Metalsite} \rightarrow \text{C}_{\text{Ads}} \text{---} * + 2 \text{H}_2$

This mechanism leads to the formulation of rate equations of the following form:

$$r_{\text{CH}_4} = -k p_{\text{CH}_4} p_{\text{H}_2}^\alpha$$

In this equation, the value of  $\alpha$  is found to depend on temperature, having a value close to  $-1$  at low temperatures ( $< 700^\circ\text{C}$ ) and approaching  $0$  at high temperatures ( $> 700^\circ\text{C}$ ).

Kinetic rate expressions for the steam reforming of methane found in the literature use the steady state approximation and take the form:

$$r_{CH_4} = -k p_{CH_4} \frac{f(p_{H_2O}, p_{H_2})}{(1 + f(p_{CH_4}, p_{H_2O}, p_{H_2}, p_{CO}, p_{CO_2}))} \times \left( 1 - \frac{p_{CO} p_{H_2}^3}{p_{CH_4} p_{H_2O} K_1} \right)$$

Wei and Iglesia<sup>45, 46</sup> measured CH<sub>4</sub> reaction rates on 7 % Ni/MgO catalyst in the absence of detectable deactivation and of transport or thermodynamic corruption of rate measurement. CH<sub>4</sub> reaction rates remained constant for 100 h and transport artifacts were ruled out by dilution of the catalyst pellet with inert Al<sub>2</sub>O<sub>3</sub> and dilution of the catalyst bed with ground quartz. Reforming rates can be rigorously obtained from measured net rates using an approach to equilibrium parameter ( $\eta$ ) evaluated from CH<sub>4</sub>-H<sub>2</sub>O thermodynamic reaction data and measured reactant and product partial pressures:

$$\eta = \frac{[P_{CO}] [P_{H_2}]^3}{[P_{CH_4}] [P_{H_2O}]} \frac{1}{K_{eq}}$$

In this expression, [P<sub>j</sub>] is the average partial pressure of species j (in atm); it is also used to correct for reactant depletion. K<sub>eq</sub> is equilibrium constant for CH<sub>4</sub>-H<sub>2</sub>O reaction. Forward turnover rates (r<sub>f</sub>) are given by:

$$r_f = \frac{r_n}{(1 - \eta)}$$

where r<sub>n</sub> is the net CH<sub>4</sub> conversion turnover rate. CH<sub>4</sub> reaction rate increased linearly with increasing CH<sub>4</sub> pressure, but it is not influenced by H<sub>2</sub>O pressure. H<sub>2</sub> and CO products added to CH<sub>4</sub>-H<sub>2</sub>O reactant mixture influenced net CH<sub>4</sub> conversion rate at 600°C, but forward rates were unaffected, indicating that H<sub>2</sub> and CO affected only the extent to which reforming reactions approach equilibrium, but not the kinetics of CH<sub>4</sub> reforming reaction. Thus, previously reported inhibition of CH<sub>4</sub> reaction rates by products may reflect unrecognized contributions from reverse reaction rates. CO adsorption enthalpies are 135 kJ/mol at low coverages (< 0.02) and much lower at higher coverages on Ni (1 0 0). These adsorption enthalpies indicate that CO coverages should be well below 0.01 monolayer at 600°C and even at equilibrium CH<sub>4</sub> conversions. The lower adsorption enthalpies typically reported for H<sub>2</sub> (92 kJ/mol) would make hydrogen coverages even lower than for CO. Thus, competitive adsorption is unlike to

influence the availability of metal sites for CH<sub>4</sub> activation and reported inhibition effects predominately reflect contributions from reverse reactions.

These kinetic responses to reactant and product concentrations are consistent with determining CH<sub>4</sub> activation steps on surfaces, essentially free of reactive intermediates or co-adsorbed products. CH<sub>4</sub>-derived chemisorbed intermediates appear to be readily removed via reactions with H<sub>2</sub>O co-reactant; as a result, the identity and concentration of co-reactant become kinetically irrelevant and forward rate data for the steam reforming reaction is accurately described by:

$$r_f = k P_{\text{CH}_4}$$

Catalytic reaction of CH<sub>4</sub> with H<sub>2</sub>O to form H<sub>2</sub>-CO mixtures on Ni depends only on the rate of the initial activation of C — H bonds, catalyzed by surface Ni atoms. Co-reactant activation is easy and CH<sub>4</sub>-derived intermediates, including reactive chemisorbed carbon, are kept well below monolayer coverages by their rapid reactions with intermediates derived from H<sub>2</sub>O.

Isotopic tracing and exchange measurements confirmed the mechanism proposed based on measured kinetic effects of reactant and product concentrations of forward reaction rates.

Methane decomposes to chemisorbed carbon (C\*) via sequential elementary H-abstraction steps, which become faster as H atoms are sequentially abstracted from CH<sub>4</sub> reactants. Density-functional theory led to an activation energy of 142 kJ/mol for the first H-abstraction step in CH<sub>4</sub> on Ni clusters, which decreased to 25-40 kJ/mol for CH<sub>2</sub> formation from CH<sub>3</sub>. This cascade process leads to low CH\* coverages and to C\* as the most abundant carbon-containing reactive intermediate. Chemisorbed carbon is then removed using CO<sub>2</sub> or H<sub>2</sub>O as co-reactants (Fig. 1. 16)<sup>45</sup>. These elementary steps are consistent also with kinetic and isotopic measurement on Ru, Pt, Ir and Rh catalysts. When exposed metal atoms (\*) are the most abundant surface species, only the rate constant for the activation of the first C — H bond in CH<sub>4</sub> appears in the rate expression and reaction rates become first order in CH<sub>4</sub> and independent of the presence or concentration of H<sub>2</sub>O or CO<sub>2</sub> co-reactants. Wei and Iglesia noted that these elementary steps provide pathways for reactions of CH<sub>4</sub> with either H<sub>2</sub>O or CO<sub>2</sub> and also for water gas shift reaction which have been typically, but inappropriately and non-rigorously, treated as independent kinetic process during CH<sub>4</sub> reforming<sup>45, 46</sup>.

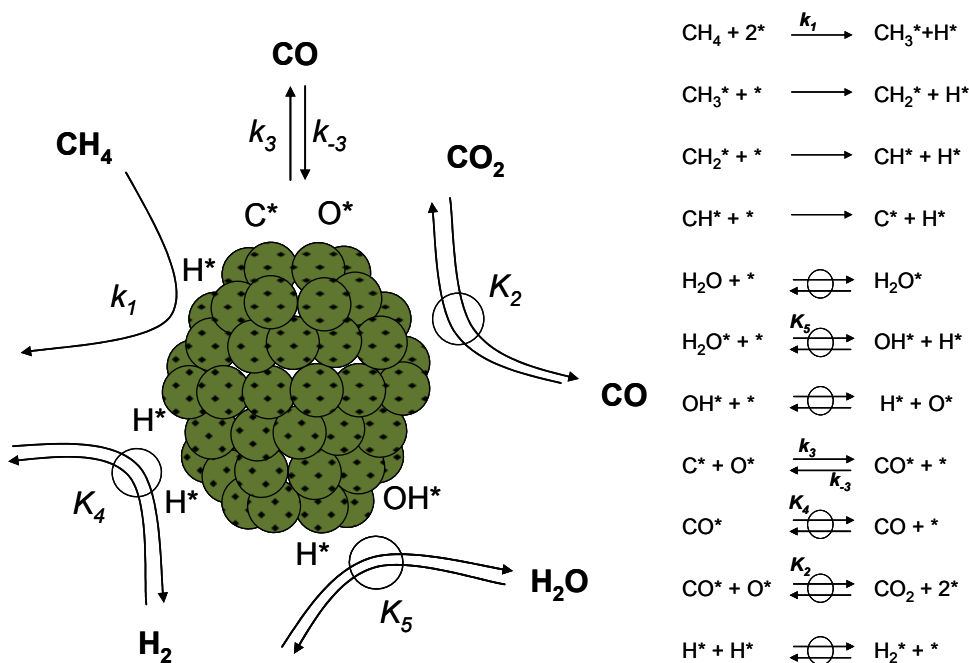


Fig. 1. 16 - Sequence of elementary steps for CH<sub>4</sub> reforming and water gas shift reactions on Ni based catalysts (—→ irreversible step,  $\rightleftharpoons$  quasi-equilibrated step,  $\rightleftharpoons$ , reversible step,  $k_i$  is the rate coefficient and  $K_i$  is the equilibrium constant for a given step i)<sup>45</sup>.

The mechanism of steam reforming of higher hydrocarbons is more complex than that of methane, since break of carbon-carbon bond is necessary to produce single carbon surface species. The order with respect to higher hydrocarbon in most published work is zero over nickel or rhodium catalysts, reflecting the ease of fragmentation of higher hydrocarbons and a consequent high surface coverage. The order with respect to water ranges from zero to one.

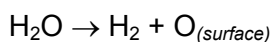
Microkinetic model assisted catalyst design seems to be a powerful tool for catalyst development and can be used to study methods for decreasing the carbon formation. Model simulations indicate that the use of Ni alloys and alkali promoters reduce the potential of carbon formation, but it also reduces the activity of methane reforming. Co, Pd, Pt, Ag and Au are candidates as dopants for Ni catalysts to form surface alloys<sup>47</sup>.

Decomposition of methane on nickel surface is believed the first step of the steam reforming of methane; then the carbon species formed on the surface react subsequently with steam or surface oxygen species. To follow the reaction

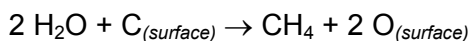
steps, Matsumura and Nakamori<sup>48</sup> separately fed methane and steam to the catalysts at 500°C and analyzed the mechanism at the initial stage of the reaction in which surface-active species participate.

The rate of the reaction of methane in absence of steam is significantly lower than that of the steady steam reforming, suggesting that the presence of steam which can oxidize the surface of Ni accelerates the decomposition of methane to hydrogen<sup>48</sup>. The formation rate of hydrogen is high at the initial stage of the reaction with methane on Ni/SiO<sub>2</sub> and Ni/Al<sub>2</sub>O<sub>3</sub> catalysts, and formation of carbon oxides, which evidences presence of surface oxygen species, is accompanied. Carbon monoxide is selectively formed in the reaction with methane over the catalyst containing NiO. Hence, the reduction of nickel oxide results in formation of carbon monoxide.

Formation of hydroxyl group on the surface of nickel (Ni-OH) is hypothesized in the reduction process of NiO particles. It is also supposed that the hydroxyl group is more reactive to methane and/or carbon monoxide than the lattice oxygen of nickel oxide. Accumulation of oxygen on the surface of these catalysts can be detected at the initial stage of the reaction with steam after methane decomposition. In this process, reaction of:



and



are also probable. However, the contribution will be small because formation of carbon monoxide, which is produced in presence of nickel oxide is small in the reaction with methane after the contact with steam. Since the formation rates of hydrogen and carbon dioxide increases gradually in the reaction with steam, carbon dioxide cannot be formed in the direct reaction between steam and surface carbon, but probably formed by the reaction with surface hydroxyl groups whose concentration should be saturated under the continuous feed of steam.

That is:

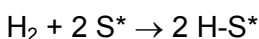
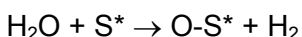
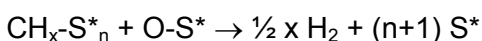


will take place on the surface. Little methane is formed after the formation rate of carbon dioxide is saturated, implying that the surface is mostly oxidized, because formation of methane does not proceed in absence of metallic nickel which accepts the oxygen in steam. After the feed of steam, following the reaction with methane, formation of carbon dioxide

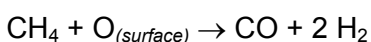


can be observed with re-feed of methane, suggesting formation of surface hydroxyl groups during the previous reaction with steam.

Mechanism of methane steam reforming at low temperature can be schematized as:



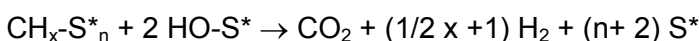
In the mechanism, where S\* represents an active site, the presence of oxide causes formation of carbon monoxide and the process is similar to:



in the reaction solely with the methane

No reaction was observed at the initial stage of the methane decomposition over 20 % Ni/ZrO<sub>2</sub> without reduction, suggesting that methane does not reduce nickel oxide. Just after the induction period, CH<sub>x</sub> is probably formed on the partially reduced surface and this leads to the formation of carbon monoxide and hydrogen which also reduces the surface. Thus, formation of CO in the steam reforming at 500°C will be caused from surface NiO species.

Since formation of carbon dioxide takes place in the presence of surface hydroxyl groups [ $\text{CH}_4 + 2 \text{OH}_{(\text{surface})} \rightarrow \text{CO}_2 + 3 \text{H}_2$ , and  $\text{C}_{(\text{surface})} + 2 \text{OH}_{(\text{surface})} \rightarrow \text{CO}_2 + \text{H}_2$ ],



may proceed on the surface in the steam reforming. Formation of hydroxyl groups on the surface should be an important step also in the steam reforming at 500°C. In the case of Ni/ZrO<sub>2</sub>, accumulation of water on the support assists formation of the hydroxyl groups, and this is probably the reason why zirconia is an effective support of nickel in the steam reforming at 500°C. Formation of carbon dioxide from carbon monoxide by water–gas shift reaction is possible in the reaction mechanism, but no relationship between production of carbon monoxide and carbon dioxide can be found in the reactions solely with methane or steam<sup>7</sup>.

### 2.1.3. Steam reforming catalysts

The catalyst must promote the desired reaction and be as inactive as possible towards unwanted side-reactions, particularly to the formation of carbon. The catalyst should also be as resistant as possible to poisons<sup>7</sup>.

The catalyst must be able to maintain its activity under the demanding process conditions, necessary to promote the desired reaction (800-1000°C and 20-30 bar). With impregnated catalysts, an important parameter in maintaining activity over prolonged periods is the nature of the support material and its pore structure<sup>7</sup>.

The catalyst must be strong enough to withstand the handling it receives; from manufacture to charging into the reformer, as well as the stresses generated by the process conditions and the thermal cycles arising from plant start-up and shutdown. The catalyst also must be of a suitable physical shape to provide an appropriate geometric surface area to give an acceptable activity per unit volume of packed bed whilst possessing acceptably low-pressure drop characteristics. The support must not be affected by water condensing on it, nor must it produce an unacceptable quantity of dust and material carryover, which could foul heat exchangers and other catalysts downstream<sup>7</sup>.

For many years nickel has been recognized as the most suitable metal for steam reforming of hydrocarbons, other metals can be used; for example cobalt, platinum, palladium, iridium, ruthenium and rhodium. Although some precious metals are considerably more active per unit weight than nickel, nickel is much cheaper and sufficiently active to enable suitable catalysts to be produced economically.

The reforming reaction takes place on the nickel surface, so the catalyst must be manufactured in a form that produces the maximum stable nickel surface area available to reactants. This is generally done by dispersing the nickel as small crystallites on a refractory support, which must be sufficiently porous to allow access by the gas to the nickel surface.

This is usually achieved by precipitating nickel as insoluble compound, from a soluble salt, in the presence of a refractory support such as mixtures of aluminum oxide, magnesium oxide, calcium oxide and calcium aluminate cement. Alternatively, the nickel can be incorporated by impregnating a preformed catalyst

support, such as alumina or an aluminate, with a solution of a nickel salt which is subsequently decomposed by heating to the oxide.

In either case, the nickel oxide is reduced to the metal by hydrogen supplied from another plant, or by cracking a suitable reactant gas (e.g. ammonia) over the catalyst as the reformer is being started up. In some instances process gas itself is used to reduce the nickel oxide to metal as the reformer is gradually brought on line.

Impregnated catalysts are generally stronger than precipitated catalysts, and this is one of the reasons for their widespread use.

The activity of a steam reforming catalyst in service is closely related to the available surface area of the nickel metal and the access the reactants have to it. Most commercial natural gas catalysts are now of the impregnated type and give a relatively high surface area when first reduced, but under normal reforming conditions the surface area falls as sintering of nickel crystallites occurs. The higher the temperature is, the more rapidly the sintering proceeds.

Activity is a function of the overall nickel content. However, it has been demonstrated that with both impregnated and precipitated catalyst there is an optimum beyond which an increase in nickel content does not produce any further significant increase in activity. Typically, these optima are approximately 20 % for precipitated and up about 15 % for impregnated catalyst, but this depends on the nature and physical properties of the actual support.

Steam reforming catalysts differ in the ease with which they reduce, and the extent of reduction is influenced by the chemical nature of the catalyst support, the reduction temperature and time, and the composition of the reducing gas. The highest initial nickel surface area is obtained when the reduction is done using pure hydrogen (rather than steam and hydrogen) and when the reduction temperature is ~ 600°C. Below this temperature, reduction can be slow and incomplete. Above 600°C, some sintering may take place, which lowers the nickel surface area.

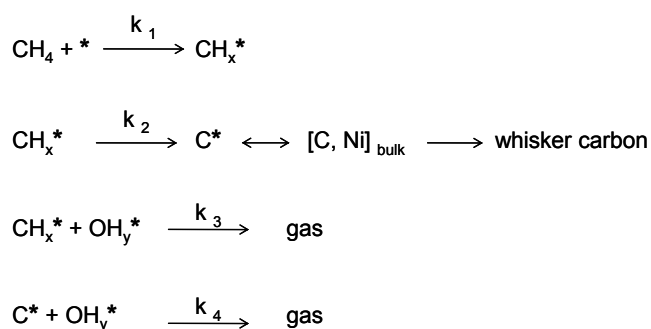
When steam is present, the surface areas can result lower, because sintering is enhanced, and this process proceeds further to give even lower surface areas if excessive reduction periods are employed. Nevertheless, for some catalyst, particularly precipitated catalysts for naphtha reforming, reduction periods up to twenty-four hours are recommended.

In order to optimize the development of superior catalysts, it is essential to understand the catalyst surface at the molecular level<sup>18</sup>. Choudhary and Goodman<sup>18</sup> summarize the studies related to methane activation on Ni catalyst. The interaction of methane with Ni surfaces is of considerable importance because steam reforming of methane is carried out on nickel catalysts.

The dissociation of methane is considered to be the rate-limiting step in SMR. This has led to a great interest in investigating the fundamental sticking process of methane on nickel single crystals. Ni single crystal studies have shown methane dissociation to be structure sensitive<sup>18</sup>.

At a given temperature and for a given hydrocarbon feed carbon will be formed below a critical S/C ratio<sup>49</sup>. This critical S/C ratio increases with temperature. By promotion of the catalyst, it is possible to push this limit towards the thermodynamic limit reflecting the principle of the equilibrated gas: "Carbon formation is to be expected on nickel catalysts if the gas shows affinity for carbon after the establishment of the methane reforming and the shift equilibria".

By use of noble metals or sulphur passivation, it is possible to push the limit at lower values. A safe design criterion is to require that the actual gas shows no affinity for carbon formation. Whether carbon free operation is possible depends on the kinetic balance as illustrated in the simplified two-step mechanism:



where \* represents nickel site disregarding the ensemble size<sup>7</sup>.

For a nickel catalyst, carbon is normally formed by the whisker mechanism. Adsorbed carbon atoms that do not react to gaseous molecules are dissolved in the nickel crystal and carbon whiskers nucleate from the nickel support interface of the crystal. Carbon formation is avoided when the concentration of carbon dissolved in the nickel crystal is smaller than that at equilibrium, in other words, when the steady state activity of carbon is smaller than one. The steady state activity is proportional with [C\*] which can be expressed by:

$$a_c^s \sim [C^*] \sim \frac{k_1 k_2}{k_3 k_4} \cdot \frac{1}{[OH_y^*]^2}$$

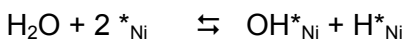
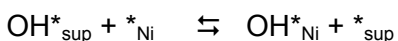
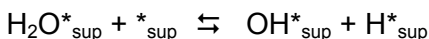
Hence, the steady state carbon activity can be decreased by:

- Enhancing the adsorption of steam or CO<sub>2</sub>
- Enhancing the rate of the surface reaction
- Decreasing the rate and degree of methane activation and dissociation.

The whisker mechanism may also be blocked by use of noble metal catalysts because these metals do not dissolve carbon.

Kinetic studies indicated that the adsorption of steam was enhanced by active magnesia and alkali and that spill-over of adsorbed steam to the metal surface may play a role. This was reflected by negative reaction orders with respect to steam.

The improved adsorption of steam on magnesia supports, resulting in improved resistance to carbon formation, is not a static but a dynamic effect. Enhanced steam adsorption cannot reflect a true equilibrium constant. This would violate the principle of microscopic reversibility, because steam is also adsorbed directly on the nickel surface.



The above means that the spill-over of steam probably involves OH species instead of molecular water<sup>7</sup>.

Apart from the enhanced steam adsorption on alkali promoted catalyst, it is well known that the addition of alkali to steam reforming catalysts results in a decrease of the reforming rate sometimes by more than one order of magnitude. The effect has been observed on a number of different group VIII metals and on a variety of supports. The decrease in reaction rate is due to lower pre-exponential factors whereas the activation energies are almost unchanged. In contrast, the enhancement of steam activation on magnesia-based catalyst has no impact on pre-exponential factor. It is remarkable that the decline in activity when promoting with alkali is also observed when testing the catalyst for hydrogenolysis of ethane, i.e. without the presence of steam.

The impact of alkali is stronger on less acidic supports, which suggest that the alkali partial pressure over the catalyst is important. A less acidic support has a

weaker bounding of alkali resulting in easier transport (via the gas phase) from the support to the metal. This effect of alkali on the activity of nickel is not fully understood<sup>7</sup>.

The influence of alkali on the chemisorption of a number of different molecules on transition metal surfaces has been explained as the result of electrostatic interaction. It was found that, above a critical alkali coverage, the adsorbed H<sub>2</sub>O is dissociated into OH and H. The maximum OH coverage is equal to the alkali coverage. Both adsorbed H<sub>2</sub>O and OH are strongly stabilized by the presence of alkali<sup>7</sup>.

A direct blockage of surface nickel atoms, with resulting ensemble control, was observed over partly sulphur poisoned nickel catalysts. By controlling the sulphur content in the feed, it is possible to establish a situation on the nickel surface with ensembles available for the dissociation of methane, but not for the dissolution of carbon atoms into the nickel crystal and nucleation of the whisker carbon. This way of obtaining carbon free operation was brought into practice in the SPARG process. Carbon formation on noble metals is probably prevented because carbon is not dissolved in these metals, thus preventing the diffusion of carbon through the metal to form whisker carbon. Palladium is the only noble metal that still forms carbon, probably because of the formation of a carbide<sup>7</sup>.

Takehira et al<sup>50, 51, 52, 53</sup> have proposed a solid phase crystallization (spc-) method for the preparation of well-dispersed and stable metal supported catalyst, starting from perovskite compounds (PVK) and hydrotalcite-like compounds (HTlc) as the precursors. Starting from Mg–Al hydrotalcite precursors containing Ni at the Mg sites, spc-Ni/MgAl catalysts have been prepared and were successfully applied in the partial oxidation, the steam reforming, and the CO<sub>2</sub> reforming of CH<sub>4</sub>.

There has been for the past decade an increased interest in the preparation of mixed oxide catalysts using hydrotalcite-like compounds as precursors for various reactions. Recently it was reported that spc-Ni/MgAl catalyst showed high and stable activity for both steam reforming and autothermal reforming of CH<sub>4</sub>. Such characteristics are equal to the ability of 1 wt. % Rh/MgO, reported as the best catalyst. In spite of such good catalytic performance due to stable and highly dispersed Ni metal particles, spc-Ni/MgAl catalysts have a drawback. Active Ni species distribute uniformly from the surface skin to the core of catalyst particles, since the catalysts was prepared by heating Mg(Ni)–Al hydrotalcite to form

Mg(Al)–Ni–O solid solutions, followed by the reduction of Ni(II) included in the structure. As a result, a considerable amount of Ni included in the catalyst bulk becomes irreducible and therefore ineffective for catalysis. The preparation of metal-loaded catalysts in egg shell-type will be anticipated, since active metal species are concentrated in the surface layer of the catalyst particles where gas-phase reactions preferentially proceed in the micro- or meso-porous space<sup>52</sup>.

Hydrotalcite is an anionic clay, layered mixed hydroxide containing exchangeable anions and affords the mixed oxide by heating; it shows an interesting property, i.e., a “memory effect”. This “memory effect” allows the reconstitution of the original hydrotalcite structure under mild conditions when the product of the thermal treatment is brought into contact with aqueous solutions containing anions. By adopting this “memory effect” on the surface of Mg–Al mixed oxide particle after thermal treatment, Takehira and coworkers<sup>52</sup> have prepared egg shell-type Ni-loaded catalysts. When the Mg–Al mixed oxide particles were dipped in aqueous solution of Ni(II) nitrate, Mg–Al hydrotalcite was reconstituted on the surface of particles and Ni(II) substituted for the Mg(II) sites. After the calcination followed by the reduction of the particles, active spc-Ni/MgAl phase was formed in the surface layer of the particle, resulting in the formation of egg shell-type Ni-loaded catalyst as s(surface)-spc-Ni/MgAl. The egg shell-type loading was substantially affected by the heating rate and the calcinations temperature of Mg–Al hydrotalcite to the mixed oxide and by the dipping conditions, i.e., pH of aqueous solution of Ni(II) nitrate and the dipping time.

Surface-solid phase crystallization (s-spc) Ni/MgAl catalyst was prepared by adopting the “memory effect”, i.e., reconstitution of Mg–Al hydrotalcite from Mg–Al mixed oxide and spc-method was just applied in the surface layer of the mixed oxide particle. Mg–Al (3/1) mixed oxide particles were prepared as the catalyst supports starting from Mg–Al (3/1) hydrotalcite,  $[\text{Mg}_6\text{Al}_2(\text{OH})_{16}\text{CO}_3] \cdot 4 \text{H}_2\text{O}$ , and were dipped in an aqueous solution of Ni(II) nitrate. Upon dipping, reconstitution of Mg–Al hydrotalcite took place in the surface layer and a part of the Mg(II) sites were replaced by Ni(II). After the calcination, followed by the reduction, s-spc-Ni/MgAl catalysts were obtained and showed high activity due to surface enrichment of highly dispersed Ni metal particles. Egg shell-type Ni-loaded catalysts showed a high and stable activity in the steam reforming of CH<sub>4</sub>. It was concluded that the high activity is mainly due to the enrichment of stable and highly dispersed Ni metal particles in the surface layer of the catalyst particles<sup>52</sup>.

Catalysts were prepared from hydrotalcite precursors, characterized and tested in the reaction of methane steam reforming to produce hydrogen also by Assaf and Fonseca<sup>54</sup>. The precursors were synthesized by the traditional technique, with co-precipitation of Ni, Mg and Al nitrates with carbonate; co-precipitation of Mg and Al nitrates with pre-synthesized nickel chelate and anion-exchange of NO<sub>3</sub><sup>-</sup> of hydrotalcite with nickel chelate. The catalytic tests demonstrated high methane conversion, high activity for hydrogen production and high stability during the time of reaction for a molar ratio in the feed H<sub>2</sub>O:CH<sub>4</sub> = 2:1. The low quantity of carbon formed on the catalysts surface confirmed the hypothesis that the structure of hydrotalcite layers leads to a homogeneous distribution of the active phase. Comparing the different methods of preparation, it was shown that the precursors obtained by means of Ni chelates were the most active in converting methane, with a high hydrogen yield, probably because they provided the best distribution of the active phase<sup>54</sup>.

Recently, Struzzenegger and coworkers<sup>55</sup> have tested nickel iron oxide (NiFe<sub>2</sub>O<sub>4</sub>) as a combined catalyst precursor and oxygen transfer material for improved conversion of methane into syngas.

Alloying Fe<sub>3</sub>O<sub>4</sub> with NiO to a spinel-type nickel iron oxide turned out to be a promising path for adding catalytic functionality to the native iron oxide. The reaction of the ternary metal oxide with humidified CH<sub>4</sub> comprises two characteristic phases. During the early phase, oxidation of methane by lattice oxygen is the prevailing reaction. This leads to a two-phase mixture consisting of a nickel-deprived spinel phase and a Ni-rich alloy. As the amount of the Ni-rich alloy increases, catalyzed steam reforming of CH<sub>4</sub> becomes increasingly important. Once all Ni is deprived from the spinel phase, the bulk reaction terminates and steam reforming of methane is the only reaction.

The reduction of the bed material is reversed by exposure to steam. Though this reaction is slower than that with pure or diluted O<sub>2</sub>, it is advantageous because it produces H<sub>2</sub> rather than heat. The reaction with steam is also a key step in catalyst regeneration. First, oxidation and re-integration of Ni drives off many prominent catalyst poisons, specifically sulfur, as thermodynamics predicts conversion of nickel sulfides into nickel iron oxides at high water vapor pressure. Recycling of the parent spinel phase has thus a similar purification effect as re-crystallization and minimizes the accumulation of undesired elements in the fixed

bed. Second, each recovery of the parent spinel phase re-disperses the nickel on an atomic scale, allowing for a repeated formation of fresh Ni-alloy particles under conditions similar to those during the first reduction. The benefit of re-dispersion was also emphasized by Provendier et al.<sup>56</sup> while discussing regeneration of Ni/LaFeO<sub>3</sub>/La<sub>2</sub>O<sub>3</sub> to the parent perovskite-type LaNi<sub>1-x</sub>Fe<sub>x</sub>O<sub>3</sub> by calcination in air.

The design of a steam reforming catalyst support must reflect the need for it to be robust at high temperature and pressure. It must also be suitable for the dispersion of nickel crystallites and allow access of the reacting species, but it must not interfere with their activity. If possible, it should promote or at least sustain the activity of the nickel, but it must not catalyze side-reactions, particularly those which produce carbon deposits.

Good physical properties can be obtained by using a simple  $\alpha$ -alumina that is calcined at 1500°C.

A particularly useful range of catalysts are produced from a support which is derived from a mixture of alumina and hydraulic cement that is processed to a porous calcium aluminate. This support is less acidic than  $\alpha$ -alumina, and is therefore less susceptible to carbon formation initiated by hydrocarbon-cracking reactions.

Spinel is a ternary oxide with a chemical formula of AB<sub>2</sub>O<sub>4</sub>, where A is a divalent metallic cation in a tetrahedral site and B is a trivalent metallic cation in an octahedral site of the cubic structure<sup>57</sup>. Magnesium aluminate spinel (MgAl<sub>2</sub>O<sub>4</sub>) has a specific combination of desirable properties such as: high melting point (2135°C), high resistance to chemical attack, good mechanical strength from room temperature to high temperatures, low dielectric constant, excellent optical properties, low thermal expansion and good catalytic properties. Conventionally, the spinel (MgAl<sub>2</sub>O<sub>4</sub>) is prepared through a reaction in the solid state using MgO and Al<sub>2</sub>O<sub>3</sub>. In this process, the mixture is calcined at high temperatures such as 1400–1600°C. An effort to synthesize MgAl<sub>2</sub>O<sub>4</sub> at lower temperatures has been reached by using chemical synthesis processes, especially chemical co-precipitation and sol–gel processes, where the spinel phase is formed at temperatures around 700°C. The MgAl<sub>2</sub>O<sub>4</sub> can be formed at temperatures lower than 675°C by the co-precipitation method involving the dehydration of a solution of metallic ion complexes with tri-ethanolamine. However, these chemical

processes have disadvantages over the conventional solid-state reaction. The co-precipitation method has difficulties in pH control because there is solid precipitation and the removal of anions that are in the solids as impurities, changing the final composition. The sol-gel method, which uses a mixture of aluminum and magnesium salts that are submitted to pyrolysis, also has impurities in the solids. Catalysts obtained through nickel impregnation in inorganic supports have been employed in industry to catalyze the steam reforming of hydrocarbons. Due to its resistance to sintering, the magnesium aluminate spinel has been used as a catalyst support for methane reforming. It was observed a high activity and stability of a Ni/MgAl<sub>2</sub>O<sub>4</sub> catalyst for dry reforming of methane, which was attributed to the interaction between the active phase Ni and the support, resulting in highly dispersed active Ni species. This catalyst exhibited higher activity and better stability when compared to Ni/ $\gamma$ -Al<sub>2</sub>O<sub>3</sub> and Ni/MgO- $\gamma$ -Al<sub>2</sub>O<sub>3</sub> catalysts.

The addition of small amounts of Pt (0.09%) to Ni/Al<sub>2</sub>O<sub>3</sub> catalyst resulted in a significant increase of its activity in methane reforming with CO<sub>2</sub> and O<sub>2</sub>. It was found that the addition of Pt, Pd and Ir (< 0.3 %, by weight) in Ni/ $\gamma$ -Al<sub>2</sub>O<sub>3</sub> catalysts (15 % Ni, w/w) strongly promoted conversion of methane in an autothermal reforming reaction.

MgAl<sub>2</sub>O<sub>4</sub> was synthesized by Foletto and coworkers<sup>57</sup> through hydrolysis of metallic alkoxides of Mg<sup>2+</sup> and Al<sup>3+</sup>. The formed spinel precursor phase was calcined at temperatures between 600 and 1100°C, for 4 h. The spinel was utilized as a Ni/Pt catalyst support. The Ni/MgAl<sub>2</sub>O<sub>4</sub> catalysts (15 % Ni, w/w) containing small amounts of Pt were tested for methane steam reforming. The spinel phase was formed at temperatures above 700°C. The addition of small amounts of Pt to Ni/MgAl<sub>2</sub>O<sub>4</sub> promoted an increase in surface area. This noble metal promoted an increase in the surface area. This probably caused the considerable increase in methane conversion<sup>57</sup>.

Nickel is increasingly studied for the methane-reforming catalysis with various oxides, either classical (Al<sub>2</sub>O<sub>3</sub>, SiO<sub>2</sub>, MgO, TiO<sub>2</sub>) or less conventional ones (ThO<sub>2</sub>, CeO<sub>2</sub>, ZrO<sub>2</sub>, Cr<sub>2</sub>O<sub>3</sub>, Nb<sub>2</sub>O<sub>5</sub>)<sup>58</sup>. It appears that, besides the elaboration process, the nature of the interaction between the nickel and the support, in the form of specific phases, plays a determinant role for the catalytic properties. For example, the formation of phases, such as nickel aluminate spinel, NiAl<sub>2</sub>O<sub>4</sub>, on

alumina leads after reduction to highly dispersed catalysts with a high selectivity and a great resistance against sintering and poisoning. However, these phases are only partially reduced by conventional methods (hydrogen reduction at high temperature) and their activity is drastically low. Nevertheless, even though the role of the tight interaction support metal is widely studied, it is still subject to discussion and yet far from being well understood. The catalyst properties may be due to a combination of intrinsic size effects and support effects<sup>58</sup>.

As an alternative way, irradiation has been proven to be a powerful tool to reduce metal ions into highly dispersed and size-controlled metal clusters. Actually, the specific properties, distinct from the bulk, of 'quasi-atomic' metal were demonstrated for the first time for nascent metal produced by irradiation. The aggregates of a few atoms only were much easily oxidized than the bulk metal. These new specific properties could explain why nanosized metal clusters are difficult to stabilize but they could induce higher activity. The radiation-induced reduction of metal ions into atoms is achieved by solvated electrons generated from the solvent and by electrons generated from the support, both having the strongest reducing power. Therefore, all ions, including non-noble metals, are reducible by electrons. Due to the radiation penetration, the reducing species are produced - without any chemical additive. In addition, the reduction is carried out at room temperature, which is favorable to prevent sintering. The radiolytic process has been extensively used to synthesize noble metals as nanocolloids or supported clusters. Using the radiolytic technique in both regimes (steady-state and pulsed radiolysis), it was improved the understanding of the primary steps of the formation of mono- and multi-metal aggregates and the nucleation-coalescence processes. This has permitted to obtain clusters of controlled size and structure (alloyed or core shell)<sup>58</sup>.

Non-noble metal clusters are still more difficult to synthesize at very small sizes, since their fragility to oxidation still exists up to high nuclearities. The atoms and the primary oligomers are highly oxidable and can be corroded as soon as they are produced. However, using appropriate conditions, nickel and other metal nanocolloids were produced by radiation-induced reduction. Irradiation has also been used in some cases as a complementary treatment of Ni-alumina samples, before or after the classical reduction by hydrogen gas, in view of creating defects in the support and improving the catalytic properties of the solids<sup>58</sup>.

A series of Ni aggregates supported on  $\alpha$ -Al<sub>2</sub>O<sub>3</sub> at different nickel contents are prepared by ionic exchange of Ni<sup>2+</sup> followed by  $\gamma$ -irradiation under inert atmosphere. The radiation-induced reduction of Ni ions and the synthesis of Ni clusters, under wet conditions already known for nanocolloids, was successfully adapted to the elaboration of Ni particles supported on  $\alpha$ -alumina. When used as catalysts for the steam-reforming methane reaction to produce synthesis gas, they act with a remarkable high selectivity in CO (80%), even at low temperature (550°C). The reasons are probably due to combination of the influence of the radiation on both the metal and the support, particularly on the interface<sup>58</sup>.

The presence of silica would further increase the already adequate strength of the support, but as silica is volatile in the presence of steam at high temperatures only very small quantities can be used, except in naphtha steam reforming catalysts when it is combined with potassium which significantly reduces its partial pressure under reforming conditions.

Magnesia can also be included in some formulations, but has to be used with caution and understanding, however, as under certain conditions, it can hydrate and markedly weaken the catalyst. During start-up or shutdown in the presence of reaction steam only, hydration of the magnesia can take place below 425°C and, since the molar volume of Mg(OH)<sub>2</sub> is almost twice that of MgO, a dramatic weakening of the support may result unless the MgO is formulated in such a way that is chemically associated with other refractory oxides. If this is not done reformer start-ups and shutdowns must ensure that, the catalyst is in a dry atmosphere whilst temperatures are below the critical hydration temperatures<sup>7</sup>.

Effects of supports such as silica,  $\gamma$ -alumina, and zirconia for nickel catalysts have been studied in steam reforming of methane at 500°C<sup>48</sup>. The activity of the nickel supported on silica reduced with hydrogen at 500°C decreases with oxidation of nickel particles by steam during the reaction. Nickel supported on  $\gamma$ -alumina is not much reduced with hydrogen at 500°C and is inactive in the reforming at 500°C. However, the catalyst reduced at 700°C is fairly active while nickel is partially oxidized during the reaction. Nickel supported on zirconia is the most effective in the steam reforming at 500°C<sup>7</sup>.

Fujimoto and coworkers<sup>59</sup> studied a Ni-Mg-O solid solution with low Ni content (Ni<sub>0.03</sub>Mg<sub>0.97</sub>O, atomic ratio) which was reduced at high temperature (> 800°C) and was found to be an active and stable catalyst for the steam reforming of

methane in a steam to carbon ratio of 1.0. The reduced Ni<sub>0.03</sub>Mg<sub>0.97</sub>O catalyst showed higher activity and much higher stability than a commercial reforming catalyst (Ni/Al<sub>2</sub>O<sub>3</sub>-MgO). The catalyst kept its activity for 60 h or more at 900°C and a steam to carbon ratio of 1.0, giving little coke on the catalyst (< 1 wt %), whereas the commercial steam reforming catalyst lost its activity at 20 h because of severe coking under the same reaction conditions. For both Ni<sub>0.03</sub>Mg<sub>0.97</sub>O and Ni/Al<sub>2</sub>O<sub>3</sub>-MgO, the rate equations were similar. Thus, it was suggested that the suppressed coke formation of the Ni<sub>0.03</sub>Mg<sub>0.97</sub>O catalyst is caused by the very small nickel particles and the difference in the composition of surface carbonaceous species on the Ni metal particles as the reaction intermediate.

Ni<sub>0.03</sub>Mg<sub>0.97</sub>O solid solution catalyst has high resistance to carbon deposition in steam and dry reforming of methane, but the deactivation due to oxidation of active nickel species was observed under some reaction conditions. This deactivation was avoidable by the addition of hydrogen to reactant gas. On Ni<sub>0.03</sub>Mg<sub>0.97</sub>O catalyst, nickel particles were much more dispersed than that on 3 mol % Ni/MgO and CO<sub>2</sub> was adsorbed on Ni<sub>0.03</sub>Mg<sub>0.97</sub>O similarly to MgO. In addition, CO<sub>2</sub> was activated on Ni<sub>0.03</sub>Mg<sub>0.97</sub>O at 60°C lower temperature than on 3 mol % Ni/MgO. This is suggested to be promoted by large interface between metal and support, and strong interaction of CO<sub>2</sub> with support surface. Combined with the results of reaction order, it is suggested that high resistance to carbon deposition in methane dry reforming is closely related to high ability of CO<sub>2</sub> activation and this causes rapid oxidation if carbon species on nickel before converting to deposited carbon<sup>60</sup>.

Reactions used to model the steam reforming of natural gas show that the influence of the support on the performances of the metal is minimal. On the other hand, hydrogen produced during the reactions adsorbs on the metal and can spill over to the support. The spilt over hydrogen could be responsible in part for the gasification of carbonaceous residues<sup>61</sup>.

In the industrial viewpoint, Al<sub>2</sub>O<sub>3</sub>-based supports are preferred because of their easier availability in the reforming processes. Therefore, Ni/Al<sub>2</sub>O<sub>3</sub> and Ni/MgAl<sub>2</sub>O<sub>4</sub> have been used as catalysts for SMR. As an alternative, Ni/γ-Al<sub>2</sub>O<sub>3</sub> could be considered. However, it is unstable at high temperature (>700°C) because of the thermal deterioration of the γ-Al<sub>2</sub>O<sub>3</sub> support that causes sintering and leads to pore closing and reduction in surface area as well as phase transformation into

$\alpha$ - $\text{Al}_2\text{O}_3$  which changes an active surface layer and promotes a low surface area structure. Thus, Jun and coworkers<sup>62, 63, 64</sup> carefully changed  $\gamma$ - $\text{Al}_2\text{O}_3$  into  $\theta$ - $\text{Al}_2\text{O}_3$  and modified  $\theta$ - $\text{Al}_2\text{O}_3$  with Ce-ZrO<sub>2</sub> because Ni/Ce-ZrO<sub>2</sub> exhibited good performance in methane reforming reactions. The catalyst was remarkably deactivated by steam treatment but reversibly regenerated by H<sub>2</sub>-reduction. The steam treatment resulted in the formation of NiAl<sub>2</sub>O<sub>4</sub>, which is inactive for SMR, but it was reversibly converted to Ni by the reduction. The reversible oxidation-reduction of Ni state was evidenced and it was observed that the formation of NiAl<sub>2</sub>O<sub>4</sub> is more favorable at higher temperature. It is most likely that the alumina support is only partially covered with Ce-ZrO<sub>2</sub> and most Ni directly interacts with  $\theta$ - $\text{Al}_2\text{O}_3$ , which would probably make easy formation of NiAl<sub>2</sub>O<sub>4</sub> in the presence of steam alone. The results imply that, during the start-up procedure in SMR, too high concentration of steam could deactivate seriously Al<sub>2</sub>O<sub>3</sub> supported Ni catalysts<sup>62</sup>.

Xu et al<sup>65</sup> had explored the use of oxide nanoparticles for catalysts founding that the Ni catalyst 'supported' by small nanoparticles of ZrO<sub>2</sub> (7–25 nm) or MgO (10–12 nm) can be highly active and extremely stable for the steam and the dry methane reforming reactions at 700–800°C. In contrast to conventional oxide-supported metal catalyst having discrete metal nanocrystals (1–20 nm) supported on oxide particles that are often one to several orders of magnitude larger than the metal nanocrystals, the stable Ni/ZrO<sub>2</sub> catalysts appear as nanocomposites of comparably sized Ni-metal (10–15 nm) and zirconia nanocrystals (7–25 nm). Ni catalysts supported on conventional oxide supports are not able to avoid coking and deactivate rapidly under the same conditions. They tested nanocomposite Ni/ZrO<sub>2</sub> catalyst for the SMR reaction with a stoichiometric mixture of steam and methane in a wide range of feed space velocities. The nanocomposite catalyst is claimed to be superior to Ni catalysts supported on bigger particles of conventional oxides (Ni/ZrO<sub>2</sub> and Ni/Al<sub>2</sub>O<sub>3</sub>) for the SMR reaction<sup>65</sup>.

Addition of promoters into the catalysts is the simplest and cheapest way to improve their quality. For example, molybdenum added to nickel catalysts in small amounts ( $\leq 0.5$  wt. %) is a promoter, which significantly increases catalysts resistance to coking in the steam reforming (decreasing coking rate and lengthening induction time). With the addition of such amounts of Mo, loss of

catalytic activity was not observed<sup>66</sup>. Effectiveness of promoter depends on the type of hydrocarbon reaction (reforming, hydrogenolysis, cracking), and in the case of steam reforming on the ratios of reactants (H<sub>2</sub>O/C<sub>n</sub>H<sub>m</sub>) and  $p_{H_2O}/p_{H_2}$  in the reaction mixture. The prepared catalyst<sup>66</sup> was Ni–Mo/ $\gamma$ -Al<sub>2</sub>O<sub>3</sub>. Heating of the catalysts in the H<sub>2</sub>O : H<sub>2</sub> mixtures at the temperature 500–600°C caused important changes in the mean oxidation number of surface Mo atoms. The same treatment at the higher temperature resulted in the bulk changes and the formation of MoO<sub>2</sub> phase. H<sub>2</sub>O into gaseous atmosphere affects the oxidation states of Mo and Ni. Concentration of oxygen atoms on the surface of Ni–Mo/Al<sub>2</sub>O<sub>3</sub> catalysts after heating in the H<sub>2</sub>O : H<sub>2</sub> mixture (so at conditions similar to the steam reforming of hydrocarbons) was higher than that on the nickel catalyst surface. The experiments confirmed surface reactions between water vapor and molybdenum under the conditions of steam reforming of hydrocarbons, which change the oxidation state of promoter atoms due to their oxidation. Hence, it was supposed that in the steam reforming reaction of hydrocarbons the presence of larger number of oxygen atoms on the surface of Ni–Mo catalysts may facilitate gasification of the “CH<sub>x</sub> species” and limit their transformation into inactive deposit. It decreases the rate of carbon deposit formation<sup>66</sup>.

Nickel catalysts supported on silica–zirconia mixed oxides were prepared<sup>67</sup> by homogeneous precipitation in sol–gel-derived wet silica gel. Their structural properties and catalytic performance in steam-reforming of methane were investigated from the viewpoint of steam resistance. Ni/SiO<sub>2</sub> without zirconia readily loses its catalytic activity during the reaction because the coarsening of silica that occurs in the presence of high-temperature steam hinders the active surface of Ni. The addition of zirconia drastically increases the steam resistance of silica. Ni/SiO<sub>2</sub>-ZrO<sub>2</sub> catalyst shows steady activity in steam-reforming of methane without any changes in pore structure<sup>67</sup>.

From an industrial point of view, the development of nickel catalysts with greater resistance to coking is thus an attractive research goal<sup>68</sup>.

An effective approach to developing such nickel catalysts is to focus on the selection and modification of catalyst supports. It is widely accepted that the addition of alkali, alkali earth oxides and rare earth metal oxides to the  $\alpha$ -Al<sub>2</sub>O<sub>3</sub> support or the use of basic metal oxides as the support improves resistance to

coking. This positive effect is understood to result from the enhancement in steam adsorption, in the oxidation rate of  $\text{CH}_x$  fragments adsorbed on metallic nickel and/or the reduction of methane activation and dissociation.

Although improvements of the support greatly influence catalytic activity and/or resistance to coking, limited attempts have been made to apply oxygen-ion conducting oxides, for instance  $\text{CeO}_2$  and perovskite-type oxides, to the steam reforming catalysts.

It is mechanistically expected that oxidation of  $\text{CH}_x$  fragments adsorbed on metallic nickel would be promoted by the lattice oxygen in oxygen-ion conducting oxides and that the consumed lattice oxygen would be regenerated by steam. Such a mechanism has specifically been proposed for CO oxidation and dry reforming of methane. Huang and coworkers<sup>69, 70, 71</sup> have evaluated the activity of nickel supported on ceria-based ion-conducting oxides for dry reforming of methane and have pointed out that the lattice oxygen in modified ceria may play some positive roles in the activation of methane and carbon dioxide. Takehira et al.<sup>50</sup> have reported that the perovskite-type oxides such as  $\text{SrTiO}_3$ ,  $\text{CaTiO}_3$ ,  $\text{BaTiO}_3$  that contain a small amount of nickel in the titanium sites show high catalytic activities with high resistance to coking, due to the high dispersion of nickel. These researchers also examined oxygen mobility in perovskites, and found that the high resistance to coking might be partly due to the migration of mobile oxygen from the perovskite support to the metallic nickel particles.

The catalytic activity and resistance to coking of nickel catalysts supported on a variety of the perovskite-type oxides ( $\text{LaAlO}_3$ ,  $\text{LaFeO}_3$ ,  $\text{SrTiO}_3$ ,  $\text{BaTiO}_3$ ,  $\text{La}_{0.4}\text{Ba}_{0.6}\text{Co}_{0.2}\text{Fe}_{0.8}\text{O}_{3-\delta}$ ) were compared to those of the conventional  $\text{Ni}/\alpha\text{-Al}_2\text{O}_3$  catalyst for steam reforming of methane under the conditions of  $800^\circ\text{C}$ , atmospheric pressure and a molar  $\text{H}_2\text{O}/\text{CH}_4$  ratio of 2<sup>68</sup>. To investigate differences in catalytic activity among the Ni/perovskite catalysts examined, the dispersion and reduction properties of nickel and the roles of the lattice oxygen on the catalytic activity and carbon deposition were examined. Ni/ $\text{LaAlO}_3$  and Ni/ $\text{SrTiO}_3$  showed high catalytic activities among the Ni/perovskites and longer-term stabilities than the conventional catalyst. Temperature programmed oxidation of carbon deposited on used catalysts revealed that inactive carbon species detected on Ni/ $\alpha\text{-Al}_2\text{O}_3$  were not formed in the case of Ni/ $\text{LaAlO}_3$ . The results of temperature programmed reduction confirmed that consumption and recovery of the lattice oxygen in perovskites occurred during the reaction, and

that the reducibility of perovskites had a great impact on the steam reforming activity. The lattice oxygen in perovskites is considered to play important roles in promoting the oxidation of CH<sub>x</sub> fragments adsorbed on metallic nickel.

Both the reducibility and the particle size of nickel were found to be related to catalytic activities. These results suggest that the lattice oxygen in LaAlO<sub>3</sub> and SrTiO<sub>3</sub> accesses CH<sub>x</sub> fragments adsorbed on nickel readily due to the large amount of lattice oxygen near the surface of the perovskite, and interfaces between the nickel particles and the support. Thus, Ni/LaAlO<sub>3</sub> and Ni/SrTiO<sub>3</sub> have high catalytic activities. The lattice oxygen in LaAlO<sub>3</sub> and SrTiO<sub>3</sub>, thus plays a positive role in both promoting the oxidation of CH<sub>x</sub> fragments adsorbed on metallic nickel and in hindering the production of inactive carbon species<sup>68</sup>.

A novel anode La<sub>1-x</sub>Sr<sub>x</sub>Cr<sub>1-y</sub>Ni<sub>y</sub>O<sub>3-δ</sub> (x = 0.1, 0.2, 0.3, 0.4 and y = 0.05, 0.1) for solid oxide fuel cells (SOFCs) operated under methane has been tested regarding its catalytic activity for methane steam reforming and its structure characterized<sup>72</sup>. Powders were synthesized by solid-state reaction. The steam/methane ratio was between 0.5 and 1.

The strontium and nickel-doped lanthanum chromite has been shown to have some catalytic activity for methane steam reforming. The main point was the absence of carbon deposition for a steam/methane ratio equal to 1 or less at 850°C. The highest catalytic activity was obtained with 30 mol % of strontium and 5 mol % of nickel, synthesized at 1400°C during 4 h. This synthesis temperature seems to be necessary in order to obtain a complete solid-state reaction. The maximum in conductivity seemed to be either between 30 and 40 mol % of strontium, or slightly above 40 mol %. With nickel content higher than 5 mol % of nickel, the catalytic activity decreased and some nickel/chromium agglomerations were observed after catalytic tests<sup>72</sup>.

Wang et al prepared a series of Rh/MgO - Al<sub>2</sub>O<sub>3</sub> catalysts with varying Rh loadings (1, 5 and 10 %) and 6 wt % MgO by an incipient wetness method. Rh loading was optimized on a stable MgO - Al<sub>2</sub>O<sub>3</sub> support to improve the volumetric productivity for methane conversion. Catalyst activities were stable over a wide range of steam/carbon ratios. In particular, experimental results demonstrated that Rh/MgO - Al<sub>2</sub>O<sub>3</sub> catalysts are extremely active for methane steam reforming and are resistant to coke formation at stoichiometric steam/carbon ratio of 1 for

over 14 h time-on-stream with no sign of deactivation. Methane steam reforming activities on this catalyst were compared in both a microchannel reactor and a conventional micro-tubular reactor. Significant performance enhancement was observed in microchannel reactors owing to improved heat and mass transfer<sup>73</sup>.

Highly active and coke-resistant Rh catalysts were developed for methane steam reforming in micro-channel chemical reactors<sup>73</sup>. Conventional methane steam reforming processes suffer severe mass and heat transfer limitation, and the effectiveness factors of catalysts are typically less than 5%. Micro-channel reaction technology, which has been developed over the past decade, provides a potential breakthrough solution to the challenge of methane steam reforming processes. Micro-channel reactors have a sandwich-like multi-layer structure consisting of a large number of closely spaced channels with a gap of less than 1 mm, which reduces heat and mass transport distance and thus enhancing the overall efficiency. Consequently, micro-channel reactors allow process intensification and unprecedented temperature control. Heat transfer coefficients in micro-channel reactors are as high as 10,000–35,000 W/m<sup>2</sup>K compared to 100–700 W/m<sup>2</sup>K in conventional reactors. Such high heat transfer coefficients coupled with the high surface-to-volume ratio achievable in micro-channel reactors permit the operation of highly endothermic methane steam reforming at near isothermal conditions and provide the potential to improve significantly the efficiency of methane steam reforming process<sup>73</sup>.

The effect of Ru loading added to the Ni-catalyst was investigated<sup>74</sup>, it was found that the presence of Ru strongly enhances the catalytic performance of the Ni-based catalyst when increasing Ru loading up to 2 wt %. Effect of Ni loading to the Ru-based catalyst system was also investigated. It was found that the addition of nickel to the Ru-based catalyst up to 15 wt% enhanced significantly the catalytic activity of the catalyst. The lifetime of the Ru–Ni catalysts in the reforming of m-cresol was tested at 750°C (m-cresol was used as a representative model compound for the coal tar or lignin-derived oils). In agreement with general observations of the use of Ni monometallic catalyst, deactivation of the catalyst due to the carbon deposition reaction already occurred in the reforming of the oxygenated compound. On the other hand, a reasonable high resistant on the carbon deposition in the reforming of m-cresol

was given by the 2 wt % Ru – 15 wt % Ni catalyst system. An effort in improving the strength of the catalyst support with this catalyst system was also conducted, and the catalyst showed significant increase in the stability of the reforming of oxygenated aromatic compound<sup>74</sup>.

Palladium (Pd) supported on CeO<sub>2</sub>-promoted  $\gamma$ -Al<sub>2</sub>O<sub>3</sub> with various CeO<sub>2</sub> (ceria) crystallinities, were used as catalysts in the methane steam reforming reaction<sup>75</sup>. Pd was found present on the oxidized CeO<sub>2</sub>-promoted catalysts as Pd<sup>0</sup>, Pd<sup>+</sup> and Pd<sup>2+</sup>, at ratios strongly dependent on CeO<sub>2</sub> structure. Pd was well dispersed (particles < 2 nm) on crystalline CeO<sub>2</sub> and was agglomerated as large clusters (particles in 10–20 nm range) on amorphous CeO<sub>2</sub>. After pre-treatment under H<sub>2</sub> or in the presence of amorphous CeO<sub>2</sub>, partial encapsulation of Pd particles occurred. CeO<sub>2</sub> structure influenced the CH<sub>4</sub> steam reforming reaction rates. Crystalline CeO<sub>2</sub> and dispersed Pd favor high reaction rates (low activation energy). The presence of CeO<sub>2</sub> as a promoter conferred high catalytic activity to the alumina-supported Pd catalysts. The catalytic activity was significantly lower on Pd/ $\gamma$ -Al<sub>2</sub>O<sub>3</sub> or on amorphous (reduced) CeO<sub>2</sub>/Al<sub>2</sub>O<sub>3</sub> catalysts. The reaction rates were found two orders of magnitude higher on Pd/CeO<sub>2</sub>/ $\gamma$ -Al<sub>2</sub>O<sub>3</sub> than on Pd/ $\gamma$ -Al<sub>2</sub>O<sub>3</sub>, due to a catalytic synergism between Pd and CeO<sub>2</sub>. The low rates on the reduced Pd/CeO<sub>2</sub>/Al<sub>2</sub>O<sub>3</sub> catalysts were correlated with the loss of Pd sites through encapsulation or particle agglomeration, a process found mostly irreversible after catalyst regeneration<sup>75</sup>.

CeO<sub>2</sub> (ceria) has been extensively employed as a textural and structural promoter for supported noble metal catalysts. Its promotion effect was attributed to excellent thermal and mechanical resistance, propensity to non-stoichiometry and oxygen-storage capacity. Due to its properties, structure and capabilities of storing and releasing oxygen, CeO<sub>2</sub> is an important component in automotive, emission-control (oxidation) catalysts, selective oxidation in fine chemicals synthesis and solid oxide fuel cell applications.

CeO<sub>2</sub> addition to a Ni-supported catalyst was found to decrease carbon deposition and increase the catalyst life and activity. Noble metal based catalysts (Pt, Pd and Rh) deposited on various supports such as Al<sub>2</sub>O<sub>3</sub>, CeO<sub>2</sub>, ZrO<sub>2</sub>, or NiO, tested in regular tubular reactors or more recently in membrane design reactors, provided good catalytic activity in methane, propane or n-butane steam reforming reactions. The promoting effect of CeO<sub>2</sub> on Pt, Pd and Rh catalysts

was proven for CO oxidation, water gas shift and CH<sub>4</sub> steam reforming. The state of CeO<sub>2</sub> reduction affects the activity of Pt/Ce–Zr oxides in CO oxidation. For various CeO<sub>x</sub> stoichiometries corresponding to various degrees of reduction, the activation energy increases as the degree of ceria reduction increases.

#### 2.1.4. Carbon formation on reforming catalyst

Coking or the formation of carbonaceous deposits is an important side reaction in many industrial processes. Very often, measures to eliminate or depress coke formation are more decisive for the process layout than, for instance, the activity of the catalyst<sup>76</sup>.

Deactivation of supported metal catalysts by carbon or coke formation is a problem of serious magnitude in steam reforming. Its causes are generally threefold:

- 1) fouling of the metal surface,
- 2) blockage of catalysts pores and voids,
- 3) actual physical disintegration of the catalyst support.

Carbon may chemisorb strongly, as a monolayer, or physically adsorb in multi-layers and, in either case, block access of reactants to metal surface sites. Furthermore, carbon may totally encapsulate a metal particle, and thereby completely deactivate that particle, and plug micro- and macropores such that access of reactants is denied to many crystallites inside this pores. Finally, in extreme cases, strong carbon filaments may build-up in pores to the extent that they stress and fracture the support material, ultimately causing disintegration of catalyst pellets and plugging of reactor voids<sup>77</sup>.

Since loss of catalytic activity and physical destruction of the catalyst by carbon deposits can occur rapidly (within hours or days) under unfavorable conditions, understanding and control of these effects are of major technological and economical importance<sup>78</sup>.

Carbon accumulation can also cause spalling and pulverization of catalysts, which can also lead to poor heat distribution<sup>79</sup>.

Carbon is a product of CO disproportionation while coke is produced by decomposition or condensation of hydrocarbon on metals. Nevertheless, coke forms may vary from high molecular weight hydrocarbons such as condensed

polyaromatics to carbon such as graphite, depending upon the conditions under which the coke was formed and aged (Fig. 1. 17).

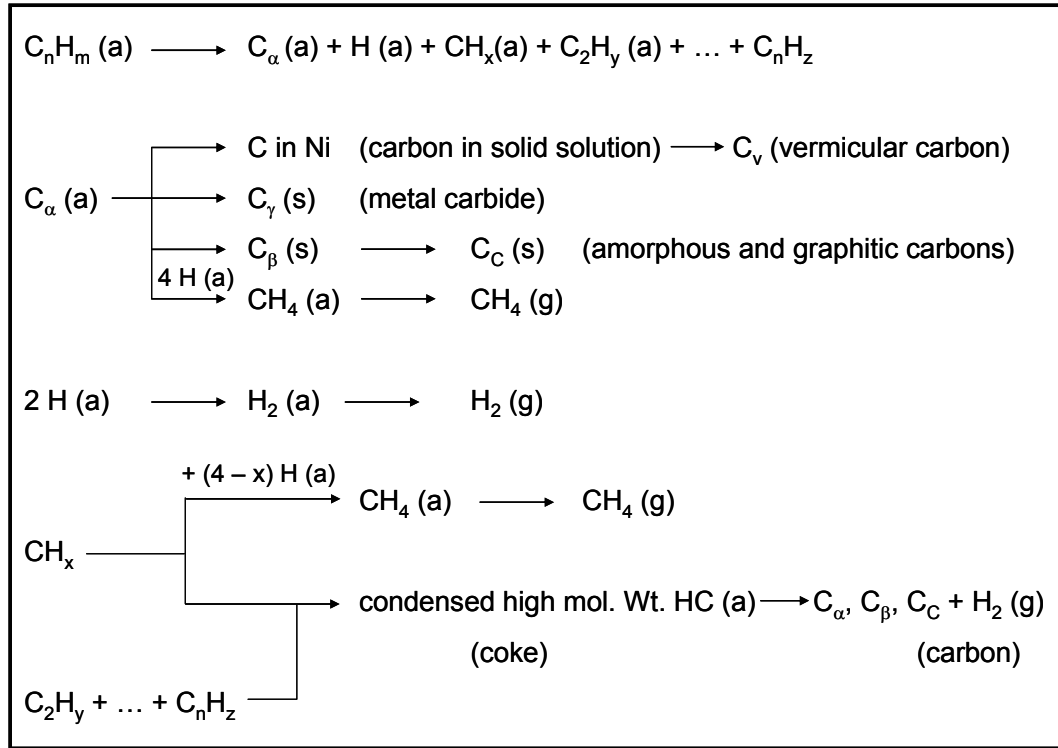


**Fig. 1. 17 - Formation, gasification and transformation of coke and carbons on metal surfaces from hydrocarbons (a = adsorbed, g = gaseous, s = solid).**

Three different kinds of carbon or coke species are observed in steam reforming (Tab. 1. 2):

- 1) whiskers like carbon formed at temperature greater than 450°C,
- 2) encapsulating hydrocarbon films formed by polymerization at less than 500°C,
- 3) pyrolytic carbon from cracking of hydrocarbon above 600°C.

Formation of carbon deposits via CO decomposition (Fig. 1. 18) may involve the production and transformation of various carbon forms, adsorbed atomic carbon ( $C_\alpha$ ), amorphous carbon ( $C_\beta$ ), vermicular carbon ( $C_v$ ), bulk nickel carbide ( $C_\gamma$ ) and crystalline, graphitic carbon ( $C_C$ ), the structural reactivities of which are summarized in the Tab. 1. 3. The presence of dispersed or atomic carbon, stable below 325°C, which can be also surface nickel carbide, and polymerized carbon stable above 325°C was confirmed. Nickel carbide can be easily removed by H<sub>2</sub> at the same temperature.

	Whisker like	Encapsulating film	Pyrolytic carbon
<b>Formation</b>	Diffusion of C through Ni crystal, nucleation and whisker growth with Ni crystal at top	Slow polymeraization of $C_nH_m$ radicals on Ni surface into encapsulating film	Thermal cracking of hydrocarbon. Deposition of C precursors on catalyst
<b>Temperature range</b>	> 450°C	< 500°C	> 600°C
<b>Critical parameters</b>	High temperature. Low $H_2O/C_nH_m$ No enhanced $H_2O$ adsorption Low activity Aromatic feed	Low temperature Low $H_2O/C_nH_m$ Low $H_2/C_nH_m$ Aromatic feed	High temperature High void fraction Low $H_2O/C_nH_m$ High pressure Acidity of catalyst

Tab. 1. 2 - Carbon species formed in steam reforming of hydrocarbons<sup>78</sup>.

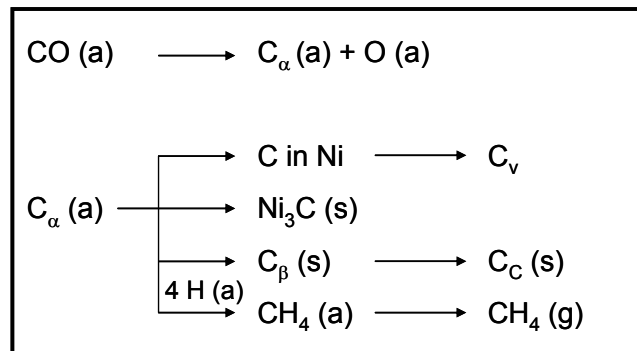


Fig. 1. 18 - Formation, gasification and transformation of carbon on nickel from carbon monoxide (a = adsorbed, g = gaseous, s = solid).

Structural type	Designation	Temperature formed	Peak temperature for reaction with $H_2$
Adsorbed, atomic (dispersed, surface carbide)	$C_\alpha$	200-400°C	200°C
Polymeric, amorphous films or filaments	$C_\beta$	250-500°C	400°C
Vermicular (polymeric, amorphous) <ul style="list-style-type: none"> <li>a. filaments</li> <li>b. fibers</li> <li>c. whiskers</li> </ul>	$C_\nu$	300-1000°C	400-600°C
Nickel carbide (bulk)	$C_\gamma$	150-250°C	275°C
Graphitic (crystalline) <ul style="list-style-type: none"> <li>a. platelets</li> <li>b. films</li> </ul>	$C_\text{C}$	500°C 550°C	550-850°C

Tab. 1. 3 - Forms and reactivities of carbon species formed by decomposition of CO on nickel<sup>78</sup>.

Several studies of carbon deposition on nickel powders, foils and single crystals show direct evidence of low density filamentous (amorphous) and high density, crystalline graphitic forms, such as platelets observed after treatment in carbonizing atmospheres at temperature above 550°C. It should be emphasized that at high temperature amorphous carbon may convert to more graphitic forms in terms of their reactivity and even crystallinity while retaining their overall film or vermicular structure.

Furthermore, some forms of carbon results in loss of catalytic activity and some do not. For example, at low temperature (< 300-375°C), condensed polymer or β-carbon films and at high temperature (> 650°C) graphitic carbon films encapsulate the metal surfaces of steam reforming catalysts.

Deactivation of steam reforming catalysts at high temperature (500-900°C) may be caused by precipitation of atomic (carbide) carbon dissolved in the Ni surface layers to a depth of more than 50-70 nm. If it accumulates on the metal surface, at high or low temperatures, adsorbed atomic carbon can deactivate metal sites for adsorption and/or reaction. For example, carbon atoms residing in the four-fold hollow sites of Rh (1 0 0) block the adsorption of hydrogen and hence could block sites for hydrogenation<sup>77</sup>. In the intermediate temperature range of 375-650°C, carbon filaments are formed by precipitation of dissolved carbon at the rear side of metal crystallites causing the metal particles to grow away from the support. Filament growth stops when sufficient carbon accumulates on the free surface to cause encapsulation by a carbon layer; however, encapsulation of the metal particles does not occur if H<sub>2</sub>/CO or H<sub>2</sub>O/hydrocarbon ratios are sufficiently high. Thus, carbon filaments sometimes formed in CO hydrogenation or steam reforming of hydrocarbons would not necessarily cause a loss of intrinsic catalyst activity unless they are formed in sufficient amount to cause plugging of the pores or loss of metal which occurs as the carbon fibers are removed during regeneration. However in practice, region of carbon forming potential in steam reforming must be carefully avoided, since once initiated, the rate of filamentous carbon formation are sufficiently high to cause catastrophic pore plugging and catalyst failure within a few hours to days.

The rate at which deactivation occurs for a given catalyst and reaction depends greatly on reaction conditions, especially temperature and reactant composition. A fundamental principle for coke insensitive reactions on metals (in which relatively reactive coke precursors formed on active sites are readily removed by

hydrogen or other gasifying agents) is that deactivation rate depends greatly on the difference in rate of formation and gasification of carbon/coke precursors:

$$r_d = r_f - r_g$$

If the rate of gasification,  $r_g$ , is equal to or greater than that of formation,  $r_f$ , carbon/coke is not deposited. Rates of carbon/coke precursor formation and gasification both increase exponentially with temperature, although the difference between them varies a great deal with temperature because of differences in pre-exponential factors and activation energies. Thus, carbon/coke formation is avoided in region of temperature in which precursor gasification rate exceeds deposition rate. Since at temperature below 320°C ( $1/T > 1.66 \times 10^{-3} \text{ K}^{-1}$ ) the rate of  $C_\alpha$  gasification exceeds that of  $C_\alpha$  formation, no carbon is deposited. However, above 320°C,  $C_\alpha$  accumulates on the surface since the rate of  $C_\alpha$  formation exceeds that of  $C_\alpha$  gasification. As  $C_\alpha$  accumulates (at 320-520°C), it is converted to a  $C_\beta$  polymeric chain or film which deactivates the nickel catalyst; however, above 520°C ( $1/T < 1.43 \times 10^{-3} \text{ K}^{-1}$ ) the rate of  $C_\beta$  hydrogenation exceeds that of formation and no deactivation occurs.

In steam reforming, filamentous carbon formation rate is strong function of hydrocarbon structure; for example, it decreases in the order acetylenes, olefins, paraffins, i.e. in order of decreasing reactivity, although activation energies for nickel are in the same range independent of hydrocarbon structure and about the same as those observed for formation of filamentous carbon from decomposition of CO. This latter observation suggests that the reaction of CO and different hydrocarbons to filamentous carbon proceed by a common mechanism and rate-determining step, probably the diffusion of carbon through the metal crystallites<sup>77</sup>. The rate at which carbon or coke is accumulated in a given reaction under given conditions can vary significantly with catalyst structure, including metal type, metal crystallite size, promoter, and catalyst support. For example, Co, Fe and Ni are active above 350-400°C for filamentous carbon formation from CO and hydrocarbons.

Pt, Ru and Rh catalysts, on the other hand, while equally or more active than Ni, Co, or Fe in steam reforming produce little or no coke or carbon. This is attributed to reduced mobility and/or solubility of carbon in the noble metals, thus retarding the nucleation process. Thus, it is not surprising that addition of noble metals to base metals retards carbon formation; for example, addition of Pt in Ni lowers

carbon deposition rate during methanation, while addition of Cu to Ni substantially lowers carbon formation in steam reforming.

Since carbon formation and gasification rates are influenced differently by modifications in metal crystallite surface chemistry, which are in turn a function of catalyst structure, oxide additive or oxide supports may be used to moderate the rate of undesirable carbon or coke accumulation<sup>77</sup>.

The high temperatures associated with steam reforming favor the formation of carbon<sup>80</sup>. Four reactions may be involved:

Thermal cracking or decomposition of methane:



Thermal cracking or decomposition of hydrocarbons:



CO disproportionation (Boudouard):



CO reduction:

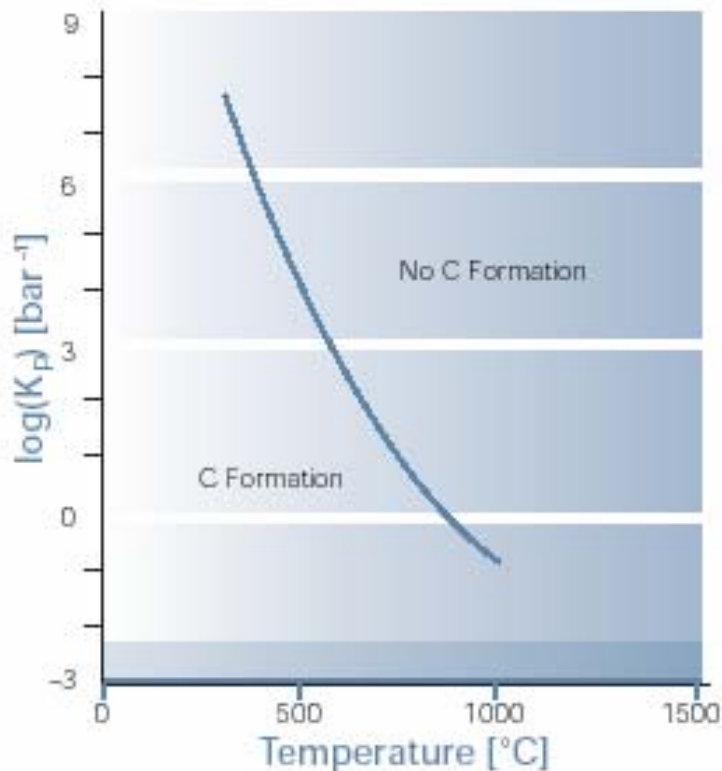
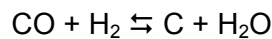


Fig. 1. 19 - Boudouard reaction: equilibrium constant.

For naphtha the decomposition is more complex because carbon can be formed by direct thermal cracking and also from various intermediates, particularly unsaturated species.

When methane or naphthas are reformed, the formation of carbon within the nickel catalyst can be prevented by ensuring the steam/hydrocarbon ratio (S/C) exceeds a certain minimum ratio. This minimum varies with pressure and temperature, and thermodynamic data can be used to calculate the minimum S/C ratio under different conditions. The exact values calculated depend on thermodynamic parameters assumed for "carbon", and a considerable amount of research has shown that different forms of carbon can be produced, depending on the prevailing conditions. There is a greater tendency for higher hydrocarbon than for methane to form carbon, because on pyrolysis the readily formed initial intermediates is an important factor, and is critical in influencing the delicate balance between carbon-forming and carbon-removing reactions.

Both the nickel and the support play dual roles, contributing to the reforming process and to the formation of carbon. This problem was solved (by ICI) by introducing an alkali metal component into the catalyst. This accelerates the carbon-steam reaction and, at the same time, the alkali neutralizes the acidity in the catalyst support, so retarding cracking and polymerization. The most effective alkali was found to be  $K_2O$  (potash). The potassium is effective by being mobile on the catalyst surface.

Accurate formulation combines the potassium as a complex potassium alumina-silicate (Kalsilite:  $K_2O \cdot Al_2O_3 \cdot SiO_2$ ) and monticellite ( $CaO \cdot MgO \cdot SiO_2$ ). The potassium is liberated at a very slow rate as non-volatile  $K_2CO_3$  which is hydrolyzed as fast it is formed, producing KOH, which is very mobile on the catalyst surface and is the effective carbon-removing agent. Potassium is therefore slowly lost from the catalyst into the product gases, but the rate of evolution is very slow, being kinetically controlled by its release from the Kalsilite compounds. The higher the temperature and the higher the feedstock throughput, the more rapid is the potassium depletion. Careful formulation of the catalyst ensures that lives of several years are obtained in most reformers.

Most of the complex reactions associated with naphtha reforming are completed in the top half of the catalyst bed, with methane reforming taking place in the lower part of the tubes. It is therefore possible to use an non-alkalized steam reforming catalyst in the bottom half of the reformer tube. This has several

beneficial effects. It reduces the total quantity of potash in the reformer, and takes potash out of the hottest part of the reformer. Since the potash depresses the activity of the nickel catalyst to some degree with respect to the methane reforming, a non-alkalized catalyst at the bottom of the reformer improves the approach to equilibrium at the exit of the reformer for a given throughput and exit temperature.

Non-acidic magnesium spinel (MgAl<sub>2</sub>O<sub>4</sub>) based catalysts containing no mobile alkali are effective under certain operating conditions, but formulation is critical. However, given good control of temperature throughout a reformer, it is possible to achieve the delicate balance between carbon formation and removal. Systems of this sort have lower tolerance to variation in operating conditions, changes in reformer firing patterns or temperature profiles which can disturb the balance and give carbon lay-down<sup>7</sup>.

The reduction or elimination of coke formation often results in constraints on the operating conditions to be applied. Steam and hydrogen are the most important retarding reactants. In steam reformers, carbon will be formed below a certain steam to carbon ratio which means that in many cases the steam reformer has to operate with a surplus of steam and, hence that a larger reformer is required. When using a catalyst with enhanced steam adsorption, the critical steam to carbon ratio can be reduced. This can be obtained by adding alkali to the catalyst or using active magnesia as support. In tubular reforming, no carbon is accepted because of the break-down of the catalyst will result in build up of pressure drop with uneven flow distribution and hot spots. The progressive deactivation can be followed from the movement of temperature profile of the catalytic bed.

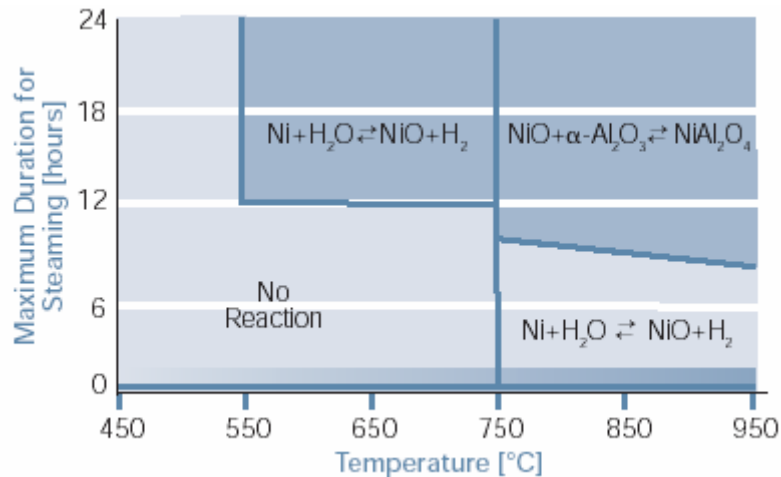


**Fig. 1. 20 - Steaming: recommended durations.**

Regeneration of coke deposits can be carried out in various ways depending on the reactivity of the coke. The encapsulating deposits which cause deactivation of the nickel based catalysts can be removed by treatment in hydrogen at 500°C depending on the age of the carbon. Newly formed carbon in tubular steam reformers can be removed by increasing the S/C ratio or by steaming of the catalyst (Fig. 1. 20). However, aged coke deposits require regeneration by means of air. At sufficiently high temperatures (typically above 500°C), the regeneration process becomes limited by the diffusion of the oxygen through the carbon free pores as the burn-off progresses after a core/shell mechanism. If the carbon is highly reactive, the regeneration may easily become heat transfer limited meaning that the temperature of the catalyst pellet may be heated up to a temperature corresponding to the adiabatic temperature increase of the combustion process. In the case of a metal catalyst, the metallic phase will also be oxidized. Therefore, in many cases it is necessary to carry out the regeneration with controlled addition of air to nitrogen or steam<sup>76</sup>.

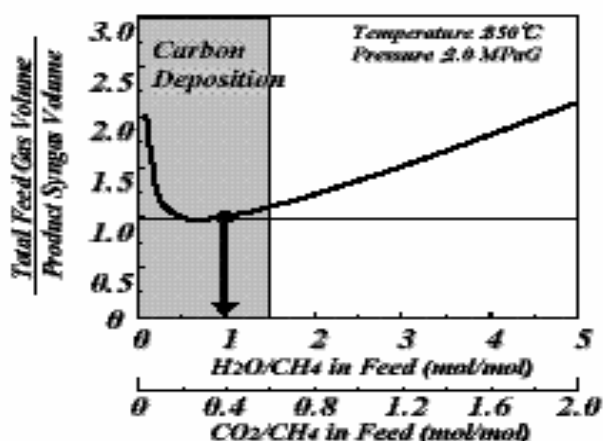


Fig. 1. 21 - Optimal values of H<sub>2</sub>O/CH<sub>4</sub> and CO<sub>2</sub>/CH<sub>4</sub> ratios.

Because of the reactions that lead to carbon formation are reversible, and it is possible to calculate limits based on the ratio of carbon in the feedstock to steam beyond which carbon will not be formed, there is a continuing pressure to work at high steam/carbon ratio<sup>80</sup>. The situation can be worse when dealing with heavier feedstocks. The first problem arises with traces of sulphur that may be present in the feed. When the level of sulphur is very low, this may be advantageous. Under most circumstances, however this leads to the formation of nickel sulphide and to catalyst deactivation.

So, the carbon formation may be avoided by controlling the surface reactions, by sulphur addition. It has been demonstrated that minimal coking can be observed, during steam reforming, if traces of sulphur are added to the feed<sup>81, 82</sup>. Sulphur obtained from traces of hydrogen sulphide in the feed chemisorbs on the surface. At low coverages on a (1 0 0) surface, sulphur occupies a fourfold hollow site independent of coverage. At higher coverages the surface involves a (2 x 2) structure on the (1 0 0) surface, which is probably best described as a nickel sulphide surface containing islands of free nickel sites<sup>80</sup>.

Adsorbed sulphur will deactivate nickel but will also delineate ensembles of sites where sulphur is not adsorbed. Rostrup-Nielsen<sup>82</sup> suggested that the size of these ensembles was critical in allowing steam reforming with minimal formation of coke. Steam reforming was found to involve ensembles of 3-4 nickel atoms, while carbon formation required six or seven atoms.

Dissociation of methane to form C<sub>α</sub> requires a given number of sites. If the formation of dissolved carbon occurs mainly through C<sub>β</sub>, then

polymerization/isomerization of  $C_\alpha$  to  $C_\beta$  is required. This, in turn, requires at least twice the number of sites associated with the formation of  $C_\alpha$ . The critical ensemble size was found to be generated at sulphur coverages in excess of 0.7-0.8 (corresponding to  $H_2S/H_2$  ratios of greater than about  $7.5 \times 10^{-7}$ ). The rate of steam reforming was decreased, but carbon formation was essentially eliminated. Some amorphous carbon was laid down and it was possible, under extreme conditions, to produce carbon whiskers<sup>80</sup>.

The formation of carbon is very dependent on the system pressure, and the industry seeks high pressure  $H_2/CO$ , not low-pressure product. It is known that if one operates these reforming reactions at elevated pressures ( $\sim 12$  atm), dramatic increases in the rates of coke formation are observed over most types of Ni based catalysts. Formation of carbon on a catalyst can be difficult to follow at elevated pressure running in continuous mode<sup>79</sup>.

Carbon formation may also have an effect on construction materials. Pyrolytic coke deposited on the tube walls may lead to harmful carburization of the high alloy steel tubes. A critical phenomenon is metal dusting corrosion, which may take place if a CO-containing process gas is cooled below the equilibrium temperature of the CO-decomposition reaction. The resulting carbon will typically react with the steel forming iron carbide which will decompose and fall off leaving the construction material with heavy pitting<sup>76</sup>.

### 2.1.5. Sintering of reforming catalysts

Nickel steam-reforming catalysts are subject to several deactivation mechanisms including coking, poisoning, and sintering. Sintering is the reason for loss of activity for many industrial catalyst systems.

Thermally induced deactivation of catalysts results from<sup>77</sup>:

- (i) loss of catalytic surface area due to crystallite growth of the catalytic phase;
- (ii) loss of support area due to support collapse and of catalytic surface area due to pore collapse on crystallites of the active phase,
- (iii) chemical transformations of catalytic phases to non-catalytic phases.

Sintering processes generally take place at high reaction temperatures ( $> 500^\circ\text{C}$ ) and are generally accelerated by water vapor.

Sintering of heterogeneous catalysts is often referred to as the loss of catalytic surface area due to growth of large particles at the expense of smaller particles. Sintering is complex and may be influenced by many parameters such as sintering time, temperature, chemical environment, catalyst composition and structure, and support morphology. A good understanding of the sintering mechanism is necessary, both to predict the extent of deactivation by sintering and to design catalysts that maintain a high activity<sup>83</sup>.

Particle growth via sintering influences the resistance of the catalyst toward coking and poisoning with sulfur. The coking limits are affected by the nickel particle size and the nickel surface area determines the sulfur capacity of the catalyst. Furthermore, the activity of a steam-reforming catalyst is related to the nickel surface area. To model an industrial reformer with regard to activity and the effect of sulfur poisoning, it is necessary to know the nickel surface area as a function of time, temperature, feed gas composition, chemical composition including promoters, and extent of poisoning.

Several studies of sintering of Ni particles supported on a ceramic carrier are reported in the literature. The most important parameters are the sintering temperature and the composition of the gas over the catalyst. Increasing temperature and the presence of steam accelerates the sintering process. High surface areas of the carrier, on the other hand, increase the stability toward sintering.

Three mechanisms for the metal particle growth have been proposed:

- (i) particle migration, where entire crystallites migrate over the support followed by coalescence;
- (ii) Ostwald ripening (atom migration), where metal atoms emitted from one crystallite migrate over the support and are captured by another crystallite;
- (iii) vapor transport between particles (at high temperatures).

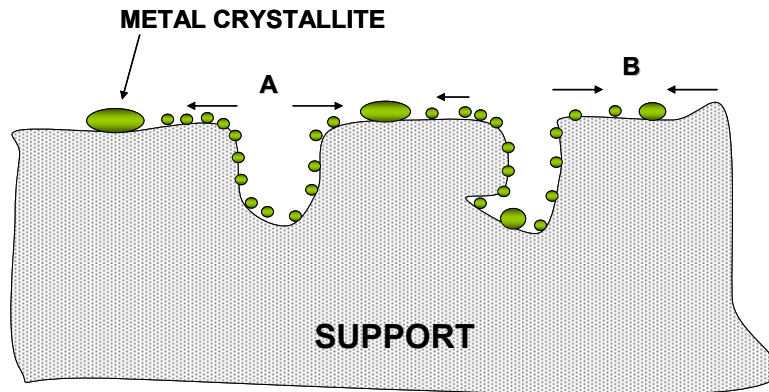


**Fig. 1. 22 - Two conceptual models for crystallite growth due to sintering by (A) atomic migration or (B) crystallite migration<sup>77</sup>.**

Crystallite migration involves the migration of entire crystallites over the support surface followed by collision and coalescence. Atomic migration involves detachment of metal atoms from crystallites, migration of these atoms over the support surface and ultimately, capture by large crystallites<sup>77</sup>.

Each of the three sintering mechanisms is a simplification, which ignores the possibility that all mechanisms may occur simultaneously and may be coupled with each other through complex physicochemical processes including:

- a) dissociation and emission of metal atoms or metal-containing molecules from metal crystallites,
- b) adsorption and trapping of metal atoms or metal-containing molecules on the support surface,
- c) diffusion of metal crystallites across support surfaces,
- d) metal or metal oxide particle spreading,
- e) support surface wetting by metal or metal oxide particles,
- f) metal particle nucleation,
- g) coalescence of, or bridging between, two metal particles,
- h) capture of atoms or molecules by metal particles,
- i) liquid formation,
- j) metal volatilization through volatile compound formation,
- k) splitting of crystallites in  $O_2$  atmosphere due to formation of oxides of a different specific volume,
- l) metal atom vaporization.

Depending upon reaction or redispersion conditions, a few or all of these processes may be important; thus, the complexity of sintering/redispersion process is emphasized.

In general, sintering processes are kinetically slow at moderate reaction temperature and irreversible or difficult to reverse. Thus, sintering is more easily prevented than cured<sup>77</sup>.

Temperature, atmosphere, metal type, metal dispersion, promoters/impurities and support surface area texture and porosity, are the principal parameters affecting rates of sintering. Sintering rates increase exponentially with temperature. Metals sinter relatively rapidly in oxygen and relatively slowly in hydrogen, although depending upon the support. Water also increases the sintering rate of supported metals. In reducing atmosphere, metal crystallite stability generally decreases with decreasing metal melting temperature, in the order: Ru > Ir > Rh > Pt > Pd > Ni > Cu > Ag, although this order may be affected by relatively stronger metal –support interactions.

Promoters or impurities affect the sintering by either increasing (chlorine and sulphur) or decreasing (oxygen, calcium and cesium) metal atom mobility on the support. Similarly, support surface defects or pores impede surface migration of metal particles, especially micropores and mesopores with pore diameters about the same size as the metal crystallite.

Sehested et al.<sup>84</sup> studied the mechanism for sintering of nickel steam-reforming catalysts at 500°C, 30 bar, H<sub>2</sub>O : H<sub>2</sub> = 10 : 1 and concluded on the basis of the particle size distributions that sintering occurred via the crystallite migration mechanism. For this sintering mechanism, mass transport by diffusion of nickel atoms on the nickel crystallite surfaces is necessarily an important step, so the diffusivity and concentration of single metal atoms and small clusters are central parameters in the understanding of the sintering phenomenon.

Campbell et al.<sup>85</sup> reported that the heat of adsorption of metal atoms to metal particles depends more strongly on the particle size than assumed previously leading to faster rates of sintering via both Ostwald ripening and particle migration and coalescence. This phenomenon is most important for small particles (diameter < 50 Å for Pb particles). A nickel particle with a diameter of approximately 36 Å contains the same number of atoms as a Pb particle with a diameter of 50 Å due to the size difference of the atoms. In the study of Sehested<sup>83</sup>, the nickel particles are generally larger than this particle size. The

smallest average nickel particle diameters estimated from the nickel surface areas in the catalysts used are of the order of 75–90 Å, indicating that the effect of fast sintering of small particles can be ignored. On the contrary, ASAXS (anomalous small angle X-ray scattering) gives lower estimates of the nickel particle diameters, indicating that sintering of small particles is significant. However, they believe that the measurements of the nickel areas in that case give the most reliable estimates of the nickel particle diameters as these measurements are carried out using reduced catalysts as opposed to ASAXS, where passivated catalysts are used. Nickel may move significantly during passivation.

Recently, a simple expression for the development of the nickel surface area as a function of time, temperature, nickel loading, and carrier surface area was derived<sup>86</sup>.

$$A_{\text{Ni}} = \pi c_{\text{cat}} d_{\text{Ni}}^2 = \text{const. } X_{\text{Ni}} d_{\text{Ni}}^{-1} \approx \text{const.} \frac{X_{\text{Ni}}^{0.86} (1 - X_{\text{Ni}})^{0.14} A_{\text{car}}^{0.14}}{K_1^{0.14} D_{\text{Ni}}^{0.14} t^{0.14}}$$

$A_{\text{Ni}}$  = nickel surface area

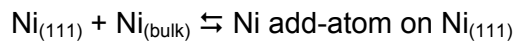
$c_{\text{cat}}$  = number of particles per gram of catalyst

$d_{\text{Ni}}$  = number averaged particle diameter

$X_{\text{Ni}}$  = fractional mass of nickel (g metal/g catalyst)

$A_{\text{car}}$  = surface area of the carrier (m<sup>2</sup>/g of the carrier)

$K_1$  = equilibrium constant for the reaction:



$D_{\text{Ni}}$  = diffusion coefficient of an add-atom on a Ni surface

$t$  = time

To obtain the expression it was assumed that the sintering mechanism was particle migration and coalescence, that the particle sizes were log normally distributed with constant relative standard deviation, and that the carrier acted only as an area dispersing the metal particles. The expression included a parameter, which depends on the atmosphere over the catalyst and the chemical environment on the catalyst. It was investigated experimentally and theoretically the effects of steam and hydrogen over nickel catalysts as a function of temperature. The relative nickel areas of Al<sub>2</sub>O<sub>3</sub> and MgAl<sub>2</sub>O<sub>4</sub>-supported nickel catalysts are determined after sintering at 1, 31, and 40 bar total pressure at various steam and hydrogen ratios.

The increased rate of sintering in the presence of steam is attributed to formation of Ni<sub>2</sub>-OH species at the surface of nickel particles. The energy of formation of this species at the nickel surface is low, compared to that of nickel atoms while the energy of diffusion is highest for the Ni<sub>2</sub>-OH complex. It was concluded that, in the presence of steam and hydrogen, the surface transport at nickel particles will be dominated by Ni<sub>2</sub>-OH dimers. The calculated energies of formation and diffusion are used in a simple model that is able to predict the rate of sintering of nickel catalysts. The predicted dependencies of temperature, P<sub>H<sub>2</sub>O</sub>, and P<sub>H<sub>2</sub></sub> are in good agreement with those obtained experimentally.

The experimental data showed a change in the activation energy of sintering at high temperatures. The temperature for this change is at approximately 600°C at 40 bar total pressure and H<sub>2</sub>O:H<sub>2</sub> = 2.5:1 when the catalyst is sintering for 700 h. At ambient pressure, the change is observed to happen at approximately 700°C after sintering at 1 bar total pressure and H<sub>2</sub>O:H<sub>2</sub> = 1:1 for 50 h. It is speculated that the rate of sintering, at high temperatures, may be determined by Ostwald ripening<sup>83</sup>.

Sintering of the support may also occur. Single-phase oxide carriers sinter by one or more of the following processes:

- 1) surface diffusion,
- 2) solid-state diffusion,
- 3) evaporation/condensation of volatile atoms or molecules,
- 4) grain boundary diffusion,
- 5) phase transformation.

Additives and impurities affect the thermal properties of carriers by occupying defect sites or forming new phases. Alkali metals, for example, accelerate sintering, while calcium, barium, nickel and lanthanum oxides form thermally stable spinel phases with alumina. Steam accelerates support sintering by forming mobile surface hydroxyl groups that are subsequently volatilized at higher temperatures. Chlorine also promotes sintering and grain growth in magnesia and titania during high temperature calcination.

Dispersed metals, in supported metal catalysts, can also accelerate support sintering, for example, dispersed nickel accelerates the loss of Al<sub>2</sub>O<sub>3</sub> surface area in Ni/Al<sub>2</sub>O<sub>3</sub> catalysts<sup>77</sup>.

### 2.1.6. Catalyst shape and dimensions

Reforming catalysts can be produced in different shapes and sizes by pelleting or extrusion technique. Since it is used in tubular reactors, it must be of a shape and size which packs easily and homogeneously into the tubes to give an active bed which does not have an unacceptably high pressure drop. As much as possible of the active nickel surface must be accessible to the reactant gas, while the catalyst must be strong enough to resist abrasion and breaking during handling or during any thermal cycling that might occur. It must also generate enough turbulence in the gas to give good heat transfer between the tube wall and the body of the catalyst<sup>7</sup>.

Obvious, possible simple shapes are pellets, spheres, rings and various extrusions in the shape of tubes, cylinders, rods and bars of different sizes and cross sections (Fig. 1. 23).

For reforming it has been found that a thick-walled ring meets all of the above criteria, and the dimensions most commonly used are a diameter of 17 mm with lengths of 17 mm, 10 mm and even 6 mm. If the outside dimensions of the ring are reduced, then an equivalent packed volume will have an increase of pressure drop and slightly higher activity resulting from the larger geometric surface area.

By using different ratio of the various sized catalyst, it is possible to balance gas flows through individual reformer tubes and to compensate for asymmetric heat fluxes in the furnace<sup>7</sup>.



Fig. 1. 23 - Different shapes and forms for steam reforming catalysts.

To enhance steam reformer performances a possible route can be to modify catalyst shape rather than changing the fundamental chemistry of the support or the catalytically active phase.

The two main objectives are to reduce pressure-drop across the reformer, and/or lower tube wall temperatures (particularly in the region of maximum heat flux) via increased activity through higher geometric surface area and heat transfer properties. The major benefits that can be obtained are either longer life or the possibility of increased throughput, or a combination of both effects<sup>7</sup>.

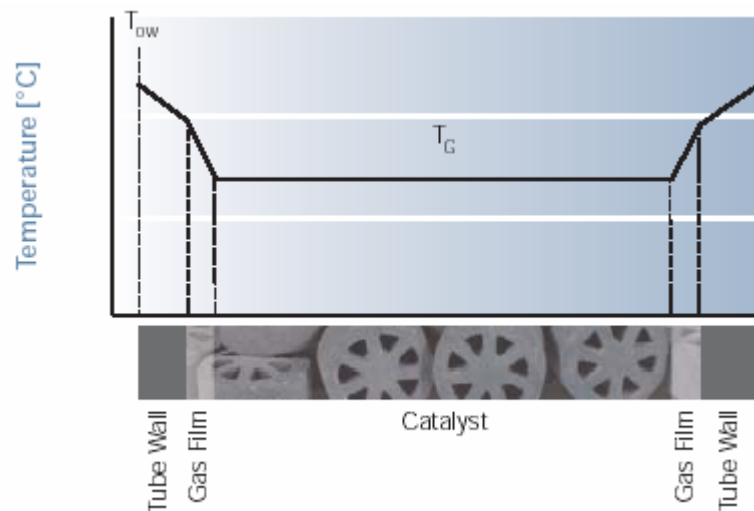


Fig. 1. 24 - Radial temperature profile – top fired furnace / 40 % down the tube.

In designing shaped steam reforming catalysts a number of factors have to be taken in account. These include the packing characteristics of the catalyst particles in relatively narrow tubes, pressure drop, geometric surface area, heat transfer properties and physical strength. Whilst some of these properties may be enhanced with a particular shape, others may be diversely affected. For example, some high geometrical surface area shaped particles tend to bridge across the tube walls when they are being charged, and this makes uniform packing difficult. Subsequently, when the reformer is running, this problem can lead to severe hot spots at regions where there is little catalyst in the tube. Other high geometric surface area shapes may have low strength. A further consideration is the pattern of breakage of the catalyst particles. If a ring breaks, it is preferable that forms two large pieces, which do not cause a detrimental increase in pressure drop. However, with shapes having open structures there is the danger of them shattering into a number of small pieces when they break and these can give rise to a high-pressure drop<sup>7</sup>.

### **2.1.7. Practical aspects of steam reformers**

Although steam reforming is the most mature and the best established technology for hydrogen production, the continuous research on reforming catalysis, reactor engineering, and process modeling brought several improvements in the new installed plants.

A typical design for a SMR reactor and a scheme for the whole process of hydrogen production are presented in Fig. 1. 25. For this kind of endothermic process, the catalyst is usually loaded into a number of tubes and placed inside of a furnace. There are several factors that are of fundamental importance in the reformer design: i.e., the geometry and number of single reformers; the heat transfer from the burners to the reforming units; and the catalyst design, including its intrinsic activity and physical properties (size, form, etc.)<sup>37</sup>.

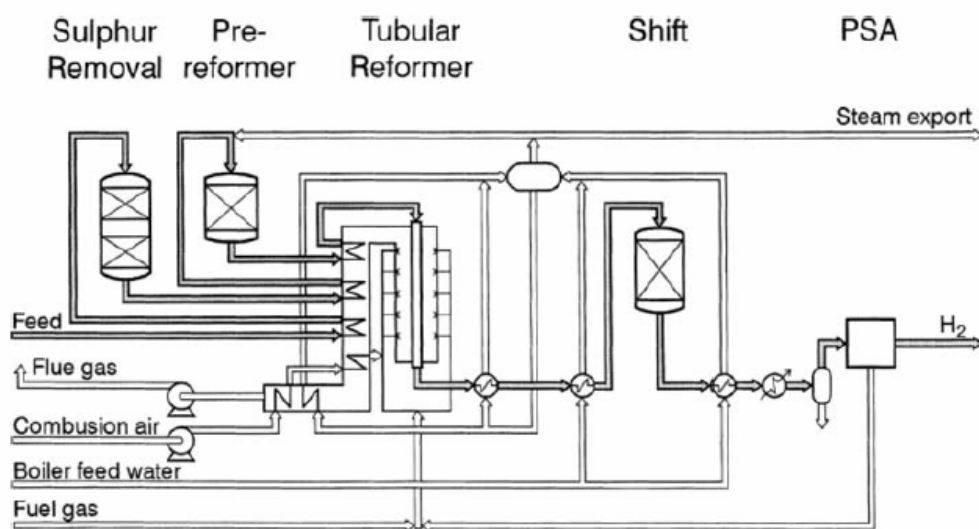


**Fig. 1. 25 - Typical process layout for a hydrogen plant based on advanced tubular steam reforming technology. The hydrogen is purified by shift conversion followed by pressure swing adsorption (PSA) to delivery pressure<sup>37</sup>.**

The primary reformer consists essentially of two main sections: the furnace, containing the tubes charged with the catalyst, and the convection section, where heat is recovered from the flue gas by such duties as preheating feedstock, process air and/or combustion air, boiler feedwater heating and steam raising, and super heating.

The steam reforming reactions are usually carried out at a pressure up to 35 bar and temperatures of 800°C or higher, while the flue gas may reach a temperature in excess of 1000°C. Consequently, the design of the primary reformer is complex and depends on the duty and on the philosophy of the chemical contractor engineering the plant. The furnace can be top-fire, terrace wall-fire or side-fire, and in the case of small hydrogen plants it can be of a bottom-fired design<sup>37</sup>.

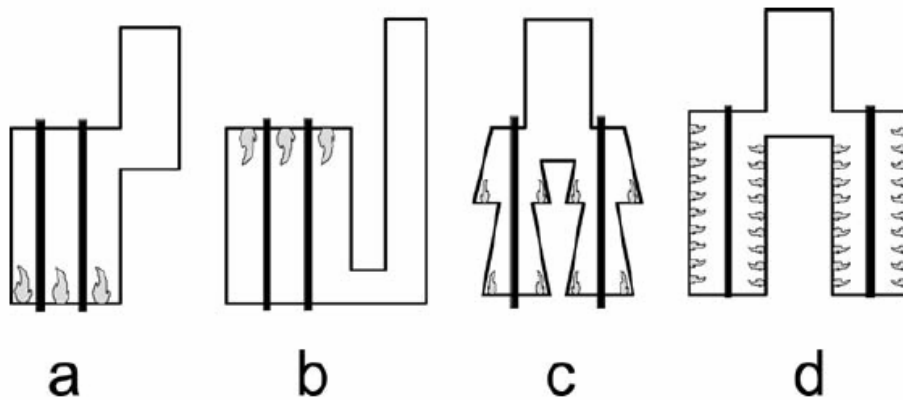


Fig. 1. 26 - Typical configurations of reformer furnaces: a) bottom fired, b) top fired, c) terrace wall, d) side fired<sup>37</sup>.

Typical throughput, which is usually expressed as the amount of steam plus feedstock per hour per liter of catalyst, is in the range 2-7 Kg h<sup>-1</sup>l<sup>-1</sup>. The overall length of reformer tubes is usually in the range 7.5 – 12.0 m although the heated charged length may be up to 9.0 m; tube diameter usually lies between 7 cm and 13 cm. The number of tubes depends on output, and for a large reformer there may be as many as 650 tubes<sup>7</sup>.

Conventional steel tubes do not possess the material characteristics to withstand the pressure and temperature at which a modern reformer operates. A suitable cost-effective material is a chromium/nickel alloy with the following composition: Cr 24-28 %, Ni 18-22%; C 0.35-0.45%; Mn 2 %; Si 2 %; P and S 0.05 %. The melting point of the alloy is close to 1370°C, and it is suitable for use at temperatures up to 1150°C. Other materials such as Pyrotherm G24/24 Nb and Manaurite 36X can also be used, since they allow operation of the reformer at higher temperatures and pressures. However, they are more expensive<sup>7</sup>.

If the diameter of the tube is too large, heat transfer to the catalyst in the centre of the tube will be restricted and the reaction rate limited. On the other hand, if the tube diameter is too small the pressure drop will be high.

In operation, there is a gradation of temperature longitudinally from the inlet to the outlet of the tube, as well as radially across the wall of the tube. Creep occurs with time at normal operating conditions. The temperature which the tube wall experiences depends on the distribution of heat input and the heat adsorbed by the reaction taking place on the catalyst in the tubes. Uneven heat input uneven catalyst activity caused by uneven packing or catalyst poisoning will cause local

overheating, resulting in excessive creep in that location, which will hasten tube rupture. Normally reformers are designed with a tube life of about 10 years using creep strength data based on creep-rupture tests of varying duration available from a number of sources<sup>7</sup>.

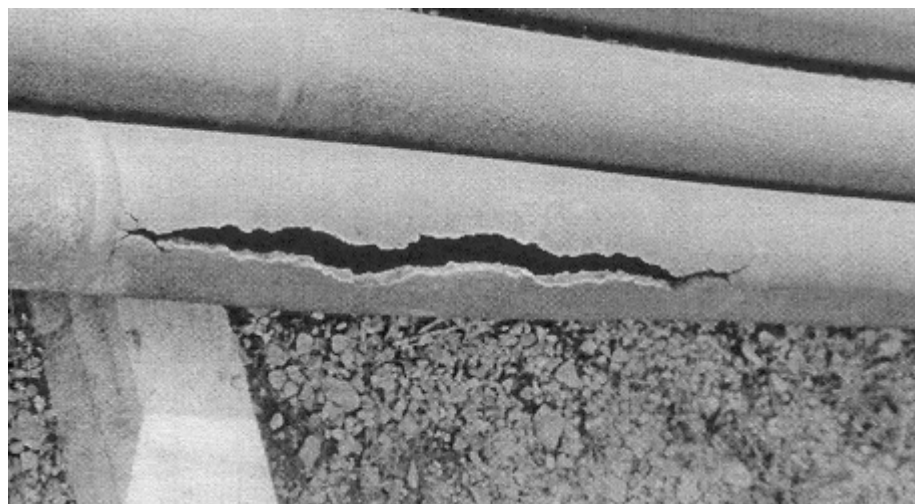


**Fig. 1. 27 - Creep occurred in a reforming tube.**

The higher the temperature and pressure are, the greater the creep and the shorter the tube life. This applies to all parts of each tube, and if part of any tube is subjected consistently to higher-than-average temperatures, it will fail prematurely. It is therefore important that hot spots, due to catalyst poisoning or carbon deposition, are removed as soon as possible<sup>7</sup>.

Other practical aspects of steam reformers are:

- Reactant gas distribution (both steam/feedstock and fuel for the burners)
- Firing the reformer
- Expansion and contraction of reformer tubes
- Facilities to charge and discharge catalyst
- Designing a reformer for efficient operation
- Catalyst reduction (with hydrogen, with ammonia, with methanol, with natural gas or other hydrocarbons)

The life of a catalyst can be affected by the following factors: *catalyst breakdown, tube blockage, overheating of the catalyst, poisoning of the catalyst, and thermal ageing.*

Catalyst breakage and blockage of the tubes causes an increased pressure drop across the reformer, and if the effect is random, it shows as an uneven appearance of the tubes in the furnace. More fundamentally, it can lead to overheating of the catalyst, loss of activity and a reduction of throughput. All of these effects may be caused by the deposition of carbon. Overheating of the catalyst can also be caused by maloperation of the reformer. Loss of activity through poisoning by contaminants in the process gas is important, since this can cause carbon deposition and result in overheating, catalyst breakage and, in extreme cases, even partial blocking of the tubes. Gradual loss of activity or thermal ageing caused by progressive loss of nickel surface area through sintering places a limit on the life of a catalyst charge, and for a particular catalyst, this depends on the actual operating conditions. In practice, the most important effects are catalyst sintering, catalyst poisons and carbon formation<sup>7</sup>.

Carbon can be deposited in primary reforming catalyst by different mechanisms and to varying degrees. Complete loss of reaction steam results in a massive deposit of carbon, and the reformer will develop a very large pressure drop within a few seconds. It will not then be possible to run the reformer again without replacing the catalyst. Running a reformer with a slightly deficient steam/carbon ratio will result in slight carbon deposition, which will slowly increase the reformer pressure drop, and the tubes will appear hotter than normal. If detected soon enough this carbon can often be removed satisfactorily, but this depends on the type of catalyst being employed. Removing the feed flow and sustaining normal reformer temperatures with only steam and hydrogen will convert the carbon to carbon dioxide, which can be detected by an analyzer at the reforming exit. The hydrogen will keep the catalyst in a reduced form. When the carbon has been deposited within the catalyst pores by carbon monoxide disproportionation, steaming will increase the reformer pressure drop. In this case, the carbon expands within the catalyst pores and cracks the pellet and, although the carbon in situ retains the pellet strength, when the carbon is removed, the pellet collapses. If this happens, it is necessary to change the catalyst<sup>7</sup>.

Slow deposition of carbon can occur for a number of reasons. Careful catalyst formulation is essential to maximize selectivity, and to eliminate acid sites, which can promote carbon formation. When a predominantly methane feedstock is reformed, low catalyst activity in the inlet portion of the tube can lead to carbon deposition, which restricts heat transfer and give rise to the phenomenon known

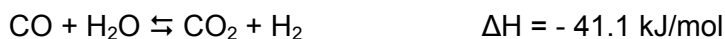
as “hot bands”. Both the CO disproportionation and reduction reactions are always in the carbon-free side of the equilibrium throughout the reformer tube, regardless of catalyst activity. However, the methane cracking reaction is on the carbon forming side equilibrium for a significant portion of the tube. Carbon is not, however, produced at the lower temperatures near the inlet, because both reactions which remove carbon (reverse CO disproportionation and reverse CO reduction) are faster at these temperatures than the rate of carbon formation by methane cracking. However, as the temperature increases, so does the rate of carbon formation and at a temperature of about 650°C, the carbon forming reaction becomes faster than the carbon removing ones. If the rates of these reactions are fixed, then it is essential that the catalyst has enough activity to produce sufficient hydrogen via steam reforming below this temperature, so that the gas composition lies on the carbon removal side of the methane cracking equilibrium<sup>7</sup>.

“Hot bands” always format about the same position on all tubes in the furnace and approximately the same position in all reforming furnaces.

As expected, heavily loaded top-fired furnaces are the most susceptible to forming “hot bands”. The low catalyst activity can arise from a number of causes – catalyst may be old and at the end of its useful life, it may be poisoned or inadequately reduced. If no hydrogen is recycled with the feedstock, then the catalyst in the inlet portion remains in the oxidized state until reforming or cracking of the feedstock occurs, and produces some hydrogen. This increases the load on the catalyst further down the tube, since the inlet portion is then functioning simply as a heat exchanger. Further, if reformer conditions change, then unreduced catalyst may be called upon to do some reforming. It will be unable to do so, carbon will be deposited and hot areas will appear at the top of the tubes<sup>7</sup>.

### 2.1.8. Water gas shift reaction (WGS)

The water gas shift reaction is moderately exothermic and hence its equilibrium constant decreases with temperature and high conversions are favored by low temperatures. The water gas shift reaction is:



The position of equilibrium is virtually unaffected by pressure. As expected, additions of greater than stoichiometric quantities of steam improve conversion. Under adiabatic conditions, conversion in a single bed of catalyst is thermodynamically limited – as the reaction proceeds the heat of reaction increases the operating temperature, and so restricts of the conversion are possible. Typical carbon monoxide levels that are achieved at the exit with a single adiabatic bed of chromia-supported iron-based shift catalyst in an ammonia plant are in the range 2-4 %, and because it is necessary to operate these catalysts at high inlet temperatures (typically in the range 370-400°C) they are known as high temperature (HT) shift catalysts<sup>7</sup>.

The thermodynamic equilibrium limitation on the reaction can be reduced by using two or more beds of HT shift catalyst with inter-bed cooling and, perhaps, removal of carbon dioxide between the stages. In this way, it was possible in the late 1950s to decrease the thermodynamic limitation, and achieve carbon monoxide levels of less than 1 % at the exit. The limitation on conversion was then catalyst activity.

When a single stage or two stages of HT shift were used, the final carbon monoxide removal stage was generally absorption in copper liquor, although some plants used a methanator, because of the simplicity of the process, and accepted the attendant hydrogen loss. At this time, attempts were made to improve the carbon monoxide conversion so that methanation could be used more economically as a means of removing the remaining traces of carbon oxides. This impetus led to the development and introduction of copper-based shift catalysts in the early 1960s<sup>7</sup>.

A significant improvement in the conversion of the carbon monoxide could then be obtained with two-bed operation, with the second bed operating at the lowest possible inlet temperature, which in practice was dictated by the dew-point (about 200°C). The conventional iron based catalysts are not sufficiently active for such low temperature operation, but copper based water gas shift catalyst are, and

when they are used in the second bed, carbon monoxide exit concentrations as low as 0.1-0.3 % can be achieved, which is an acceptable economic level for subsequent methanation. These copper-based catalysts are known as low temperature (LT) shift catalysts.

In this arrangement, it is necessary to lower the temperature of around 200°C, which is suitable for the inlet of the LT shift catalyst. Inter-bed cooling is usually achieved by heat exchange, which, depending on the steam pressure levels in the plants, may be used to heat boiler feedwater or to raise steam. In some cases, the temperature may also be trimmed by injecting either steam or condensate into the process gas. In such plants, the life of the LT shift catalyst may be shortened because of physical damage from entrained water droplets or because of the presence of catalyst poisons in the water itself<sup>7</sup>.

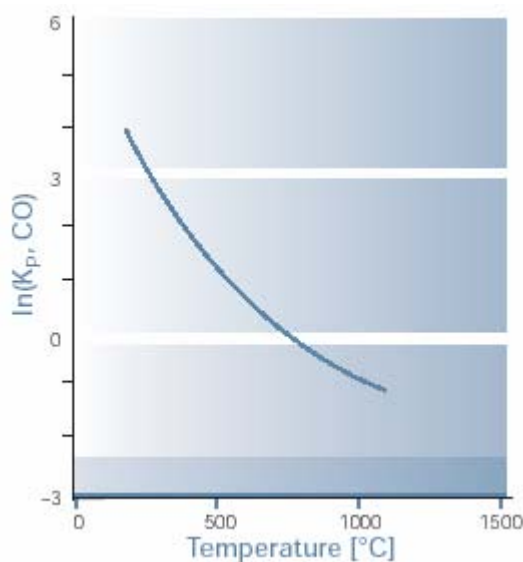


**Fig. 1. 28 - Water gas shift reaction: equilibrium constant**

Numerous studies of the kinetics of the water gas shift reaction over iron oxide/chromia catalysts have been reported and more than 20 different kinetic equations have been proposed. Differences among authors have been especially marked in their opinion of the reaction mechanism, and the effect of pressure on the reaction rate. The reasons for this conflict have been attributed to the presence of impurities in the gases used, to varying degrees of mass transfer limitation and to the fact that kinetic measurements have been mostly obtained

with integral rather than differential reactors, which were often only operating at or near atmospheric pressure<sup>7</sup>.

The importance of mass transfer effects in the reaction over a commercial catalyst was assessed and the conclusions obtained were:

1. the activation energy in the absence of diffusion effects for the water gas shift reaction over iron oxide / chromia catalyst is 121.8 kJ/mol
2. the reaction over 5.4 x 3.6 mm pellets is not pore diffusion limited at temperatures below 370°C and at pressure up to 31 bar. Over larger pellets, 8.5 x 10.5 mm, the reaction becomes diffusion limited at temperature above 350°C at 31 bar pressure.

Fewer publications have appeared on the mechanism and kinetics of the water gas shift reaction over copper based catalysts than over high temperature iron based catalysts, but similar types of kinetic expressions have been proposed. Indeed, the pore diffusion limited version of the Langmuir-Hinshelwood equation for copper-based shift catalysts is consistent with plant data and semi-technical scale results. There is little doubt that the copper LT shift catalysts generally operate in a pore-diffusion limited regime, although there is debate over the extent of this limitation on typical industrial catalyst pellets. In addition, they are often self-guarding with respect to poisons (sulphur and chlorine compounds). The pick-up of which is evidently a very rapid process and may itself also be pore-diffusion limited.

The mechanism of the catalyzed shift reaction remains in dispute for copper and iron-based catalysts. Briefly, two types of mechanism have been proposed – adsorptive and regenerative.

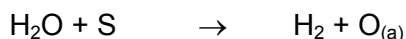
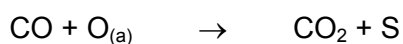
In the former mechanism, reactants adsorb on the catalyst surface, where they react to form surface intermediates such as formate, followed decomposition to products and desorption from the surface.

In the regenerative mechanism, the surface undergoes successive oxidation and reduction cycles by water and carbon monoxide, respectively, to form the corresponding hydrogen and carbon dioxide products of the water gas shift reaction.

Dealing first with iron oxide/chromia catalysts, the adsorption mechanism has been supported by tracer studies and apparent stoichiometric number analyses. Unfortunately, however, the kinetics of the water gas shift reaction can equally

well be described either by the adsorptive mechanism or by the regenerative mechanism, which was first proposed. Support for the regenerative mechanism is that the rate at which water oxidized the magnetite surface and carbon monoxide reduces it, corresponds to the rate of the water gas shift reaction. In an in situ gravimetric study of oxygen removal from and incorporation into magnetite/chromia catalyst in CO<sub>2</sub>/CO and H<sub>2</sub>O/H<sub>2</sub> gas mixtures at about 350°C further supported the regenerative mechanism.

For the copper based LT shift catalysts the regenerative mechanism was rejected on the basis that neither cupric nor cuprous oxide could be formed under reaction conditions from copper metal and steam. An adsorptive mechanism with a surface formate intermediate was proposed. However, an analysis of transient kinetics of the shift reaction over a Cu/ZnO catalyst supports the regenerative mechanism. With both Cu/ZnO/Al<sub>2</sub>O<sub>3</sub> catalysts and unsupported polycrystalline copper catalysts, it was also produced results consistent with the regenerative mechanism. The occurrence of the four separate steps needed for both forward and reverse reaction shown in the following equations (in which S is a vacant site) has been demonstrated on copper.



For oxygen coverage of half-monolayer or less there is no equilibrium limitation to the second reaction, in contrast with the equivalent reaction forming cuprous oxide, so that objection to regenerative mechanism is invalid for adsorbed oxygen formation. Therefore, it seems likely that the water gas shift reaction proceeds by the same regenerative mechanism on both Fe<sub>3</sub>O<sub>4</sub>/Cr<sub>2</sub>O<sub>3</sub> and Cu/ZnO/Al<sub>2</sub>O<sub>3</sub> catalysts.

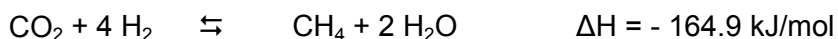
The catalyst used for HT-WGS duty consists of magnetite crystallites stabilized with the addition of a small amount of chromia, although fresh unreduced catalyst contains hematite (Fe<sub>2</sub>O<sub>3</sub>) 90-95% with 5-10% Cr<sub>2</sub>O<sub>3</sub>.

Iron based catalysts are not very sensitive to poisoning by sulphur, which is commonly present in feed gas derived from coal or fuel oil, and if the catalyst must be operated under highly sulphiding conditions the deactivated effect can be compensated for by increasing the volume of catalyst used.

Magnetite (Fe<sub>3</sub>O<sub>4</sub>) has good activity for the reaction at moderately high temperatures and, provided the magnetite crystallites are stabilized by the

addition of a refractory oxide component such as chromia ( $\text{Cr}_2\text{O}_3$ ), satisfactory long lives are obtained.

The formulation of LT shift catalyst is important in terms of selectivity and resistance to poisoning, as well as activity. Selectivity is important because under LT shift conditions methanation of both carbon monoxide and carbon dioxide is thermodynamically very favorable:



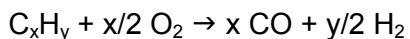
If these reactions take place to any extent, then valuable hydrogen would be consumed; in addition, since they are very exothermic they could give rise to dramatic and dangerously destructive rises in temperature.

Copper based catalyst have good activity for the water gas shift reaction, and have no methanation activity so they are well suited for use in water gas shift duties.

Alumina together with zinc oxide was a desirable support that could significantly stabilize the copper crystallite against thermally induced sintering, and also enhanced the strength of the catalyst and minimize shrinkage during reduction.

## 2.2. Partial oxidation of fossil fuels (POX)

The other major route to hydrogen is non-catalytic partial oxidation of fossil fuels, often referred to as POX (or gasification). One key advantage of this approach is that it accepts all kinds of hydrocarbon feeds. The thermal oxidation is run at 30-100 atm with pure O<sub>2</sub> using a special burner inside a refractory lined vessel at ~1300°C. The general reaction is described by:



There are several plants that produce hydrogen by the partial oxidation of hydrocarbons. In the non-catalytic process, a mixture of oxygen and natural gas is pre-heated, mixed and ignited in a burner. In the absence of catalyst, the reactor temperature must be high enough to reach complete CH<sub>4</sub> conversion. Combustion products like CO<sub>2</sub> and H<sub>2</sub>O are also formed to a certain extent. Subsequently, endothermic reaction as steam reforming is also involved, which determine the outlet temperature in the order of 1000-1200°C. At this stage, the gas composition is near thermodynamic equilibrium. According to the stoichiometry of reaction the consumption of O<sub>2</sub> should be, in the absence of combustion products, approximately 0.5 O<sub>2</sub>/CH<sub>4</sub>. However, actual use requires O<sub>2</sub>/CH<sub>4</sub> ratio of about 0.7. It appears that if the reactor in principle is simple, the cost of an oxygen plant is considerable. One advantage of this process is that it can work at high pressures, thereby saving costly compressors. Some carbon is formed by the thermal cracking of methane and has to be removed by washing. The outer reactor walls are cold being insulated on the inside. Using this technology, Texaco and Shell commercialize this conversion process<sup>41</sup>.

In non-catalytic partial oxidation process, steam is not used as a feed, but with higher hydrocarbon feeds there can be a lot of coke as by-product. Since conditions are maintained net reducing, no NO<sub>x</sub> or SO<sub>x</sub> are produced; however, if the feed contains any sulfur compounds, H<sub>2</sub>S and COS are by-product which must be scrubbed. A clear disadvantage is the need to have huge quantities of O<sub>2</sub> available continuously, thus requiring the substantial investment in an adjoining O<sub>2</sub> plant<sup>41</sup>.

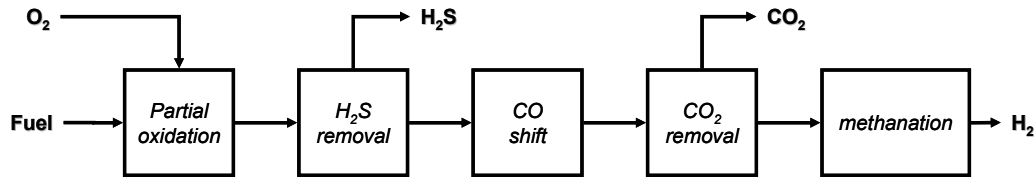


Fig. 1. 29 - Block diagram of the whole non catalytic partial-oxidation of methane.

Methane is reacted with  $O_2$  in a flame, then after desulphurization, the WGS reaction is used to shift essentially all CO to  $H_2$ , and  $CO_2$  is removed. If complete removal of residual CO and  $CO_2$  is required, methanation on a Ni catalyst can reduce carbon oxides to less than 10 ppm (Fig. 1. 29)<sup>41</sup>.

Since CO is also a co-product, one has to use high temperature water gas shift to convert CO with steam to  $H_2$ . Additional unit operations are required for gas purification (largely to remove  $H_2S$ ) and to remove soot from the waste water. In addition, the  $CO_2$  can be removed by adsorption, and final traces of CO destroyed by follow-up methanation. Thus POX operations can get quite complex, and in comparison to SMR they are less energy efficient, while eliminating more  $CO_2$  co-product<sup>39</sup>.

In the Fig. 1. 30 it is only shown part of the POX process, steam must also be generated and the product  $CO/H_2$  must also be purified. A strong feature of POX technology versus SMR is that the former is a very attractive process when dealing with the increasing amounts of bottom-of-the-barrel feedstocks. It was estimated that the thermal efficiency of a POX plant feed with heavy hydrocarbons to be ~ 70 % versus 81 % with SMR. Secondary reforming with added  $O_2$  is used in some operations employing SR technologies, especially in connection for the high  $H_2$  demands of ammonia synthesis. In the exothermic, secondary reforming, air is added to the effluent of the primary reformer. The residual methane reacts with the air providing heat for this CO producing reaction, and the unreacted  $N_2$  is used for  $NH_3$  synthesis<sup>39</sup>.

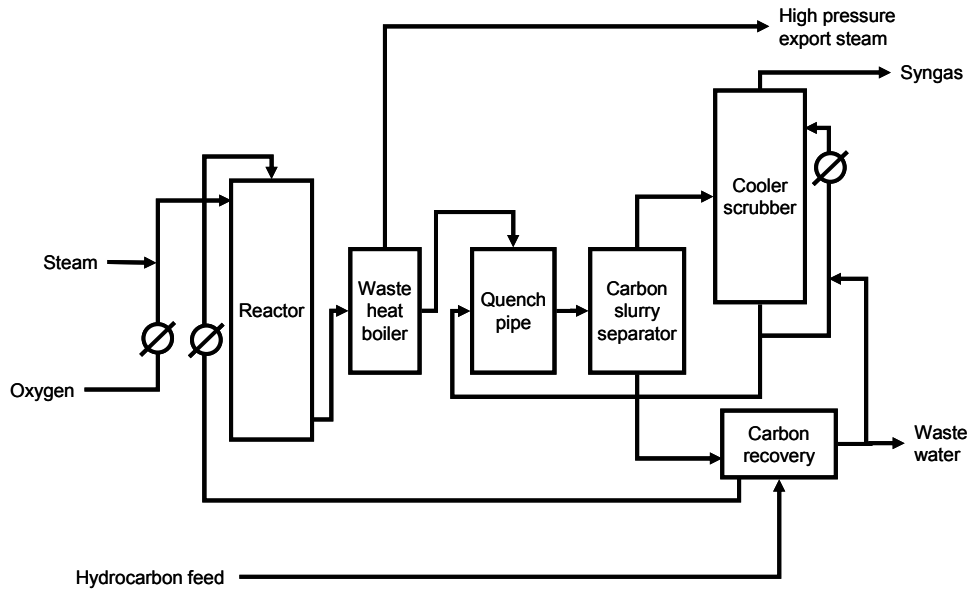


Fig. 1. 30 - Process flow diagram for POX.

### 2.3. Autothermal reforming (ATR)

An alternative approach to POX and SMR is autothermal reforming (ATR), which is a combination of both technologies.

This process was developed by Haldor Topsoe in the late 1950s with the aim of performing reforming in a single reactor. In autothermal reforming, the energy for the production of CO and H<sub>2</sub> is produced by partial oxidation of the hydrocarbon feedstock. Like POX, the feeds first react in a large refractory lined vessel with O<sub>2</sub> for non-catalytic combustion at 1200-1250°C. If the product H<sub>2</sub> is intended for NH<sub>3</sub> production, an air feed could be used.

The reformer basically consists of a ceramic lined tube and a fixed catalyst bed for equilibration of the gas. The preheated streams (CH<sub>4</sub> + H<sub>2</sub>O and H<sub>2</sub>O + O<sub>2</sub>) are mixed in a burner placed at the top where the POX reactions take place. The final steam reforming and equilibration take place in the catalyst bed below the burner. Typically, the ATR operates at high temperatures ca. 1200-1300°C in the combustion zone and 950-1200°C in the catalytic zone. This results in a lower oxygen consumption (O<sub>2</sub>/CH<sub>4</sub> = 0.55-0.60), however, with a certain amount of steam added to the feedstock to eliminate carbon formation. Carbon and soot formation in the combustion zone is an undesired reaction, which leads to carbon

deposition on downstream tubes causing equipment damage, pressures losses and heat transfer problems.

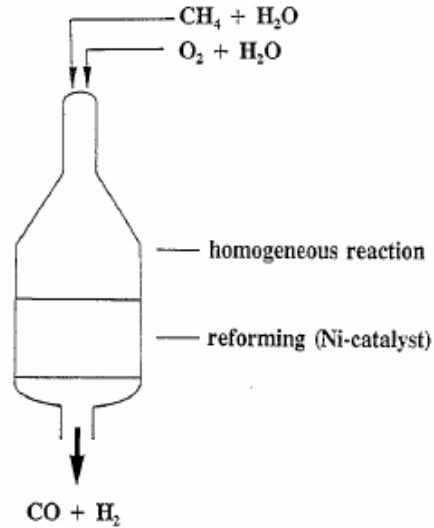


**Fig. 1. 31 - Autothermal reformer.**

Although the ATR was originally used to maximize  $\text{H}_2$  production in ammonia plants, it can be applied in the production of CO rich gases. In all cases, the  $\text{H}_2/\text{CO}$  ratio at the outlet of the reactor can be precisely adjusted by varying the  $\text{H}_2\text{O}/\text{CH}_4$  and/or  $\text{O}_2/\text{CH}_4$  molar ratios in the feed.

Since autothermal reforming uses less  $\text{O}_2$  than POX, the economics are less sensitive to the price of  $\text{O}_2$  when  $\text{O}_2$  is cheap. It requires no external fuel while offering some flexibility in feedstock.

## 2.4. Catalytic partial oxidation of methane (CPO)

A new interesting process for conversion of methane into synthesis gas is catalytic partial oxidation. In the 1940s, Prettre et al first reported the formation of synthesis gas by the catalytic partial oxidation of CH<sub>4</sub>:



They used a Ni-containing catalyst. In contrast to steam reforming of methane, methane partial oxidation is exothermic. However, the partial oxidation requires pure oxygen, which is produced in expensive air separation units that are responsible for up to 40% of the cost of a synthesis gas plant (in contrast, the steam reforming process does not require pure oxygen)<sup>87</sup>.

In the early 1990s, several papers<sup>88, 89, 90, 91, 92</sup> reported that one can reach CO and H<sub>2</sub> concentrations in excess of those expected at thermodynamic equilibrium by operating the CH<sub>4</sub> oxidation reaction at exceptionally high space velocities (GHSV = 52,000 ml (g catalyst)<sup>-1</sup> h<sup>-1</sup>) in a fixed-bed reactor. The following catalysts were employed: Ni/Yb<sub>2</sub>O<sub>3</sub>, Co/rare earth oxide, Co/MgO, and Ni/Al<sub>2</sub>O<sub>3</sub>.

According to the partial oxidation reaction, such a process yields the desired H<sub>2</sub>/CO molar ratio of 2 required for methanol or Fischer-Tropsch synthesis. From thermodynamic simulations, it is clear that the reaction is favored at T > 850°C in excess of CH<sub>4</sub>, although both CO and H<sub>2</sub> selectivities are modified by the formation of CO<sub>2</sub> and H<sub>2</sub>O in combustion reactions which are much more exothermic:



Since CPO reaction is slightly exothermic, a process based on this reaction would be much more energy efficient than the energy intensive SMR process. In addition the partial oxidation reaction is also much faster than the reforming reactions, suggesting that a single stage process for syngas production would be an attractive alternative to SMR and also results in smaller reactors and higher productivity.

The direct oxidation has not been developed at industrial scale, and it is difficult to study because it involves co-feeding CH<sub>4</sub>/O<sub>2</sub> mixtures and reaction close flammable or even explosive conditions.

Local hot spots are usually formed which can irreversibly damage the active catalyst. Moreover, the gas phase reactions in a high reducing atmosphere can lead to carbon and soot deposition over the catalyst surface.

The actual reaction temperatures could be much higher than those reported. By using an optical pyrometer, it was found that, during the catalytic oxidation of methane to CO and H<sub>2</sub>, the combination of a high space velocity, an exothermic reaction, and an active catalyst (Ni/Yb<sub>2</sub>O<sub>3</sub>) gave rise to steep temperature gradients (hot spots). Furthermore, the temperature of the hot spot was greater by as much as 370°C than the temperature measured with a thermocouple located at a distance of only 1 mm from the hot spot in the catalyst bed. If a temperature lower than that of the hot spot is used to calculate the equilibrium concentrations of CH<sub>4</sub>, CO, CO<sub>2</sub>, and H<sub>2</sub>, one can draw the conclusion that the concentrations of CO and H<sub>2</sub> exceeded their thermodynamic equilibrium values. However, if the true maximum (hot spot) temperature is used in the calculation, the observed concentrations are found to be somewhat less than those predicted at equilibrium. Indeed, using a careful temperature measurement method, in which a thermocouple end contacted just the top surface of the catalyst bed, it was found that the CH<sub>4</sub> conversion in the presence of Ni/Al<sub>2</sub>O<sub>3</sub> catalyst was less than that predicted by thermodynamic equilibrium.

Furthermore, Hu and Ruckenstein<sup>93</sup> observed hot layers (thinner than 1 mm) in NiO/MgO solid solution catalysts and in NiO/Al<sub>2</sub>O<sub>3</sub> and NiO/SiO<sub>2</sub> catalysts during the partial oxidation of methane in a fixed-bed reactor. The hottest layers were located at the top of the bed of the NiO/MgO and NiO/Al<sub>2</sub>O<sub>3</sub> catalysts, but they were observed to move down and then up for the NiO/SiO<sub>2</sub> catalyst bed. The down-and-up movement resulted in an oscillatory temperature of the NiO/SiO<sub>2</sub> catalyst at a given position in the bed, which was absent when the catalyst was NiO/MgO or NiO/Al<sub>2</sub>O<sub>3</sub>.

The different temperature behaviors of the three catalysts were attributed to the different strengths of the interactions between the metal oxide and the support. Temperature-programmed reduction (TPR) experiments with 4% H<sub>2</sub> in argon indicated that the initial reduction temperature was about 330°C for 13.6 wt % NiO/SiO<sub>2</sub>, which is near that of pure NiO (about 300°C). In contrast, for 13.6 wt % NiO/Al<sub>2</sub>O<sub>3</sub> the initial reduction temperature was high (670°C) and no marked reduction peak could be detected even at 800°C for 13.6 wt % NiO/MgO. These

results clearly indicate that there are weak interactions between NiO and SiO<sub>2</sub> and much stronger interactions between NiO and Al<sub>2</sub>O<sub>3</sub> and between NiO and MgO. The weak interactions in Ni/SiO<sub>2</sub> might have been responsible for the temperature oscillation by allowing a facile redox behavior of the active nickel sites, namely, the oxidation of Ni<sup>0</sup> to NiO by O<sub>2</sub> and the reduction of NiO to Ni<sup>0</sup> by CH<sub>4</sub>. The strong interactions characteristic of NiO/Al<sub>2</sub>O<sub>3</sub> and NiO/MgO were inferred to inhibit in part the redox behavior of the nickel sites. In the case of NiO/SiO<sub>2</sub>, according to this interpretation, the freshly reduced NiO located at the inlet of the bed became highly active, causing a hot layer to be generated. The high temperature of this hot layer resulted in sintering of the nickel particles, which led to the loss of activity. Therefore, the reaction is inferred to have taken place in the neighboring section of the catalyst. As a result, a hot layer propagated downward in the reactor. However, the sintered nickel particles were re-dispersed on the SiO<sub>2</sub> support when they were re-oxidized by O<sub>2</sub>, because the oxygen concentration is high when the reaction of CH<sub>4</sub> with O<sub>2</sub> does not take place. After a certain time, the re-oxidized layer near the entrance was again reduced by CH<sub>4</sub> and became active again, resulting in a hot layer. The following part of re-oxidized nickel on SiO<sub>2</sub> can be reduced rapidly by H<sub>2</sub> and CO generated near the entrance of the reactor. The redox of the Ni/SiO<sub>2</sub> catalyst constitutes a cycle of deactivation and reactivation in each part of the catalyst. The hot layer moved downward in the bed during the time required for the reduction of the entrance layer. Consequently, the time scale of the oscillations was determined by the time scale of the reduction–oxidation process.

Furthermore, Basile et al.<sup>94</sup> used IR thermography to monitor the surface temperature of the nickel foil during the methane partial oxidation reaction by following its changes with the residence time and reactant concentration. Their results demonstrate that the surface temperature profile was strongly dependent on the catalyst composition and the tendency of nickel to be oxidized.

In the 1940s, Prettre et al. reported the formation of synthesis gas via the catalytic partial oxidation of CH<sub>4</sub> catalyzed by a 10 wt % refractory supported nickel, at temperatures between 700 and 900°C. Thermodynamic equilibrium corresponding to the catalyst bed exit temperature was achieved under all conditions investigated. In 1970, it was examined the effect of diffusion on methane partial oxidation catalyzed by a single grain of Ni/mullite catalyst in the temperature range of 760 and 900°C and examined the ignition and extinction

characteristics of this catalyst. It was observed that the nickel catalyst deactivated in an oxidative environment but could recover on reduction. In 1984, Gavalas et al<sup>95</sup> investigated the effects of the calcination temperature, pre-reduction, and feed ratio on the reaction of CH<sub>4</sub>/O<sub>2</sub> mixtures catalyzed by NiO/ $\alpha$ -Al<sub>2</sub>O<sub>3</sub> at 570–800°C. However, under their experimental conditions, the main products were CO<sub>2</sub> and H<sub>2</sub>O. Since 1990, researchers have continued to examine nickel-containing catalysts for the partial oxidation of methane, and they also started to use noble metals as catalysts. In 1990, it was reported a methane conversion of about 90 % and more than 90 % selectivity to CO and H<sub>2</sub> at 770°C, atmospheric pressure, and at the high GHSV of 4 x 10<sup>4</sup> ml (ml catalyst)<sup>-1</sup> h<sup>-1</sup> for a reaction catalyzed by lanthanide ruthenium oxides, such as Pr<sub>2</sub>Ru<sub>2</sub>O<sub>7</sub>, Eu<sub>2</sub>Ru<sub>2</sub>O<sub>7</sub>, Gd<sub>2</sub>Ru<sub>2</sub>O<sub>7</sub>, Dy<sub>2</sub>Ru<sub>2</sub>O<sub>7</sub>, or Lu<sub>2</sub>Ru<sub>2</sub>O<sub>7</sub>. In 1992, Hickman and Schmidt<sup>96</sup> used platinum monoliths to achieve high selectivities to CO and H<sub>2</sub> in the partial oxidation of methane. In the following 10 years, various noble metal catalysts have been examined. Compared with the non-noble metal catalysts, the noble metals exhibit high stability with excellent activities and selectivities. The major drawback of the noble metal catalysts is their high cost, which restricts their potential use in industrial processes. Non-noble metal catalysts, particularly those containing nickel, have also been investigated extensively since 1990.

The authors observed that, under their operating conditions, the calcined catalyst bed consisted of three regions, NiAl<sub>2</sub>O<sub>4</sub> (upstream, section), NiO + Al<sub>2</sub>O<sub>3</sub> (middle section), and reduced Ni/Al<sub>2</sub>O<sub>3</sub> (downstream section). In the upstream section of the reactor, the CH<sub>4</sub>/O<sub>2</sub>/He feed contacted NiAl<sub>2</sub>O<sub>4</sub>, which exhibited only a moderate activity for the complete oxidation of methane to CO<sub>2</sub> and H<sub>2</sub>O. The next section of the reactor contained NiO + Al<sub>2</sub>O<sub>3</sub>, which catalyzed the complete exothermic oxidation of methane to CO<sub>2</sub>. Because of the complete consumption of O<sub>2</sub> in the second section, the third (downstream) section of the catalyst bed consisted of a reduced Ni/Al<sub>2</sub>O<sub>3</sub>. The formation of the CO and H<sub>2</sub> products, corresponding to thermodynamic equilibrium at the temperature of the bed exit, occurred in this section, as a result, of the reforming reactions of CH<sub>4</sub> with CO<sub>2</sub> and H<sub>2</sub>O produced during the complete oxidation reaction catalyzed by the NiO/Al<sub>2</sub>O<sub>3</sub>.

The activity of NiO in the total oxidation reaction was excluded by Basile et al<sup>94</sup> using IR thermography and evidencing the low temperature of oxidized Ni particles placed at the entrance of the bed.

Choudhary et al. reported a high conversion of CH<sub>4</sub> and high selectivities to CO and H<sub>2</sub> with Ni/CaO, Ni/Al<sub>2</sub>O<sub>3</sub>, NiO-rare earth oxide, and Co/rare earth oxide catalysts<sup>88, 89, 90, 91, 92</sup>.

The major problem encountered with these non-noble metal catalysts is their relatively low stability. The main causes of the deactivation of the catalysts are carbon deposition and metal sintering in the catalyst. Nevertheless, numerous effective nickel-containing catalysts have been developed by incorporation in suitable supports, such as La<sub>2</sub>O<sub>3</sub>, MgO, SrTiO<sub>3</sub>, and CeO<sub>2</sub>; effective promoters, including La<sub>2</sub>O<sub>3</sub>, Li<sub>2</sub>O, and iron oxide; and novel preparation methods, such as a solid phase crystallization method, a sol–gel method, and a citrate method<sup>87</sup>. However, because the high stabilities reported for these effective nickel-containing catalysts were based on short-term tests (< 100 h), it is unclear how stable these catalysts will be in long term tests (> 1000 h), which is the first step that any candidate catalyst for commercialization must pass.

In the last decade, numerous attempts have been made to understand the mechanism of the partial oxidation of methane. Mechanistic investigations of the partial oxidation are still challenging, because this exothermic reaction is very fast and causes extremely high catalyst temperature rises, so that the usual methods of investigation are unsuitable.

Two kinds of pathways have been suggested:

- (i) a combustion-reforming pathway, in which CO<sub>2</sub> and H<sub>2</sub>O are the primary products, and CO and H<sub>2</sub> are formed by their reactions with CH<sub>4</sub>,
- (ii) a pyrolysis or dissociative adsorption pathway, in which CO is the primary product formed by the dissociation of methane, CH<sub>4</sub> → CH<sub>x</sub> + (2 – 1/2 x) H<sub>2</sub>; followed by the oxidation of carbon containing species to give CO without the pre-formation of CO<sub>2</sub>.

For methane partial oxidation to syngas, the thermodynamic calculation results suggest a high temperature is advantageous for high methane conversion and selectivity to CO and H<sub>2</sub>. However, increasing the pressure in the reactor is unfavorable for CH<sub>4</sub> conversion and CO and H<sub>2</sub> selectivity. The prediction of the CH<sub>4</sub> conversion and product selectivity under specific conditions is shown in two-dimensional forms (Fig. 1. 32 (a) and (b)). Apparently, under 1 bar at 800°C, theoretical CH<sub>4</sub> conversion should be up to 90 %, and selectivities to CO and H<sub>2</sub>

are 97 %. At 8 bar and 800°C, CH<sub>4</sub> conversion is only 70 %, and CO and H<sub>2</sub> selectivities are around 85 %.

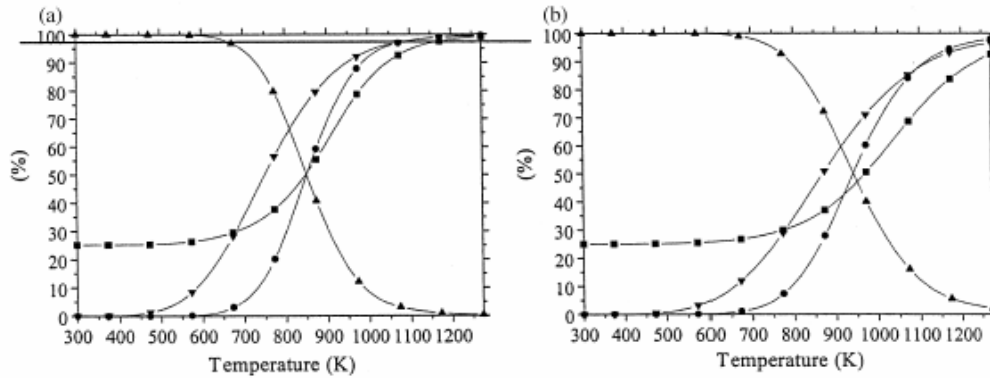


Fig. 1.32 - Thermodynamic equilibrium calculations at: (a) atmospheric pressure and (b) at 8 bar); (■) XCH<sub>4</sub>; (●) S[CO], (▲) S[CO<sub>2</sub>], (▼) S[H<sub>2</sub>]<sup>98</sup>.

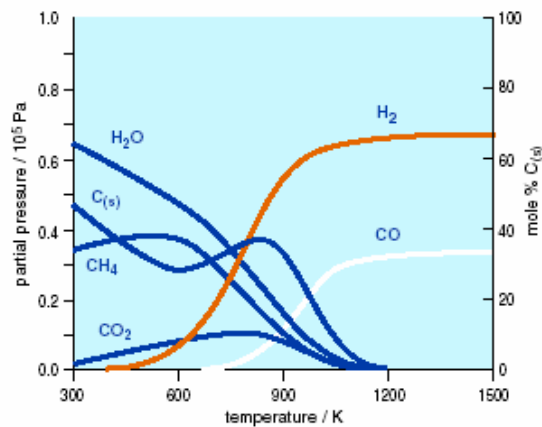


Fig. 1.33 - Composition of equilibrium mixture as a function of temperature when oxygen and methane are mixed in a 2/1 ratio<sup>97</sup>.

This process is likely to become more important in the future of methane conversion due to the thermodynamic advantages this process has over steam reforming:

1) Partial oxidation is mildly exothermic, while steam reforming is highly endothermic. Thus, a partial oxidation reactor would be more economical to heat. In addition, it can be combined with endothermic reactions, such as steam reforming or dry reforming with carbon dioxide to make these processes more energy efficient.

2) The H<sub>2</sub>/CO ratio produced in stoichiometric partial oxidation is around 2, and this ratio is ideal for downstream processes, in particular methanol and FT synthesis. This avoids the need to reverse shift hydrogen, which is produced in excess in steam reforming.

3) The product gases from methane partial oxidation can be extremely low in carbon dioxide content, which must often be removed before synthesis gas can be used downstream.

4) Partial oxidation technology avoids the need for large amounts of expensive superheated steam. However, an oxygen separation plant, which is also costly, may be required in cases where nitrogen (from air) is undesirable in high-pressure downstream processes.

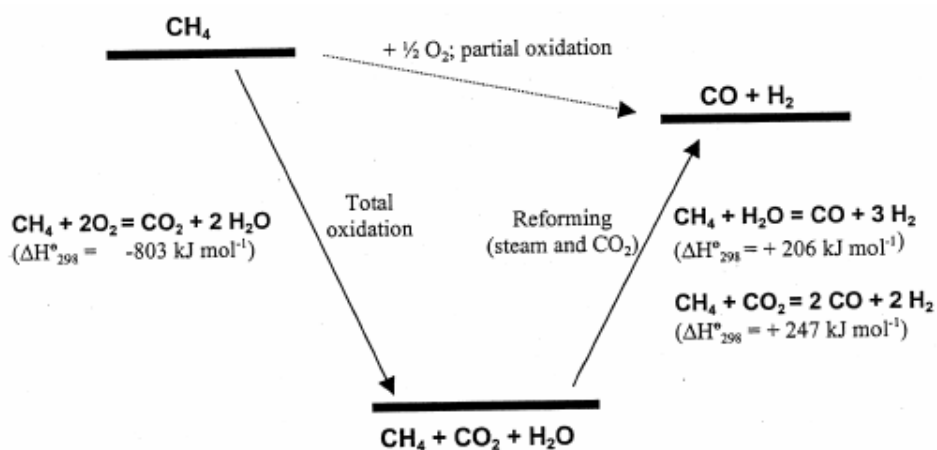


Fig. 1. 34 - Thermodynamic representation of the partial oxidation of methane<sup>98</sup>.

# EXPERIMENTAL SESSION

## 1. Catalysts preparation

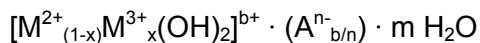
### 1.1. Perovskite type catalysts (PVK)

The perovskite type catalysts of general formula  $La_{(1-x)}Ce_xFe_{(1-y-z)}Ni_yRh_zO_3$  were synthesized in the laboratory using the following method, known as citrate method:

- 1) Preparation of aqueous solution (1 M) of the nitrate of the metals:
  - »  $La(NO_3)_3 \cdot H_2O$  (99.9 %),
  - »  $Ce(NO_3)_3 \cdot 6H_2O$  (99.5 % )
  - »  $Fe(NO_3)_2 \cdot 9H_2O$
  - »  $Ni(NO_3)_2 \cdot 6 H_2O$  (99 %)
  - »  $Rh(NO_3)_3$  (10 % solution)
- 2) Preparation of an aqueous solution (1 M) of citric acid, which act as ligand for increasing the solubility and as reducing agent;
- 3) The cation solution is dropped into the citric acid solution under vigorous magnetic stirring;
- 4) The final solution is placed in an electric oven and treated at 90°C for 4 h, then at 180°C for 12 h;
- 5) After grinding of the obtained precursor, the powder was calcined at 900°C (or in one case at 1100°C) in a muffle furnace for 12 h (heating rate 10°C/min)

## 1.2. Catalysts obtained from hydrotalcite type precursors

The hydrotalcite type precursors (HT) of general formula



with  $M^{2+} = Ni^{2+}$  and  $Mg^{2+}$

$M^{3+} = Rh^{3+}$  and  $Al^{3+}$

$A^{n-} = \text{silicate}$

were synthesized in the laboratory using the following coprecipitation method:

1) Preparation of aqueous solution (0.2 M) of the nitrate of the metals:

- »  $Mg(NO_3)_2 \cdot 6H_2O$  (99 %)
- »  $Al(NO_3)_3 \cdot 9H_2O$  (98 %)
- »  $Ni(NO_3)_2 \cdot 6H_2O$  (99 %)
- »  $Rh(NO_3)_3$  (10 % solution)

2) Preparation of aqueous silicate solution (30 % in excess with respect to the amount required by the stoichiometry)

- »  $SiO_2 \cdot NaOH$  27%

3) The cation solution is dropped, under magnetic stirring, into the solution of silicates, at constant temperature (50-60°C). The pH was maintained constant ( $10.5 \pm 0.1$ ) by adding NaOH (3 M). Once the dropping was finished, the obtained dispersion was maintained under magnetic stirring for 45 minutes (at 50-60°C and pH = 10.5).

4) The precipitate has been then separated from the mother liquor by filtration under vacuum, washed with abundant hot water (60°C) and dried overnight at 100°C.

5) The dried precursor samples were grinded to obtain powder.

The catalysts (ex-HT) were obtained from the precursors by calcination at 900°C for 12 h (heating rate 10°C/min).

## 2. Characterization of the catalysts

### 2.1. X-Ray diffraction analysis (XRD)

The XRD powder analyses were carried out using a Philips PW1050/81 diffractometer equipped with a graphite monochromator in the diffracted beam and controlled by a PW1710 unit (Cu K $\alpha$ ,  $\lambda = 0.15418$  nm). A  $2\theta$  range from  $10^\circ$  to  $80^\circ$  was investigated at a scanning speed of  $70^\circ/\text{h}$ .

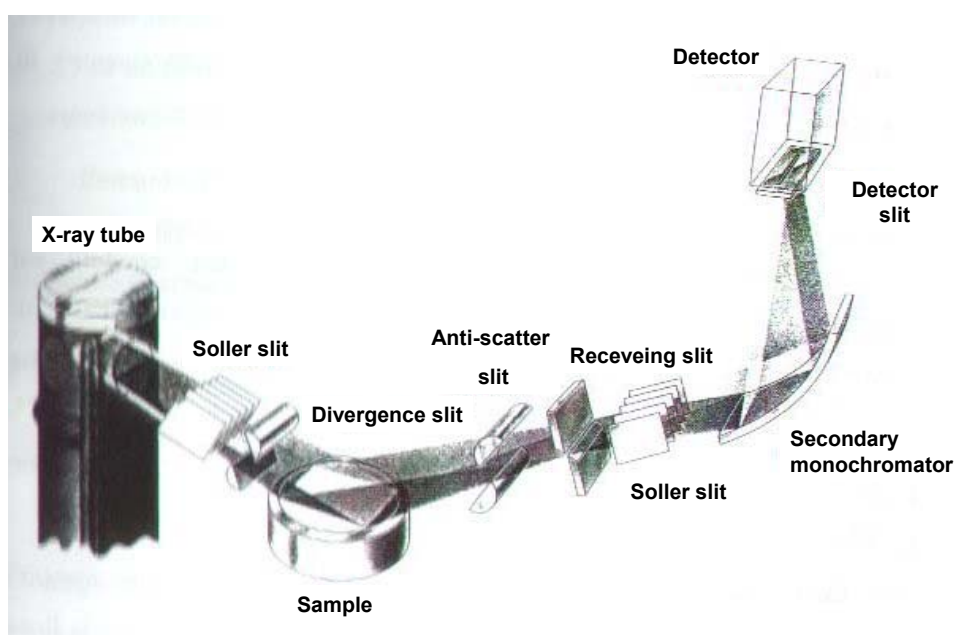


Fig. 2. 1 – Scheme of the instrument for the X-ray diffraction analysis.

The analysis of the phases present in the patterns were analyzed using the Bragg's Law:

$$n\lambda = 2dsen\vartheta$$

in order to calculate the  $d$  values to compare with those reported in the literature [Powder Diffraction Files - Inorganic Phase, ICDD (International Centre for Diffraction Data)]. In addition, the particle sizes are calculated using the Sherrer's Law:

$$D = \frac{k\lambda}{\cos\vartheta\sqrt{B^2 - b^2}}$$

## 2.2. Surface area and porosimetry analyses

The surface area of the catalysts were determined by N<sub>2</sub> adsorption at 77 K using the one point B.E.T. method, using a Carlo Erba Sorpty Instrument (model 1700). The porosimetry analysis were carried out with a Micromeritics ASAP 2020 (Accelerated Surface Area and Porosimetry System). This instrument measures the adsorption and desorption isothermal curve (at 77 K) by the volume of adsorbed/desorbed N<sub>2</sub>, as a function of relative pressure.

## 2.3. Temperature programmed reduction (TPR) and oxidation (TPO)

The reduction and oxidation profiles have been measured using a ThermoQuest Instrument TPD/R/O 1100 Catalytic Surface Analyzer. The analyses were carried out loading 0.1 g of sample, using the following procedure:

- Pre-treatment : the sample was pre-treated under N<sub>2</sub> (20 ml/min) from room temperature to 150°C (temperature rate of 20°C/min) and hold for 30 minutes at 150°C.
- Reduction : after cooling until 100°C, the reduction analysis was carried out with 5 % of H<sub>2</sub> in Ar (20 ml/min) from 100 to 950°C (temperature rate of 10°C/min) and hold for 30 minutes at 950°C.
- Oxidation : after cooling until 100°C, the oxidation analysis was carried out with 5 % of O<sub>2</sub> in He (20 ml/min) from 100 to 950°C (temperature rate of 10°C/min) and hold for 30 minutes at 950°C.

The oxidation step was carried out after the reduction on fresh samples to evaluate the reoxidation of the active metals, or after the pretreatment (coupled with quadrupole mass analyzer) on the used samples to evaluate possible carbon deposits on the surface of the catalyst.

## 2.4. H<sub>2</sub> Chemisorption analysis

The instrument used for the H<sub>2</sub> chemisorption analysis is a ASAP 2020C (Micromeritics) in which the analysis were carried after a pre-treatment under

vacuum at 100°C, reduction with a H<sub>2</sub> flow at 750°C for 2 hours and again vacuum treatment at 740°C for 2 h for the cleaning of the surface of the catalyst. The analyses are carried out at different H<sub>2</sub> pressure and 35°C. The H<sub>2</sub> chemisorbed is calculated from the difference of two consecutive analyses: in the first the measured adsorbed H<sub>2</sub> correspond to chemisorbed and physisorbed H<sub>2</sub>, while in the second to H<sub>2</sub> only physisorbed.

The dispersion of the metal is given by:

$$D_{\text{metal}} (\%) = [(100 \% \cdot 100 \%) / 22414^*] \cdot [(V \cdot SF_{\text{calc}}) / (\text{wt } \% / \text{AW})]$$

in which:

$D_{\text{metal}} (\%)$  = metal dispersion

$V$  (cm<sup>3</sup>/g STP) = chemisorbed H<sub>2</sub> volume calculated from the difference of the two consecutive analyses (Chemisorbed and Physisorbed H<sub>2</sub> – Physisorbed H<sub>2</sub>)

$SF_{\text{calc}}$  = stoichiometric factor

wt % = weight percent of the metal in the sample

AW (g/mol) = atomic weight of the metal

\* = (22414 cm<sup>3</sup> STP/mol<sub>gas</sub>) volume of 1 mol of gas

The surface area of the metal is calculated by:

$$\text{MSAs} = (6.023 \cdot 10^{23} / 22414^*) \cdot V \cdot SF_{\text{calc}} \cdot A$$

in which:

MSAs (m<sup>2</sup>/g of sample) = Metallic Surface Area per gram of sample

$V$  (cm<sup>3</sup>/g STP) = chemisorbed H<sub>2</sub> volume calculated from the difference of the two consecutive analyses (Chemisorbed and Physisorbed H<sub>2</sub> – Physisorbed H<sub>2</sub>)

$SF_{\text{calc}}$  = stoichiometric factor

$A$  (m<sup>2</sup>/atom) = area of the section of one atom of the active metal

The apparent particle size of the metal were calculated by:

$$D (\text{nm}) = 6 / (\text{MSAm} \cdot \rho)$$

in which:

$D$  (nm) = apparent metal crystal size

MSAm (m<sup>2</sup>/g of metal) = Metallic surface area per gram of metal

$\rho$  = metal density

## 2.5. Shaping in form of the catalysts

The powder catalysts prepared in the laboratory (PVK or ex-HT) were pressed, at 10 ton for 30 min, in form of round plate pellet (diameter ~ 1 cm and thickness ~ 4 mm) and then shivered in smaller particles, using apposite sieves, of different dimensions depending on the catalytic process requirements:

- for CPO tests, the pellets were between 0.841 and 0.595 mm (corresponding to granulometry of 20-40 mesh),
- for SMR tests, the pellets were between 1.410 and 0.841 mm (corresponding to granulometry of 14-20 mesh).

For what concern the commercial catalysts, both fresh and used samples, being already in form of large pellets, were directly crushed and sieved

## 2.6. CPO laboratory plant

The scheme of the reactor used for the catalytic partial oxidation tests of methane are reported in the Fig. 2. 2.

The catalytic tests were carried out in a quartz microreactor (fixed bed) with a internal diameter of 0.8 cm. the reactor was packed firstly inserting a monolith of  $\alpha$ -Al<sub>2</sub>O<sub>3</sub> in the part of the reactor where there is a restriction of the quartz tube. The monolith has the function of support for a layer of quartz wool used to create a plane and uniform surface where the catalytic bed can be placed.

In the middle of the catalytic bed, a quartz thermocouple shell is positioned. The cromel-alumel thermocouple, of 0.5 mm diameter, inserted in the shell can be moved in the axial direction in order to measure the outlet and the maximum temperatures of catalytic bed.

The reactor is placed inside an electric oven (500 W). The catalytic partial oxidation process is carried out at atmospheric pressure, which was monitored by a manometer placed before the reactor.

The feed gas (CH<sub>4</sub>/O<sub>2</sub>/He) flow was injected from the top, passed through the catalytic bed and the produced syngas (CH<sub>4</sub>/H<sub>2</sub>/CO/CO<sub>2</sub>/H<sub>2</sub>O/He) leave the reactor from the bottom. The syngas pass through a condenser and a trap containing dehydrator agent (Drierite, CaSO<sub>4</sub>, 8 mesh, containing an indicator) in order to remove all the water produced during the reaction (Fig. 2. 3).

The dry syngas is analyzed on line using two gas-chromatograph equipments. The first one is a Fisons Instruments 8000 series equipped with a TCD detector and is used to separate  $O_2$ ,  $CO$ ,  $CH_4$  and  $CO_2$ , using a Carbosieve S-II packed column [Isotherm at  $55^\circ C$  for 3 min, ramp  $10^\circ C/min$  until  $220^\circ C$ , isotherm at  $220^\circ C$  for 5 min, cooling; carrier gas: He 20 ml/min].

In the second gas-chromatograph, a Perkin Elmer Instrument, the hydrogen was analyzed using a similar Carbosieve S-II packed column. The analysis was carried out at  $35^\circ C$  using as carrier gas  $N_2$ , (20 ml/min).

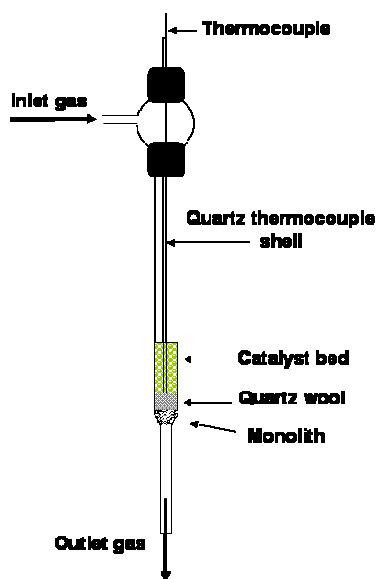


Fig. 2. 2 – Scheme of CPO laboratory reactor.

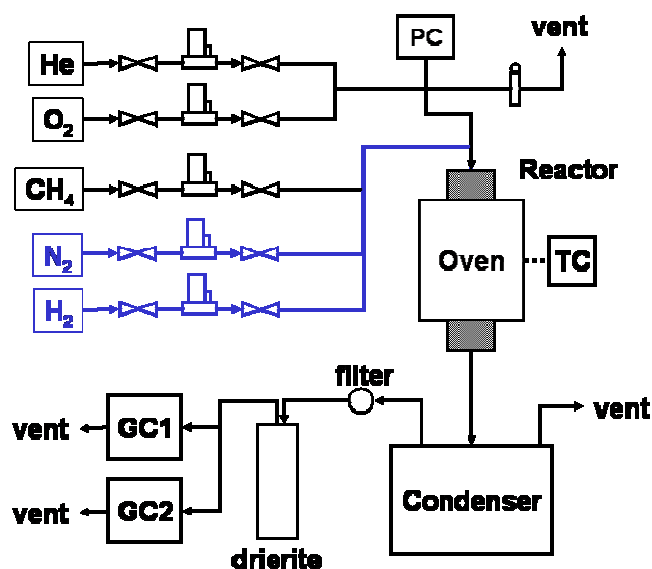


Fig. 2. 3 – Scheme of the CPO laboratory plant.

All the samples, before the catalytic tests were subjected to in situ reduction at 750°C for 12 h, in order to activate the active metals, using a H<sub>2</sub>/N<sub>2</sub> equimolar flow (total flow 150 ml/min).

The reactor, operating at atmospheric pressure is fed with CH<sub>4</sub>/O<sub>2</sub>/He mixtures with different volumetric ratios (Tab. 2. 1). Each mixture allows to study different catalytic behavior. Using the diluted mixture, the temperature profiles are smoothed, indeed it is possible a better control of the temperature in the catalytic bed. In fact, this volumetric ratio among the inlet gases allows a lower heat produced by exothermic reactions and improved thermal diffusion, obtaining a measured temperature value of the gas phase, by the thermocouple inserted in the catalytic bed, more similar to the real temperature at the surface of the catalyst.

The more concentrated mixtures approach to the possible industrial conditions. The CH<sub>4</sub>/O<sub>2</sub>/He = 2/1/4 v/v mixture simulates the use of air, while the CH<sub>4</sub>/O<sub>2</sub>/He = 2/1/1 v/v ratio the use of O<sub>2</sub> rich air.

The oven temperature was set at 500°C, to evaluate the activity in condition far from thermodynamic equilibrium, or 750°C, to study the real operative conditions.

CH <sub>4</sub>	O <sub>2</sub>	He	T <sub>oven</sub>	CT (ms)
2	1	20	500°C	65
2	1	20	750°C	65
2	1	4	750°C	65
2	1	1	750°C	112
4	2	2	750°C	56
2	1	20	500°C	65

Tab. 2. 1 – List of the tests carried out for the catalytic partial oxidation of methane.

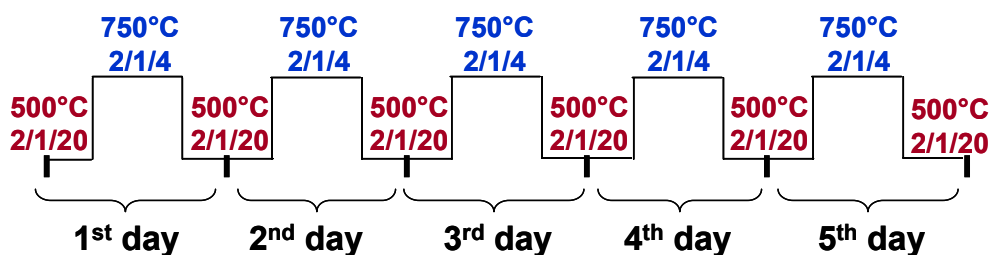


Fig. 2. 4 – Scheme of the tests carried out with time-on-stream.

Some catalysts were subjected to duration tests for 5 days, to evaluate the stability with time-of-stream. The tests were carried out feeding at the beginning and at the end of each day the dilute mixture ( $\text{CH}_4/\text{O}_2/\text{He} = 2/1/20$  v/v) at  $500^\circ\text{C}$ , while for all the day the  $\text{CH}_4/\text{O}_2/\text{He} = 2/1/4$  v/v at  $750^\circ\text{C}$  was fed.

The methane conversion and  $\text{H}_2$ , CO,  $\text{CO}_2$  selectivities were calculate by:

$$\text{Conv. CH}_4 = \frac{\text{CH}_4 \text{ in} - \text{CH}_4 \text{ out}}{\text{CH}_4 \text{ in}} = \frac{\text{F}_{\text{CO out}} + \text{F}_{\text{CO}_2 \text{ out}}}{\text{F}_{\text{CO out}} + \text{F}_{\text{CO}_2 \text{ out}} + \text{F}_{\text{CH}_4 \text{ out}}}$$

$$\text{Sel. CO} = \frac{\text{F}_{\text{CO out}}}{\Delta \text{CH}_4} = \frac{\text{F}_{\text{CO out}}}{\text{F}_{\text{CO out}} + \text{F}_{\text{CO}_2 \text{ out}}}$$

$$\text{Sel. CO}_2 = \frac{\text{F}_{\text{CO}_2 \text{ out}}}{\Delta \text{CH}_4} = \frac{\text{F}_{\text{CO}_2 \text{ out}}}{\text{F}_{\text{CO out}} + \text{F}_{\text{CO}_2 \text{ out}}}$$

$$\text{Sel. H}_2 = 0.5 \frac{\text{F}_{\text{H}_2 \text{ out}}}{\Delta \text{CH}_4} = 0.5 \frac{\text{F}_{\text{H}_2 \text{ out}}}{\text{F}_{\text{CO out}} + \text{F}_{\text{CO}_2 \text{ out}}}$$

## 2.7. SMR laboratory plant

In order to study the methane steam reforming reaction, a laboratory plant with a fixed bed reactor was built (Fig. 2. 5). The plant can be divided in four zone:

(1) methane and water feeds mixing and preheating, (2) microreactor, (3) water condenser, and (4) analyzer.

The water used as feed is ultrapure (with a conductivity of  $18.2 \mu\text{S}$ ), it is fed by a HPLC pump and pre-heated at  $400^\circ\text{C}$  before enter in the reactor. Water and methane are mixed before the pre-heating zone.

Due to the hard reaction conditions, such as high temperature ( $870\text{-}950^\circ\text{C}$ ), pressure (until 20 bar) and reducing atmosphere, the constituting material of the reactor undergoes to severe restrictions. To avoid the break of the reactor in

these conditions, it was built in a special alloy material (Incoloy 800HT) constituted by chromium (20-25%), nickel (30-35 %) and iron (40-45 %).

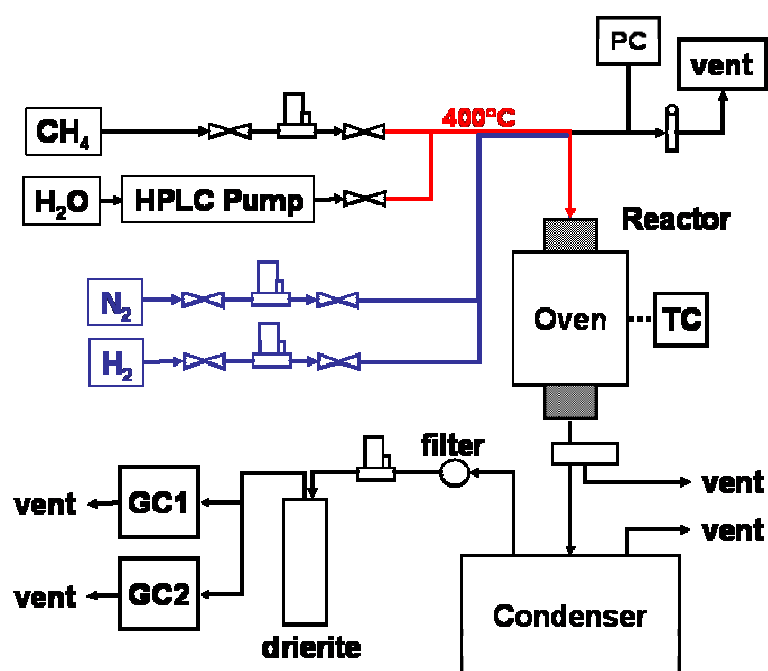


Fig. 2. 5 - Scheme of the SMR laboratory plant.

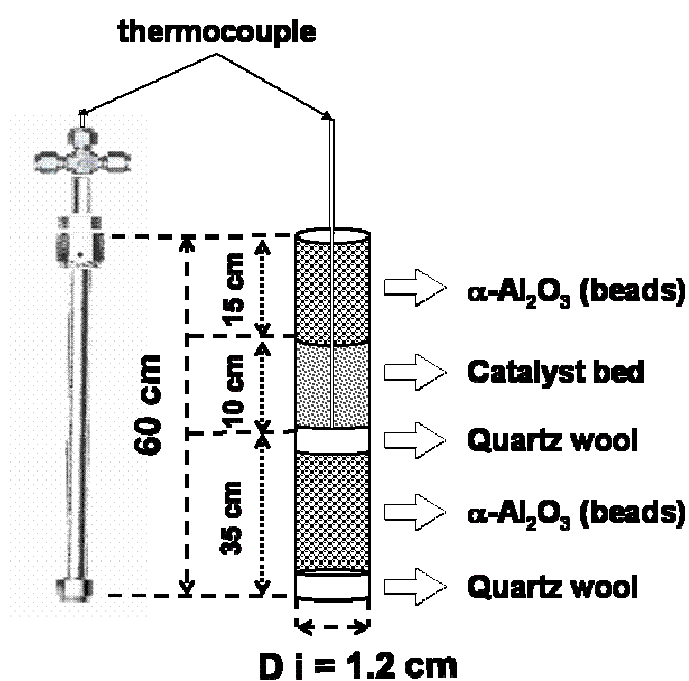


Fig. 2. 6 – Scheme of the laboratory SMR reactor.

Inside the reactor (Fig. 2. 6), along the axial direction a thermocouple shell is inserted, in this fixed shell it is possible to move the cromel-alumel thermocouple (0.8 mm of diameter) in the axial direction in order to measure the axial thermal profile during reaction. The reactor is placed inside an electric oven.

The wet syngas, going out from the reactor, pass through a water condenser that separates the major amount of non reacted water and through a trap containing a dehydrator agent (Drierite,  $\text{CaSO}_4$ , 8 mesh, containing an indicator) in order to remove any residual traces of water.

Between the water condenser and the dehydration trap, a pressure regulator is placed to maintain the feed zone and the microreactor under the operative pressure conditions, while after this control device the pressure is atmospheric, that is useful for the analysis.

The dry syngas is then analyzed on line using two gas-chromatograph equipments (the system is the same used for catalytic partial oxidation plant).

The first gas-chromatograph is a Fisons Instruments 8000 series equipped with a TCD detector and is used to separate  $\text{O}_2$ ,  $\text{CO}$ ,  $\text{CH}_4$  and  $\text{CO}_2$ , using a Carbosieve S-II packed column [Isotherm at  $55^\circ\text{C}$  for 3 min, ramp  $10^\circ\text{C}/\text{min}$  until  $220^\circ\text{C}$ , isotherm at  $220^\circ\text{C}$  for 5 min, cooling; carrier gas: He 20 ml/min].

The second gas-chromatograph is a Perkin Elmer Instrument, for the hydrogen analysis using a similar Carbosieve S-II packed column. The analysis was carried out at  $35^\circ\text{C}$  using as carrier gas  $\text{N}_2$ , (20 ml/min).

The catalytic tests were carried out in the following reaction conditions:

- $P = 10 \text{ bar}$ ,  $15 \text{ bar}$  and  $20 \text{ bar}$
- $CT = 4 \text{ s}$ ,  $2 \text{ s}$ ,  $1.1 \text{ s}$  and  $0.83 \text{ s}$
- $T_{\text{out}} = 870^\circ\text{C}$  and  $930^\circ\text{C}$  (measured temperature at the outlet of the catalytic bed)
- $T_{\text{oven}} = 800^\circ\text{C}$  and  $950^\circ\text{C}$  (oven set temperature)
- $S/C = 1.7$  and  $2.5 \text{ ml/mol}$  (and in one case 1.1, 1.4, 3 and 4 mol/mol)
- $D_p = 1.410 - 0.841 \text{ mm}$  (granulometry of 14-20 mesh)
- $V_{\text{cat}} = 6 \text{ ml}$ ,  $10 \text{ ml}$  and  $12 \text{ ml}$ .

Before testing catalysts, the laboratory plant was subjected to preliminary activity tests loading all the reactor tube with corundum beads ( $\alpha\text{-Al}_2\text{O}_3$ ), to evaluate the activity of this material chosen as inert and to evaluate if the reactor itself has some activity due to the high % of Ni in the special alloy material (30-35%).

These blank tests were carried out at different temperatures (870°C and 950°C) and S/C ratio. In the tests at 870°C a methane conversion lower than 1 % was observed, while at 950°C it was about of 7 % with very poor selectivities (Tab. 2. 2).

	S/C = 1.7	S/C = 2.5
<b>Conv. CH<sub>4</sub></b>	7.0	6.5
<b>Resa H<sub>2</sub> (*)</b>	7.8	7.5
<b>Sel. CO</b>	19.6	11.2
<b>Sel. CO<sub>2</sub></b>	80.4	88.8

**Tab. 2. 2 – Catalytic activity of the inert material ( $\alpha$ -Al<sub>2</sub>O<sub>3</sub>) and reactor at T = 950°C, P = 10 bar, CT = 1 s, S/C = 1.7 and 2.5.**

The start up of a new load of catalyst was made reducing in situ the sample and switching to reaction conditions:

1. Feeding of N<sub>2</sub>, then start-up of heating
3. When the temperature measured inside the reactor (close to the first layer of catalyst) is greater than 600°C, reduction of the catalyst is carried out by adding H<sub>2</sub> to N<sub>2</sub> flow, in equimolar ratio, for at least 30 minutes and until 800-850°C, depending on the catalyst.
4. When the temperature measured inside the reactor is greater than 800°C, the injection of the steam is started, maintaining the H<sub>2</sub>/N<sub>2</sub> flow and then, the flow is quickly switched from N<sub>2</sub> to CH<sub>4</sub>. After that, the H<sub>2</sub> flow is turned off.
5. Finally, the temperature of the oven was adjusted to reach the desirable outlet temperature of the catalytic bed.

The composition of the dry syngas at the exit of the SMR reactor, the total condensed water permit to calculate the methane and water conversions, the hydrogen selectivity (and yield) and CO and CO<sub>2</sub> selectivities, using the following calculations:

$$\text{Conv. CH}_4 = 100 * \frac{\text{CO}_{\text{out}} + \text{CO}_{2\text{out}}}{(\text{CH}_{4\text{out}} + \text{CO}_{\text{out}} + \text{CO}_{2\text{out}})}$$

$$\text{Conv. H}_2\text{O} = 100 * \frac{\text{CO}_{\text{out}} + 2\text{CO}_{2\text{out}}}{\text{H}_2\text{O}_{\text{in}}}$$

$$\text{Sel. H}_2 = 100 * \frac{\text{H}_{2\text{out}}}{(3 * (\text{CO}_{\text{out}} + \text{CO}_{2\text{out}}))}$$

$$\text{Sel. CO} = 100 * \frac{\text{CO}_{\text{out}}}{(\text{CO}_{\text{out}} + \text{CO}_{2\text{out}})}$$

$$\text{Sel. CO}_2 = 100 * \frac{\text{CO}_{2\text{out}}}{(\text{CO}_{\text{out}} + \text{CO}_{2\text{out}})}$$

## RESULTS AND DISCUSSION

### 1. Aim of the work

The aim of this work was the study of new catalysts, active and stable in the hydrogen production from methane/natural gas, using either a new process, the catalytic partial oxidation (CPO), or an enhanced well-established process, the steam methane reforming (SMR).

Two types of catalytic materials were examined:

- Bulk catalysts, i.e. non-supported materials, in which the active metals (Ni and/or Rh) are stabilized inside an oxidic matrix, obtained from perovskite type compounds (PVK) and from hydrotalcite type precursors (HT);
- Structured catalysts, i.e. catalysts supported on materials having high thermal conductivity (SiC and metallic foams).

The study of the two reactions was carried out differently due to the different industrial development stage of these processes.

As first, regarding the catalytic partial oxidation, new catalysts (PVK and HT) were examined. The effect of the metal, the role of the metal/matrix ratio and the matrix formulation was studied extensively.

In the second part of the work related to the steam methane reforming, the study was carried out first on the commercial catalysts examining the deactivation in industrial conditions, the role of the operating conditions (P, T, CT, S/C, V<sub>cat</sub> and D<sub>p</sub>) and the activity of different types of catalysts. Then, innovative materials bulk (PVK and HT) and structured catalysts (SiC and metallic foam) were studied.

## 2. Catalytic partial oxidation of methane

The study of new catalysts, active and stable in the catalytic partial oxidation reaction, was focused on two types of bulk active materials: perovskite type catalysts (PVK) and catalysts obtained from hydrotalcite type precursors (HT).

In both cases the effect of the metal, the role of the metal/matrix ratio and the matrix formulation was studied.

### 2.1. Perovskite (PVK) type catalysts

Perovskite-type oxides (general formula  $ABO_3$ ) with the typical crystal structure of perovskite, shown in the Fig. 3. 1, ave been used<sup>99</sup>. The A cations are in dodecahedral sites, while the B cations are in octahedral sites.

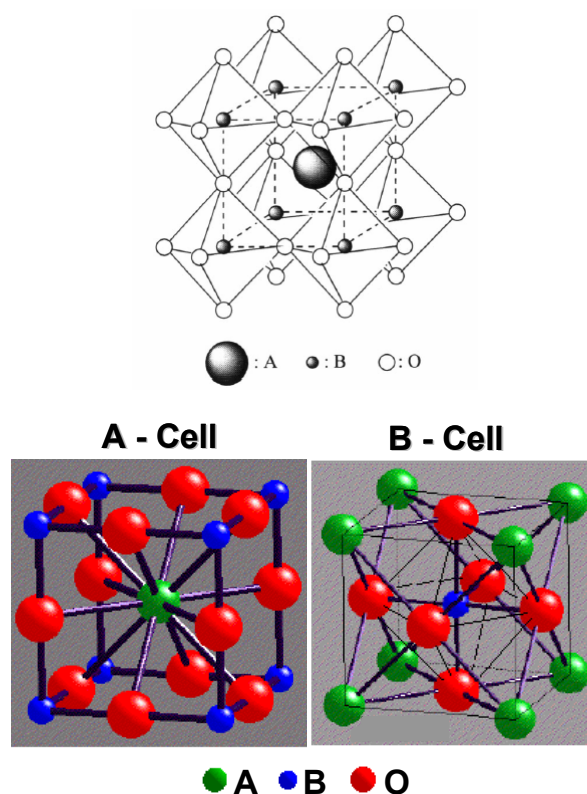


Fig. 3. 1 - Crystal structure of perovskite-t ype oxides ( $ABO_3$ ). A: La, Sr, Ba, Ca, etc. B: Ti, V, Cr, Mn, Fe, Co, Ni, Cu, Zr, Nb, Ru, etc.

One of the more successful applications is their use as combustion catalysts in exhaust gas cleaning utilizing low temperature burners. Furthermore, the perovskite materials can find important application in O<sup>2-</sup> active membrane applications. The reason for the catalytic intent of perovskite oxides lies mainly in the high mobility of oxygen and the stabilization of unusual cations oxidation states in this structure, together with their stability at high temperature. Modulation of these characteristics could be done by appropriate partial substitution of cations in A and B positions. The substitution in B position has the additional advantage that the cations in these sites are transition cations that usually have an important role in the catalytic processes<sup>99</sup>.

Provendier et al<sup>100</sup> reported that LaFeO<sub>3</sub> was relatively stable and the substitution of a part of Fe with Ni resulted in an increase in the activity in partial oxidation of methane, in which Ni alone was reduced to form the highly dispersed metal particles without collapsing the LaFeO<sub>3</sub> perovskite structure. This system permits to control the reversible migration of nickel from the structure to the surface. The best system for the partial oxidation of CH<sub>4</sub> is LaNi<sub>0.3</sub>Fe<sub>0.7</sub>O<sub>3</sub>, which showed no deactivation at 800°C during 250 h and no coke formation. These results strongly suggest that stable perovskite permit to produce stable finely dispersed Ni metal particles on the supports, which should be effective for the CH<sub>4</sub> reforming reaction.

In this work, perovskite type catalysts were studied with the general formula<sup>101</sup>



Varying the amount of the different cations and the calcination temperature, different type of catalyst were prepared in order to study the role and the effect of the active metal, the role of the metal/matrix ratio and the matrix formulation and in order to find the best catalyst composition. Different catalysts were prepared varying:

- the Rh amount            z = 0.00      0.01      0.1
- the Ce amount            x = 0.0      0.1      0.2
- the Ni amount            y = 0.0      0.1      0.3      0.5
- the calcination temperature      900°C      1100°C

All the PVK samples tested in the partial oxidation reaction were characterized before and after use by X-ray diffraction analysis and single point B.E.T. surface area analysis. The surface areas of all the samples were very low ( $< 5 \text{ m}^2\text{g}^{-1}$ ), indeed it was impossible using this technique to distinguish among the samples and to determine if deactivation by support sintering occurs.

The activity was studied monitoring the methane conversion and the synthesis gas selectivity during reaction in different reaction conditions (see the experimental section chapter). The oxygen conversion is not reported because it is 100%. Before the catalytic tests, all the samples were pretreated in a  $\text{H}_2/\text{N}_2$  flow in order to reduce the active metal for the reaction.

### 2.1.1. Effect of Rh amount ( $\text{La}_1\text{Fe}_{(0.7-z)}\text{Ni}_{0.3}\text{Rh}_z$ )

The insertion of Rh was suggested from previous studies on hydrotalcite type precursors where Ni/Rh catalysts show to be the best formulation.

The catalyst chosen for studying the effect and the role of the rhodium content and role have the general formulation  $\text{La}_1\text{Fe}_{(0.7-z)}\text{Ni}_{0.3}\text{Rh}_z$  with  $z = 0.0, 0.01$  and  $0.1$ . The rhodium content was increased 10 times:  $z = 0.01$  corresponds to about 0.4 wt %, while  $z = 0.1$  to 4 wt %. In the XRD patterns of all the fresh samples it is possible to observe that only the perovskite and a side NiO phases are present, while no rhodium containing phases are detected due to its complete insertion in the PVK structure (Fig. 3. 2).

The samples were reduced in situ at  $750^\circ\text{C}$  for 12 h before the use in the partial oxidation reaction to extract the rhodium from the structure in the metallic form.

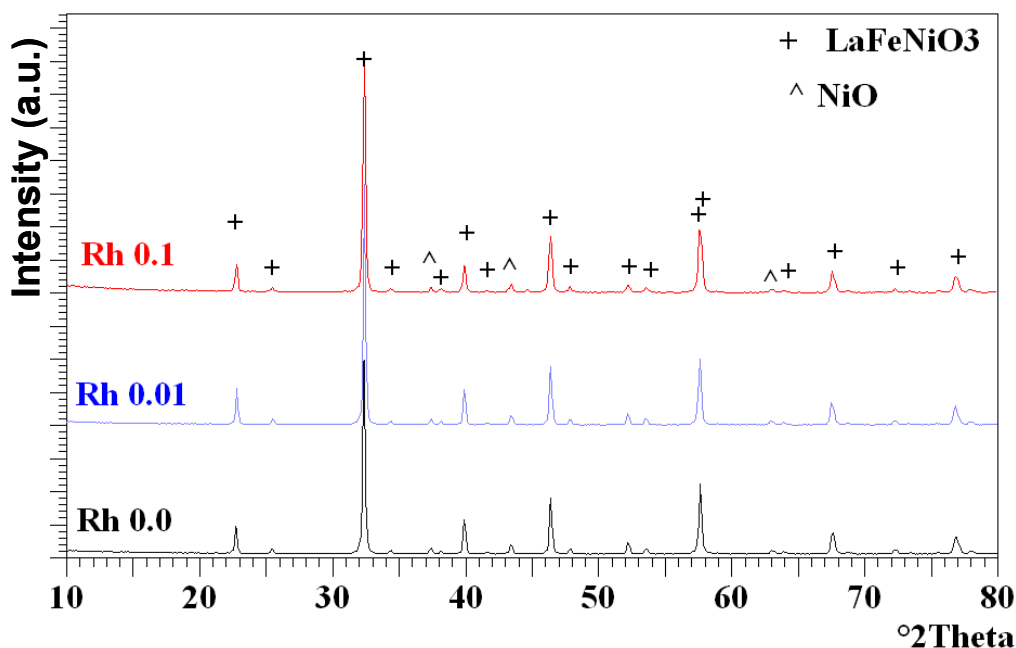


**Fig. 3. 2 – XRD patterns of fresh PVK catalysts:  $\text{LaFe}_{(0.7-z)}\text{Ni}_{0.3}\text{Rh}_z$ , containing different amount of rhodium ( $z = 0.0, 0.01, 0.1$ ).**

At low temperature, in the initial test feeding the diluted mixture, the presence of considerable amount of Rh the activity increases with respect to the sample without rhodium, but the latter shows an increase of the activity in the final tests, carried out in the same conditions, due to activation with time-on-stream, effect not observed for the catalysts containing Rh (Fig. 3. 3).

However, at high temperature and increasing the concentrations of the feed, the effect given by increasing the content of the noble metal is evident, both the methane conversion and the syngas selectivity are significantly improved. The activity, in terms of methane conversion, increases from about 60 % of the sample without Rh to more of 80 % obtained using the sample with  $z = 0.1$ .

Indeed, it is clear that the rhodium can be a very important element for improving the catalysts activity, especially in reaction conditions that are desirable for an industrial process, probably due to the improved redox properties of the couple Rh/Ni with respect to Ni. Furthermore, it is well-known that noble metals are coke-resistant and can give a further beneficial effect, also in this way, to the catalyst performance and life.

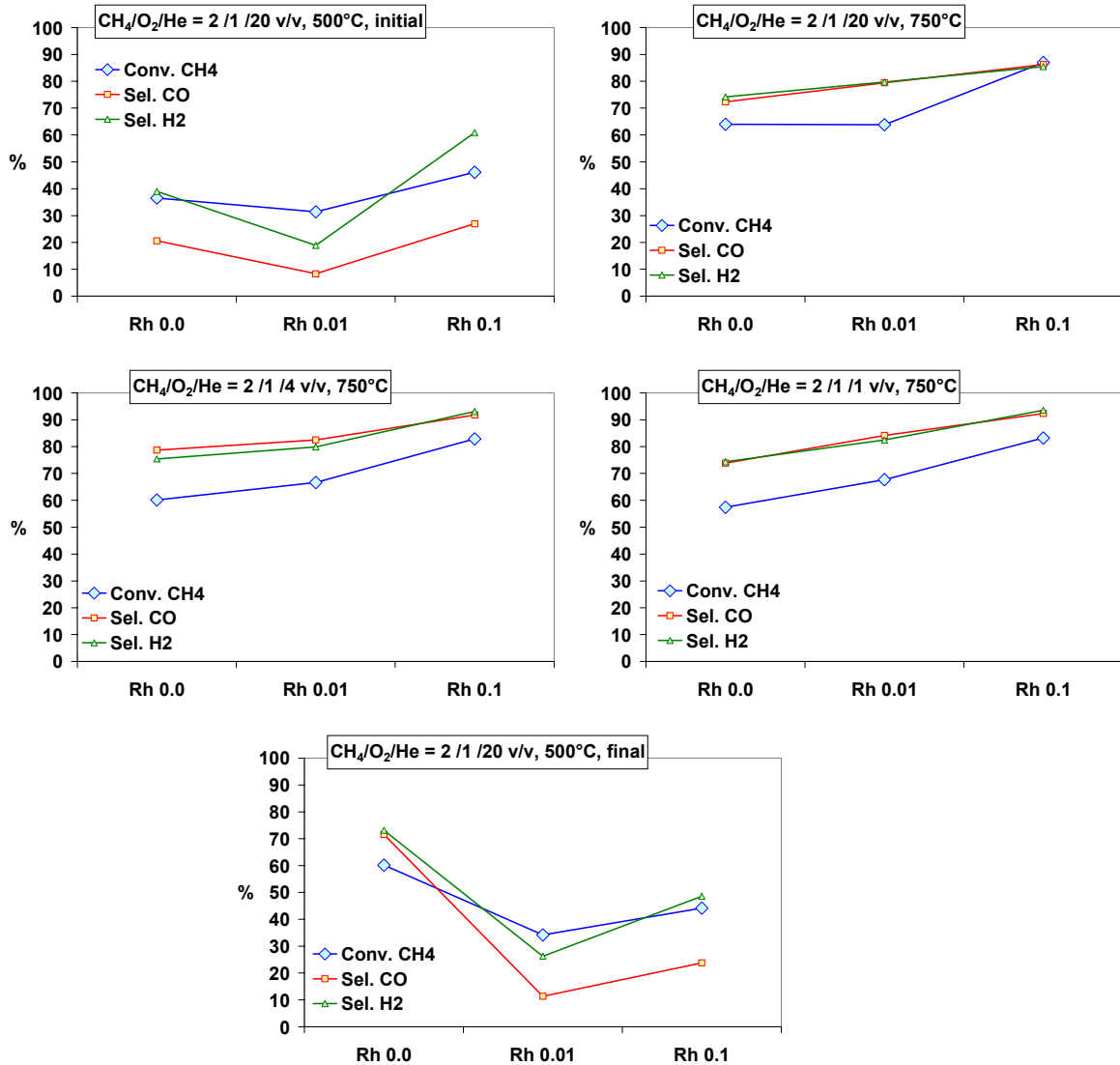


**Fig. 3. 3 - Activity of PVK catalysts: LaFe<sub>(0.7-z)</sub>Ni<sub>0.3</sub>Rh<sub>z</sub>, containing different amount of rhodium (z = 0.0, 0.01 and 0.01).**

The XRD pattern of the used sample does not show any segregated phase containing rhodium (Fig. 3. 4). All the used samples present again the LaFeNiO<sub>3</sub> PVK type structure and metallic Ni. The La<sub>2</sub>O<sub>3</sub> type phase is also present, because of the extraction of Ni (B cation) during reduction creates an excess of La (A cation) with respect to the perovskite stoichiometry. The absence of the metallic Rh phase, also in the sample with z = 0.1, may be due to the great stability and good dispersion of the noble metal, indeed probably it is present as very small particles, not detectable using this method.

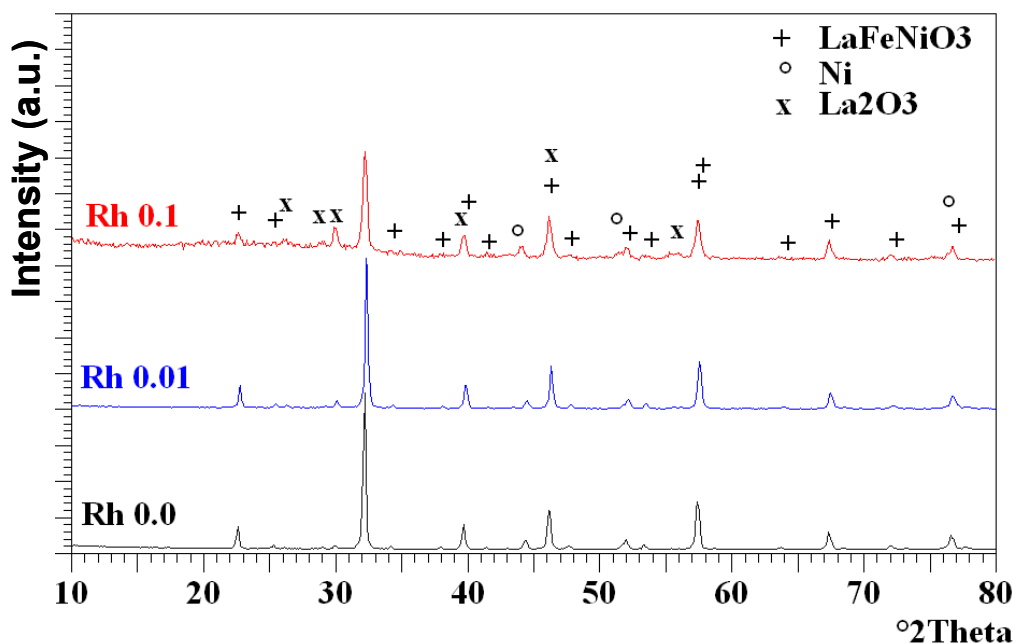


Fig. 3. 4 - XRD patterns of used PVK catalysts:  $\text{LaFe}_{(0.7-z)}\text{Ni}_{0.3}\text{Rh}_z$ , containing different amount of rhodium ( $z = 0.0, 0.01, 0.1$ ).

### 2.1.2. Effect of Ce amount ( $\text{La}_{(1-x)}\text{Ce}_x\text{Fe}_{0.69}\text{Ni}_{0.3}\text{Rh}_{0.01}$ )

The catalysts used to study the role of the cerium and the effect of its amount have a general formula  $\text{La}_{(1-x)}\text{Ce}_x\text{Fe}_{0.69}\text{Ni}_{0.3}\text{Rh}_{0.01}$  ( $x = 0.0, 0.1$  and  $0.2$ ). These samples were prepared by the citrate method and were calcined in static air at  $900^\circ\text{C}$  for 12 h (heating rate  $10^\circ\text{C}/\text{min}$ ).

The cerium was introduced because it can easily store and release oxygen atoms due to the redox properties of Ce ions ( $\text{Ce}^{4+}$  to  $\text{Ce}^{x+}$ ,  $x < 4$ ), facilitating the oxidation reaction of adsorbed carbon atoms during the reaction. Theoretically, the Ce cations is inserted in the perovskite structure in the A dodecahedral sites together with the lanthanum cations. However, the XRD pattern of the fresh samples shows, besides the perovskite structure,  $\text{LaFeNiO}_3$ , a minor phase constituted of  $\text{CeO}_2$  that increase with increasing the amount of Ce added during the preparation. Probably, only low amount of cerium can be inserted in the perovskitic structure and part of it segregate to cerium oxide during the thermal treatment at  $900^\circ\text{C}$ , due to the high stability of the  $\text{CeO}_2$  phase. It can be noted from the XRD pattern that, increasing the cerium amount, the crystallinity of the perovskitic structure is lower and the reflections are slightly shift towards higher

d-spacing (Å), due to the insertion in the  $\text{LaFeNiO}_3$  structure of cerium cations, which are bigger than the lanthanum ones.

Furthermore, also the nickel is not completely inserted in the structure and NiO type phase is present, especially in the sample that not contain Ce.

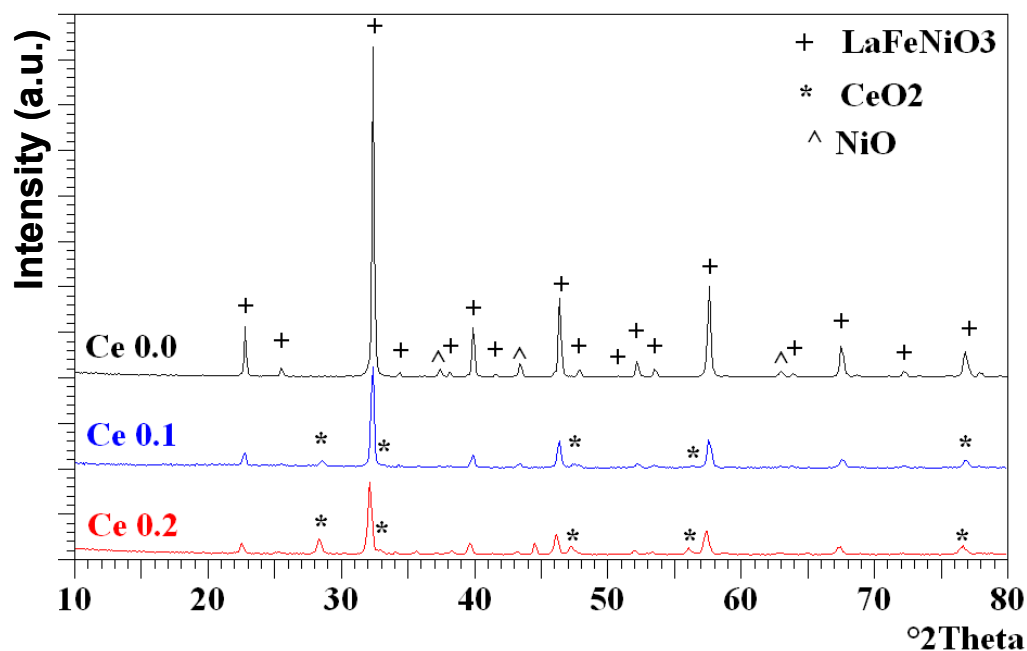


**Fig. 3. 5 – XRD patterns of fresh PVK catalysts:  $\text{La}_{(1-x)}\text{Ce}_x\text{Fe}_{0.69}\text{Ni}_{0.3}\text{Rh}_{0.01}$ , containing different amount of cerium ( $x = 0.0, 0.1$  and  $0.2$ ).**

The three samples containing different amount of Ce were tested in the catalytic partial oxidation of methane after an in situ activation carried out with  $\text{H}_2/\text{N}_2$  equimolar flow at  $750^\circ\text{C}$  for 12 h. The catalytic performances obtained in the different reaction conditions were compared (Fig. 3. 6).

In all the reaction conditions it is possible to note that the sample that does not contain cerium (denoted as Ce 0.0) presents the worst activity, both considering the methane conversion and syngas selectivity.

In particular, in the initial test at low temperature and diluted mixture ( $\text{CH}_4/\text{O}_2/\text{He} = 2/1/20$  v,v) this sample show very poor activity, probably it is re-oxidized (i.e. deactivated) in the oxidizing atmosphere of diluted conditions due to the low temperature. Increasing the temperature and the concentration of the feed, the differences are less evident, due to further reduction. The presence of low amount of Ce in the catalyst ( $x = 0.1$ ) increases the activity and also the syngas selectivity. However, further increase of cerium amount ( $x = 0.2$ ) does not cause

a further improvement, but neither a decrease of the catalyst performances. In fact, the Ce 0.2 sample shows about the same activity of the Ce 0.1. Effectively, the cerium oxide present on the surface of the catalyst can release oxygen atoms and actively participate to the CPO reaction.

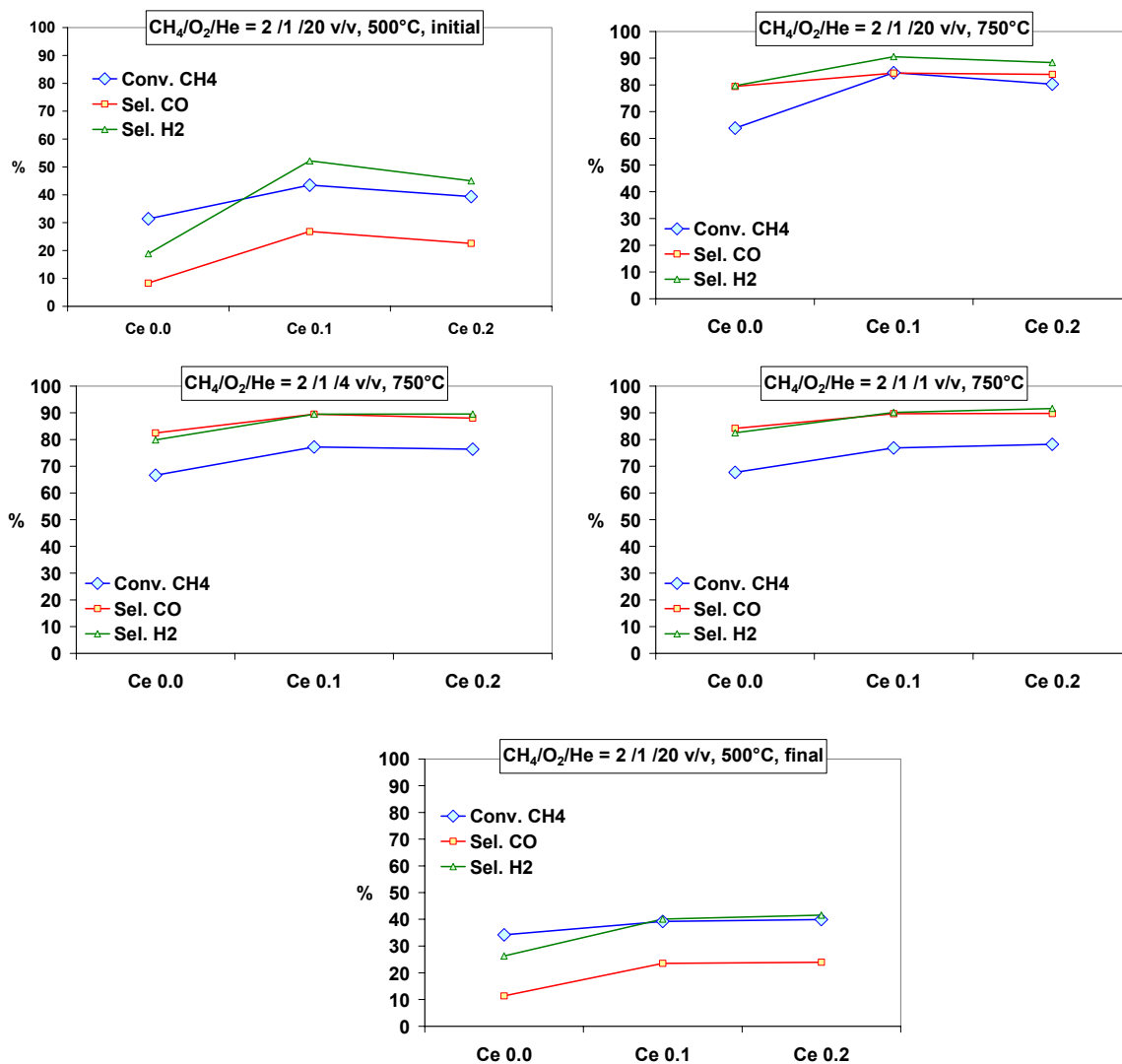


**Fig. 3. 6 – Activity of PVK catalysts: La<sub>(1-x)</sub>Ce<sub>x</sub>Fe<sub>0.69</sub>Ni<sub>0.3</sub>Rh<sub>0.01</sub>, containing different amount of cerium (x = 0.0, 0.1 and 0.2).**

The XRD pattern of the used catalyst without cerium shows, after reaction, a slight decrease of crystallinity and, besides the reduction of nickel oxide to metallic nickel, the segregation of La<sub>2</sub>O<sub>3</sub> (Fig. 3. 7). On the contrary, increasing the amount of cerium leads to lower La<sub>2</sub>O<sub>3</sub> segregation and a decrease of the CeO<sub>2</sub> phase with respect the respective fresh samples, probably due to insertion

of  $\text{CeO}_2$  in the structure and higher stability of the structure due to the presence of cerium (Fig. 3. 8 and Fig. 3. 9). Furthermore, the sample with Ce 0.2 does not show at all the presence of the  $\text{La}_2\text{O}_3$  phase, while the Ce seems to be partially reduced to  $\text{Ce}_7\text{O}_{12}$  type phase. Indeed, the samples containing cerium show better resistance in the reaction conditions than the catalyst without cerium.

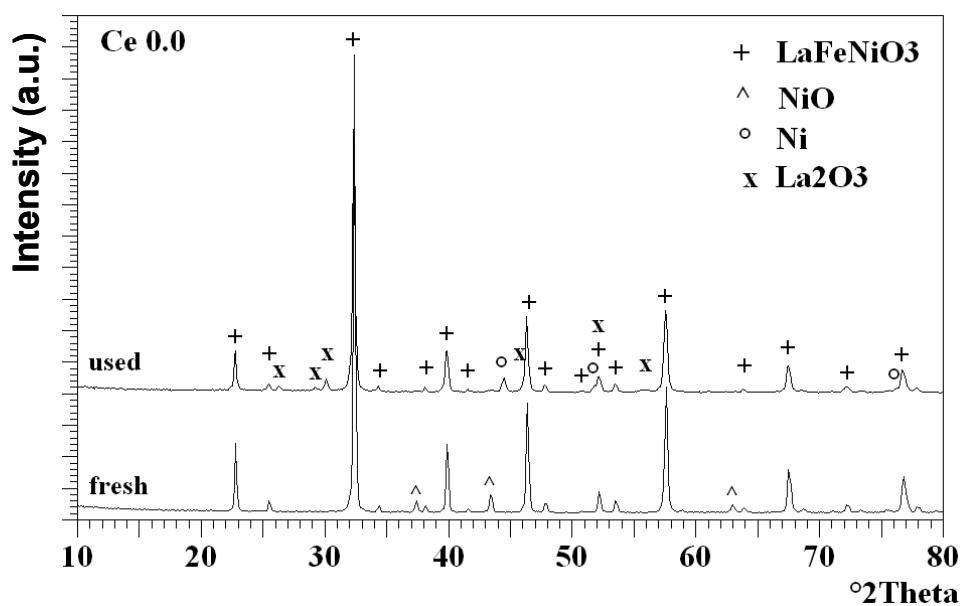


Fig. 3. 7 - Comparison of the XRD patterns of fresh and used PVK catalyst  $\text{LaFe}_{0.69}\text{Ni}_{0.3}\text{Rh}_{0.01}$ ,  $x = 0.0$ .

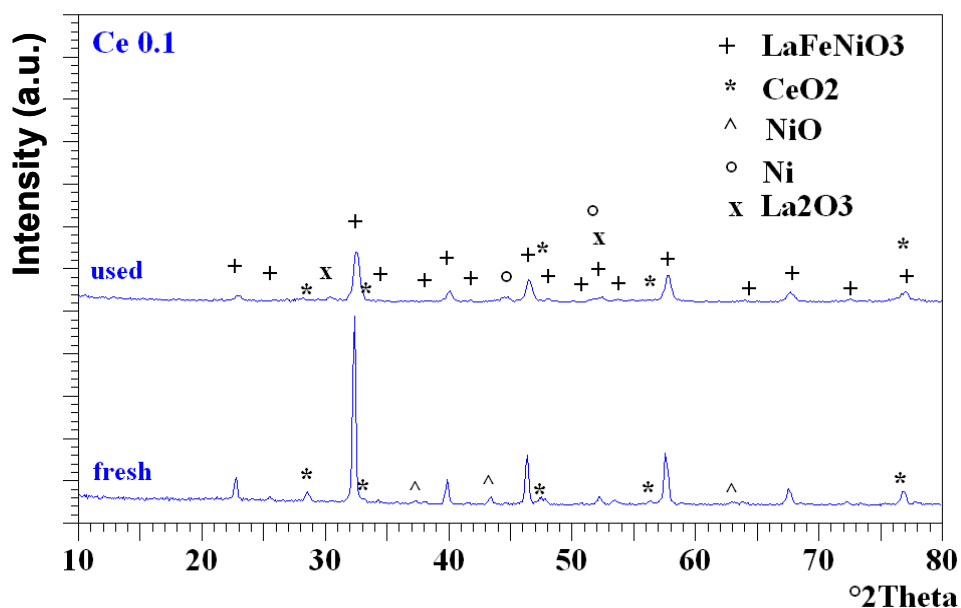


Fig. 3. 8 - Comparison of the XRD patterns of fresh and used PVK catalyst  $\text{La}_{0.9}\text{Ce}_{0.1}\text{Fe}_{0.69}\text{Ni}_{0.3}\text{Rh}_{0.01}$ ,  $x = 0.1$ .

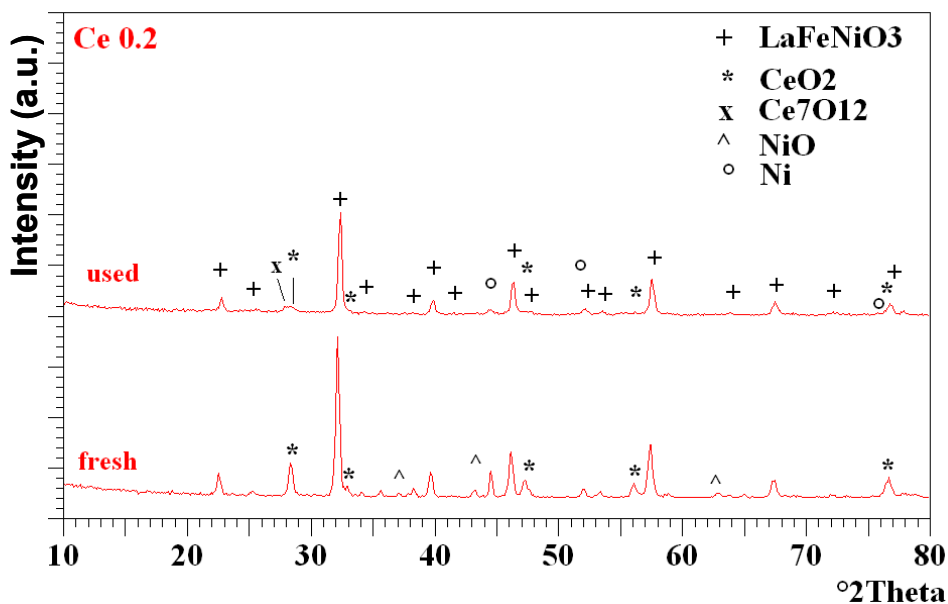


Fig. 3. 9 – Comparison of the XRD patterns of fresh and used PVK catalyst  $\text{La}_{0.8}\text{Ce}_{0.2}\text{Fe}_{0.69}\text{Ni}_{0.3}\text{Rh}_{0.01}$ ,  $x = 0.2$ .

### 2.1.3. Effect of Ni amount ( $\text{La}_{0.8}\text{Ce}_{0.2}\text{Fe}_{(0.98-y)}\text{Ni}_y\text{Rh}_{0.02}$ )

The catalysts used to study the role of the nickel as active metal and the effect of its amount have a general formula  $\text{La}_{0.8}\text{Ce}_{0.2}\text{Fe}_{(0.98-y)}\text{Ni}_y\text{Rh}_{0.02}$  ( $y = 0.0, 0.1, 0.3$  and  $0.5$ ). These samples were prepared by the citrate method and were calcined in static air at  $900^\circ\text{C}$  for 12 h (heating rate  $10^\circ\text{C}/\text{min}$ ).

The XRD patterns of the fresh samples are reported in Fig. 3. 10. The sample that does not contain nickel presents, beside the expected  $\text{LaFeO}_3$  and the  $\text{CeO}_2$  phases, a segregated  $\text{Fe}_2\text{O}_3$  type phase.

Inserting a low nickel amount,  $y = 0.1$ , the hematite type phase is not present, but a spinel type phase,  $\text{NiFe}_2\text{O}_4$ , is formed. However, also the presence of NiO cannot be excluded in this sample. With increasing the amount of nickel to 0.3 and 0.5, segregated iron containing phases are not present, while the amount of segregated nickel oxide phase is higher. This can be easily seen observing the increasing importance of the reflection at  $\sim 43.3^\circ 2\theta$ . The amount of NiO is nevertheless only a small part of Ni, being in the perovskite phase.

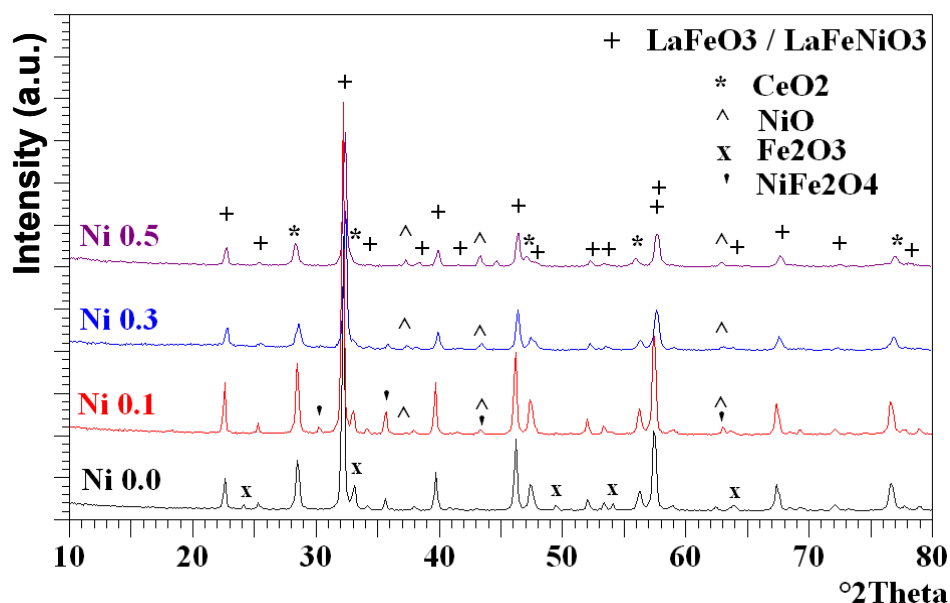


Fig. 3. 10 – XRD patterns of fresh PVK catalysts:  $\text{La}_{0.8}\text{Ce}_{0.2}\text{Fe}_{(0.98-y)}\text{Ni}_y\text{Rh}_{0.02}$ , containing different amount of nickel ( $y = 0.0, 0.1, 0.3$  and  $0.5$ ).

In situ reduction of the catalysts was carried out at  $750^\circ\text{C}$  for 12 h, before the activity tests, to reduce Ni and Rh, obtaining the active metals. The activity of these catalysts is strongly dependent on the nickel amount (Fig. 3. 11). It was observed that up to content of nickel of 0.3, especially with diluted mixtures ( $\text{CH}_4/\text{O}_2/\text{He} = 2/1/20$  v/v), methane conversion increase linearly with increasing the active metal amount. Feeding more concentrated mixtures of reactants the differences are smoothed, however the best nickel content appears to be 0.3, because further increase to 0.5 does not improve the catalytic performances. In the final test, in the same reaction condition of the initial tests, i.e. low temperature and diluted feed, only the sample without nickel shows a deactivation with respect to the initial performances.

Furthermore, it was observed that the maximum temperature measured during reaction decreases by increasing the amount of nickel in the catalysts (Tab. 3. 1). This is probably due to the high activity, which leads to the presence on the same pellets of simultaneous exothermic oxidation reaction and endothermic reforming reactions.

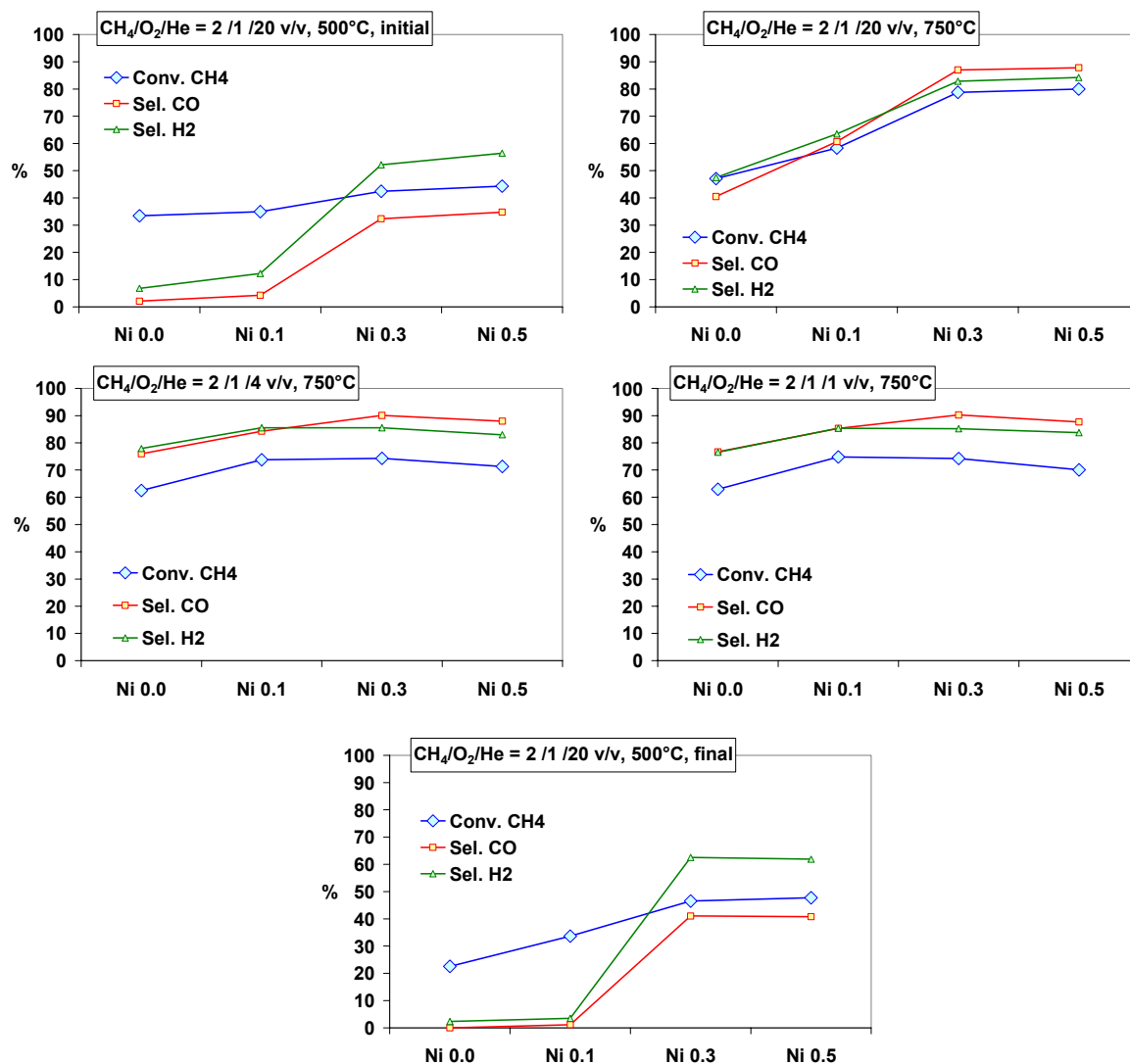


Fig. 3. 11 – Activity of PVK catalysts: La<sub>0.8</sub>Ce<sub>0.2</sub>Fe<sub>(0.98-y)</sub>Ni<sub>y</sub>Rh<sub>0.02</sub>, containing different amount of nickel (y = 0.0, 0.1, 0.3 and 0.5).

Ni y	CH <sub>4</sub> /O <sub>2</sub> /He T (°C)	2/1/20 v/v	2/1/20 v/v	2/1/4 v/v	2/1/1 v/v	2/1/20 v/v
		500°C, initial	750°C	750°C	750°C	500°C, final
0.0	T <sub>out</sub>	550	764	778	775	576
	T <sub>max</sub>	678	856	957	952	670
0.1	T <sub>out</sub>	544	758	763	759	550
	T <sub>max</sub>	681	849	937	930	683
0.3	T <sub>out</sub>	578	758	769	767	575
	T <sub>max</sub>	653	804	869	870	650
0.5	T <sub>out</sub>	560	761	773	771	565
	T <sub>max</sub>	651	808	887	890	662

**Tab. 3. 1 – Outlet (T<sub>out</sub>) and maximum (T<sub>max</sub>) temperatures observed in the catalytic bed, during different CPO reaction conditions, with the catalysts containing different amount of Ni.**

After the partial oxidation reaction the structure of the samples containing no (y = 0.0) or very low (y = 0.1) nickel amount (Fig. 3. 12 and Fig. 3. 13) present only perovskite type phase. The presence of metallic nickel in the sample with y = 0.1 is supposed, but both due to the low amount and the overlapping with other phases cannot be identify without doubt. The Al phase present in some patterns is due to interference of the sample holder used for XRD measurement.

The sample containing y = 0.3 (La<sub>0.8</sub>Ce<sub>0.2</sub>Fe<sub>0.68</sub>Ni<sub>0.3</sub>Rh<sub>0.02</sub>) presents, beside the perovskite LaFeNiO<sub>3</sub> type phase, the metallic nickel and Ce<sub>7</sub>O<sub>12</sub> phases (Fig. 3. 14). In the XRD pattern of the used sample with further increase of the nickel content (y = 0.5) segregations of the La<sub>2</sub>O<sub>3</sub> and Ce<sub>2</sub>O<sub>3</sub> phases are also evident (Fig. 3. 15). The increase of nickel amount probably increase also the amount of this metal that is inserted in the perovskite structure, which is then reduced leaving the perovskite with a lack of B cation, causing the segregation of the lanthanum and cerium oxides. Furthermore, the cerium is further reduced (CeO<sub>2</sub> → Ce<sub>7</sub>O<sub>12</sub> → Ce<sub>2</sub>O<sub>3</sub>).

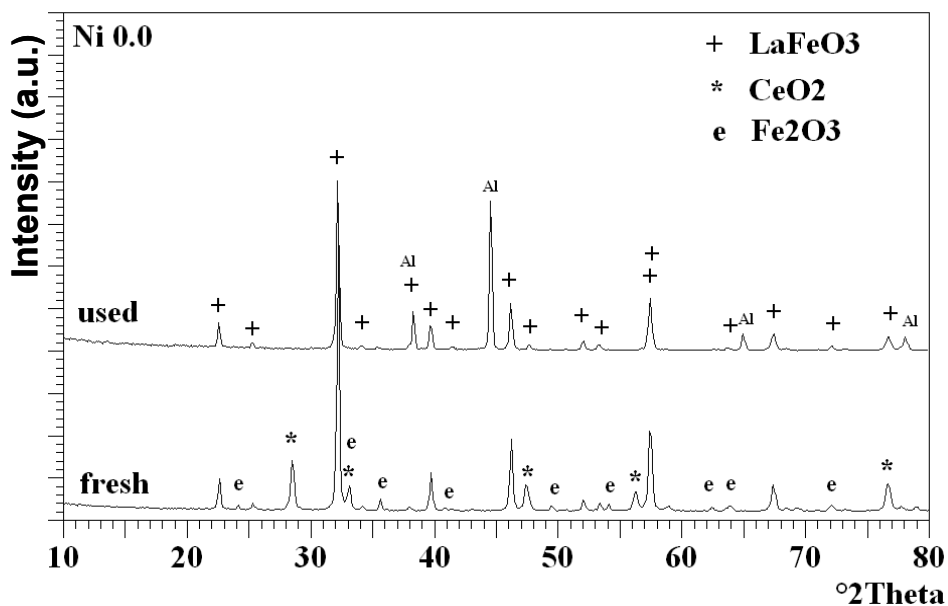


Fig. 3. 12 - Comparison of the XRD patterns of fresh and used PVK catalyst  $\text{La}_{0.8}\text{Ce}_{0.2}\text{Fe}_{0.98}\text{Rh}_{0.02}$ ,  $y = 0.0$ .

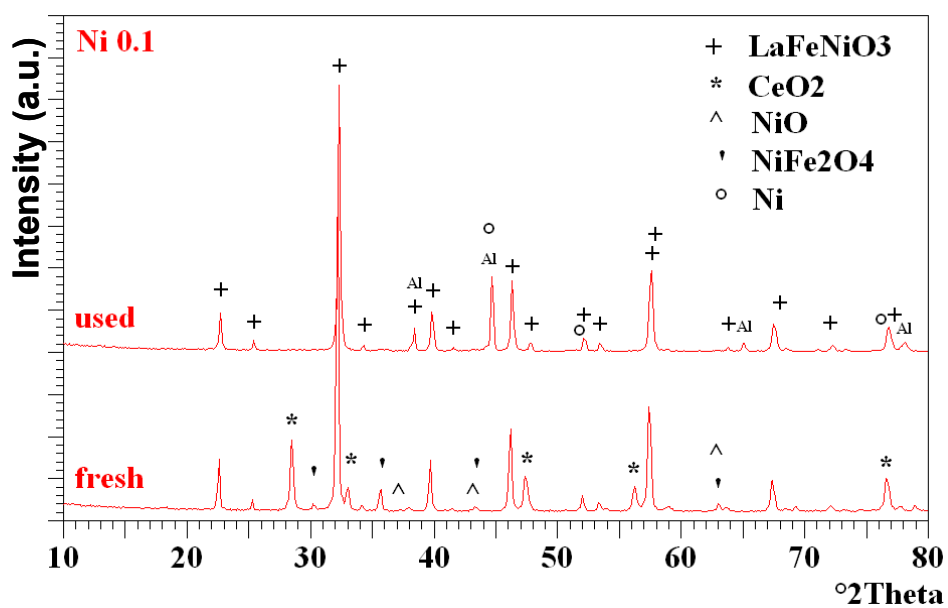


Fig. 3. 13 - Comparison of the XRD patterns of fresh and used PVK catalyst  $\text{La}_{0.8}\text{Ce}_{0.2}\text{Fe}_{0.88}\text{Ni}_{0.1}\text{Rh}_{0.02}$ ,  $y = 0.1$ .

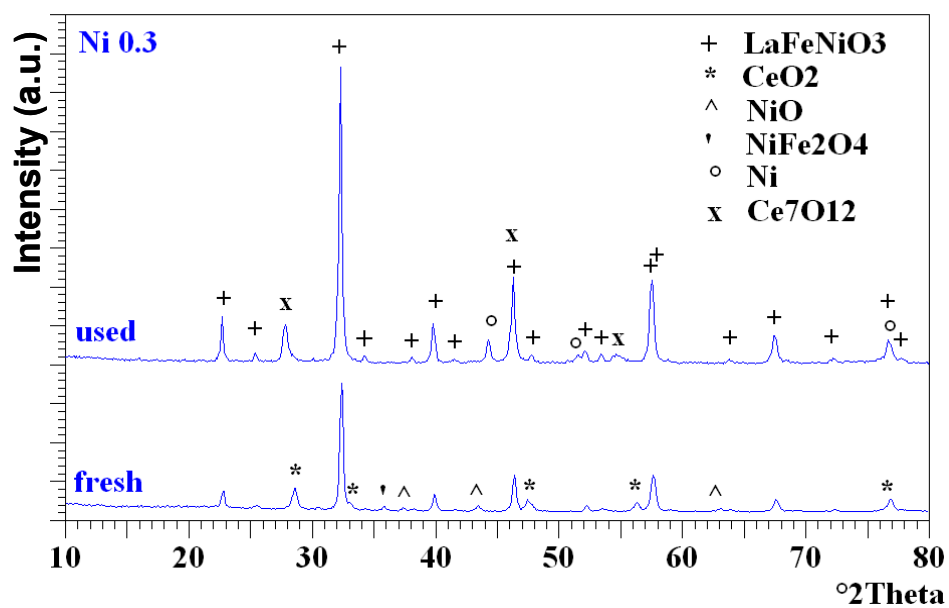


Fig. 3. 14 - Comparison of the XRD patterns of fresh and used PVK catalyst  $\text{La}_{0.8}\text{Ce}_{0.2}\text{Fe}_{0.68}\text{Ni}_{0.3}\text{Rh}_{0.02}$ ,  $y = 0.3$ .

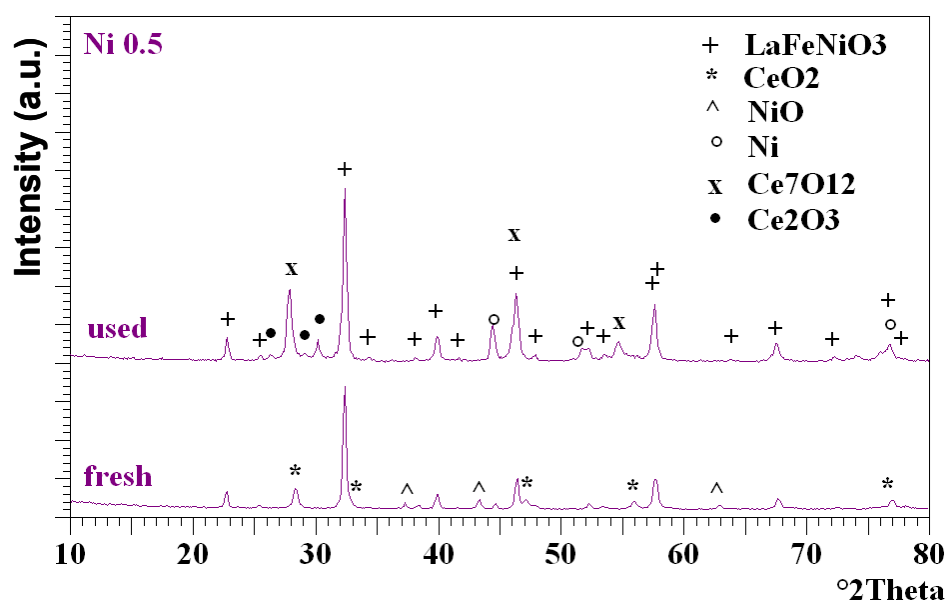


Fig. 3. 15 - Comparison of the XRD patterns of fresh and used PVK catalyst  $\text{La}_{0.8}\text{Ce}_{0.2}\text{Fe}_{0.48}\text{Ni}_{0.5}\text{Rh}_{0.02}$ ,  $y = 0.5$ .

#### 2.1.4. Effect of calcination temperature: 900 or 1100°C (La<sub>0.8</sub>Ce<sub>0.2</sub>Fe<sub>0.7</sub>Ni<sub>0.25</sub>Rh<sub>0.05</sub>)

From the study of the catalyst composition it can be concluded that a good formulation for a perovskite type catalyst is La<sub>0.8</sub>Ce<sub>0.2</sub>Fe<sub>0.7</sub>Ni<sub>0.25</sub>Rh<sub>0.05</sub>, in which cerium is contained for its beneficial effect both on the activity and on the structure stability and the active metals are present as 6 wt % of Ni and 2 wt % of Rh. On this catalyst, the effect of the calcination temperature was studied in order to optimize the stability of the sample. Two temperatures were investigated 900 and 1100°C. The samples were calcined for 12 h using a heating rate of 10°C/min.

The two samples calcined at different temperatures shows from the XRD analyses the presence of the same phases: LaFeNiO<sub>3</sub>, CeO<sub>2</sub>, NiFe<sub>2</sub>O<sub>4</sub> and NiO, even if the sample, subjected to higher temperature (1100°C), presents increased crystallinity (Fig. 3. 16).

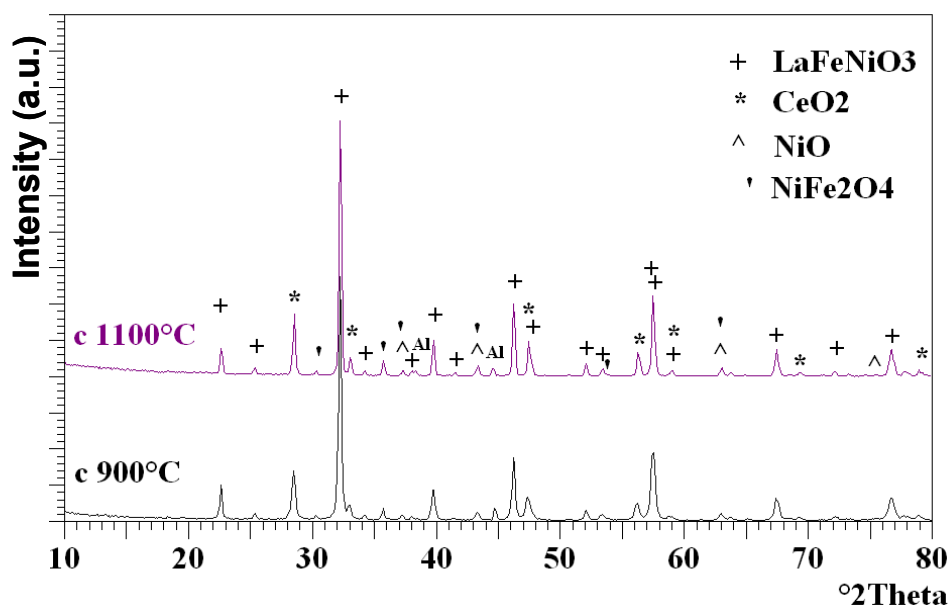


Fig. 3. 16 - XRD patterns of fresh PVK catalysts: La<sub>0.8</sub>Ce<sub>0.2</sub>Fe<sub>0.7</sub>Ni<sub>0.25</sub>Rh<sub>0.05</sub>, calcined at different temperature (900 or 1100°C).

For what concern the catalytic activity (Fig. 3. 17) of the samples calcined at different temperatures, it was observed that the catalyst calcined at 1100°C presents slightly lower methane conversion and very lower syngas selectivity,

feeding the diluted mixture at 500°C, both in the initial and in the final test, with respect those of the sample calcined at 900°C.

Increasing reaction temperature, the performances of the two samples are very similar, while increasing the reactant concentrations the sample calcined at 1100°C presents both higher methane conversion and synthesis gas selectivity. Indeed, since the only difference observed between the two samples consists in slightly increase of the crystallinity of the structure due to higher temperature, the differences in catalytic activity may be attributed to it.

The higher crystallinity, probably, makes more difficult the reduction of the active metals, because they must be extracted from the perovskite structure, and this may explain the lower activity at 500°C of the sample calcined at 1100°C in the initial test.

Nevertheless, high reaction temperature and mixture concentration yield to a more efficient activation during time-on-stream of this sample that appear for this reason more active than the one calcined at 900°C, that probably undergoes to sintering due to the severe reaction conditions.

In fact, from the XRD patterns, it was observed that the crystallinity of the two samples is the same after reaction (Fig. 3. 18). The only difference observed is that the sample calcined at 900°C shows the transformation of CeO<sub>2</sub> phase into the reduced form Ce<sub>7</sub>O<sub>12</sub>, while the sample calcined at 1100°C maintains the CeO<sub>2</sub> phase.

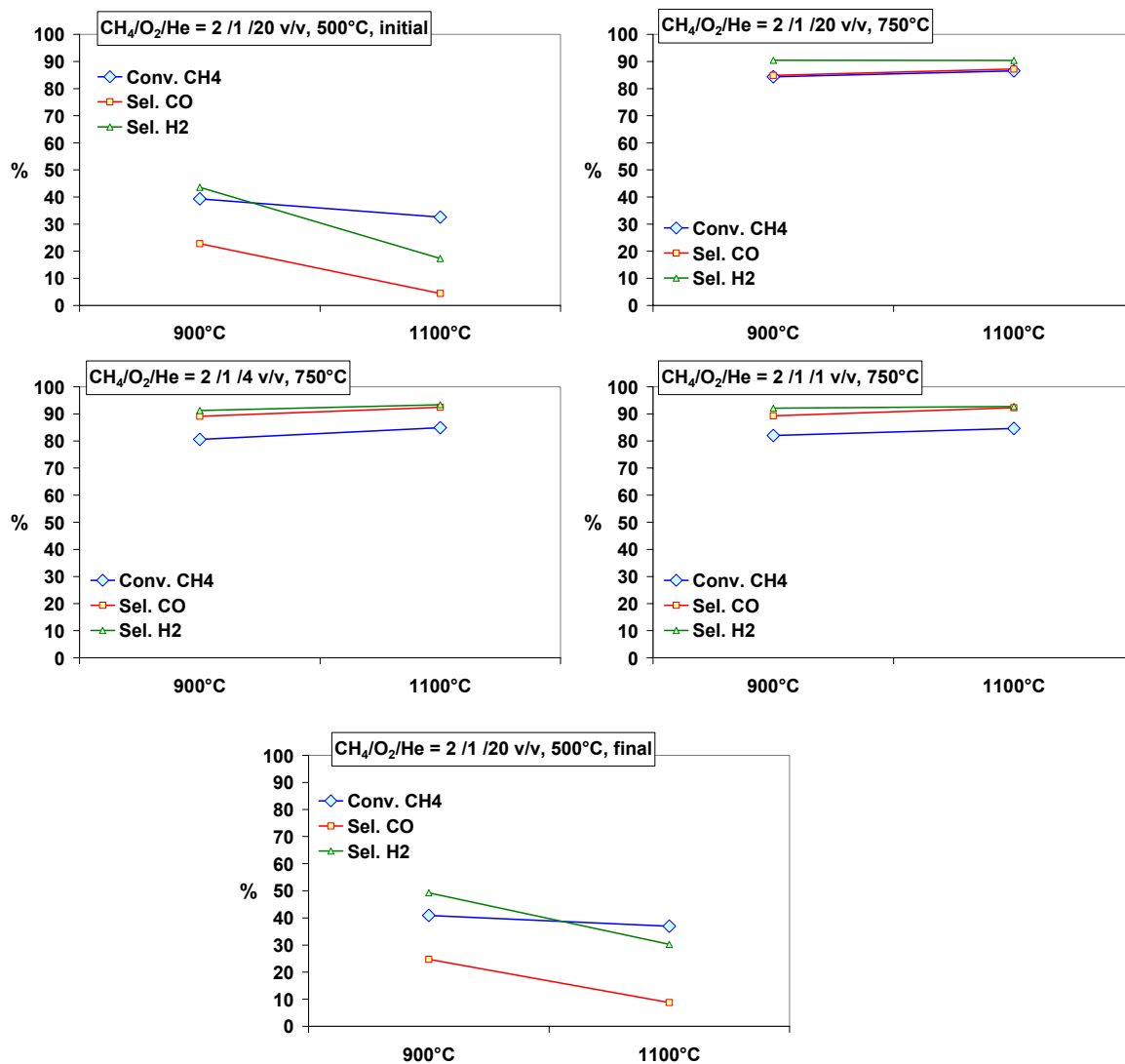


Fig. 3. 17- Activity of PVK catalysts: La<sub>0.8</sub>Ce<sub>0.2</sub>Fe<sub>0.7</sub>Ni<sub>0.25</sub>Rh<sub>0.05</sub>, calcined at different temperature (900 or 1100°C).

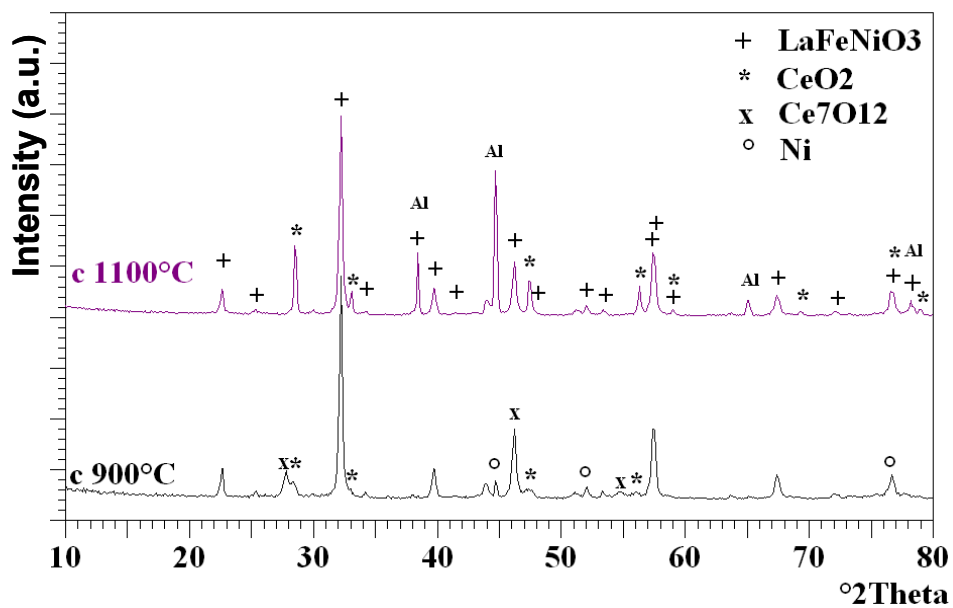
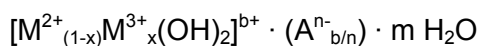


Fig. 3. 18 - XRD patterns of used PVK catalysts:  $\text{La}_{0.8}\text{Ce}_{0.2}\text{Fe}_{0.7}\text{Ni}_{0.25}\text{Rh}_{0.05}$ , calcined at different temperature (900 or 1100°C).

## 2.2. Catalysts obtained from hydrotalcite (HT) type precursor

Anionic clays or layered double hydroxides (LDHs) are lamellar mixed hydroxides with interlayer spaces containing exchangeable anions with general formula:



This class of compounds, also called hydrotalcite like compounds (HTLcs), are relatively inexpensive to prepare in the laboratory scale<sup>102</sup>. The most interesting properties are the homogeneous cation distribution and the ion exchange capacity in the precipitates. In addition, other important properties of the oxides obtained by calcination are<sup>99</sup>:

- (1) high surface area,
- (2) basic properties,
- (3) formation of homogeneous mixture of oxides with very small crystal size, stable to thermal treatments, which by reduction form small and thermally stable metal crystallites,
- (4) “memory effect”, which allows the reconstruction, under mild conditions, of the original hydrotalcite structure when contacting the product of the thermal treatment with water solutions containing various anions.

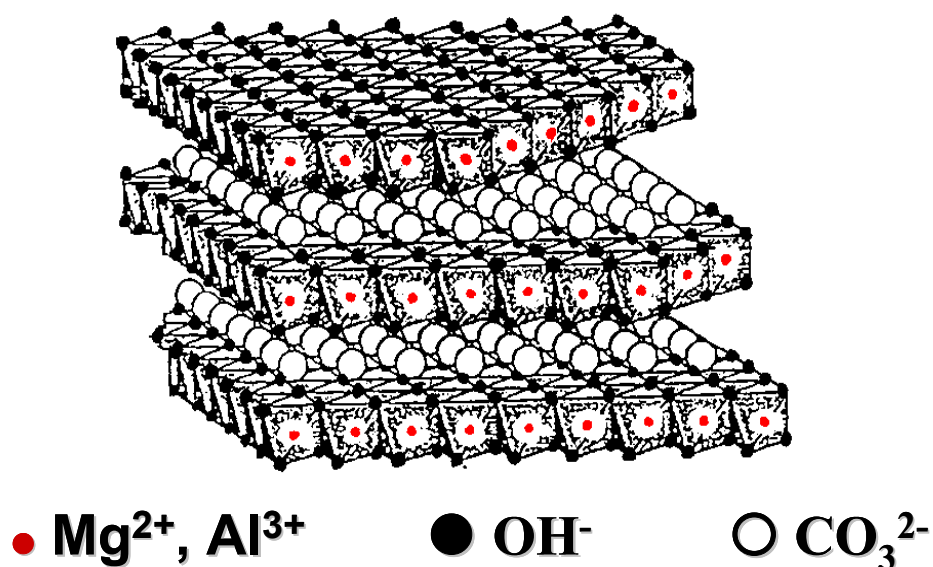


Fig. 3. 19 - Crystal structure of hydrotalcite-like precursor.

To understand the structure of these compounds, it is necessary to start from the structure of brucite  $[\text{Mg}(\text{OH})_2]$ , where octahedra of  $\text{Mg}^{2+}$  (6-fold coordinated to  $\text{OH}^-$ ) share edges to form infinite sheets. These sheets are stacked on top of each other and are held together by hydrogen bonding (Fig. 3. 20). When  $\text{Mg}^{2+}$  ions are substituted by a trivalent ion having a suitable ionic radius (such as  $\text{Al}^{3+}$  for hydrotalcite compounds), a positive charge is generated in the hydroxyl sheet. This net positive charge is compensated by  $(\text{CO}_3)^{2-}$  anions, which lie in the interlayer region between the two brucite-like sheets. In the free space of this interlayer the water of crystallization also finds a place.

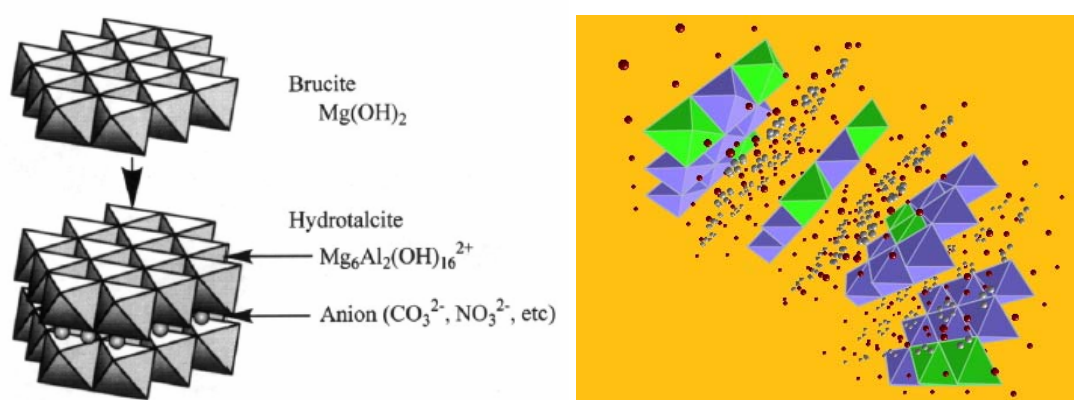
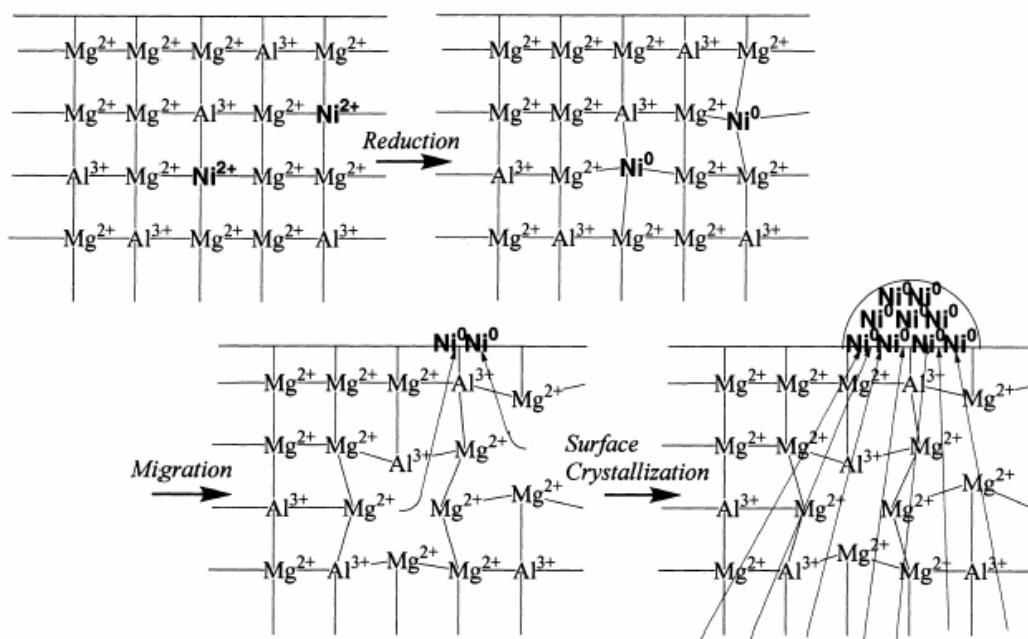


Fig. 3. 20 - Crystal structure of hydrotalcite-like precursor (2).

The hydrotalcite-derived catalysts (ex-HT), containing carbonates as interlayer anions, have already been reported as effective catalysts in the production of synthesis gas, using as active phase Ni, Rh and Ni/Rh. The characterization of these catalysts has revealed that the structure is made of MgO type and spinel type phases containing Rh and/or the Ni, which can be extracted to form rather stable metal particles.

High activity may be due to the highly dispersed Ni metal particles. Mg–Al hydrotalcite precursor, in which a part of the Mg sites were substituted by Ni, decomposed to  $\text{Mg}(\text{Al})\text{O}$  mixed oxide still containing  $\text{Ni}^{2+}$  at the  $\text{Mg}^{2+}$  site. When the mixed oxide was reduced,  $\text{Ni}^{2+}$  was reduced to  $\text{Ni}^0$ , migrated to the surface, and crystallized to form fine Ni metal particles on  $\text{Mg}(\text{Al})\text{O}$  mixed oxide as the support (Fig. 3. 21). Takehira<sup>99</sup> observed that the crystal growths of both Ni metal and  $\text{MgAl}_2\text{O}_4$  spinel after CPO reaction for 560 h, no decline was observed in the activity during the reaction under space velocity of  $1.156 \cdot 10^4 \text{ ml h}^{-1} \text{ g-cat}^{-1}$ . TEM

observation of the catalyst after the reaction for 560 h still showed finely dispersed Ni metal particles together with those of large size. The H<sub>2</sub> adsorption measurements still showed a high value of 91.3 μmol g-cat<sup>-1</sup>, corresponding to a dispersion of 8.5 %. Takehira<sup>99</sup> suggests that Ni species was continuously reduced to form fine Ni metal particles during a long term of the reaction. Active metal species is homogeneously distributed from the surface to the bulk of the catalyst particles and therefore a large part of the metal species is still located inside of the particles and cannot work as the active species.



**Fig. 3. 21 - Plausible mechanism of Ni metal crystallization from Mg(Al)O mixed oxide<sup>99</sup>.**

A general property of the ex-HT is that the amount and the nature of M(II) and M(III) modified the ratio between MgO and spinel phases.

The reducibility and stability of the Ni catalysts (in which Ni is preferentially present in a solid solution with Mg), are strongly affected by the Mg/Al/Ni ratio due to three main effects<sup>103, 104</sup>:

- (1) a low Mg content favors the formation of low active NiAl<sub>2</sub>O<sub>4</sub>,
- (2) Ni-rich samples exhibit low Ni<sup>2+</sup> reduction temperature, and fast deactivation due to the presence of large Ni particles,

(3) a decrease in reducibility of the  $\text{Ni}^{2+}$  ions is observed for high Mg/Ni ratio, due to the low concentration of Ni in the (Ni/Mg)O solid solution.

These effects limit the activity and stability of Ni containing catalysts that require new formulation. The situation for Rh catalysts is still more complicated, since it is soluted both in the spinel type and in the MgO type phases and the Mg/Al ratio affects the distribution of Rh between the two phases. The presence of other elements can change the correlation between Mg/Al ratio, spinel/MgO phase ratio and the Rh distribution<sup>105</sup>. In particular, the silicate can form with Mg or Al a specific phase, which can also incorporate Rh and or Ni. Furthermore, the presence of nesosilicate can improve thermal and mechanical resistance at high temperature.

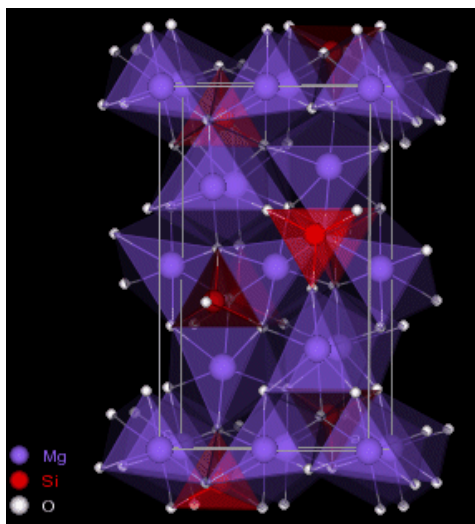


**Fig. 3. 22 – Forsterite-type structure.**

The insertion of silicates instead of carbonates as interlayer anion affects the derived structure both before and after calcination<sup>106</sup>. The silicates remain in the structure forming a new phase characterized by mixed silicate with a forsterite-type structure (Fig. 3. 22) having formula  $\text{Mg}_{2-x}\text{M}_{2/3x}\text{SiO}_4$  ( $\text{M} = \text{Al}, \text{Rh}$ ), together with a MgO-type structure, other reflections can be attributed to defective spinel-type phase. The calcined samples presented high surface area values ( $100 \text{ m}^2\text{g}^{-1}$ ) also after reaction, confirming the high thermal and mechanical stability of the materials.

These catalysts presents higher CH<sub>4</sub> conversion and CO and H<sub>2</sub> selectivity with respect to that with the same formulation, but obtained from an HT containing carbonates, in which the spinel-type phase was present<sup>107</sup>.

For a better comprehension of the catalytic behavior of the catalysts obtained by silicate containing hydrotalcite like precursors, the composition of the matrix was studied, with particular interest in the effect of the M(II)/M(III) ratio and in the role of the active metals inserted (Rh, Ni and Rh/Ni).

Furthermore, the role of the matrix as support was investigated comparing three catalysts based on hydrotalcite precursors, but prepared with different methods: coprecipitation, impregnation and coprecipitation on alumina support.

### 2.2.1. Role of the M<sup>2+</sup>/M<sup>3+</sup> ratio and role of the active metal

The catalysts containing as active phase Rh (0.04 a.a., as atomic ratio) or Ni (2 a.a.) have been prepared varying the Mg/Al ratio to investigate the role of the Mg/Al ratio on the structure and on the catalytic performances of the samples. The Mg/Al ratio has been varied from 65/35 to 80/20, preparing the samples Rh<sub>0,04</sub>Mg<sub>65</sub>Al<sub>34.96</sub>, Ni<sub>2</sub>Mg<sub>63</sub>Al<sub>35</sub>, and Rh<sub>0,04</sub>Mg<sub>80</sub>Al<sub>19.96</sub>, Ni<sub>2</sub>Mg<sub>78</sub>Al<sub>20</sub>. These samples have been prepared using a low amount of one active metal (Ni or Rh), to study contemporaneously the role of each active metal in the catalyst structure and catalytic performances.

The catalysts, containing silicates as interlayer anions, with different M(II)/M(III) ratio (65/35 or 80/20) were prepared using the coprecipitation method. The active metals were inserted in the hydrotalcite-like precursors, which were dried at 100°C overnight and then calcined at 900°C for 12 h (heating rate 10°C/min).

The precursors of the catalysts (dried at 100°C overnight) containing Mg/Al 80/20 show values of surface area lower than those of the precursors containing Mg/Al 65/35, while all the calcined samples (calcination at 900°C for 12 h) show surface area values comparable (Tab. 3. 2). The M(II)/M(III) atomic ratio does not affect the surface area of the calcined samples, since they show very similar values.

Composition	Atomic ratio	$M^{2+}/M^{3+}$	B.E.T. surface area ( $m^2/g$ )	
			100°C	900°C
Rh / Mg / Al	0.04 / 65 / 34.96	65/35	262	88
Ni / Mg / Al	2 / 63 / 35	65/35	118	86
Rh / Mg / Al	0.04 / 80 / 19.96	80/20	125	82
Ni / Mg / Al	2 / 78 / 20	80/20	71	86

Tab. 3. 2 – List of the catalysts and their surface area values, after drying at 100°C overnight and after calcination at 900°C for 12 h. .

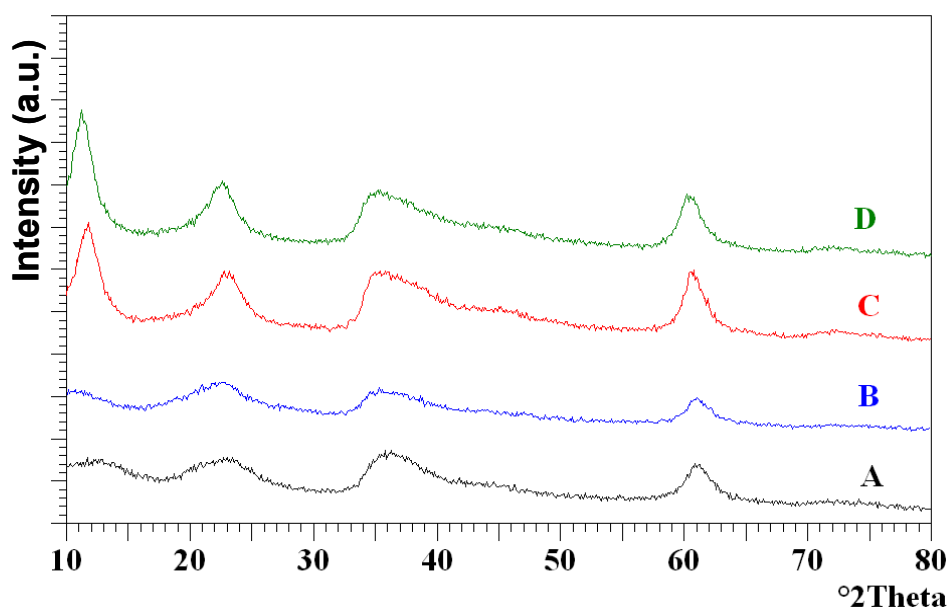


Fig. 3. 23 - XRD patterns of the HT precursors of the catalysts: (A)  $Rh_{0,04}Mg_{65}Al_{34,96}$ , (B)  $Ni_2Mg_{63}Al_{35}$ , (C)  $Rh_{0,04}Mg_{80}Al_{19,96}$  and (D)  $Ni_2Mg_{78}Al_{20}$ .

The XRD analysis of the precursors (HT) of the catalysts (ex-HT) containing Mg/Al 65/35 (Fig. 3. 23, A and B) are very similar each other, so as the patterns of the precursors of the catalysts containing Mg/Al 80/20 (Fig. 3. 23, C and D).

The precursors show the typical reflections of the hydrotalcite like-compounds containing silicates instead of carbonates anions: their broadness is due to the insertion of the silicates anions between the hydroxyl sheets. The higher amount of Mg in the samples with  $M(II)/M(III) = 80/20$  leads to a slightly crystalline structure of the precursors.

The XRD patterns of all the calcined samples show the forsterite type phase (Mg<sub>2</sub>SiO<sub>4</sub>) as main phase. All the patterns of calcined samples, whatever the Mg/Al ratio or the active metal, present similar crystallinity of this phase, indicating that the formation of the forsterite structure is the main reaction occurring during calcination (Fig. 3. 24).

The MgO type-phase is also present in all the samples. In particular, in the XRD patterns of the ex-HT catalysts containing Mg/Al 80/20 (Fig. 3. 24, C and D), the peaks of MgO phase have high intensity with respect to the samples Mg/Al 65/35. This is due to the large amount of magnesium cations and a lower amount of silicates with respect to the 65/35 matrix, due to their dependence on the M<sup>3+</sup> amount. Indeed, this leads to a lower formation of silicates that leaves part of the Mg cations free to give rise to a considerable amount of oxidic phase.

Therefore, differently to what happens to the surface area, the M(II)/M(III) ratio significantly affects the final structure of the samples. In fact, it is observed that the Mg<sub>2</sub>SiO<sub>4</sub>/MgO ratio changes in function of the Mg<sup>2+</sup>/Al<sup>3+</sup> ratio.

In addition, a defective spinel MgAl<sub>2</sub>O<sub>4</sub> phase can be detected similarly in all the XRD patterns of calcined samples. Indeed, the aluminum cations not involved in a silicate phase segregate forming this defective phase, but, probably, the thermal treatment is not sufficient to complete the formation of the spinel.

Increasing the aluminum content it was expected an increase of the spinel phase, analogously to what happens with HTlc-CO<sub>3</sub><sup>2-</sup>, while it was observed that the spinel/forsterite ratio is the same in all the samples whatever the Mg/Al ratio is. The observation indicates the presence of part of the aluminum cations in the forsterite structure.

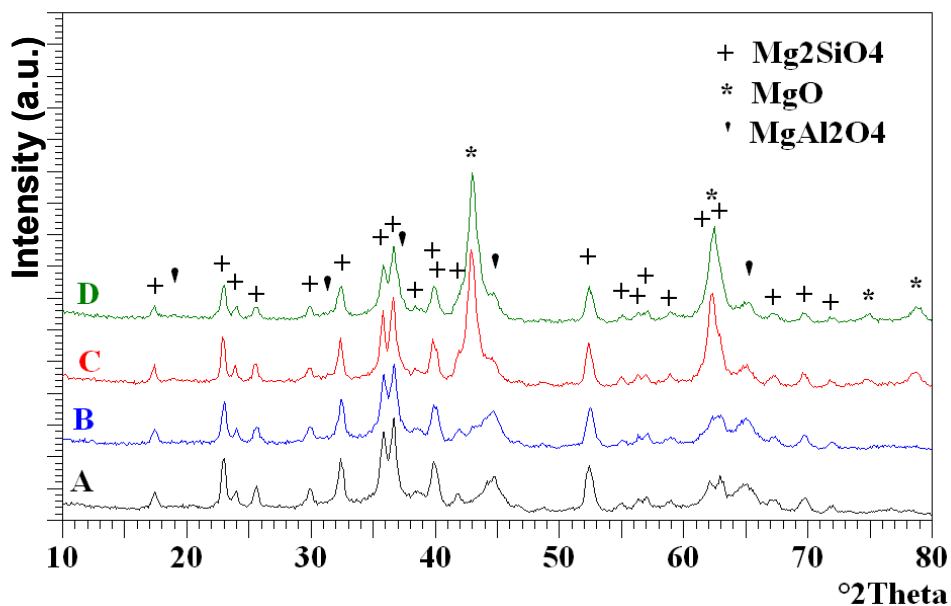


Fig. 3. 24- XRD patterns of the calcined samples (ex-HT catalysts): (A)  $\text{Rh}_{0,04}\text{Mg}_{65}\text{Al}_{34,96}$ , (B)  $\text{Ni}_2\text{Mg}_{63}\text{Al}_{35}$ , (C)  $\text{Rh}_{0,04}\text{Mg}_{80}\text{Al}_{19,96}$  and (D)  $\text{Ni}_2\text{Mg}_{78}\text{Al}_{20}$ .

All the catalysts have been tested in the partial oxidation of methane, after activation carried out in  $\text{H}_2/\text{N}_2$  equimolar flow at  $750^\circ\text{C}$  for 12 h.

Comparing the results of catalytic tests of the samples containing  $\text{Rh}_{0,04}$  but with a different ratio between Mg and Al, it can be observed that in the initial test ( $2/1/20$ ,  $500^\circ\text{C}$ ) the catalyst  $\text{Rh}_{0,04}\text{Mg}_{80}\text{Al}_{19,96}$  shows a methane conversion and a syngas selectivity appreciable, while the  $\text{Rh}_{0,04}\text{Mg}_{65}\text{Al}_{34,96}$  is totally inactive. The sample having the 80/20 matrix composition is more reducible, since it is already active in the initial test with diluted feed and low temperature, while, on the other hand, the sample with lower Mg/Al ratio seems to be not activated during the reduction procedure or re-oxidized at the light off of the reaction. The X ray diffraction analysis has shown a low amount of MgO phase in this sample, therefore only a low amount of Rh can be inserted in this phase. Most likely, the rest of the Rh, present in the Mg/Al silicate phase, is more difficult to be reduced. Feeding the reaction mixtures at  $750^\circ\text{C}$ , the Rh sample, with Mg/Al 65/35, has been reduced with the ongoing of the reaction, and even if its activity is still lower than the other sample, the differences decreases increasing the concentration of the reactants.

By increasing the concentration, also the heat produced during the reaction and the temperature in the catalytic bed increase. The higher temperature decreases

the differences between the catalyst performances which are pushed towards the equilibrium.

In the final test at 500°C and diluted mixture the sample with M(II)/M(III) 80/20 presents the same activity than in the initial test, while the other catalyst (Rh<sub>0,04</sub>Mg<sub>65</sub>Al<sub>34,96</sub>) is activated and maintains good yields in syn gas.

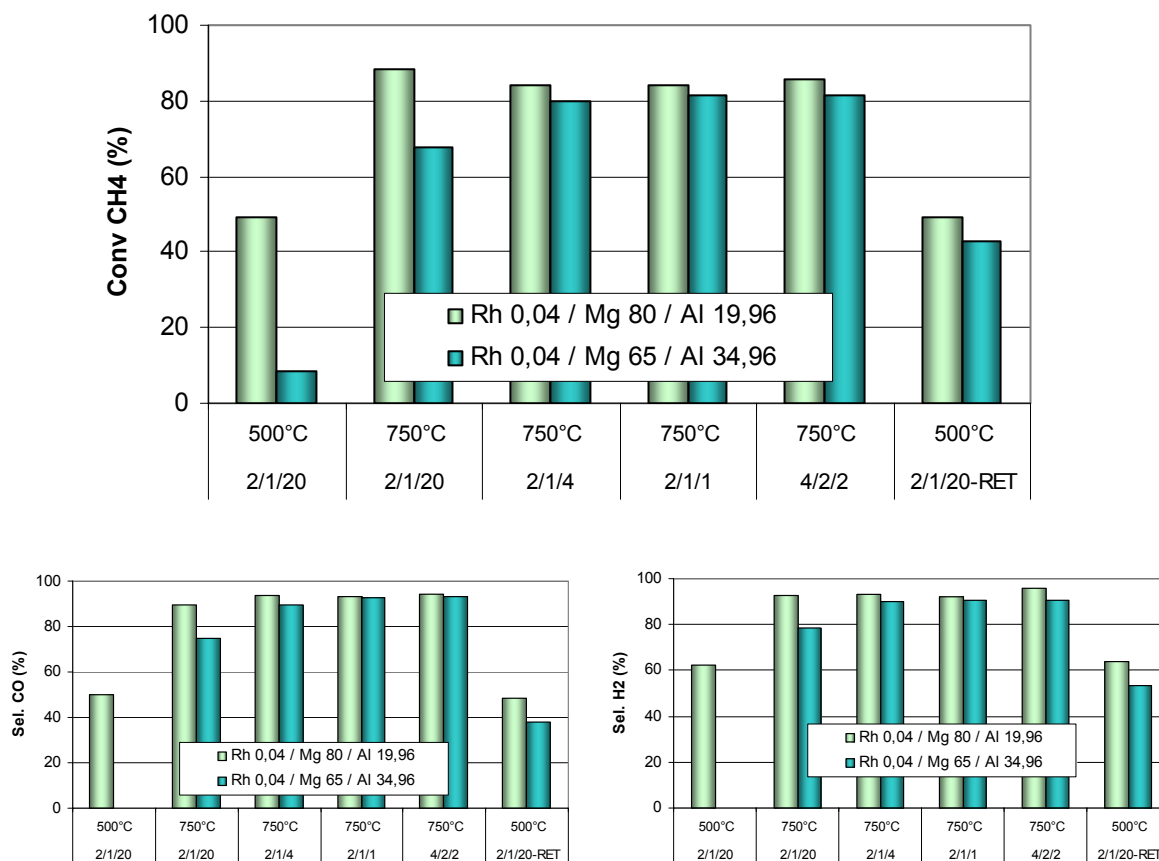


**Fig. 3. 25 - Comparison among CH<sub>4</sub> conversion and syngas selectivity of the catalysts Rh<sub>0,04</sub>Mg<sub>80</sub>Al<sub>19,96</sub> and Rh<sub>0,04</sub>Mg<sub>65</sub>Al<sub>34,96</sub>.**

The comparison between the activity results obtained using the catalysts containing Ni<sub>2</sub> but different ratio Mg/Al (80/20 and 65/35) are shown in Fig. 3. 26. In this case, both the catalysts present about the same activity and show quite the same performances. This means that the two catalysts are well reduced and keep the reduced state also at low temperature. The sample Ni<sub>2</sub>Mg<sub>78</sub>Al<sub>20</sub> presents, in all reaction conditions, slightly higher yields in syn gas than those of the sample Ni<sub>2</sub>Mg<sub>63</sub>Al<sub>35</sub>, even if by concentrating the feeds the differences are smoothed.

Both Ni samples maintain about the same values of CH<sub>4</sub> conversion and CO and H<sub>2</sub> selectivities in the final test (CH<sub>4</sub>/O<sub>2</sub>/He = 2/1/20 v/v at 500°C) with respect to the initial test performances, indicating good stability.

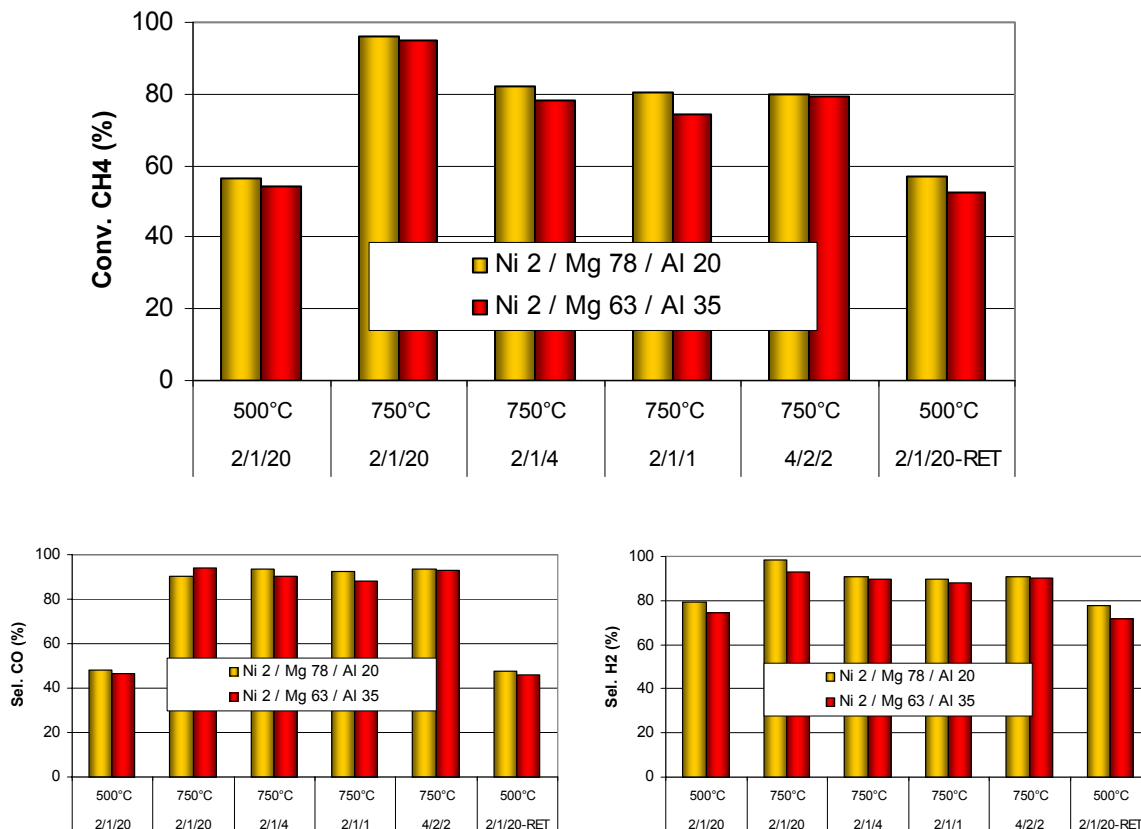


Fig. 3. 26 - Comparison among CH<sub>4</sub> conversion and syngas selectivity of the catalysts Ni<sub>2</sub>Mg<sub>78</sub>Al<sub>20</sub> and Ni<sub>2</sub>Mg<sub>63</sub>Al<sub>35</sub>.

For the study of the role of the active metal, the activities of the samples with the same Mg/Al ratio but different active metal (Rh<sub>0.04</sub> or Ni<sub>2</sub>) were compared (Fig. 3. 27 and Fig. 3. 28). It is possible to observe that feeding diluted mixture, both at low and high temperature, the samples containing Ni<sub>2</sub> are more active than those containing Rh<sub>0.04</sub>, but using harder reaction conditions (CH<sub>4</sub>/O<sub>2</sub>/He = 2/1/4, 2/1/1 and 4/2/2 v/v at 750°C) the methane conversion is higher for the samples containing Rh.

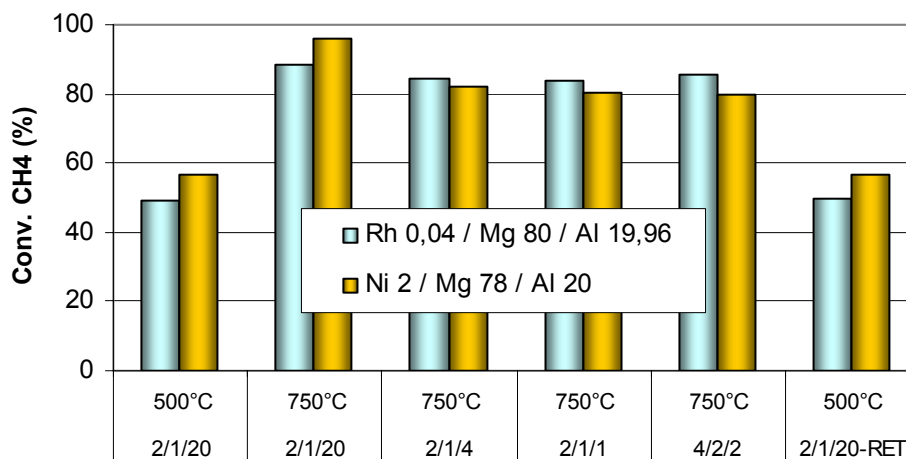


Fig. 3. 27 - Comparison between CH<sub>4</sub> conversions of the catalysts Ni<sub>2</sub>Mg<sub>78</sub>Al<sub>20</sub> and Rh<sub>0,04</sub>Mg<sub>80</sub>Al<sub>19,96</sub>.

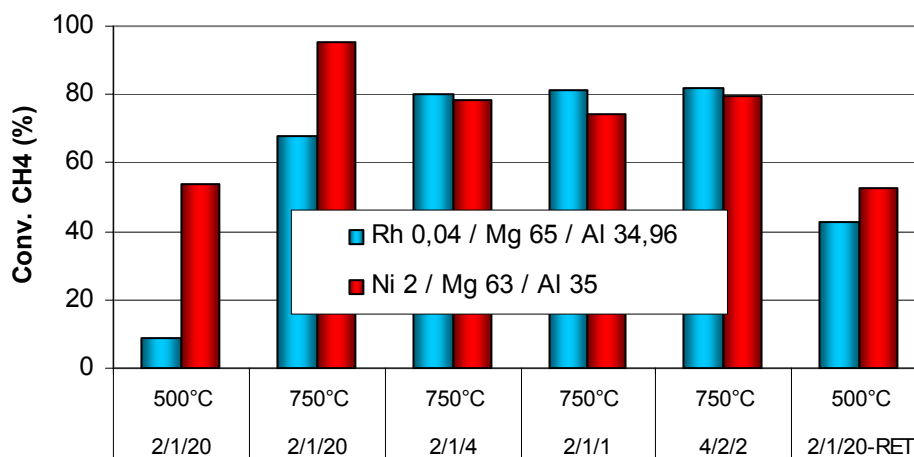


Fig. 3. 28 - Comparison among CH<sub>4</sub> conversion and syngas selectivity of the catalysts Ni<sub>2</sub>Mg<sub>63</sub>Al<sub>35</sub> and Rh<sub>0,04</sub>Mg<sub>65</sub>Al<sub>34,96</sub>.

Comparing the activity of the samples with Mg/Al 80/20 and with Mg/Al 65/35, the catalysts in which the active metal is inserted in the matrix M<sup>2+</sup>/M<sup>3+</sup> 80/20 is in all the reaction conditions more active. This is probably due to the insertion of high load of active metal in the MgO type phase, present in large amount, which leads to more reducible and stable metal crystallite.

Due to these reasons, the synergetic effect of Rh and Ni was investigated, synthesizing a catalysts with both active metals, but reducing at half amounts.

The sample has been prepared using the matrix composition having a M(II)/M(III) ratio equal to 80/20.

The surface area analysis of this new sample shows that value is similar to those of the previous samples and that a high value is maintained also after the thermal treatment at 900°C for 12 h.

<b>Composition</b>	<b>Atomic ratio</b>	<b>M<sup>2+</sup>/M<sup>3+</sup></b>	<b>B.E.T. surface area (m<sup>2</sup>/g)</b>	
			<b>100°C</b>	<b>900°C</b>
<b>Rh / Ni / Mg / Al</b>	0.02 / 1 / 79 / 19.98	80/20	111	117

**Tab. 3. 3 – Composition and surface area value, after drying at 100°C overnight and after calcination at 900°C for 12 h, of the sample containing both Rh and Ni.**

The structure of the precursor and that of the calcined sample analyzed by X-ray diffraction technique leads to the same consideration done for the samples having M(II)/M(III) ratio equal to 80/20, but containing only one metal (Fig. 3. 29 and Fig. 3. 30).

In particular, the calcined sample presents as main phases the forsterite (Mg<sub>2</sub>SiO<sub>4</sub>) and the MgO type-phases. The reflections of MgO phase have high intensity indicating that the M(II)/M(III) ratio significantly affects the final ratio between the phases.

In addition, the defective spinel MgAl<sub>2</sub>O<sub>4</sub> phase is present, but aluminium cations are probably partially inserted also in the forsterite structure.

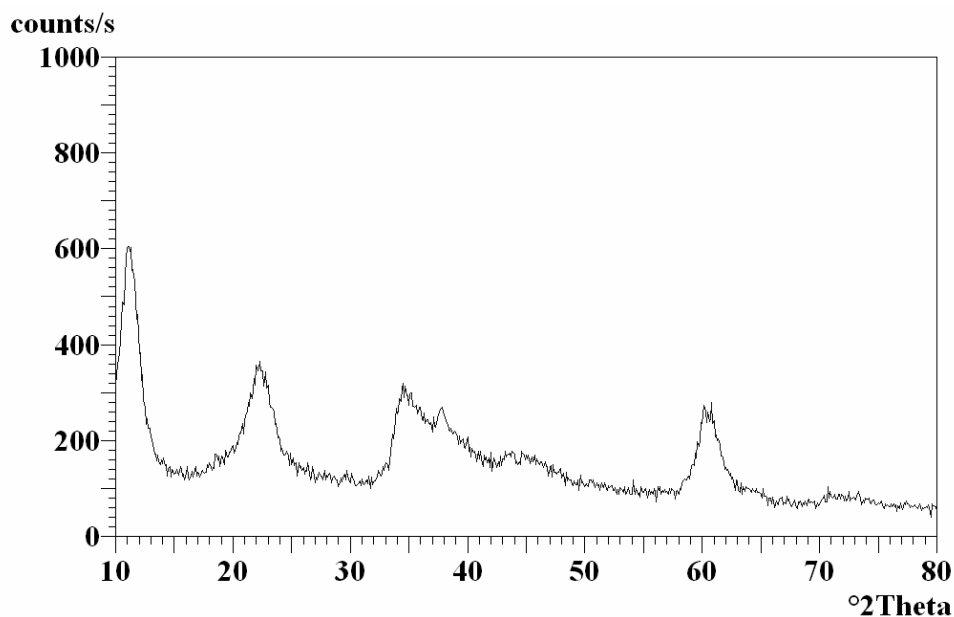


Fig. 3. 29 – XRD pattern of the hydrotalcite precursor of the sample  $\text{Rh}_{0.02}\text{Ni}_1\text{Mg}_{79}\text{Al}_{19.98}$ .

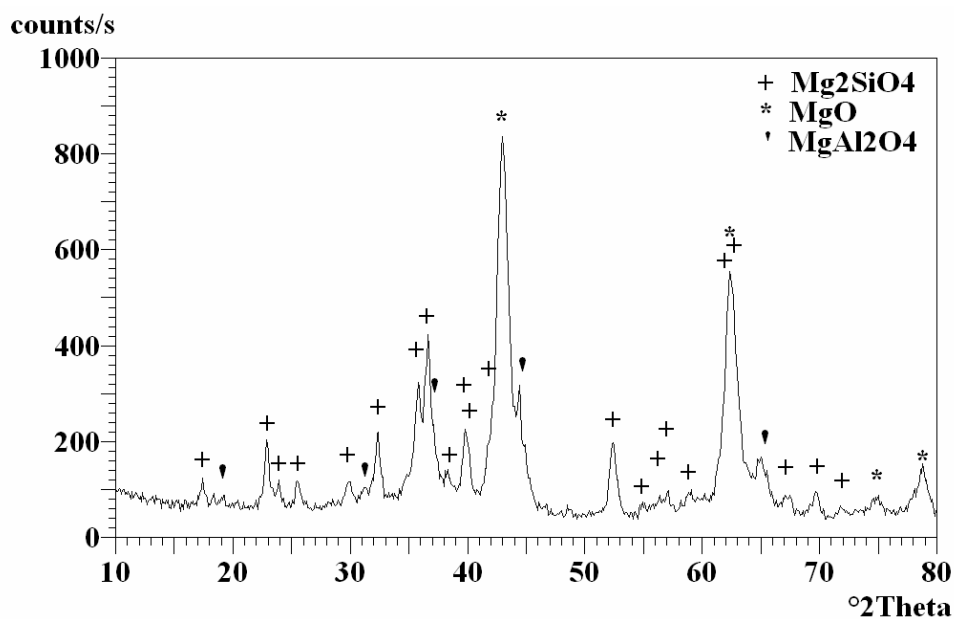


Fig. 3. 30 – XRD pattern of the sample  $\text{Rh}_{0.02}\text{Ni}_1\text{Mg}_{79}\text{Al}_{19.98}$  calcined at 900°C for 12 h.

The catalyst was tested in the lab plant for the partial oxidation of methane (Fig. 3. 31). This bimetallic catalyst presents the best catalytic performances, showing the synergetic effects between the two metals. In fact, comparing the activity of this sample with those of the monometallic samples (Fig. 3. 32), which contains only one metal, but twice the metal loading; it is evident that there is a synergetic

effect of the two metals. Indeed, the bimetallic catalyst does not presents only the good properties of the Ni at low temperature and diluted feed or the high activity of Rh using more concentrated mixtures, but also the activity is further improved.

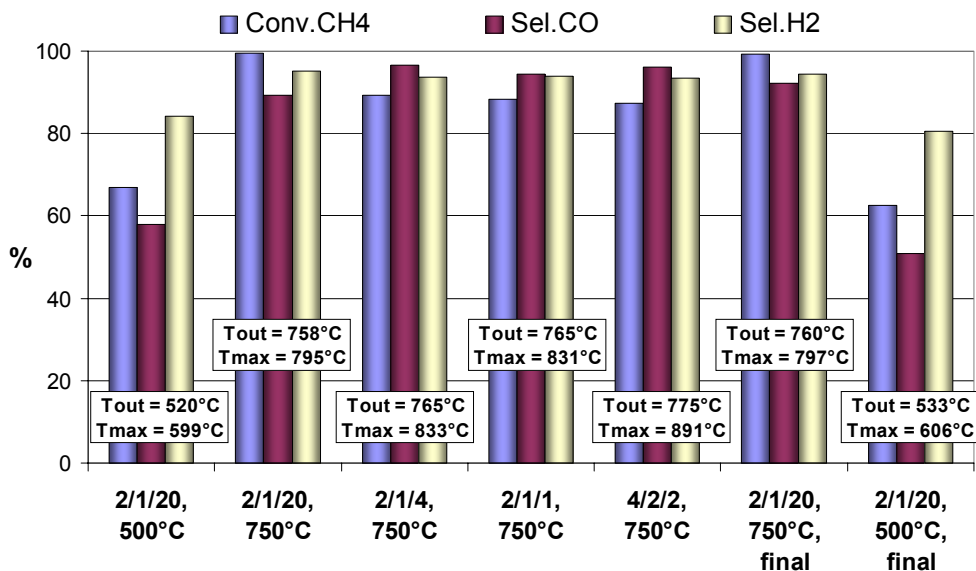


Fig. 3. 31 – Activity of the sample  $Rh_{0.02}Ni_1Mg_{79}Al_{19.98}$  in different CPO reaction conditions.

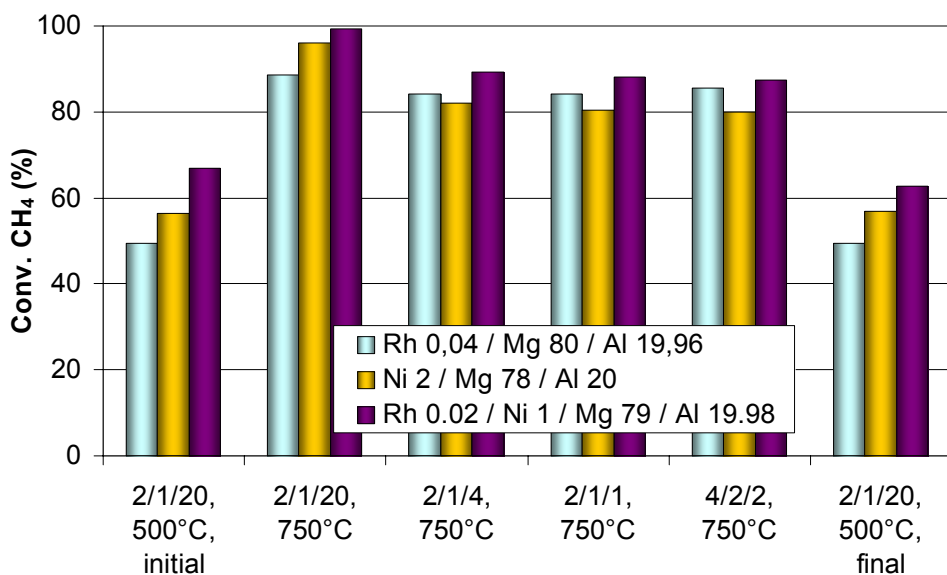


Fig. 3. 32 – Comparison of the methane conversion obtained with bimetallic and monometallic catalysts.

The bimetallic catalyst, in which the active Ni and Rh are inserted in the matrix having a M(II)/M(III) ratio of 80/20 was also subjected to duration tests (Fig. 3. 33). These tests were carried out maintaining the catalyst under operative conditions for 5 days. At the beginning and at the end of each day the diluted mixture (CH<sub>4</sub>/O<sub>2</sub>/He = 2/1/20 v/v) at 500°C was fed, while during the day reaction conditions simulating the use of air (CH<sub>4</sub>/O<sub>2</sub>/He = 2/1/4 v/v) at 750°C were fed. In both the reaction conditions, the activity of the bimetallic catalyst (Rh<sub>0.02</sub>Ni<sub>1</sub>Mg<sub>79</sub>Al<sub>19.98</sub>) is constant and similar to that obtained during the spot tests, indicating high reproducibility and high stability of the catalyst. In particular the sample shows high stability of the results feeding the diluted mixture at 500°C, either at the beginning or at the end of each days of tests, thus confirming that it was obtained very stable and well dispersed metallic particles on the catalyst surface, which do not deactivate (by sintering or coke formation) or re-oxidize during critical start up and shut down operations of the plant.

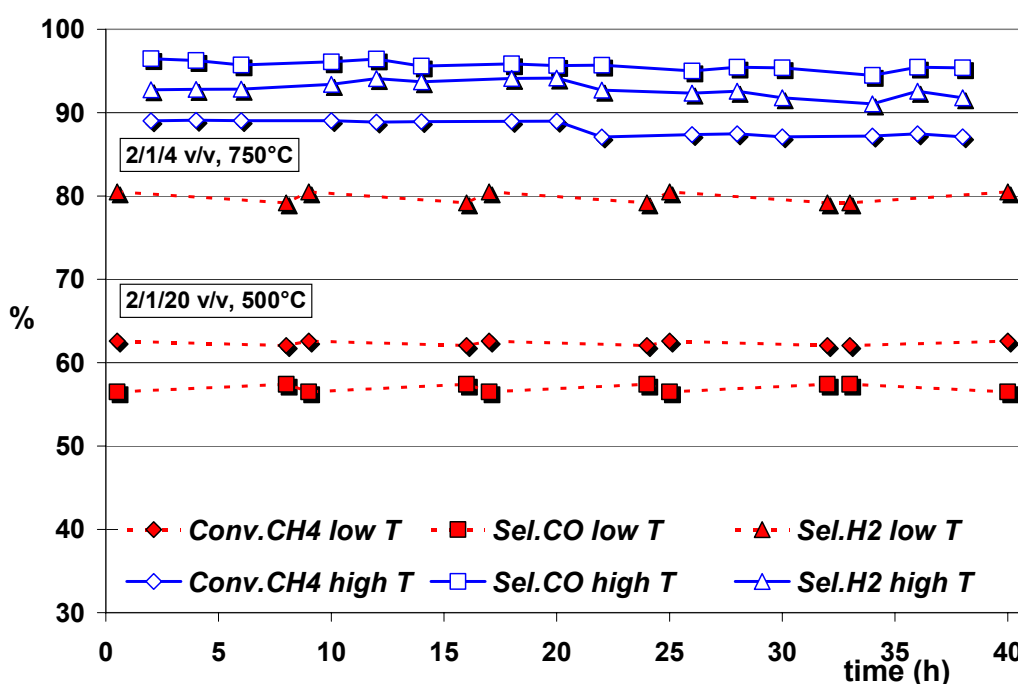


Fig. 3. 33 - Activity of the sample Rh<sub>0.02</sub>Ni<sub>1</sub>Mg<sub>79</sub>Al<sub>19.98</sub> with time-on-stream, duration test.

After the catalytic tests, the samples were characterized by XRD and B.E.T. surface area (Fig. 3. 34 and Tab. 3. 4). The XRD patterns shows the same phases present in the fresh samples (Mg<sub>2</sub>SiO<sub>4</sub>, MgO and MgAl<sub>2</sub>O<sub>4</sub> defective

phase), furthermore no changes in the crystallinity or in the ratio among the phases were observed. The metallic Ni phase was not observed in the patterns of the used samples, probably because of the good dispersion of the metal particles obtained during reduction from the mixed oxide phase.

Also the surface area values are unchanged with respect to those of the fresh samples, confirming the good stability of the catalyst structure under CPO reaction conditions.

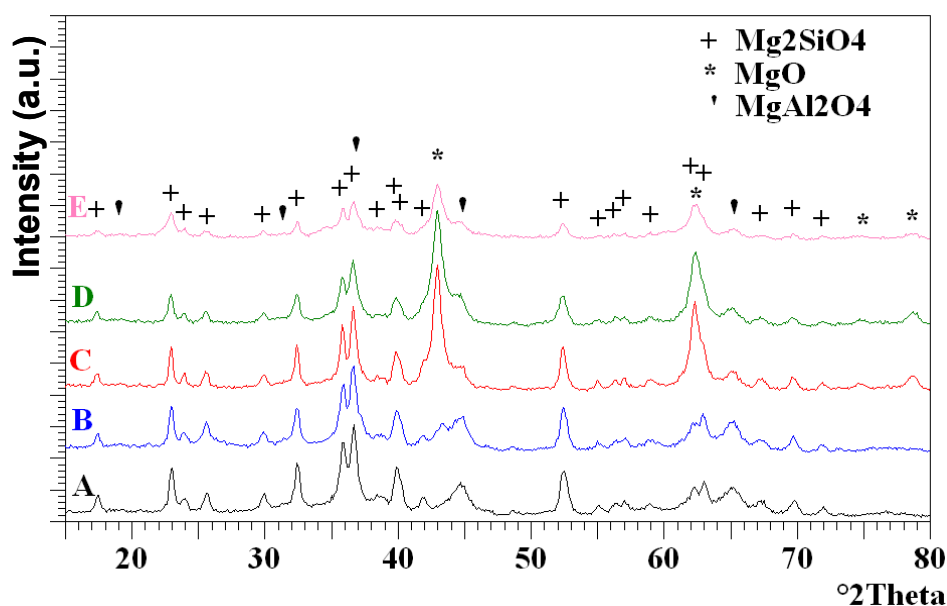


Fig. 3. 34 - XRD patterns of the used samples: (A)  $\text{Rh}_{0,04}\text{Mg}_{65}\text{Al}_{34,96}$ , (B)  $\text{Ni}_2\text{Mg}_{63}\text{Al}_{35}$ , (C)  $\text{Rh}_{0,04}\text{Mg}_{80}\text{Al}_{19,96}$ , (D)  $\text{Ni}_2\text{Mg}_{78}\text{Al}_{20}$  and (E)  $\text{Rh}_{0,02}\text{Ni}_1\text{Mg}_{79}\text{Al}_{19,98}$ .

Composition	$M^{2+}/M^{3+}$	B.E.T. surface area ( $\text{m}^2/\text{g}$ )	
		Fresh	Used
$\text{Rh}_{0,04}\text{Mg}_{65}\text{Al}_{34,96}$	65/35	88	81
$\text{Ni}_2\text{Mg}_{63}\text{Al}_{35}$	65/35	86	102
$\text{Rh}_{0,04}\text{Mg}_{80}\text{Al}_{19,96}$	80/20	82	82
$\text{Ni}_2\text{Mg}_{78}\text{Al}_{20}$	80/20	86	89
$\text{Rh}_{0,02}\text{Ni}_1\text{Mg}_{79}\text{Al}_{19,98}$	80/20	117	116

Tab. 3. 4 – Surface area values of the used samples.

### 2.2.2. Role of the hydrotalcite type matrix as support

The aim of this study was the preparation and characterization of different catalysts containing equal amounts of Ni (0.660 wt %) and Rh (0.022 wt %) obtained from hydrotalcite-type precursors (HT) and prepared according to different methodologies<sup>108</sup> (Fig. 3. 35).

In the first catalyst (*impregnated catalyst*), the active elements were introduced by impregnation, using a support obtained from a HT precursor containing silicates (ex-HT silicate Mg<sub>80</sub>/Al<sub>20</sub>). The second catalyst (*bulk catalyst*) was prepared as an example of bulk catalyst, inserting the active elements in the HT precursor by coprecipitation. The last sample (*supported bulk catalyst*) was prepared by supporting an HT phase containing the active metals on  $\alpha$ -Al<sub>2</sub>O<sub>3</sub>, preliminary washcoated by Disperal (commercial bohemite).

The hydrotalcite type precursors were prepared by coprecipitation at constant pH by dropping a 0.2 M aqueous solution containing the nitrate salts of the metal ions into a solution containing the silicates. The pH was kept constant by NaOH addition (10.5  $\pm$  0.2). The addition of the cation solution was carried out over 20 minutes; the obtained precipitate was kept in suspension under stirring at 60°C for 45 min, then filtered and washed with distilled water until a Na<sub>2</sub>O content lower than 0.02 wt % was obtained. The precipitate was dried overnight at 100°C.

Preparation of impregnated sample - The support hydrotalcite precursor was prepared as describe above using a cation solution containing Mg(NO<sub>3</sub>)<sub>2</sub> and Al(NO<sub>3</sub>)<sub>3</sub>. After washing and drying, the precursor was calcined at 900°C to obtain the support. The active metals were introduced on the powder of the support by incipient wetness impregnation using an aqueous nitrate solution (Ni(NO<sub>3</sub>)<sub>2</sub> and Rh(III) nitrate solution). The impregnated sample was dried at 120°C for 2 hours and then calcined again at 900°C for 12 h.

Preparation of bulk catalyst - The hydrotalcite type precursor was prepared using a cations solution containing: Ni(NO<sub>3</sub>)<sub>2</sub>, Rh(III) nitrate solution, Mg(NO<sub>3</sub>)<sub>2</sub> and Al(NO<sub>3</sub>)<sub>3</sub> in the right molar ratio. After washing and drying the precursor was calcined at 900°C for 12 h.

Preparation of supported bulk catalyst - The support of the third sample ( $\alpha$ -Al<sub>2</sub>O<sub>3</sub>, 4 m<sup>2</sup>/g), was washcoated using a primer, to create a  $\gamma$ - Al<sub>2</sub>O<sub>3</sub> thin layer on the  $\alpha$ -Al<sub>2</sub>O<sub>3</sub> with some OH group to which the hydrotalcite type precursor can be

grafted. The bohemite primer was prepared by dispersing the commercial bohemite in  $\text{HNO}_3$  aqueous solution. After mixing for 10 min, a stable dispersion of bohemite was obtained. The support,  $\alpha\text{-Al}_2\text{O}_3$ , in the right molar ratio, was added very slowly to the bohemite dispersion and then kept under stirring for at least 30 min at room temperature. The slurry was dried at room temperature overnight. Then the obtained  $\alpha\text{-Al}_2\text{O}_3$ /Disperal was added to the aqueous solution of the silicates and kept under stirring at  $50\text{-}60^\circ\text{C}$ , forming a homogeneous dispersion. The 0.2 M aqueous solution of the nitrates of the metals was prepared and dropped into the silicates/ $\alpha\text{-Al}_2\text{O}_3$ /Disperal dispersion, maintaining the pH constant ( $10.5 \pm 0.2$ ). At the end of the dropping, the solution was left under stirring for 45 minutes and then filtered. After washing the catalyst was dried at  $100^\circ\text{C}$  overnight and then calcined at  $900^\circ\text{C}$  for 12 h.

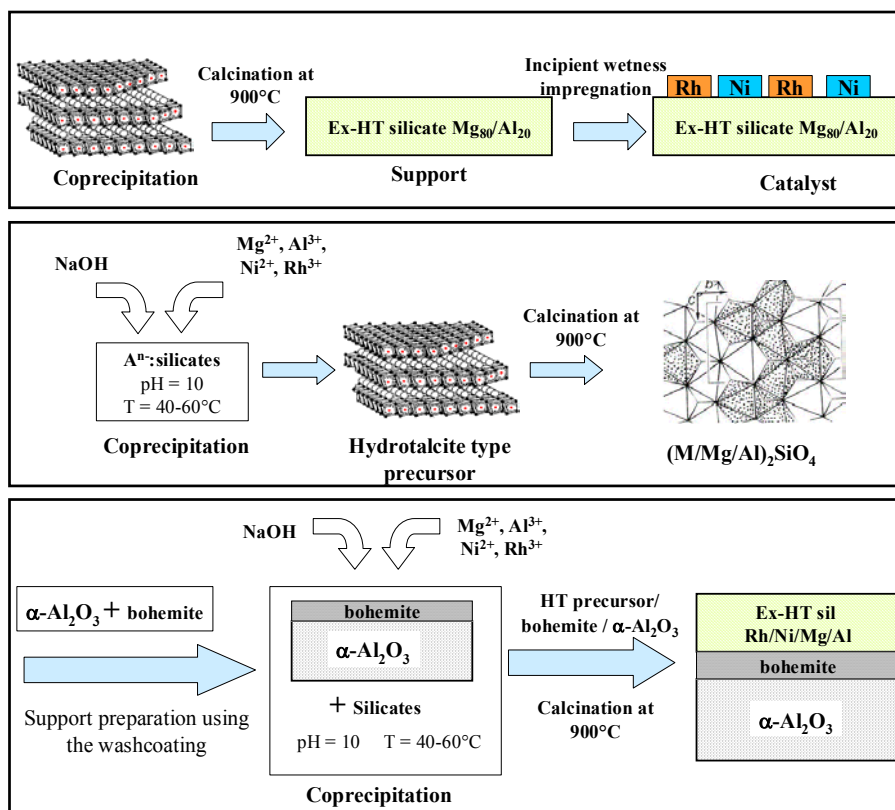


Fig. 3. 35 - Schematic preparation methods of the three investigated catalysts.

The impregnated and the bulk catalysts present high surface area values, typical of the HT samples (Tab. 3. 5). The supported bulk sample, in which the HT active phase is supported on  $\alpha\text{-Al}_2\text{O}_3$  shows a surface area only slightly higher than that

of the precursor, due to the presence of the bulk phase precipitated on the support (Tab. 3. 5). In fact, the surface area of the  $\alpha$ -Al<sub>2</sub>O<sub>3</sub> is 4 m<sup>2</sup>/g, while that of the precursor of the support  $\alpha$ -Al<sub>2</sub>O<sub>3</sub>/Disperal is 19 m<sup>2</sup>/g. Furthermore the final catalyst (after calcination at 900°C, in which the bohemite has been oxidized to  $\alpha$ -Al<sub>2</sub>O<sub>3</sub>) still shows a surface area value of 25 m<sup>2</sup>/g, due to the high surface area of the bulk phase obtained from hydrotalcite precursor (in this case 1/12 wt/wt of the whole sample). This means that the catalyst surface is probably similar to that of the bulk catalyst.

Description	B.E.T. SA (m <sup>2</sup> /g)		D (%)	MSA (m <sup>2</sup> /g <sub>metal</sub> )	ACS (nm)
	100°C	900°C			
<i>Impregnated sample:</i> Rh and Ni on ex-HT sil Mg <sub>80</sub> Al <sub>20</sub>	138	107	1.65	10.89	61
<i>Bulk sample:</i> ex-HT sil Rh <sub>0.01</sub> Ni <sub>0.57</sub> Mg <sub>79.43</sub> Al <sub>19.99</sub>	87	111	3.53	23.30	28
<i>Supported bulk sample:</i> ex-HT sil Rh <sub>0.15</sub> Ni <sub>8</sub> Mg <sub>60</sub> Al <sub>31.85</sub> on $\alpha$ -Al <sub>2</sub> O <sub>3</sub>	19	25	5.11	33.64	20

**Tab. 3. 5 - Catalyst compositions, B.E.T. surface area (SA) and results of the H<sub>2</sub> chemisorption analyses on the different catalysts having 0.660 wt % of Ni and 0.022 wt % of Rh (D = metal dispersion, MSA = metallic surface area and ACS = apparent crystallite size).**

The H<sub>2</sub> chemisorption analyses show that impregnated sample presents the lowest metal dispersion and the highest apparent crystallite size of the metals, probably due to weak interaction of the metal with the support that causes an easier sintering of the metals.

Analyzing the bulk and supported bulk samples, in which the metals are inserted inside the HT precursors, it is clear that the metal dispersions are higher than that of the impregnated one. The stronger interaction of the Ni and Rh with the support leads to smaller and stable particles, even if Ni and Rh inserted in the bulk of the catalysts are expected to be more difficult to reduce. The difference between the two coprecipitated samples is that, in the case of bulk catalyst, the concentration of the metals, in the bulk ex-HT phase, is lower because the active phase is dispersed in the whole mass of the catalyst, while for supported bulk

catalyst the mass of the bulk containing the metals is 1/12 of the whole catalyst and it is concentrated on the catalyst surface layer. Probably, the low dispersion can be due to the fact that not all the active metal is reduced in the bulk and in the supported bulk samples, however, the stronger interaction of Ni and Rh with the support phase is responsible of a lower sintering in such a hard reduction step. These hypothesis can also explain the fact that the dispersion of the metals in the supported bulk sample is higher than that of the whole coprecipitated catalyst due to the higher concentration of the active metals on the surface.

The XRD pattern of the ex-HT sil  $Mg_{80}/Al_{20}$ , calcined at  $900^{\circ}C$ , used as support, and those of the impregnated sample in different phases of preparation are reported in Fig. 3. 36. The support presents mainly  $Mg_2SiO_4$  and of MgO type-phases, but also the presence of spinel defective structure is observed. The impregnation gives rise to a decrease of crystallinity of  $Mg_2SiO_4$  and of MgO type-phases. After calcination, the XRD pattern is similar to that of the support. The XRD pattern of the spent catalyst is also reported and shows no significant differences if compared to that of the fresh catalyst. The very low amounts of Rh (0.022 wt %) and Ni (0.66 wt %) are not detectable.

The bulk catalyst, containing the same amount of Ni and Rh of the previous sample, has been prepared as a bulk ex-hydrotalcite catalyst. The XRD patterns of the fresh and used samples again reveal the presence of  $Mg_2SiO_4$ , MgO and spinel defective phases (Fig. 3. 37). There are no phases containing only Rh or Ni in both samples, because of their low amounts.

The XRD patterns of the supported bulk sample, ex-HT silicate  $Rh_{0.15}Ni_8Mg_{60}Al_{31.85}/Disperal/\alpha-Al_2O_3$  (1//1/10 wt), in different steps of preparation are reported in Fig. 3. 38. In the final catalyst, besides the support phase, the reflections of  $Mg_2SiO_4$  are present together with the spinel defective phase, even if the intensities of the peaks are low, according to the small amount of HT-silicate present in this catalyst (1/12 of the sample). The MgO type phase is not detected due to the different M(II)/M(III) ratio of this catalyst, indeed the low amount of this phase justify the absence of these reflections.

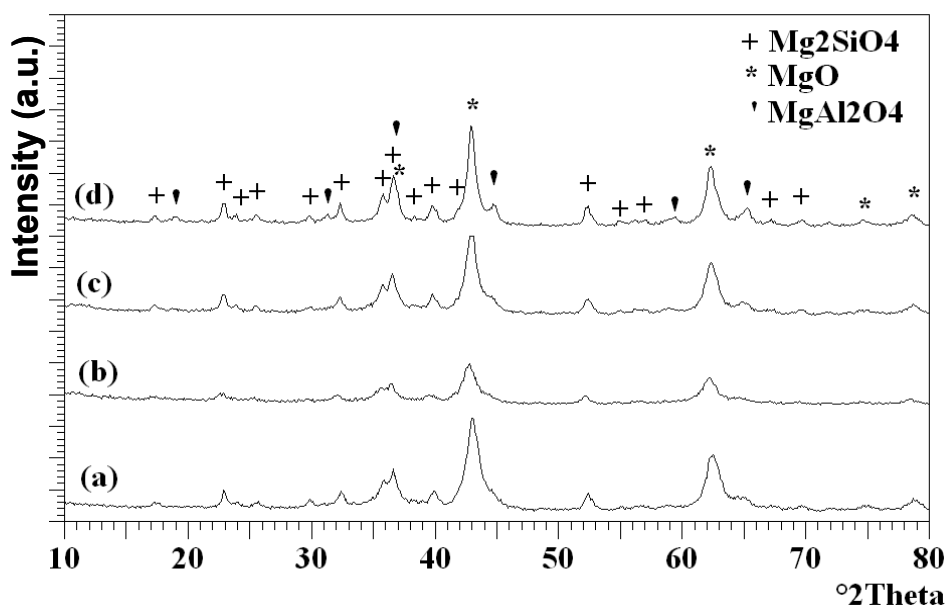


Fig. 3. 36 - XRD patterns of impregnated catalyst in different steps of preparation and after reaction: (a) Ex-HT Mg<sub>80</sub>Al<sub>20</sub>, support calcined at 900°C, (b) Ex-HT Mg<sub>80</sub>Al<sub>20</sub> impregnated with Rh and Ni, not calcined, (c) Ex-HT Mg<sub>80</sub>Al<sub>20</sub> impregnated with Rh and Ni, calcined at 900°C, (d) Ex-HT Mg<sub>80</sub>Al<sub>20</sub> impregnated with Rh and Ni, calcined at 900°C, used sample.

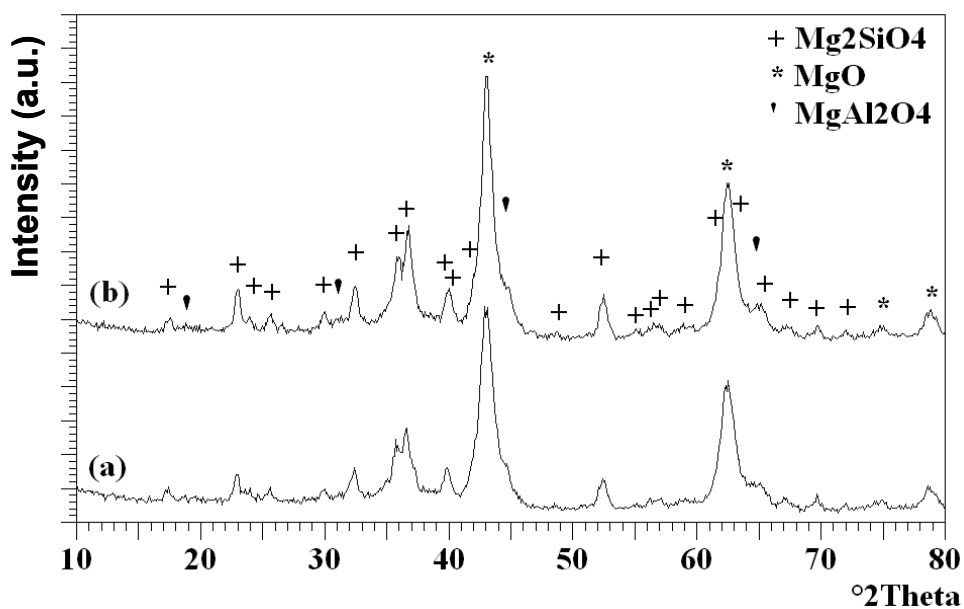
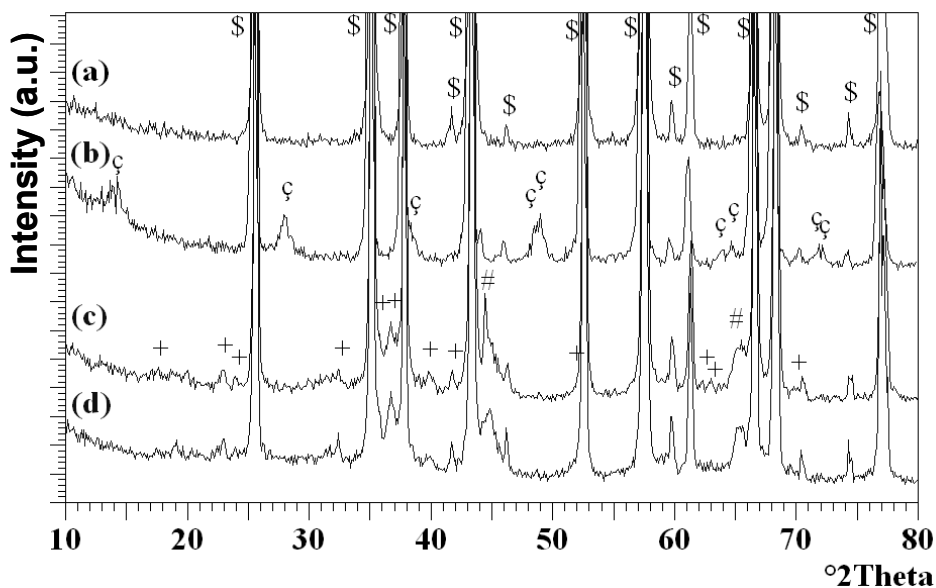


Fig. 3. 37 - XRD patterns of bulk catalyst, Ex-HT silicate Rh<sub>0.01</sub>Ni<sub>0.57</sub>Mg<sub>79.43</sub>Al<sub>19.99</sub> (a) before and (b) after reaction.



**Fig. 3. 38 - XRD patterns of supported bulk catalyst in different steps of preparation and after reaction (a)  $\alpha$ - $\text{Al}_2\text{O}_3$ , (b) Disperal/ $\alpha$ - $\text{Al}_2\text{O}_3$ , (c) Ex-HT silicate  $\text{Rh}_{0.15}\text{Ni}_8\text{Mg}_{60}\text{Al}_{31.85}$ //Disperal/ $\alpha$ - $\text{Al}_2\text{O}_3$  and (d) used Ex-HT silicate  $\text{Rh}_{0.15}\text{Ni}_8\text{Mg}_{60}\text{Al}_{31.85}$ //Disperal/ $\alpha$ - $\text{Al}_2\text{O}_3$ . [ $\$$  =  $\alpha$ - $\text{Al}_2\text{O}_3$ ,  $\text{ç}$  = bohemite, + =  $\text{Mg}_2\text{SiO}_4$ , # =  $\text{MgAl}_2\text{O}_4$  defective phase].**

In the catalytic tests at low temperature, the impregnated catalyst showed very low activity while at high temperature the activity and selectivity were high (Fig. 3. 39). The possibility of a lack of activation of the active phase by the reductant mixture  $\text{H}_2/\text{N}_2$  does not seem possible, since the metals have been impregnated on the support surface. Therefore, it may be hypothesized that in the initial conditions (2/1/20 v/v,  $500^\circ\text{C}$ ) the active metals are re-oxidized by the reaction mixture. The interaction of the impregnated metals and the support is weak and they are easily re-oxidized.

The bulk catalyst presented very low activity in the initial test. With increasing the oven temperature to  $750^\circ\text{C}$ , the methane conversion increased remarkably. By feeding the concentrated mixtures, the methane conversions were almost constant reaching values around 86%.

The activity of the supported bulk sample was high in all the reaction conditions both at  $500$  and  $750^\circ\text{C}$ .

Comparing the performances of the three samples it is evident that the worst activity is observed for the impregnated catalyst and this is probably due to the lower metal dispersion and stability of the metal particle on the surface of the

support, obtained using this preparation method. Between the bulk and the supported bulk samples the difference are significant only in the initial test due to the more difficult reduction of the metal of the bulk sample. As already observed, the concentration of the metals, in the bulk ex-HT phase, is lower and the metals must be extracted from the whole mass of the bulk, while for the supported bulk catalyst the metals are concentrated on the catalyst surface, and their reduction is easier or however more efficient.

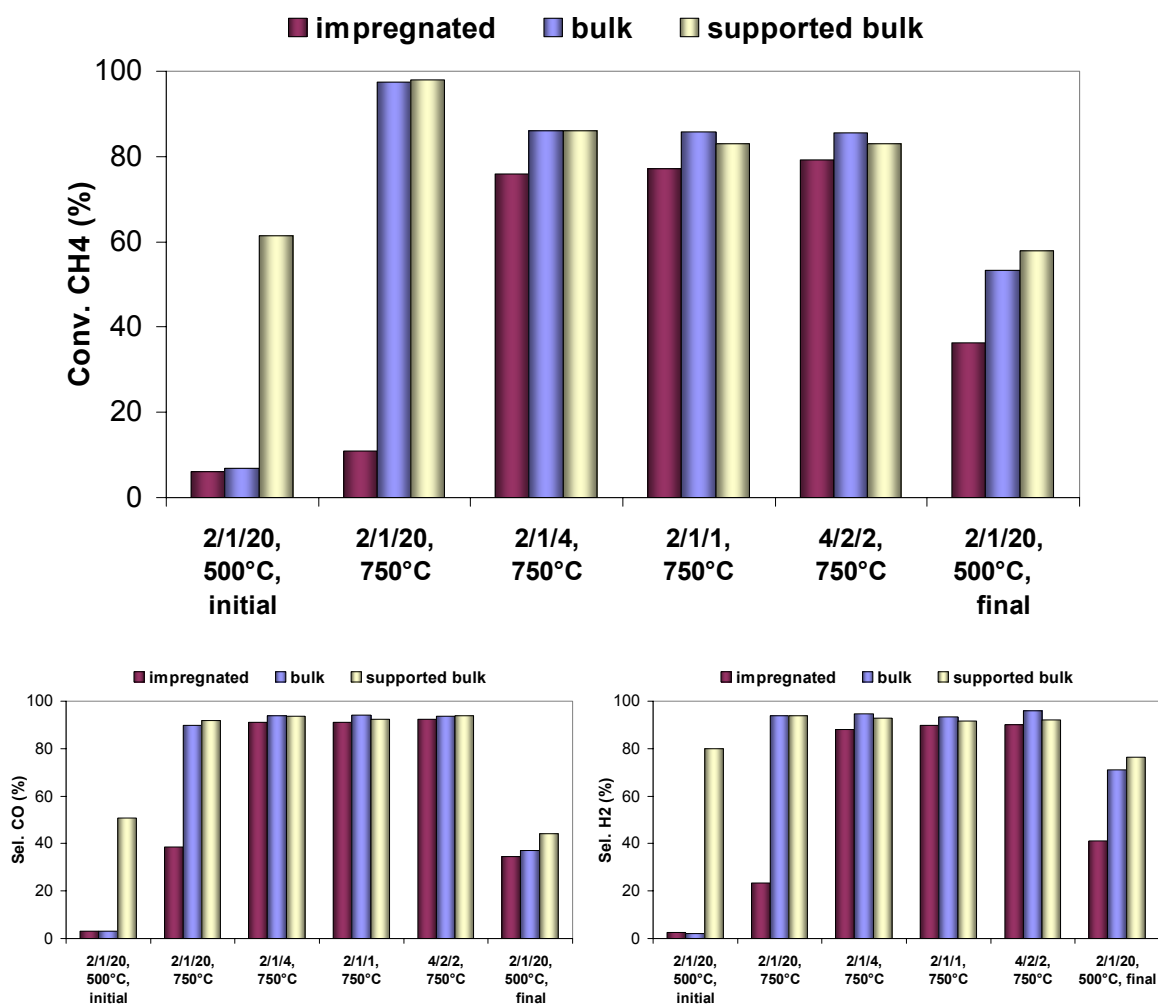


**Fig. 3.39 - Comparison of CH<sub>4</sub> conversions, H<sub>2</sub> and CO selectivities of the investigated catalysts in different reaction conditions.**

Finally, all the catalysts have been subjected to deactivation tests, while keeping the catalyst in hard reaction conditions (CH<sub>4</sub>/O<sub>2</sub>/He = 2/1/4 v/v, T<sub>oven</sub> = 750°C, CT = 65 ms) during the day (8h) and controlling the deactivation with tests at low

temperature ( $\text{CH}_4/\text{O}_2/\text{He} = 2/1/20$  v/v,  $T_{\text{oven}} = 500^\circ\text{C}$ ,  $\text{CT} = 65$  ms). The tests at low temperature were carried out for each of the run as initial tests by heating the sample from room temperature to  $500^\circ\text{C}$  and feeding the dilute mixture, and, subsequently, as final tests by cooling from the higher temperature.

Also in the lifetime test, at low temperature ( $500^\circ\text{C}$ ) the catalytic activity of the impregnated catalyst was very low, thus confirming that, for this catalyst, these conditions promote the oxidation of the catalyst. When feeding the  $\text{CH}_4/\text{O}_2/\text{He} = 2/1/4$  mixture at  $750^\circ\text{C}$  a small increase in the yields of syn gas was observed between the first day (8 h) and the second day on stream. Then the activity remained constant (Fig. 3. 40).

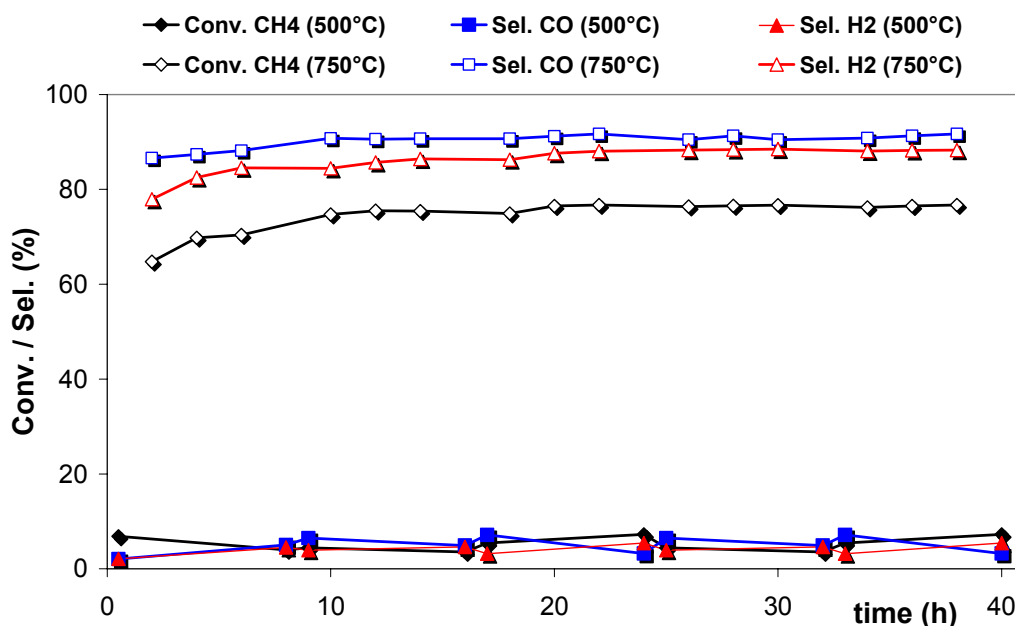


**Fig. 3. 40 - Results of the tests carried out as a function of time-on-stream on the impregnated catalyst (reaction conditions:  $T_{\text{oven}} = 500^\circ\text{C}$ ,  $\text{CH}_4/\text{O}_2/\text{He} = 2/1/20$  v/v,  $\text{CT} = 65$  ms and  $T_{\text{oven}} = 750^\circ\text{C}$ ,  $\text{CH}_4/\text{O}_2/\text{He} = 2/1/4$  v/v,  $\text{CT} = 65$  ms).**

At low temperature, the bulk catalyst presents, at the beginning of the run of the lifetime test, very low activity, but an increase in yields of syn gas in the final tests of the day (Fig. 3. 41). This is probably due to the effect of the initial conditions after start-up, in which the mixture was fed at  $500^\circ\text{C}$  after a He stream, re-oxidizing the active phase. On the contrary, the tests at the end of the day were carried out by lowering the temperature and diluting the gas in reaction stream from hard conditions (high reducing atmosphere) while keeping the reaction running (i.e. at temperature higher than  $500^\circ\text{C}$  in a  $\text{H}_2$ , CO containing

atmosphere, due to the high activity of this catalyst). In fact, in these tests the bulk sample shows high activity also at low temperature. Moreover, the activity at high temperature and with 2/1/4 v/v mixture shows very constant results all over the 5 days (both CH<sub>4</sub> conversion and syngas selectivity).

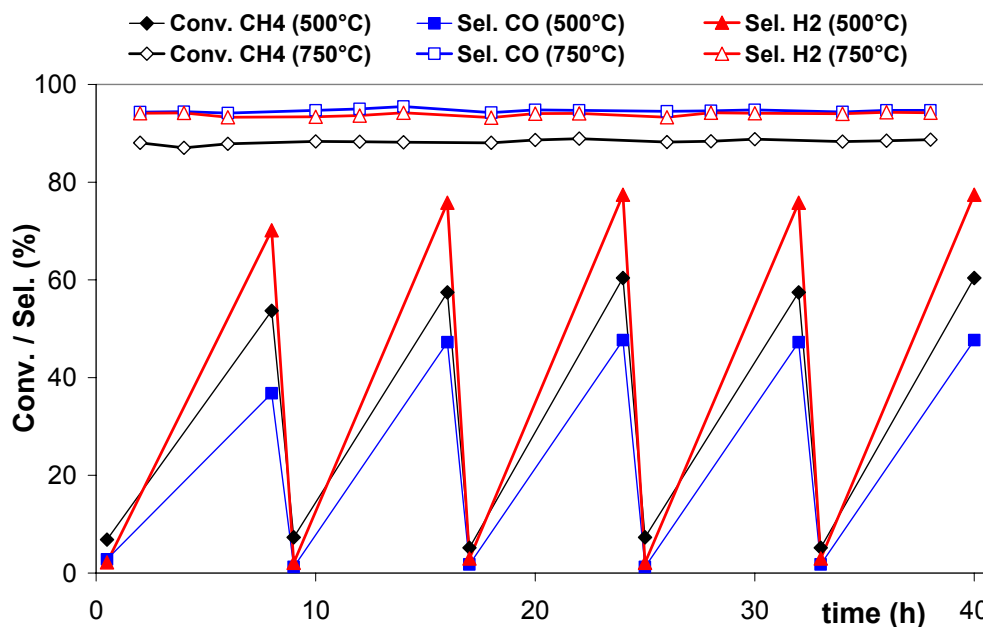


**Fig. 3.41 - Results of the tests carried out as a function of time-on-stream on the bulk catalyst (reaction conditions:  $T_{\text{oven}} = 500^{\circ}\text{C}$ ,  $\text{CH}_4/\text{O}_2/\text{He} = 2/1/20$  v/v,  $\text{CT} = 65$  ms and  $T_{\text{oven}} = 750^{\circ}\text{C}$ ,  $\text{CH}_4/\text{O}_2/\text{He} = 2/1/4$  v/v,  $\text{CT} = 65$  ms).**

The activity of the supported bulk catalyst was high in both the reaction conditions used for the deactivation test. The values of methane conversion and product selectivities remain almost constant during all the days of test. In particular, with respect to the other catalysts, feeding the diluted mixture at low temperature, the catalyst shows high and constant conversions and selectivities (Fig. 3.42).

Therefore, the catalyst with the best performances is the supported catalyst, in particular at low temperature and with the diluted mixture, since these conditions are far from the thermodynamic equilibrium. With increasing the temperature and feed concentration, the differences between the catalysts are smoothed, although the supported catalyst shows yield in syngas always higher than those of other catalysts. With the exception of the initial test at  $500^{\circ}\text{C}$  with 2/1/20 v/v mixture, the bulk catalyst also showed interesting results.

The observed scale of activity:

supported bulk catalyst > bulk catalyst > impregnated catalyst

may be attributed to the availability and to the dimensions of the metal particles on the surface, as demonstrated by the H<sub>2</sub> chemisorption results.

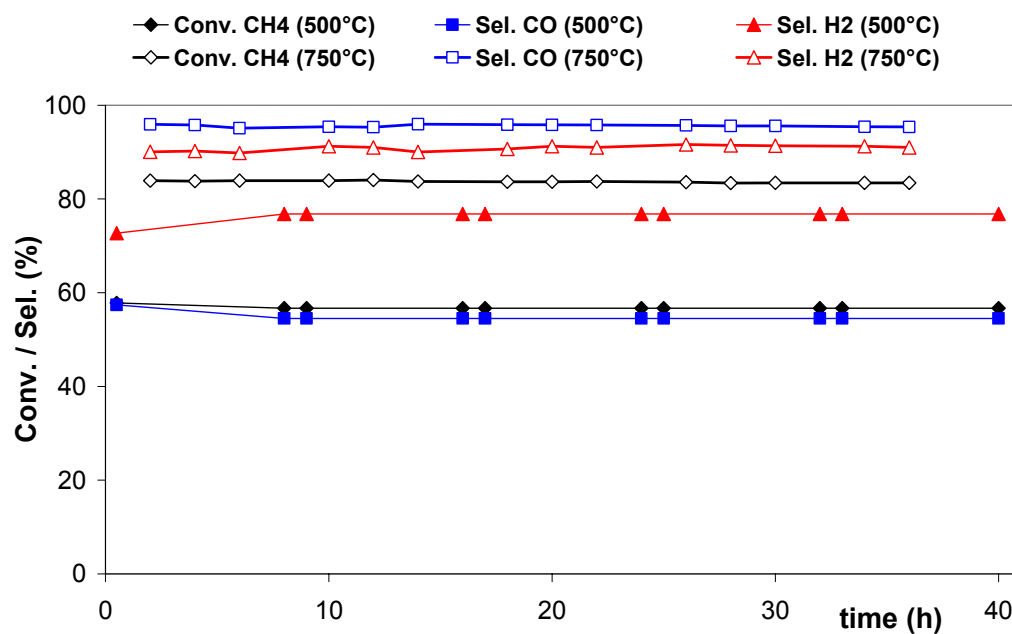


**Fig. 3. 42 - Results of the tests carried out as a function of time-on-stream on the supported bulk catalyst (reaction conditions:  $T_{\text{oven}} = 500^{\circ}\text{C}$ ,  $\text{CH}_4/\text{O}_2/\text{He} = 2/1/20$  v/v,  $\text{CT} = 65$  ms and  $T_{\text{oven}} = 750^{\circ}\text{C}$ ,  $\text{CH}_4/\text{O}_2/\text{He} = 2/1/4$  v/v,  $\text{CT} = 65$  ms).**

### 3. Steam reforming of methane

The second part of the research regards the steam methane reforming and the needs to further develop the industrial process. The study was initially focused on the investigation of commercial catalysts, examining the deactivation in industrial conditions, the role of the operating conditions (P, T, CT, S/C,  $V_{\text{cat}}$  and  $D_p$ ) and the activity of different type of catalysts.

Successively, innovative materials, as bulk (PVK and HT) and structured catalysts, (SiC and metallic foam) were studied in view of the preparation of structured reactor (wall reactor, monolith reactor and membrane reactor) that could enhance the H<sub>2</sub> production by SR.

#### 3.1. Characterization of spent industrial catalysts

Two series of used samples of the same commercial catalyst (13 wt % Ni/MgAl<sub>2</sub>O<sub>4</sub>) delivered by Air Liquide and unloaded from two industrial steam reforming plants, one locate in Portugal and the other in USA, were characterized to study the deactivation occurred during real time-on-stream.

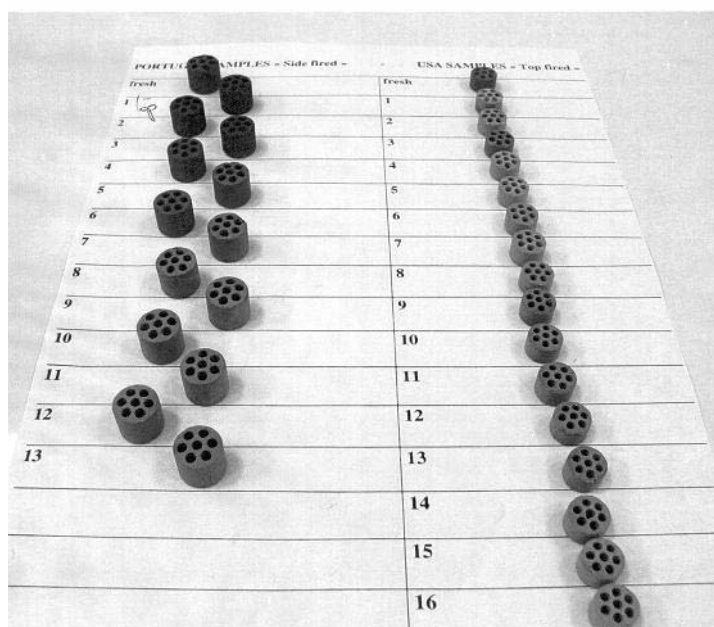


Fig. 3. 43 – Spent samples coming from the two industrial steam reforming plant.

### 3.1.1. Characterization of Portugal used samples

The spent catalyst coming from the Portugal Steam Reforming plant was constituted by 13 samples taken from a tube 13.9 m long. The samples were taken at constant distance (every 1 m); and were labeled so that the number 1 corresponds to the one of the top of the tube and the number 13 to that at the bottom. The catalyst is based on 13 % Ni / MgAl<sub>2</sub>O<sub>4</sub>.

The Portugal steam reforming plant was heated by a side fire furnace and the operating conditions to which the catalyst inside the tubes was subjected varied down the length of the tube:

- inlet conditions were: 650°C, 32.9 bar, S/C = 2.5,
- outlet conditions were: 913°C, 30.7 bar.

The plant was switched off and a tube unloaded for the characterization of the spent catalyst after about 6 years of operation. The original catalyst was identical all down the tube. The conditions of the shut down of the plant were conducted from normal operating conditions by a first flow with steam and hydrogen, and a second flow with nitrogen.

The fresh sample and a spent one, chosen in the middle of the tube (Port-7), were subjected to ICP analyses. The results show that the sample N. 7 presents a slightly higher content of Ni with respect to the fresh catalyst. It is possible that not all the pellets of the catalyst contain the same amount of Ni, due to the preparation method, by impregnation, which may leads to non-uniform distribution of the active metal on the support surface.

SAMPLE NAME	ICP (% wt of Ni)
PORT. Fresh	13,8
PORT. N. 7	14,9

**Tab. 3. 6 - Results of ICP analyses on Portugal fresh sample and on a used sample chosen in the middle of the tube.**

The fresh sample presents similar B.E.T. surface area to those of the used samples, the surface area range between 6 and 20 m<sup>2</sup>g<sup>-1</sup> (Tab. 10).

PORT Sample	BET Surface area (m <sup>2</sup> g <sup>-1</sup> )
Fresh	18
1	18
2	8
3	20
4	6
5	16
6	18
7	12
8	14
9	14
10	14
11	4
12	2
13	12

**Tab. 3. 7 - BET surface area values of fresh and used samples coming from Portugal plant.**

More detailed analyses were performed on the fresh sample and on the spent N. 1, 4, 7, 10 and 13. In the XRD patterns of these samples the phases that are present are MgAl<sub>2</sub>O<sub>4</sub> (as major phase because it is the support) and Al<sub>2</sub>O<sub>3</sub> (presents in very little amount). Moreover, the diffraction pattern of the fresh sample present the active metal (Ni) as NiO, while all the XRD patterns of spent samples contain only the reflection of Ni<sup>0</sup> (Fig. 3. 44).

The results of the XRD analyses are very interesting because they show a different degree of the Ni reduction, in spent samples, going down trough the catalytic bed. Furthermore, the crystal size of Ni metallic phase is gradually increasing descending from top (sample N.1) to the bottom (sample N.13) of the tube. The difference between the two reflections analyzed, (200) and (220) shows different increases, suggesting a not isotropic behavior (Fig. 3. 45).

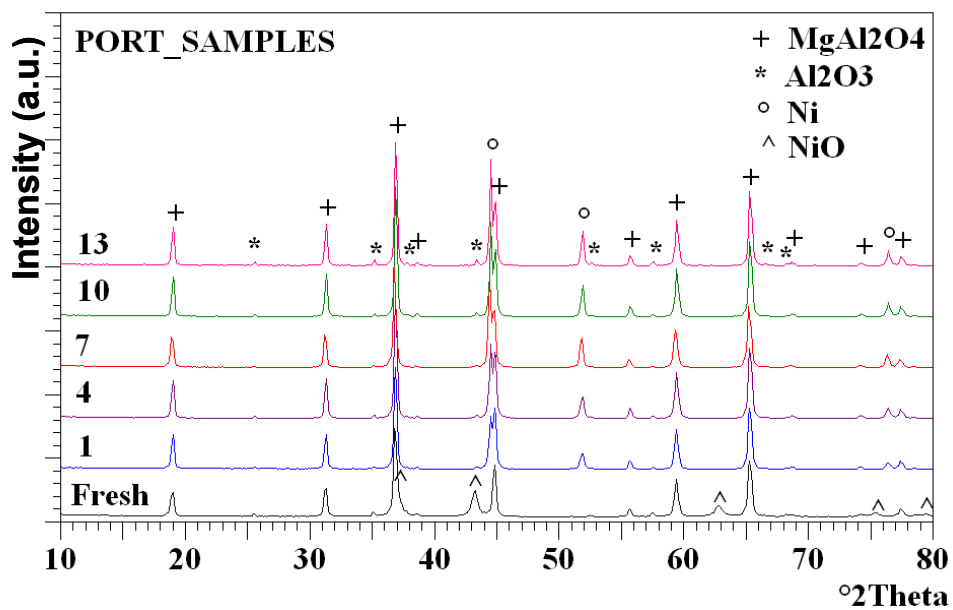


Fig. 3. 44 - XRD patterns of fresh and spent samples coming from Portugal plant.

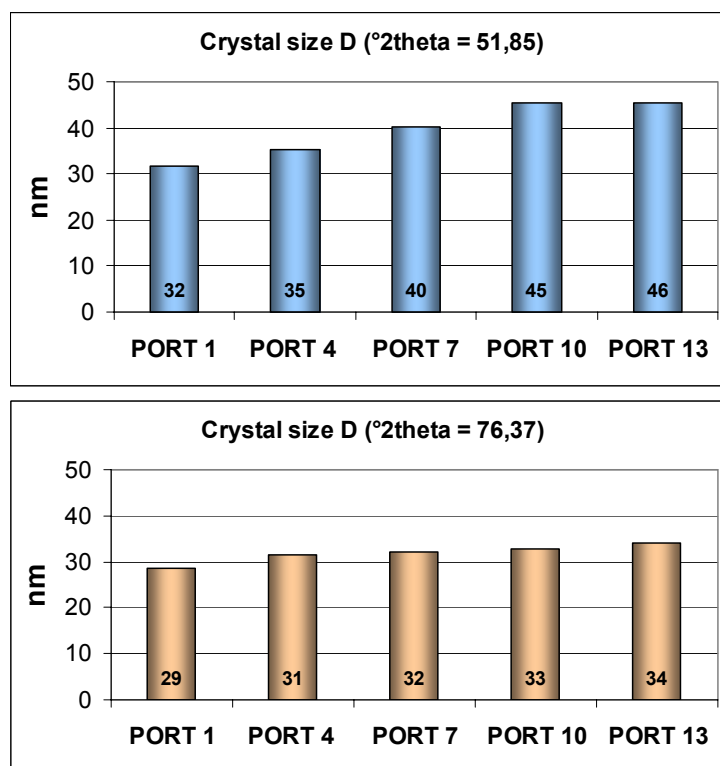


Fig. 3. 45 - Crystal size of Ni<sup>0</sup> in the Portugal used samples, calculated for two different reflections.

The fresh and spent Portugal samples were completely reduced under H<sub>2</sub>/N<sub>2</sub> flow at 750°C for 12 h. The reduced samples have been subjected to XRD analysis.

The Ni crystal sizes were calculated again for the two reflections  $d_{200}$  and  $d_{220}$  and compared to those of the unreduced samples.

The fresh sample shows the lowest value due to the fact that it was not subjected to the reaction conditions, as the used samples, and the Ni particles were not sinterized. Going down through the catalytic bed, the Ni crystal size increases, both for the unreduced samples and for the reduced catalysts, but lower values have been observed for the reduced samples.

SAMPLES	Not Reduced Samples		Reduced Samples	
	D (nm) °2θ = 51.85	D (nm) °2θ = 76.37	D (nm) °2θ = 51.85	D (nm) °2θ = 76.37
PORT_Fresh	-	-	15	19
PORT_1	32	29	38	32
PORT_5	35	31	35	29
PORT_9	40	32	36	31
PORT_13	45	33	41	33
PORT_16	46	34	39	32

Fig. 3. 46 - Ni crystal size of the USA samples calculated for two reflection.

Furthermore, the Portugal samples have been oxidized at 900°C in air for 12 h, to estimate the NiO crystal size (Fig. 3. 47).

The results of the NiO crystal size confirm the observation carried out with the Ni<sup>0</sup>. In fact also the dimension of the NiO crystal size increases, going down through the catalytic bed the because of the increase of the drastic reaction conditions in the bottom of the tube.

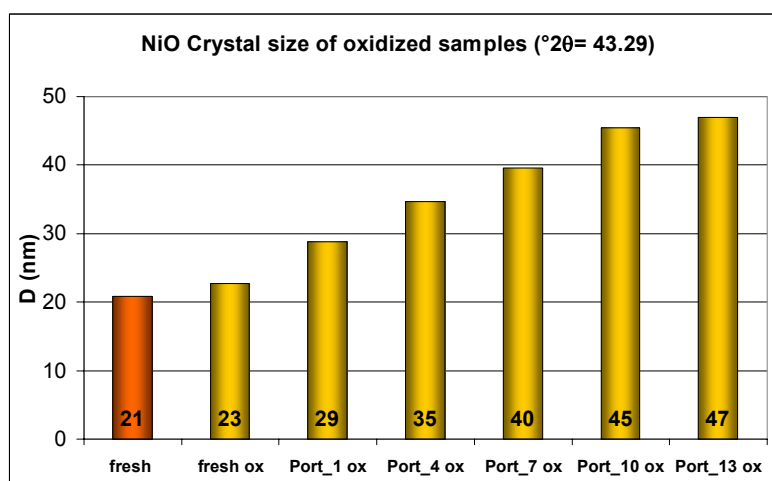


Fig. 3. 47 - NiO crystal size of calcined Portugal samples.

The samples were analyzed by temperature programmed reduction and oxidation analyses (TPR/O), using the following procedure:

- Pre-treatment : 0.1g of the samples (20-40 mesh) were pre-treated under N<sub>2</sub> (20 ml/min) from room temperature to 150°C (temperature rate of 20°C/min) and hold for 30 minutes at 150°C.
- Reduction : after cooling until 100°C, the reduction analyses were performed with 5 % of H<sub>2</sub> in Ar (20 ml/min) from 100 to 950°C (temperature rate of 10°C/min) and hold for 30 minutes at 950°C.
- Oxidation : after cooling until 100°C, the oxidation analyses were performed with 5 % of O<sub>2</sub> in He (20 ml/min) from 100 to 950°C (temperature rate of 10°C/min) and hold for 30 minutes at 950°C.

The differences among the fresh sample and the used samples are clear. Beside The NiO is responsible of the sharp reduction peak at low temperature, which for used samples is of lower intensity than the fresh sample, due to the presence of Ni partially as Ni<sup>0</sup>. In all these samples, a peak at high temperature attributable to a different oxidized Ni species is also present. Moreover, going down through the catalytic bed the TPR shows very complicated pattern in a range among 250-500°C in which free NiO species are reduced, maybe due to different size of the Ni species or access of the gas to the Ni sites.

As reported in literature<sup>109, 110, 111, 112, 113, 114, 115, 116, 117</sup>, it is possible to identify different NiO type phases that are reduced at higher temperature while the strength of interaction with the support increases and when it forms a solid solution with the Mg contained in the support. Furthermore, from the literature data it is clear that the two reduction steps at 850-890°C and at over 950°C are typical of the spinel phases with increasing reducing temperature by insertion of Mg in the spinel (Ni-MgAl<sub>2</sub>O<sub>4</sub>). A summary of the main reduction temperatures of the Portugal samples is shown in Tab. 3. 8. The NiAl<sub>2</sub>O<sub>4</sub>, which cannot be identified by XRD analysis due to the overlapping of the reflections of this phase with those of the support, is present in all the samples in a solid solution with MgAl<sub>2</sub>O<sub>4</sub>. The formation of the nickel spinel phase is due to the drastic conditions at which the Ni particles were subjected during reaction, while only the fresh sample contains peak attributable to pure NiAl<sub>2</sub>O<sub>4</sub>.

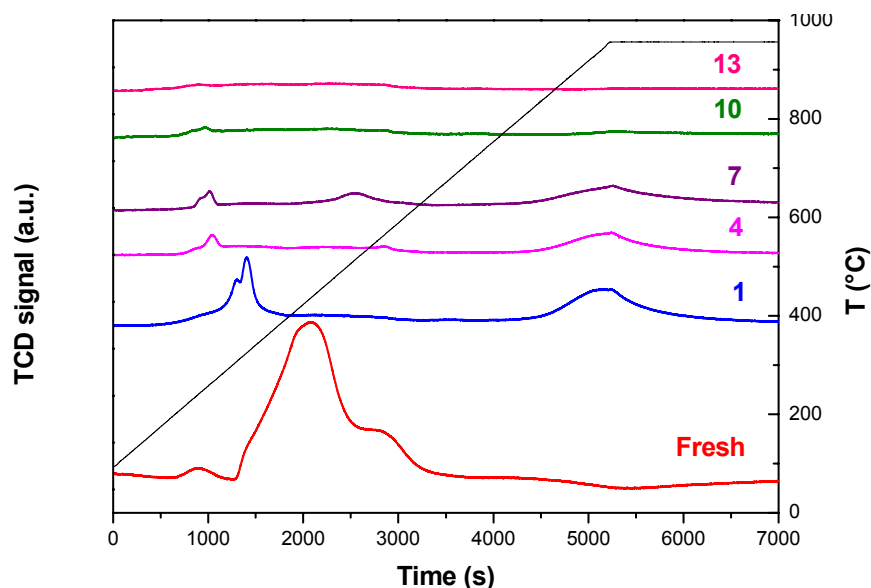


Fig. 3. 48 - TPR patterns of the fresh and used samples coming from Portugal plant.

	Port_Fresh	Port_1	Port_4	Port_7	Port_10	Port_13
<b>NiO → Ni<sup>0</sup></b> Free NiO, 220-300°C	238°C	252°C	266°C	259°C	252°C	240°C
<b>NiO → Ni<sup>0</sup></b> NiO slightly bounded with the support, 400-500°C	440°C	310-437°C	312-460°C	325-464°C	360-460°C	340-475°C
<b>NiO → Ni<sup>0</sup></b> NiO strongly interacting with the support, 500-600°C	538°C	578°C	570°C	516°C	552°C	
<b>Ni<sub>1-x</sub>Mg<sub>x</sub>O → Ni<sup>0</sup></b> Solid solution, 720°C				720°C	720°C	720°C
<b>NiAl<sub>2</sub>O<sub>4</sub> → Ni<sup>0</sup></b> Free NiAl <sub>2</sub> O <sub>4</sub> , 850°C	840°C					
<b>Ni<sub>1-y</sub>Mg<sub>y</sub>Al<sub>2</sub>O<sub>4</sub> → Ni<sup>0</sup></b> Solid solution, 1000°C		957°C	957°C	957°C	957°C	957°C

Tab. 3. 8 - Summary of the reduction temperatures observed in the TPR patterns of the Portugal fresh and spent samples.

The TPO analysis (Fig. 3. 49) shows a monotonic shift of the oxidation peaks towards higher temperature by moving from the fresh (338°C) to the used sample and from the sample N°1 (480°C) to the sample N° 13 (600°C). The differences between the samples are due to the differences in the temperature of the

catalytic bed at which they have been exposed. It can be hypothesized that the high temperature have modified the Ni species in terms of shape, size (the differences in terms of crystal size are evident in the Fig. 3. 44) and type, probably with the formation of  $\text{NiAl}_2\text{O}_4$ .

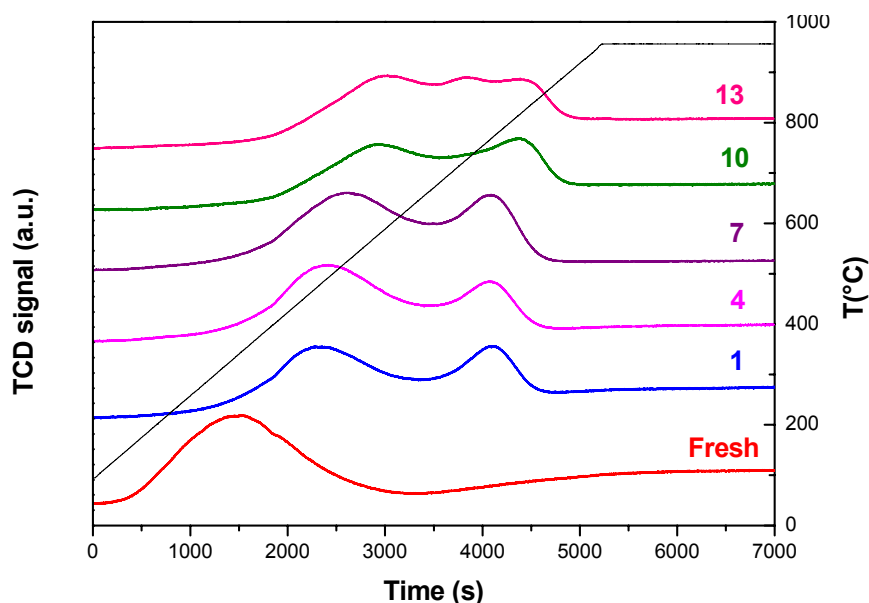


**Fig. 3. 49 – TPO patterns of the fresh and used samples coming from Portugal plant, carried out after TPR.**

Four samples coming from the Portugal plant have been characterized by porosimetry analysis: the fresh sample, Port-1 as example of first layer of the bed, Port-7 for the middle of the bed and Port-13 for the end of the bed.

The pore distributions of these samples, as pores volume vs pore widths from BJH desorption curves, are reported in Fig. 3. 50, while Tab. 3. 9 summarizes the surface area values and the pores volume and width.

The pores desorption distribution of the fresh Portugal sample is a three-modal curve (i.e. it presents three relative maximums of pore dimension: 23 Å, 37 Å and 315 Å with the last representing the most populated), while Port-1 is bimodal (pores dimensions: 37 Å and 307 Å).

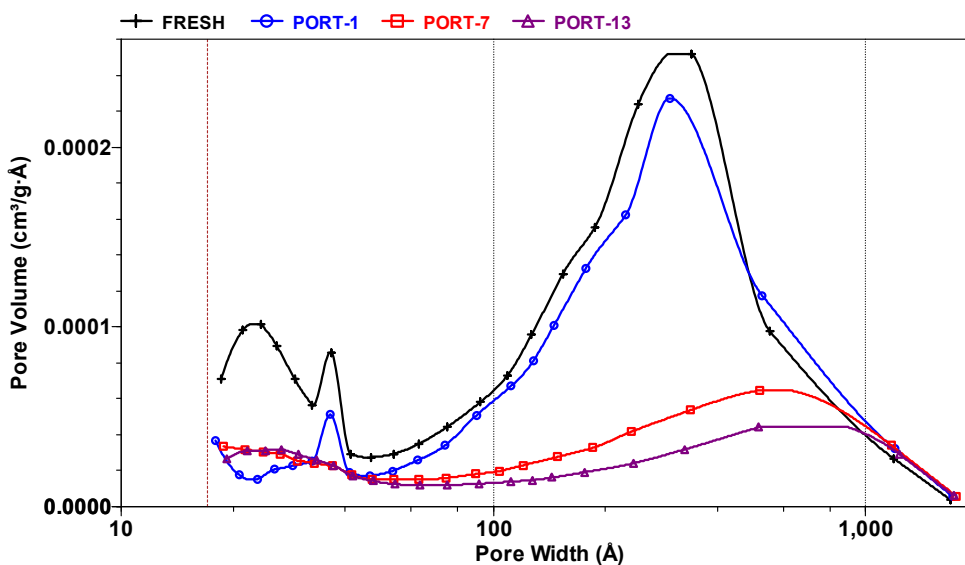


Fig. 3. 50 - Pore distribution for the Portugal samples from BJH.

Port-1 shows similar porosity with respect to the fresh sample for what concern large mesopores, while smaller pores disappear. Going down through the catalytic bed, smaller porosity further decrease, but also large mesopores significantly decrease (the maximum at around 310 Å almost disappears) and the maximum is shifted at higher values. Only macroporosity remains constant (pores with width higher than 1000 Å) and, in this region, the curves are identical for the whole series of the samples. This leads to a different pores volume, which is double for fresh Port and Port-1 with respect to the Port-7 and Port-13 (with Port 7 having higher pore volume than Port-13). The analyses confirm the progressive decrease of the surface areas going down towards the end of the bed.

The pore volume decreases from Port-7 to Port-13 can be due to the sintering of the support, in fact the spinel crystal size, calculated from XRD patterns, are 43 nm for Port-7, and 53nm for Port-13. On the other side, the disappearing of the large mesopores can be due to occlusion of the pores or to modification of the crystal and particles structure/morphology in a more close arrangement.

Two hypotheses can be done:

(a) the increase of the Ni crystal size dimensions occludes the pores. This hypothesis is corroborated by the dimension of the Ni crystal size in Port-13 and Port-7 that is analogous to the dimensions of the pores that disappeared;

(b) the elimination of coke during shut down of the plant by steam and  $H_2$  with formation of  $CH_4/CO/CO_2$  leads to the rearrangement of the pores structure (due to the over-pressure generated in the pore by the gas formation).

		Port Fresh	Port 1	Port 7	Port 13
<b>BET Sorptivity 1750</b>	$m^2g^{-1}$	18	18	12	12
<b>Single Point Surface Area</b>	$m^2g^{-1}$	18.58	16.43	7.46	5.95
<b>BET Surface Area</b>	$m^2g^{-1}$	19.10	17.12	7.71	6.12
<b>t-plot micropore area</b>	$m^2g^{-1}$	2.09	1.38	0.91	0.86
<b>t-plot micropore volume</b>	$cm^3g^{-1}$	0.000823	0.000418	0.000343	0.000348
<b>BJH desorption cumulative volume of pores</b>	$cm^3g^{-1}$	0.161980	0.170479	0.088289	0.077786
<b>BLH desorption maximums pore widths</b>	Å	23, 37, 315	37, 307	590	680
<b>BJH desorption average pore width (4V/A)</b>	Å	316.250	369.105	455.868	514.807

Tab. 3. 9 - Surface area values and pores volume and width.

### 3.1.2. Characterization of USA used samples

The spent catalyst coming from the USA Steam Reforming plant was divided in 16 samples taken from a tube 45 feet long (about 13.3 m). The samples were taken at constant distance; they were labeled so that the number 1 corresponds to the one of the top of the tube. The USA reformer tubes were heated by a top fire furnace.

The operating conditions to which it was subjected varied down the length of the tube. Outlet process gas, from the bottom of the tube, ranged from 854°C to 882°C based on plant rates, ~ 25 bar, and inlet S/C varied from 3.5 as minimum ratio to 3.0 as maximum ratio. The spent catalyst is more than 5 years old. The catalyst should be identical all down the tube. The 30 % of the top of the tube was loaded with pre-reduced catalyst, but after the first start-up, it should have the same composition of the 70 % loaded at the bottom. The shut down of the plant were carried out shifting from normal operating conditions to a 100% steaming for 3-4 hours followed by air introduction (to burn off carbon), finally the cooling was down by nitrogen circulation.

The fresh sample and a spent one, chosen in the middle of the tube, were analyzed by ICP (Tab. 3. 10). The results show that the used sample presents a lower content of Ni with respect to the fresh catalyst, but it is also possible to note that the fresh sample analyzed by ICP contains more weight % of Ni in comparison with the amount declared by seller. So two new samples of the USA fresh were analyzed by ICP: one taken from the pellet of the first sample (USA\_F\_A) and the second taken from a second pellet (USA\_F\_B). The results confirm that the sample prepared with impregnation method is not very homogeneous, and the amount of the Ni in fresh sample is significantly higher than that of the used, probably due to a loss of active metal due to the reaction atmosphere.

SAMPLE NAME	ICP (% wt of Ni)
USA fresh	16,6
USA_F_A	14,4
USA_F_B	15,7
USA N. 9	10,8

Tab. 3. 10 - Results of ICP analyses on USA fresh sample and on a used sample chosen in the middle of the tube.

USA Sample	BET Surface area (m <sup>2</sup> g <sup>-1</sup> )
Fresh	25
1	16
2	8
3	20
4	12
5	4
6	10
7	8
8	10
9	6
10	10
11	4
12	8
13	6
14	10
15	6
16	14

Tab. 3. 11 – B.E.T. surface area values of fresh and used samples, from USA plant.

The fresh sample presents also the highest B.E.T. surface area, while all the used samples show lower surface areas that range between 4 and 20 m<sup>2</sup>g<sup>-1</sup> (Tab. 3. 11).

Detailed analyses were performed on the fresh sample and on the spent N. 1, 5, 9, 13 and 16. In the XRD patterns of these samples, a MgAl<sub>2</sub>O<sub>4</sub> (as major phase because it is the support), Al<sub>2</sub>O<sub>3</sub> (presents in very little amount) and Ni<sup>0</sup> and/or NiO (as active phase) are present. The results of the XRD analyses are very interesting because they show a different degree of the Ni reduction in spent samples going down trough the catalytic bed (Fig. 3. 51). The USA used samples, which were treated with air at the shut down of the plant, present the NiO phase all along the tube. In the samples taken in the second half of the bed, the Ni<sup>0</sup> phase appears and increases going towards the bottom of the catalytic bed, implying a growth of the Ni crystal size going down through the tube (Tab. 3. 12).

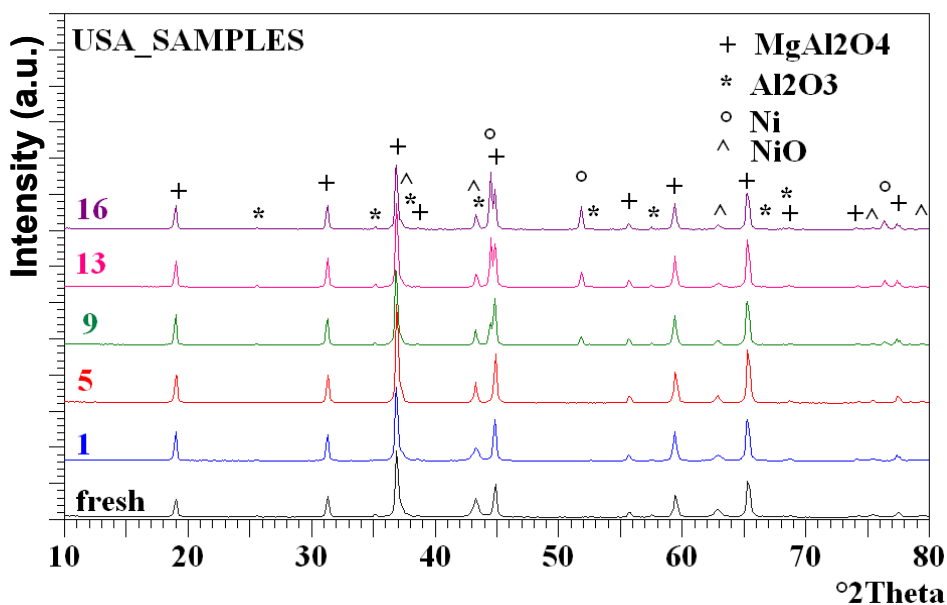


Fig. 3. 51 – XRD patterns of the fresh and used samples coming from USA plant.

The fresh and spent USA samples were completely reduced under H<sub>2</sub>/N<sub>2</sub> flow at 750°C for 12 h. The reduced samples were analyzed by XRD and the Ni crystal size for the two reflections (200) ( $2\theta = 51.85$ ) and (220) ( $2\theta = 76.37$ ) were calculated and compared to those of the unreduced samples (Tab. 3. 12). The fresh sample shows the lowest value because this sample was not subjected to the drastic reaction conditions, as the used samples, and the Ni particles are not

sintherized. Going down through the catalytic bed the Ni crystal size increases, also in the case of the reduced catalysts.

SAMPLES	Not Reduced Samples		Reduced Samples	
	D (nm) °2θ = 51.85	D (nm) °2θ = 76.37	D (nm) °2θ = 51.85	D (nm) °2θ = 76.37
USA_Fresh	-	-	16 ± 2	19 ± 2
USA_1	-	-	18 ± 2	24 ± 2
USA_5	-	-	30 ± 3	24 ± 2
USA_9	45 ± 3	37 ± 3	39 ± 3	32 ± 3
USA_13	49 ± 3	34 ± 3	38 ± 3	31 ± 3
USA_16	54 ± 3	39 ± 3	48 ± 3	34 ± 3

Tab. 3. 12 - Ni crystal size of the USA samples calculated for two reflections.

Since the USA samples are partially oxidised, they have been completely oxidised at 900°C for 12 h. The NiO crystal size has been estimated from the XRD patterns. Comparing the crystal size values obtained for the just used and one subjected to oxidation (Fig. 3. 52), the fresh and the USA\_1 samples show similar and low crystal size before and after calcination. Starting from the sample USA\_5, the dimensions of Ni (as NiO) are about doubled with respect to the fresh sample, and the maximum of NiO crystal size is reached by the USA\_9.

NiO Crystal size	D (nm)	D (nm) After calcination
USA_Fresh	25	23
USA_1	21	24
USA_5	44	43
USA_9	50	56
USA_13	41	50
USA_16	45	44

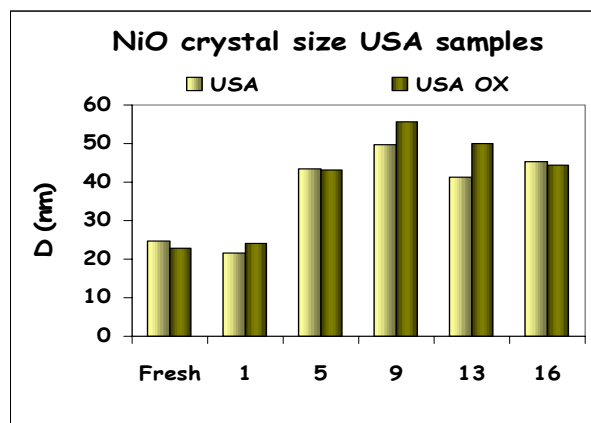


Fig. 3. 52 - Comparison between the NiO crystal size of the USA samples before and after calcination.

Three used USA samples taken from the beginning (USA-1), the end (USA-16) and from the middle of the catalytic tube (USA-9), were also subjected to porosimetry analyses. It was found that the USA-1 is very similar to the fresh sample, apart from a slight decrease of the surface area value. The USA-9 and 16 samples present a significant decrease of the surface area (especially the sample unloaded from the middle of the tube) and particularly the samples show a decrease of the large mesopores and a shift of the maximum of pore volume distribution at higher value, while the macro-porousness remains constant, analogously to the Portugal samples.

The decrease of the mesopores can be explained by the blockage of the pores due to the increase of the dimensions of the Ni particles. In fact, the sample N. 1 presents Ni crystal size not much higher than that of the fresh sample, and the porosity is very similar to that of the fresh sample. On the opposite, the USA- 9 and 16 samples present bigger Ni crystal with respect to the fresh and the N. 1 samples and their sites are similar to the mesoporous sites. As for Portugal samples can be hypothesized that the Nickel crystal occlude the pores.

		Fresh	USA 1	USA 9	USA 16
<b>Single Point Surface Area</b>	$\text{m}^2\text{g}^{-1}$	18.58	13.19	3.35	5.49
<b>BET Surface Area</b>	$\text{m}^2\text{g}^{-1}$	19.10	13.58	3.65	5.72
<b>t-plot micropore area</b>	$\text{m}^2\text{g}^{-1}$	2.09	1.11	0.00	0.38
<b>t-plot micropore volume</b>	$\text{cm}^3\text{g}^{-1}$	0.000823	0.000413	0.000000	0.000103
<b>BJH desorption cumulative volume of pores</b>	$\text{cm}^3\text{g}^{-1}$	0.161980	0.160910	0.053539	0.076358
<b>BJH desorption maximums pore widths</b>	Å	23, 37, 315	21, 36, 326	36, 740-1000	19, 36, 480-1190
<b>BJH desorption average pore width (4V/A)</b>	Å	316	401	562	527

**Tab. 3. 13 - Surface area values and pores volume and width of USA 1 and 16 samples.**

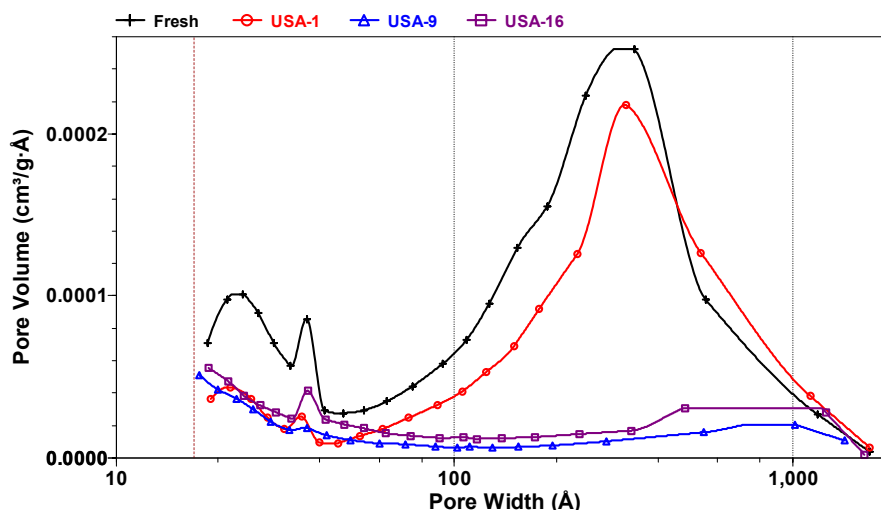


Fig. 3. 53 – Pore distribution of the fresh and used USA samples

The samples were subjected to temperature programmed reduction and oxidation analyses (TPR/O), using the same procedure used for the Portugal samples.

The comparison of the reduction profile of fresh sample with those of the used samples is very important, in fact the fresh sample shows the presence of a peak at low temperature (at about 450°C) with a shoulder at about 550°C, while the used samples shows an additional peak at high temperature very likely due to the presence of Ni<sup>2+</sup> combined in mixed oxides (Fig. 3. 54). A hypothesis can be the presence of NiAl<sub>2</sub>O<sub>4</sub> or NiO species strongly embedded in the bulk of the support that is reduced at higher temperature. Concerning the peak at low temperature the comparison shows that, its shape change along the bed due to the presence or not of the Ni<sup>0</sup> species. The samples N° 5 and N° 9 appear anomalous; the former shows a very small peak at low temperature while the latter shows a strong shift of the main peaks at higher temperature probably due to the occlusion of NiO embedded in the support. In fact the sample N° 9 shows also anomalous crystal size and pore distribution.

The TPO analysis, carried out after the TPR (Fig. 3. 55), shows the shift of the oxidation peak, moving from the fresh samples to the sample N°1, and a general increase of the temperature of the oxidation, going down trough the catalytic bed. In particular, the decrease is very clear form the sample N° 1 to the sample N° 5, in which peaks at high temperature appear. Sample N° 9 is again anomalous having a large oxidation peak at higher temperature while the sample N° 13 and 16 have a more complex pattern with an increase of the oxidation temperature might due to the presence of different Ni species.

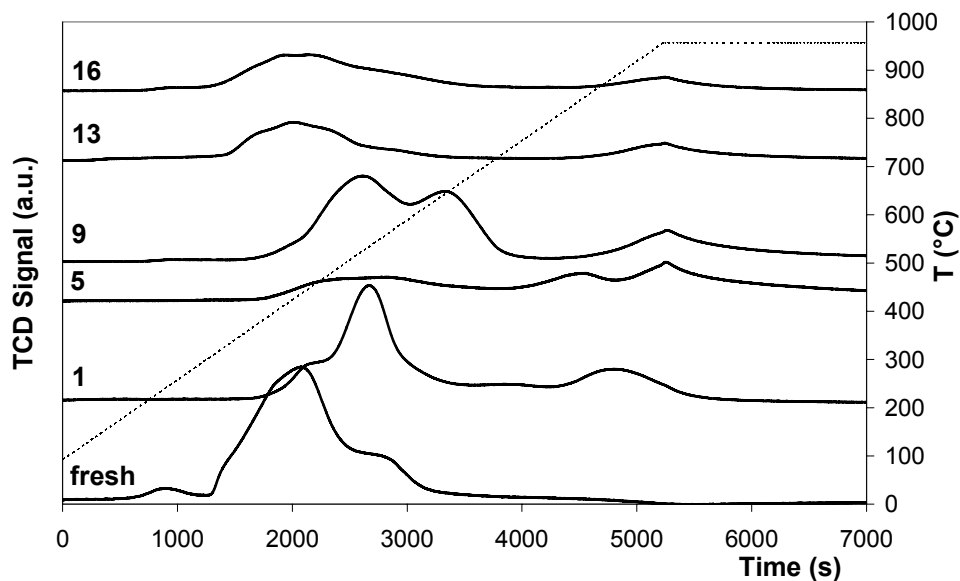


Fig. 3.54 - TPR patterns of the used samples coming from USA plant.

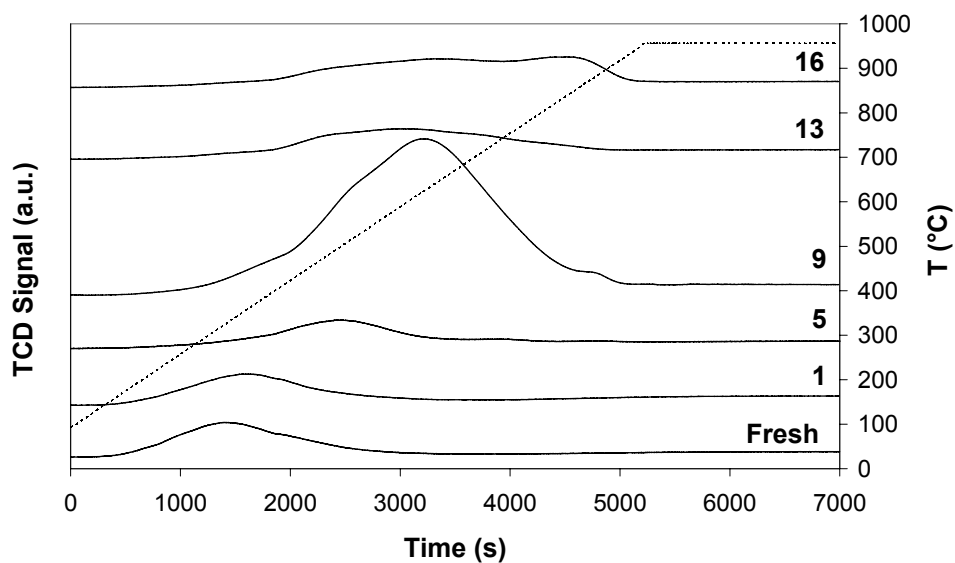


Fig. 3.55 - TPO patterns of the used samples coming from USA plant, carried out after TPR.

The Tab. 3.14 presents a schematic summary of the reduction temperatures of the TPR analyses made on the USA spent samples.

Also in this case, it is possible to identify different NiO type phases that are reduced at higher temperature while increasing of the interaction with the support and when it forms a solid solution with the Mg contained in the support. The two

reduction steps at 850-890°C and at 957°C, typical of the spinel phase can be attributed to different mixed oxide such as NiAl<sub>2</sub>O<sub>4</sub> or Ni-MgAl<sub>2</sub>O<sub>4</sub> species.

On the bases of the characterization performed on the sample used in industrial processes it was observed, for both the series of samples, decrease of surface area, decrease of the pore volume with disappearance of the mesoporosity and sintering of both support and active nickel. Furthermore, the formation of a low reducible and active nickel phase, in the form of spinel NiAl<sub>2</sub>O<sub>4</sub>, due to the reaction between nickel and support was observed.

However, it was not possible to observe the presence of carbon species on the surface of the samples because the procedure of switch off the plants caused the elimination of any carbon species.

	USA_Fresh	USA_1	USA_5	USA_9	USA_13	USA_16
<b>NiO → Ni<sup>0</sup></b> Free NiO 220-300°C	240°C					245°C
<b>NiO → Ni<sup>0</sup></b> NiO slightly bounded with the support 400-500°C	437°C	450°C	510°C	524°C	425°C	410- 441°C
<b>NiO → Ni<sup>0</sup></b> NiO strongly interacting with the support 500-600°C	540°C	535°C	551°C	643°C	560°C	
<b>Ni<sub>1-x</sub>Mg<sub>x</sub>O → Ni<sup>0</sup></b> Solid solution 720°C		740°C				
<b>NiAl<sub>2</sub>O<sub>4</sub> → Ni<sup>0</sup></b> Free NiAl <sub>2</sub> O <sub>4</sub> 850°C		885°C	846°C			
<b>Ni<sub>1-y</sub>Mg<sub>y</sub>Al<sub>2</sub>O<sub>4</sub> → Ni<sup>0</sup></b> Solid solution 1000°C			957°C	957°C	957°C	957°C

**Tab. 3. 14 - Summary of the reduction temperatures observed in the TPR patterns of the USA fresh and spent samples.**

### 3.1.3. Activity of industrial spent samples

The fresh (13 % Ni/MgAl<sub>2</sub>O<sub>4</sub>) and some used samples have been tested in the laboratory steam reforming plant to study the effect on the activity of the deactivation, observed along the catalytic tube.

For the catalytic tests, three used samples coming from the Portugal plant were chosen: Port-1 from the top, Port-7 from middle and Port-13 from bottom of the catalytic tube. Similarly, two USA used samples were selected: USA-1 from top and USA-16 from bottom of the tube.

The catalytic tests were carried out loading 10 ml of pellets of 14-20 mesh that occupy 10 cm of catalytic bed. The tests were carried out using the following reaction conditions:

- P = 10 bar
- S/C = 1.7 & 2.5
- CT = 1 s
- Tout = 870 & 950°C

In all the reaction conditions and for all the samples, the activity trend observed is quite stable during all the duration of the tests (8 h).

The activity of the fresh sample will be presented completely to give an exhaustive description of the behavior in different conditions, while for the used samples, only the comparison of the results will be shown.

Using the fresh sample, the methane conversion (Tab. 3. 15) is lower than that of the thermodynamic prediction (Fig. 3. 56). However, it can be seen that, increasing the S/C ratio and the temperature, the performances of the samples is enhanced, as expected by the thermodynamic prediction. Furthermore, the CO selectivity decrease with the increase of water content in the feed due to the enhanced water gas shift reaction promoted by this reactant, while the increase of the temperature leads to an opposite effect. In fact it is well-known that the WGS reaction is favored at low temperature and the contribution of this reaction to the H<sub>2</sub> formation is lower at higher temperature where the reverse reaction is favored. The excess of water and the temperature affect the H<sub>2</sub>/CO ratio, that is, in all the reaction conditions, higher than 3 (as expected only by the SR reaction). Increasing the S/C ratio from 1.7 to 2.5, whatever the temperature is, the obtained H<sub>2</sub>/CO ratio increases due to the promotion of the WGS reaction.

During the reaction, the axial thermal profile of the catalytic bed was measured, moving the thermocouple positioned in the middle of the catalytic bed (Fig. 3. 57). Before the catalytic bed, the temperature of the feed mixture increase along the reactor, following the oven profile. A decrease of the temperature was observed in the first zone of the catalytic bed, in particular it begins where the feed gas mixture meet the catalyst bed. The effect is due to the endothermic reforming reaction occurring mainly in this zone. After the minimum, i.e. after that the main part of methane has been converted, the axial temperature starts to increase, due mainly to the energy supplied by the electric oven, with a possible contribution of the exothermic water gas shift reaction, which can occur in the second part of the catalytic bed.

Mean composition (%)	P = 10 bar CT = 1 s S/C = 1.7 T <sub>oven</sub> = 896°C	P = 10 bar CT = 1 s S/C = 2.5 T <sub>oven</sub> = 890°C	P = 10 bar CT = 1 s S/C = 1.7 T <sub>oven</sub> = 965°C	P = 10 bar CT = 1 s S/C = 2.5 T <sub>oven</sub> = 963°C
	CH <sub>4</sub>	7.0	3.3	3.6
H <sub>2</sub>	71.3	74.3	74.3	76.9
CO	19.9	17.9	22.1	20.1
CO <sub>2</sub>	3.4	5.4	2.6	4.4
H <sub>2</sub> /CO	3.6	4.2	3.4	3.8
<b>Conv. CH<sub>4</sub></b>	<b>76.9</b>	<b>87.6</b>	<b>87.3</b>	<b>95.7</b>
<b>Yield H<sub>2</sub>(*)</b>	<b>74.8</b>	<b>86.4</b>	<b>84.5</b>	<b>94.5</b>
<b>Sel. CO</b>	<b>85.4</b>	<b>76.8</b>	<b>89.5</b>	<b>82.0</b>
<b>Sel. CO<sub>2</sub></b>	<b>14.6</b>	<b>23.2</b>	<b>10.5</b>	<b>18.0</b>
<b>Real T<sub>out</sub> (°C)</b>	870	871	950	950
<b>T<sub>in</sub> (°C)</b>	770	774	846	857
<b>DT (°C)</b>	131	80	93	83

Tab. 3. 15 - Composition of the dry gas and catalytic results of the fresh Portugal sample in the different reaction conditions (\*: Real yield in hydrogen calculated on methane conversion).

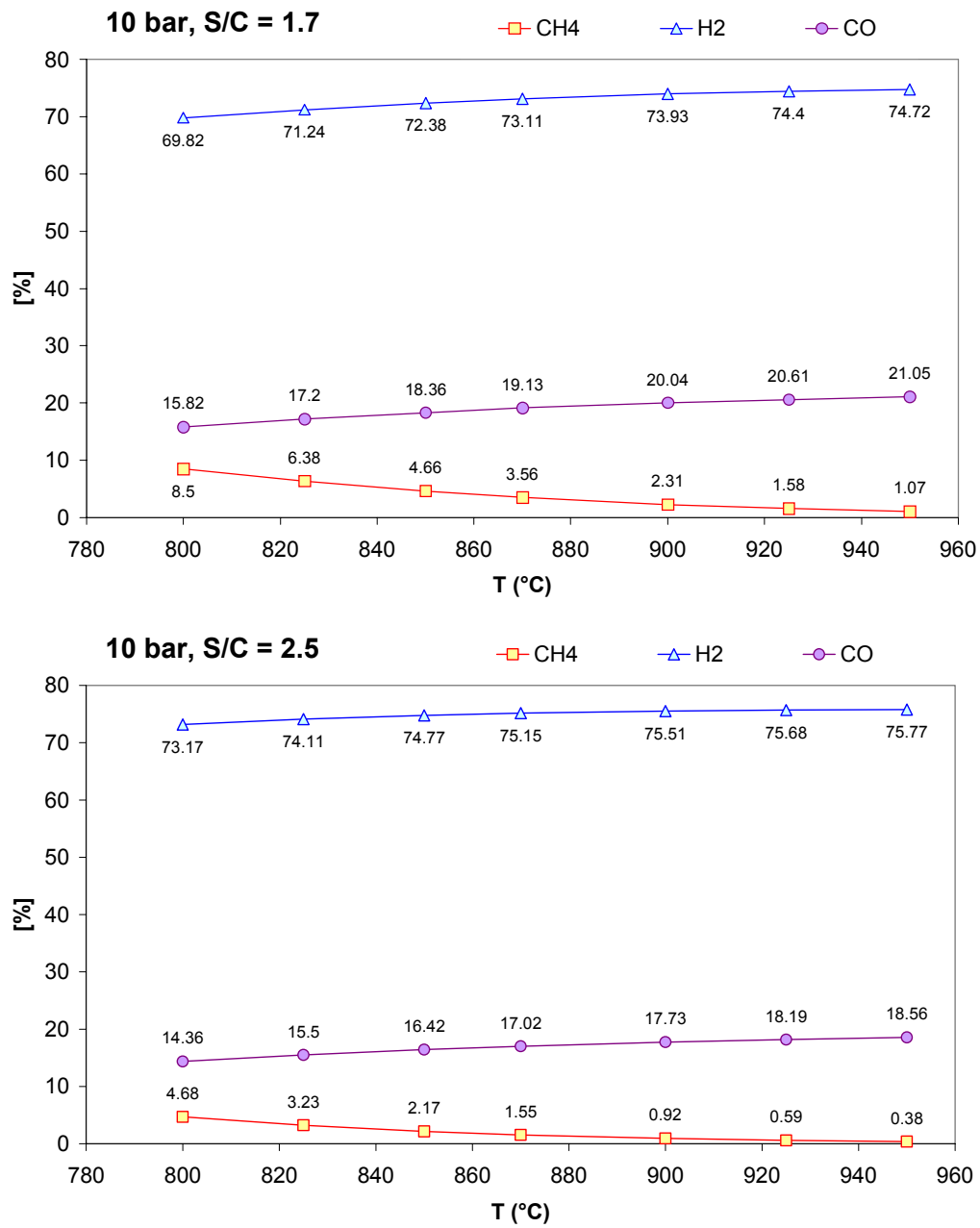
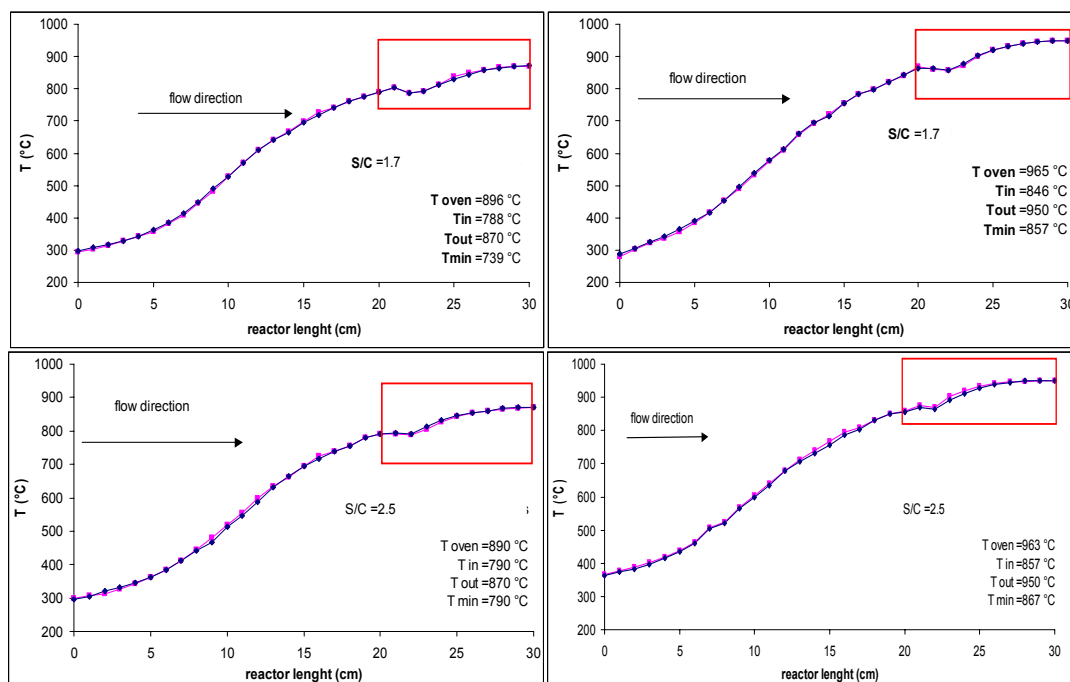


Fig. 3. 56 - Equilibrium composition of the dry syn gas as a function of temperature (Reaction conditions: P = 10 bar and S/C = 1.7 or 2.5).



**Fig. 3. 57 – Axial thermal profile during reaction of the fresh catalyst in the different reaction conditions ( $P = 10$  bar and  $CT = 1$  s).**

The used samples were tested in the steam reforming reaction feeding the same reaction conditions used for the fresh catalyst. The Fig. 3. 58 shows a comparison among the activities of the Portugal samples (fresh, 1, 7 and 13) in the different reaction conditions.

The methane conversion is in general higher for Port-1, while the fresh sample and the Port-13 are quite similar; the sample taken from the middle of the bed (N.7) presents the worse activities. Furthermore, the sample taken from the top of the industrial catalytic tube (Port-1) presents the higher hydrogen yield, followed by the fresh sample that shows also the higher CO selectivity.

Port-1 was unloaded from the top of the industrial reactor and it was the sample subjected to the less drastic conditions of temperature and reducing gases. This sample is more active with respect to the samples taken from the middle and bottom of the tube, respectively Port-7 and 13, because of its Ni crystal size dimensions (lower than those of the others) and its higher distribution of pore volume. The sample N. 7, unloaded from the middle of the tube, has the lowest activity. This is probably due to the fact that the heating of the Portugal plant was carried out using a side fire type furnace, indeed the central part of the reactor was subjected to the higher heating to maintain the right thermal profile.

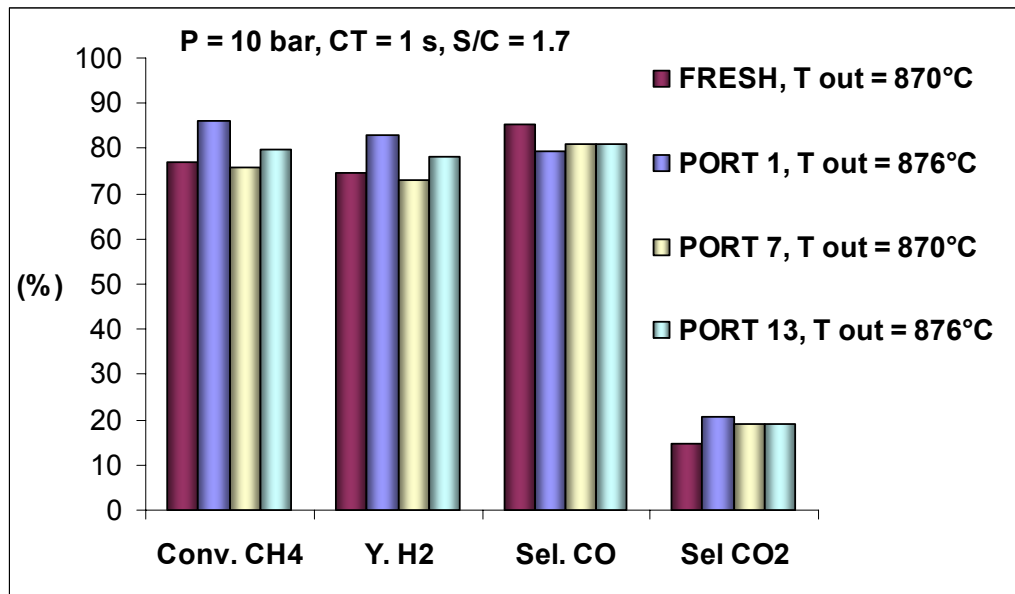


Fig. 3. 58 - Comparison among activity of Port samples (S/C = 1.7 and T<sub>out</sub> = 870°C).

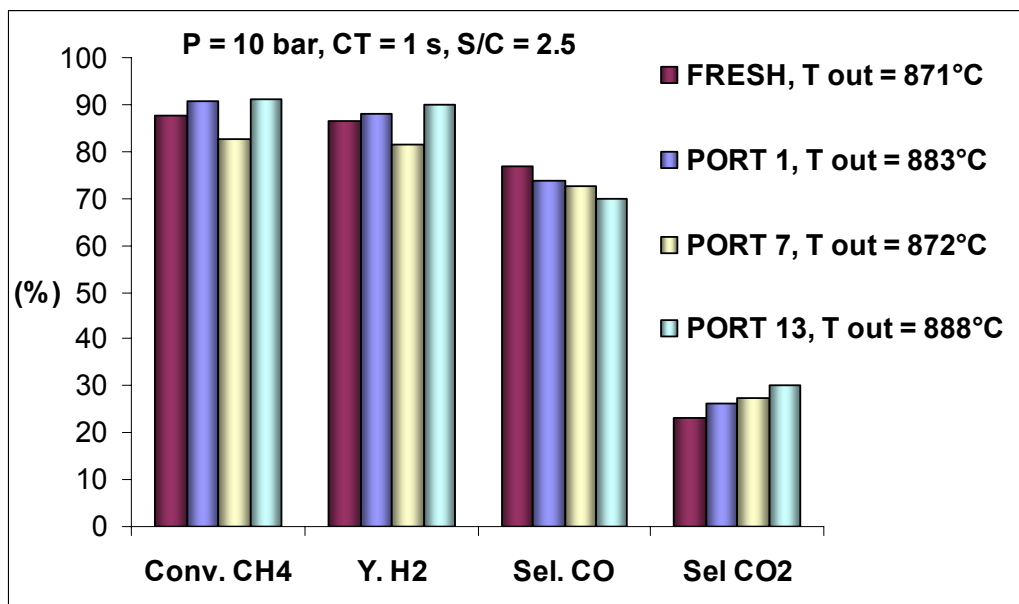


Fig. 3. 59- Comparison among activity of Port samples (S/C = 2.5 and T<sub>out</sub> = 870°C).

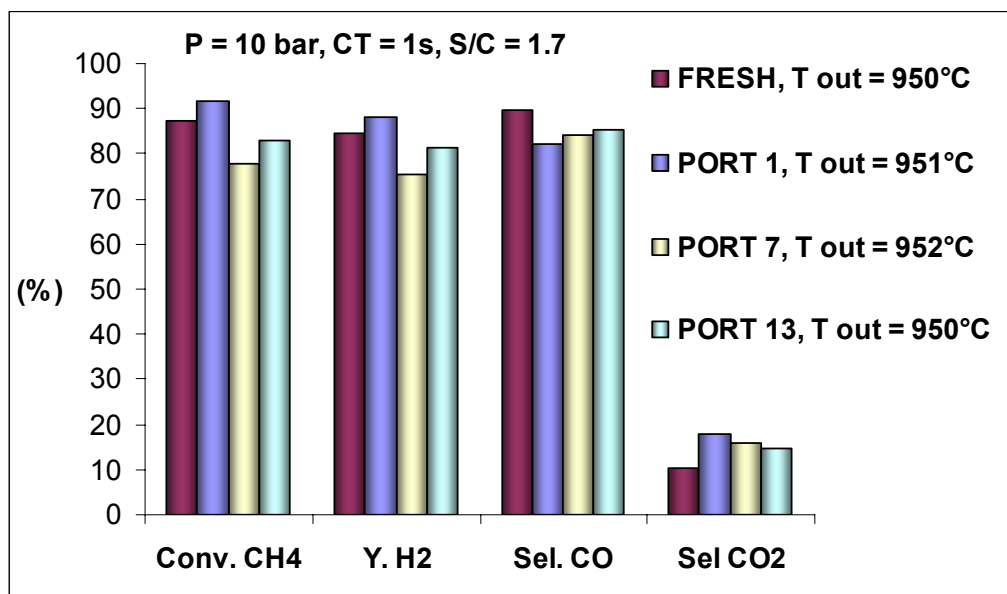


Fig. 3. 60 - Comparison among activity of Port samples (S/C = 1.7 and T<sub>out</sub> = 950°C).

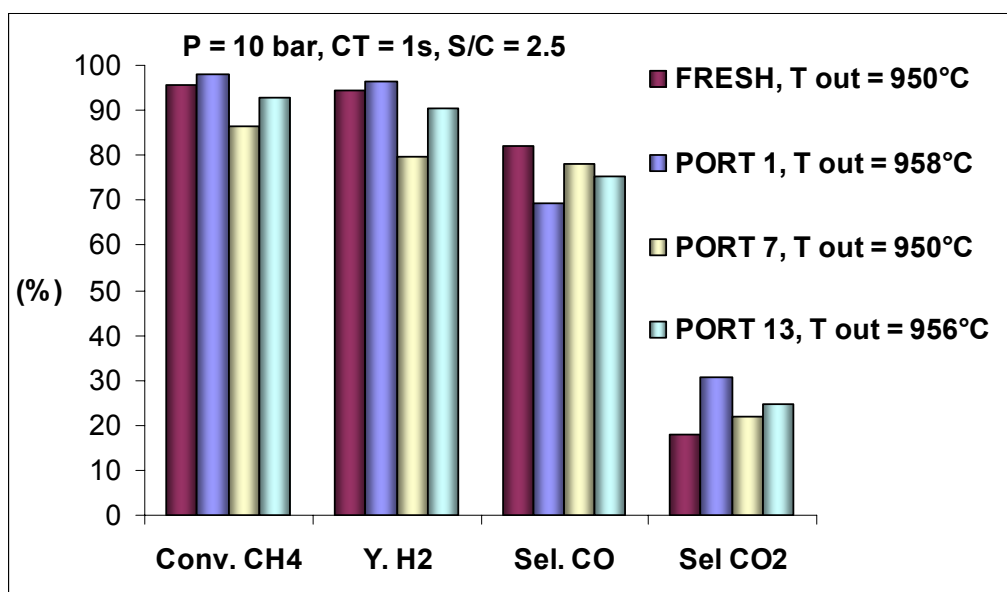


Fig. 3. 61 - Comparison among activity of Port samples (S/C = 2.5 and T<sub>out</sub> = 950°C).

Regarding the samples unloaded from the tube of the USA industrial plant, two used samples were tested in the lab plant (USA 1 and USA 16), chosen from the two extremity of the catalytic reactor, and the obtained catalytic results compared with those of the fresh sample. The SR process, in the USA plant, was carried out using a top fire furnace, differently from the Portugal plant in which it was used a side fire type, this explaining the substantial difference of thermal profile along the industrial catalytic tube.

The activity of the sample taken from the top of the catalytic bed (USA-1) shows lower performances than the respective sample of Portugal plant (Port-1).

This behavior may be mainly attributed, beside the higher temperature and S/C ratio to which the USA 1 sample was subjected during operation (with respect to the Port-1), to the oxidation of the sample by air flow during the switch off of the plant.

The USA-16 sample, taken from the bottom of the catalytic tube, presents a methane conversion slightly higher than that of the sample taken from the top of the reactor in the S/C = 1.7 conditions, while is slightly lower comparing the results obtained using the S/C = 2.5 ratio. However, the differences are smoothed because of the quite linear thermal profile and reaction conditions along the tube, during operation, as effect of the top fire furnace.

The USA used samples show in all the reaction conditions and especially in those carried out at higher temperature, lower activity than the fresh sample. Again, this behavior may be mainly attributed to the temperature of the bed and to the conditions of the shut down of the plant, which caused oxidation of the nickel, combustion of deposited carbon species, obtaining as a result effect a higher sintering of the support with respect to that observed on Portugal used samples.

In fact, on the XRD patterns, the average of  $\text{MgAl}_2\text{O}_4$  crystal size were estimated, confirming the higher sintering of the support on the USA spent samples:

Port-1	⇒	41 nm;	Port-13	⇒	44 nm
USA-1	⇒	48 nm;	USA-16	⇒	51 nm

Comparing the results of these used samples with those of the respective position, unloaded from the Portugal plant, it was observed that the Portugal samples present best performances than the USA ones.

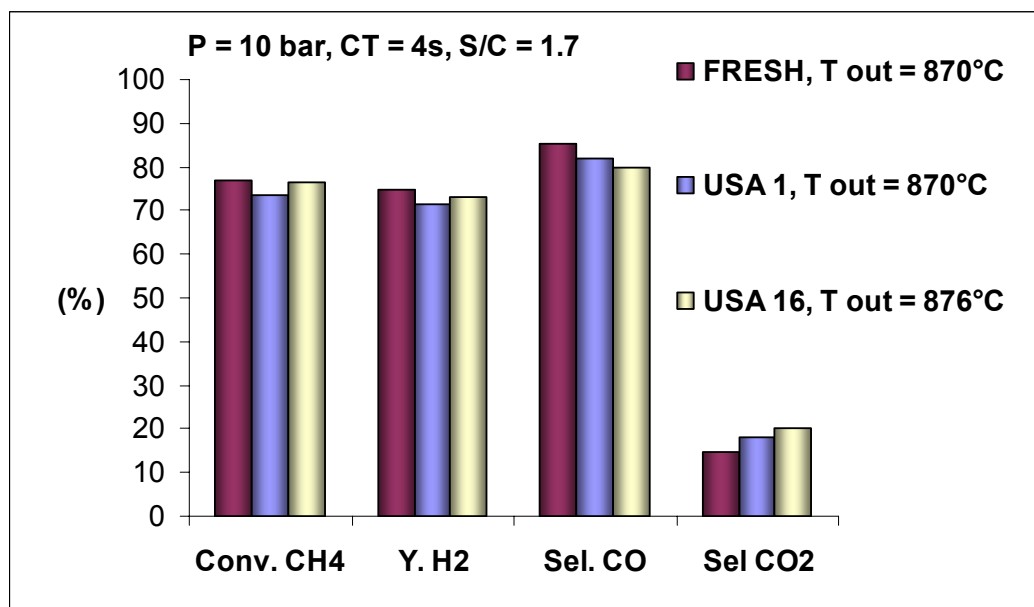


Fig. 3. 62 - Comparison among activity of USA samples (S/C = 1.7 and T<sub>out</sub> = 870°C).

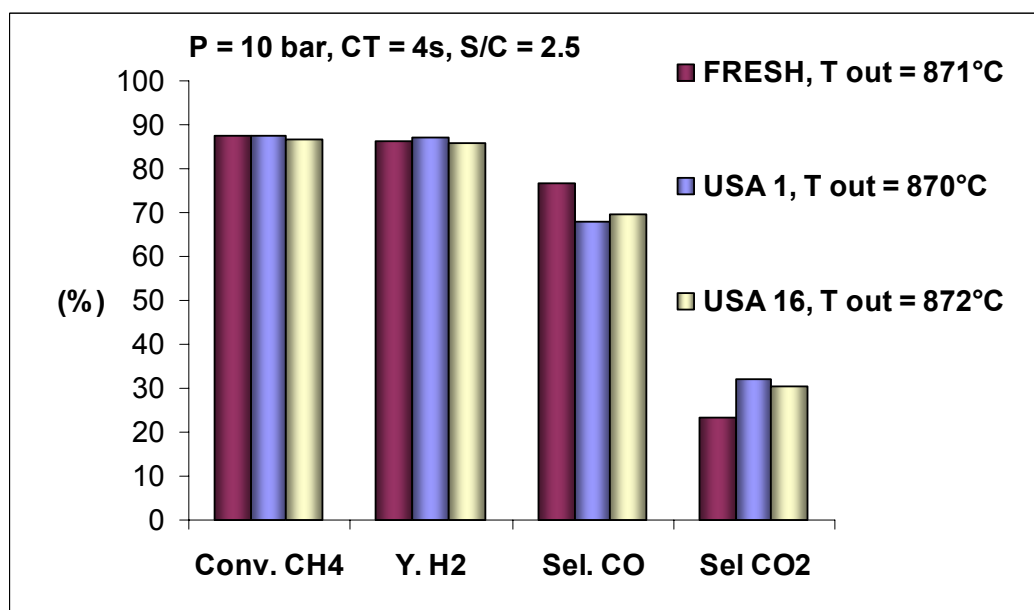


Fig. 3. 63 - Comparison among activity of USA samples (S/C = 2.5 and T<sub>out</sub> = 870°C).

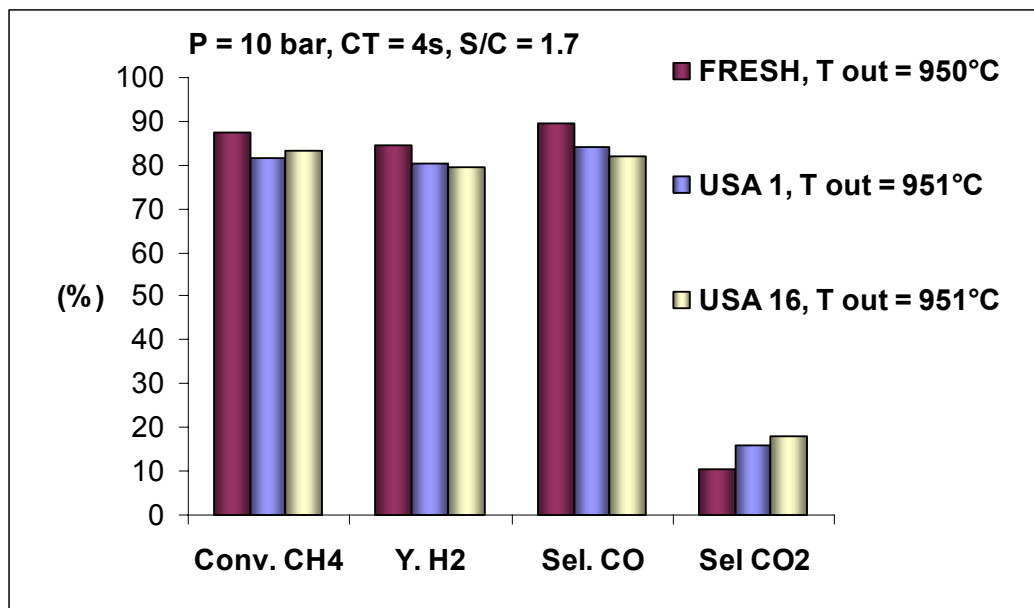


Fig. 3. 64 - Comparison among activity of USA samples (S/C = 1.7 and T<sub>out</sub> = 950°C).

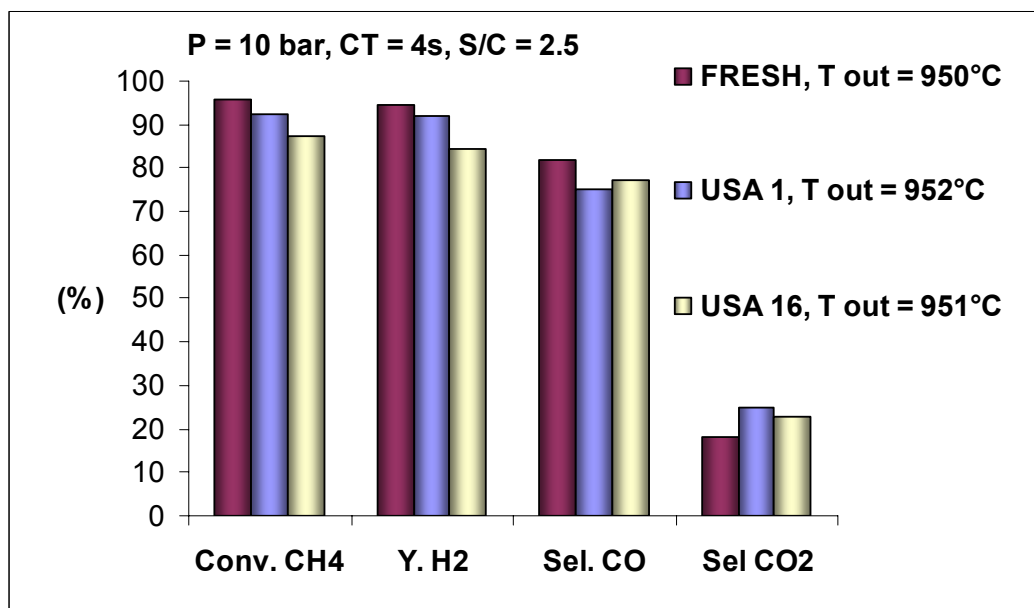


Fig. 3. 65 - Comparison among activity of USA samples (S/C = 2.5 and T<sub>out</sub> = 950°C).

The fresh and used samples, after the tests in the laboratory plant, were characterized again by XRD, B.E.T. and porosimetry analyses.

All the samples (both fresh and different used ones) contain the support phases as received samples (MgAl<sub>2</sub>O<sub>4</sub> and Al<sub>2</sub>O<sub>3</sub>) and the nickel phase present as metallic phase.

The used sample of the fresh catalyst shows after SMR tests an increase of the Ni crystal size with respect to the reduced catalyst (from 17 nm to 24nm).

Comparing the XRD pattern of lab-used Port-1 with respect to the Port-1 as received and reduced Port-1, it can be observed a different reduction degree of the Ni<sup>0</sup>. This difference probably may be due to the different reduction step to which the sample was subjected. In fact, the preliminary reduction on the as received sample was carried out at 750°C for 12 h, while before SMR tests the reduction was carried out during oven heating from 600°C to 800°C for about 30 minutes.

For this reason, the sample Port 1 was reduced again with steam reforming reduction method and this sample was characterized by XRD analysis. From the diffraction patterns the Ni crystal size was calculated, both on reflections at  $^{\circ}2\theta = 51.85$  ( $d_{200}$ ) and on  $^{\circ}2\theta = 76.37$  ( $d_{220}$ ), for different Port-1 samples (Fig. 3. 67). The results confirm that the reduction carried out for 12 h at 750°C leads to high Ni particles, while the reduction carried out before SMR test and the reaction condition do not influence the Ni crystal size dimensions.

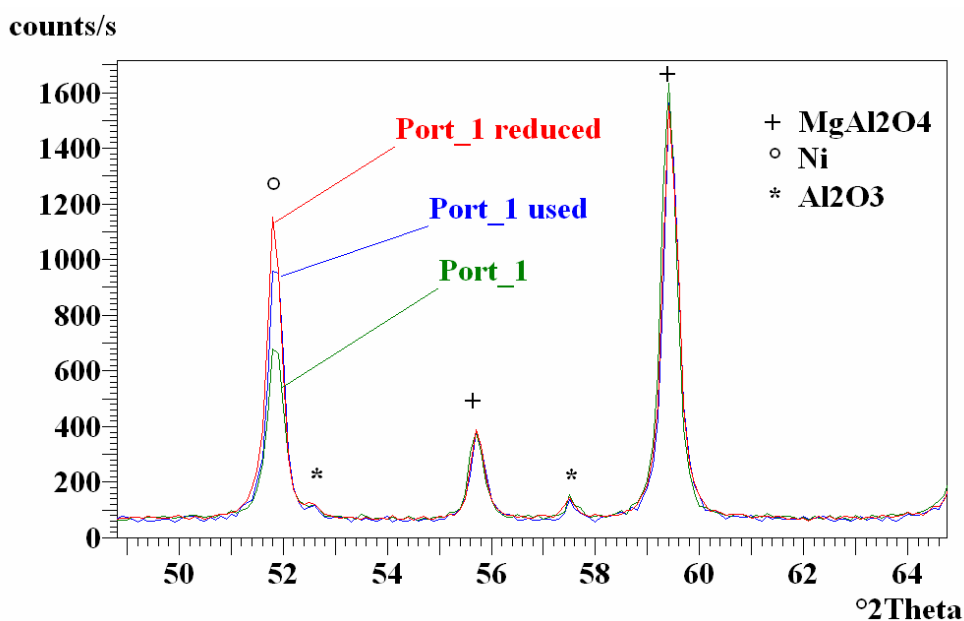


Fig. 3. 66 – Particular of the comparison of XRD patterns of Port-1, reduced Port-1 and lab-used Port-1 sample.

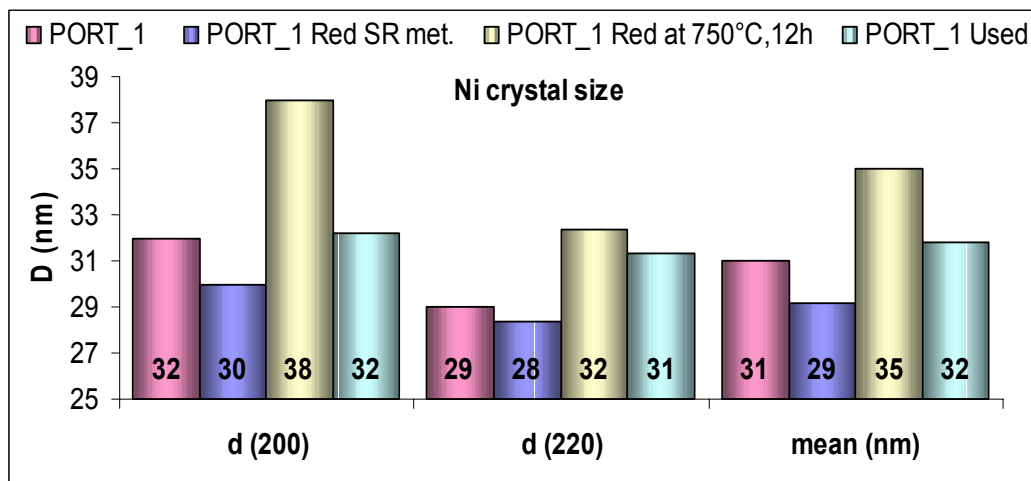


Fig. 3. 67 - Ni crystal size of Port-1 samples: as received, after different reduction method and after SMR lab tests.

The Ni<sup>0</sup> crystal size was calculated also for lab-used Port-7 and 13, on both reflections ( $d_{200}$  and  $d_{220}$ ) and the mean values compared with those of fresh and Port-1 sample (Fig. 3. 68). The different position of the samples in the catalytic tube, i.e. the different condition to which they were subjected, leads to the different trend of the Ni crystal size. Port-13 and 7 present bigger Ni particles than Port-1, both before and after steam-reforming lab tests. The Ni sintering influences the activity, in fact Port-1 presents the higher catalytic performances due to the smaller Ni particles.

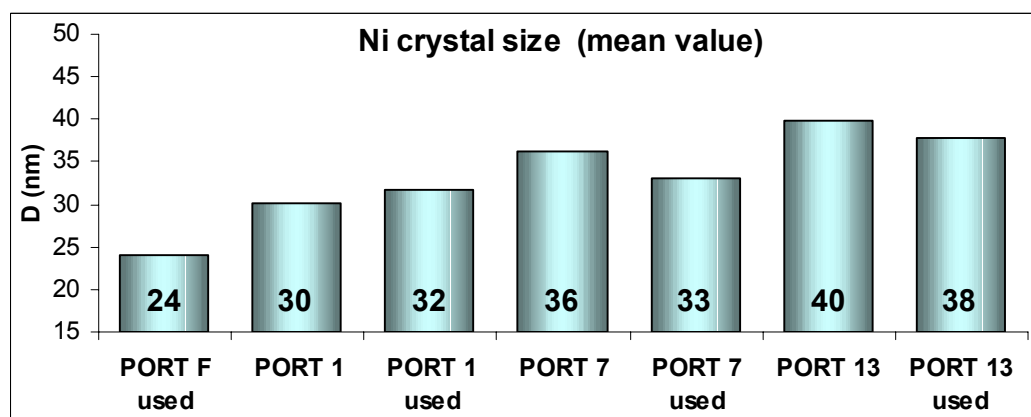
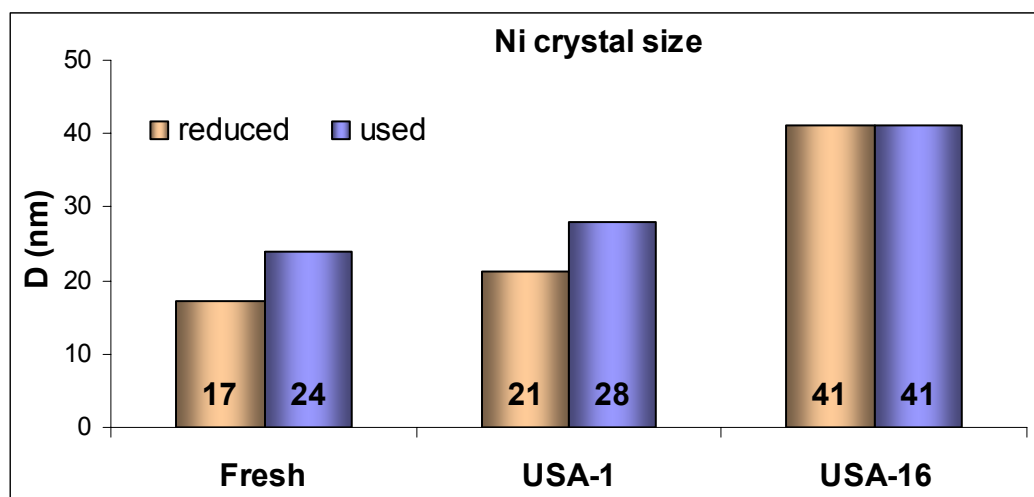


Fig. 3. 68 - Mean Ni crystal size calculated from the XRD patterns of the Port samples before and after SMR lab tests.

For what concern the USA samples, after laboratory tests, it was observed that the XRD pattern is very similar to those of as received samples, except to the

reduction of nickel in the sample N.1 where the metal was completely oxidized. For this sample (USA-1) Ni crystal size increase due to the new reduction carried out before the catalytic tests and the laboratory reaction conditions, in which the switch off of the plant does not lead the oxidation of the active phase. On the contrary, for what concern the sample taken from the bottom of the tube, the laboratory tests does not cause a further sintering of the metal (Fig. 3. 69)



**Fig. 3. 69 – Comparison of the Ni crystal size, from XRD patterns, for the reduced USA samples and after SMR lab tests.**

After the tests in lab SMR plant a further decrease of the surface area and pore volume was observed in all the samples (Tab. 3. 16 and Tab. 3. 17). The distribution of pores remains about constant at higher width, while, especially for Port 1, the micropores disappears. The decrease of surface area and disappearance of microporosity are more evident for the two samples unloaded from the top of the industrial catalytic tube, Port and USA N. 1 (Fig. 3. 70 and Fig. 3. 71).

		Fresh used	Port 1 used	Port 7 used	Port 13 used
Single Point Surface Area	$\text{m}^2\text{g}^{-1}$	9.70	13.15	7.79	5.55
BET Surface Area	$\text{m}^2\text{g}^{-1}$	9.98	13.76	8.01	5.71
t-plot micropore area	$\text{m}^2\text{g}^{-1}$	1.46	1.01	1.18	0.83
t-plot micropore volume	$\text{cm}^3\text{g}^{-1}$	0.000596	0.000266	0.000477	0.000334
BJH desorption cumulative volume of pores	$\text{cm}^3\text{g}^{-1}$	0.079673	0.156883	0.106209	0.047945
BLH desorption maximums pore widths	Å	22, 390	311	22, 555	570
BJH desorption average pore width (4V/A)	Å	308	402	502	346

Tab. 3. 16 - Surface area values and pores volume and width of the Portugal samples after lab tests.

		Fresh used	USA-1 used	USA-16 used
Single Point Surface Area	$\text{m}^2\text{g}^{-1}$	9.70	11.42	4.69
BET Surface Area	$\text{m}^2\text{g}^{-1}$	9.98	11.78	4.88
t-plot micropore area	$\text{m}^2\text{g}^{-1}$	1.46	1.49	0.37
t-plot micropore volume	$\text{cm}^3\text{g}^{-1}$	0.000596	0.000576	0.000110
BJH desorption cumulative volume of pores	$\text{cm}^3\text{g}^{-1}$	0.079673	0.173532	0.035599
BLH desorption maximums pore widths	Å	22, 390	327	20, 38, 500-1000
BJH desorption average pore width (4V/A)	Å	308	488.960	303.517

Tab. 3. 17 - Surface area values and pores volume and width of the Portugal samples after lab tests.

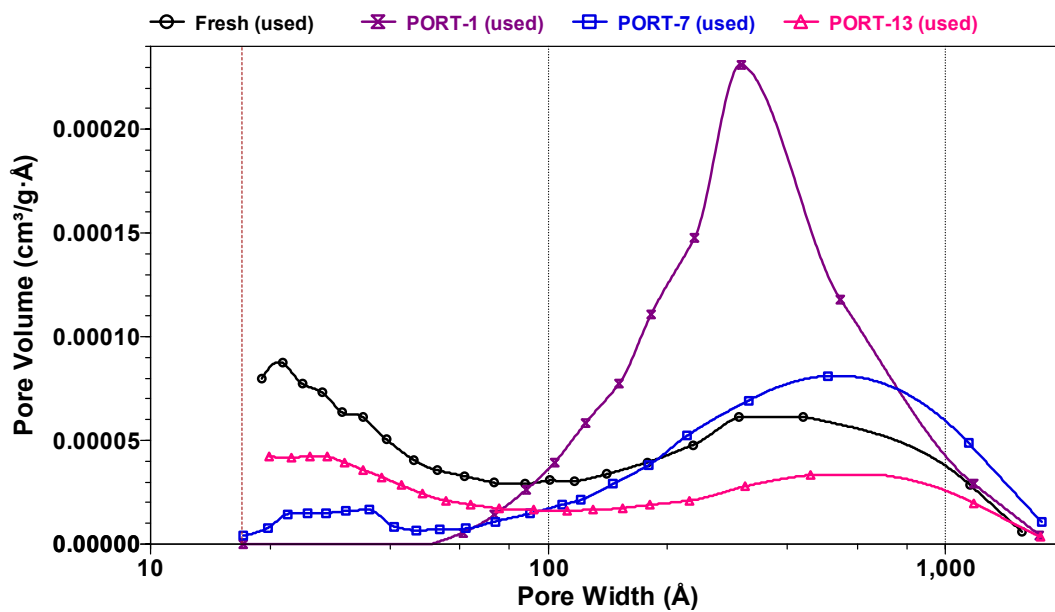


Fig. 3. 70 – Pore distribution of the Portugal samples after lab tests.

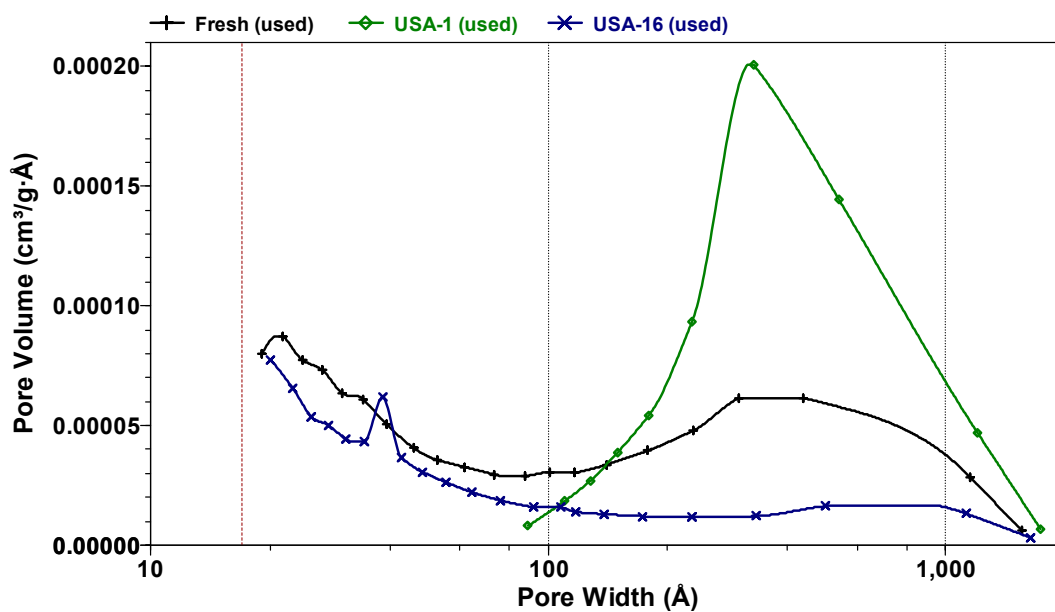


Fig. 3. 71 - Pore distribution of the Portugal samples after lab tests.

## 3.2. Comparison of different commercial catalyst

### 3.2.1. Characterization of commercial catalysts

Three commercial catalysts were characterized and tested in the laboratory steam reforming process to compare performances and deactivation.

The first sample (CAT A) was the 13 % Ni/MgAl<sub>2</sub>O<sub>4</sub>, which was characterized in detail in the previous chapter.

The features of the three steam reforming commercial catalysts are listed in the Tab. 3. 18.

	CAT A	CAT B	CAT C
Active metal	Ni	Ni	Ni
Nominal content (wt %)	13	18	14
Carrier	MgAl <sub>2</sub> O <sub>4</sub>	CaO/Al <sub>2</sub> O <sub>3</sub>	CaAl <sub>12</sub> O <sub>19</sub>
Support phase, identified by XRD	MgAl <sub>2</sub> O <sub>4</sub> /Al <sub>2</sub> O <sub>3</sub>	CaAl <sub>4</sub> O <sub>7</sub> /Al <sub>2</sub> O <sub>3</sub>	CaAl <sub>12</sub> O <sub>19</sub> / Al <sub>2</sub> O <sub>3</sub>
B.E.T. surface area (m <sup>2</sup> /g)	19	23	9

Tab. 3. 18 – Characteristic of the commercial catalysts.

The diffraction pattern of the CAT B shows mainly the presence of a calcium aluminate phase identified to be CaAl<sub>4</sub>O<sub>7</sub> together with the reflections of  $\alpha$ -Al<sub>2</sub>O<sub>3</sub> side phase, while does not show the presence of the CaO. Furthermore, in the XRD pattern are also present high intense peaks of NiO phase, but it was not possible to calculate the NiO crystal size because all the NiO reflections are partially overlapped with the support peaks (Fig. 3. 72).

The diffraction pattern of the CAT C presents mainly the reflections of the support phase (CaAl<sub>12</sub>O<sub>19</sub>), but also in this case a minor Al<sub>2</sub>O<sub>3</sub> phase is present.

Again the high amount of active metal is reflected in high intense peaks of NiO phase, but the overlapping with the complicate pattern of the support phase make impossible the calculation of NiO crystal size by XRD (Fig. 3. 73).

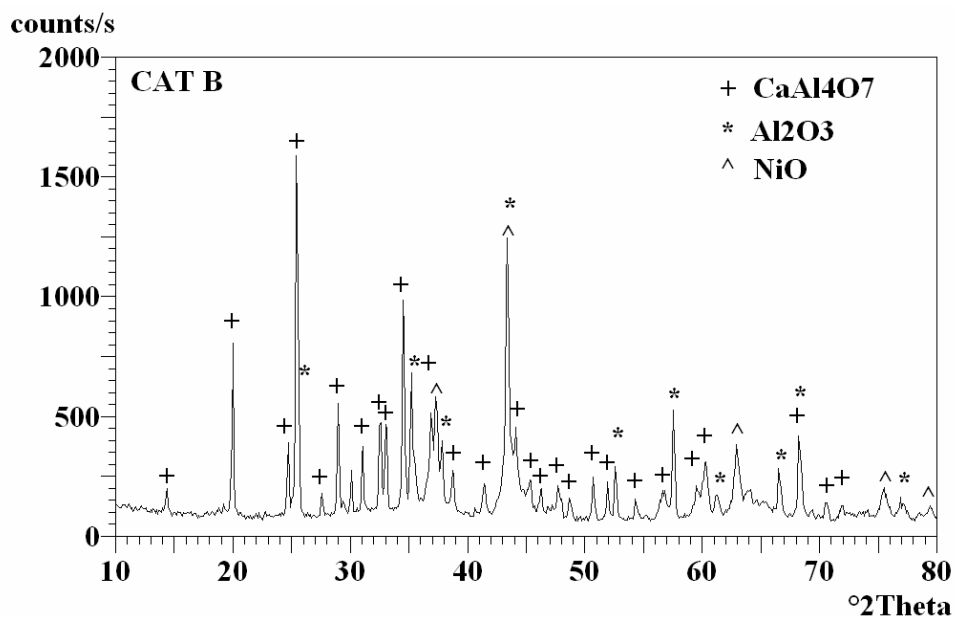


Fig. 3. 72 - XRD pattern of the sample CAT B (18 wt % Ni/CaAl<sub>4</sub>O<sub>7</sub>).

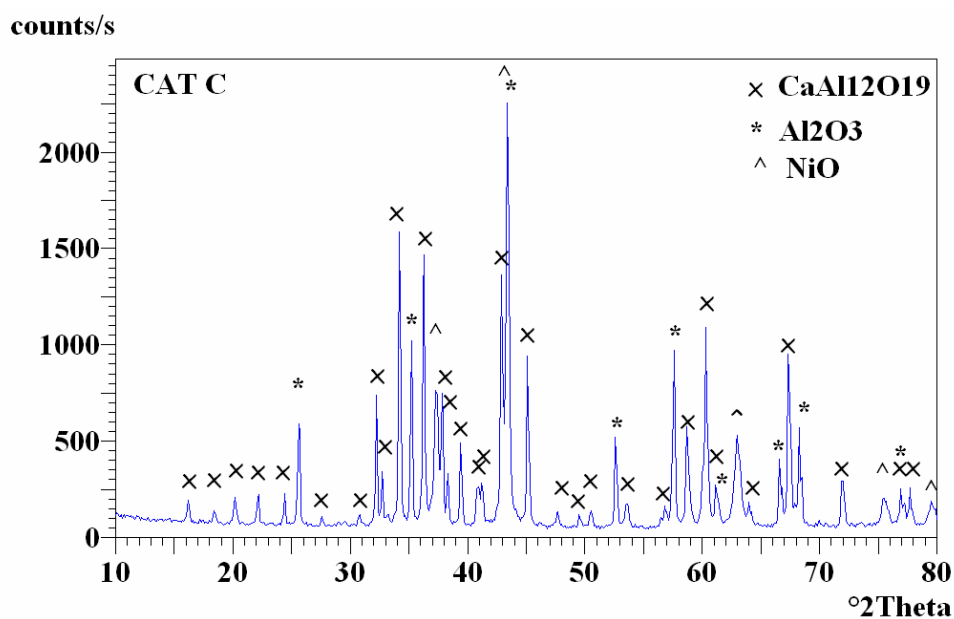


Fig. 3. 73 - XRD pattern of the CAT C sample (14 wt % Ni/CaAl<sub>12</sub>O<sub>19</sub>).

The TPR/O analyses were carried out on the three samples in order to identify the better procedure of activation of the commercial catalysts before the evaluation of the activity.

The CAT A showed three reduction steps occurring at 238, 440 and 538°C. The main reduction occurs at 440°C and is related to NiO slightly bounded with the

support; the reduction at lower temperature is related to free NiO, while that at 538°C NiO strongly interacting with the support (Fig. 3. 74).

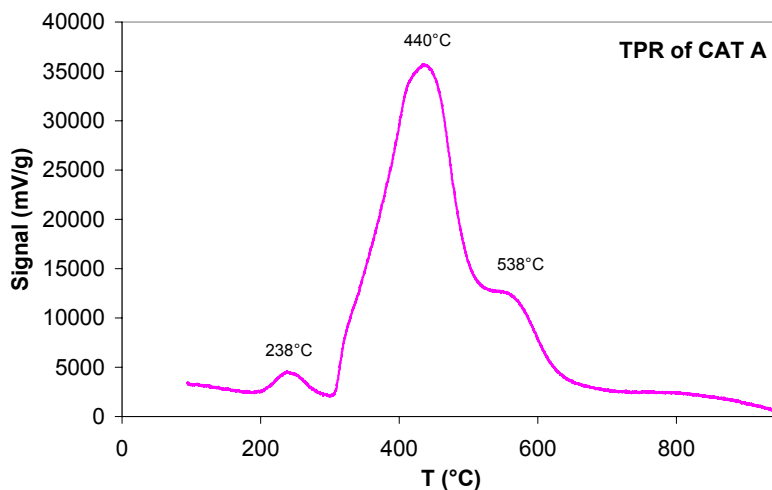


Fig. 3. 74 – TPR of CAT A.

Also for what concern the CAT B, the reduction of NiO to Ni<sup>0</sup> occurs in three steps, even if with respect to Cat A occurs at higher temperatures (Fig. 3. 75):

- at 450°C the reduction is assigned to NiO weakly interacting with the support;
- at 630°C the reduction is assigned to NiO strongly interacting with the support;
- at 755°C the reduction can be due to Ni partially soluted in the support in Ni/Al oxide amorphous phase or inside the CaAl<sub>4</sub>O<sub>7</sub> structure. The reduction at high temperature cannot be attributed to crystalline NiAl<sub>2</sub>O<sub>4</sub>, because from the XRD pattern there is no evidence of the presence of this phase.

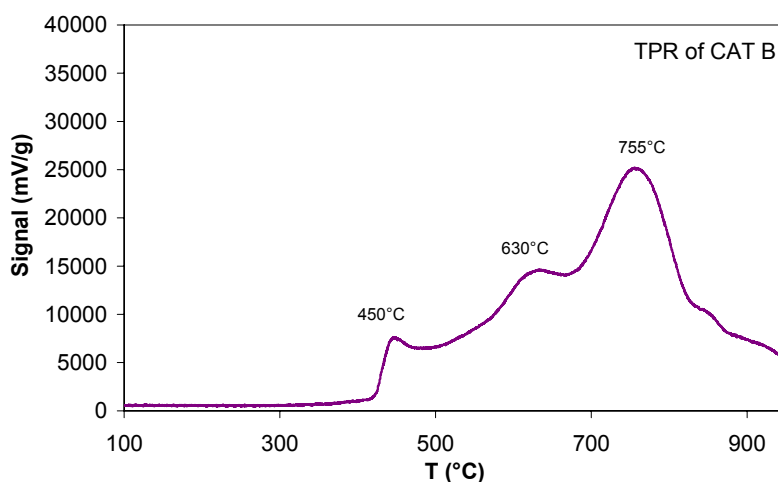
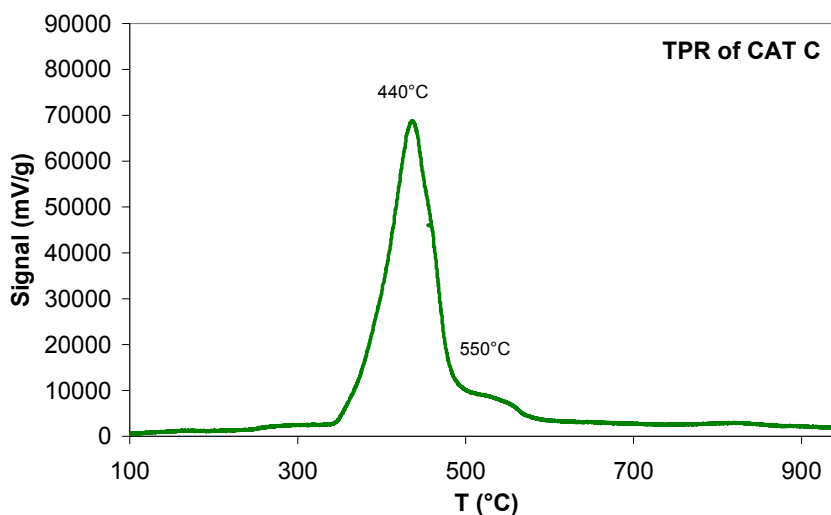


Fig. 3. 75 – TPR of CAT B.

The TPR pattern of CAT C shows mainly the reduction step of the NiO to Ni<sup>0</sup> at 440°C (i.e. NiO slightly bounded with the support). It is also present a shoulder at higher temperature (at about 550°C) probably due to some NiO strongly interacting with the support (Fig. 3. 76). The reduction profile of this sample is similar to that of the Cat A, although the different support compositions.



**Fig. 3. 76 – TPR of CAT C.**

Industrial catalysts were analyzed by porosimetry analysis (Tab. 3. 19 and Fig. 3. 77). The results on CAT B sample show that it is bimodal and its pores distribution is prevalently mesoporous, quite similar to the CAT A, even if the maximum width is lower: about 118 Å against 315 Å of the CAT A.

Very different porosity was observed for CAT C catalyst, which presents the lowest surface area and a predominant porosity at 20-40 Å. This sample shows much lower volume of pores with respect to the other commercial samples.

	CAT A	CAT B	CAT C
Single Point Surface Area	18.58	22.19	9.04
BET Surface Area	19.10	22.85	9.15
t-plot micropore area	2.09	2.93	2.41
t-plot micropore volume	0.000823	0.001152	0.001073
BJH desorption cumulative volume of pores	0.161980	0,115330	0.040404
BLH desorption maximums pore widths	23, 37, 315	37, 118	39
BJH desorption average pore width (4V/A)	316.250	188.063	196.632

Tab. 3. 19 - Surface area values and pores volume and width.

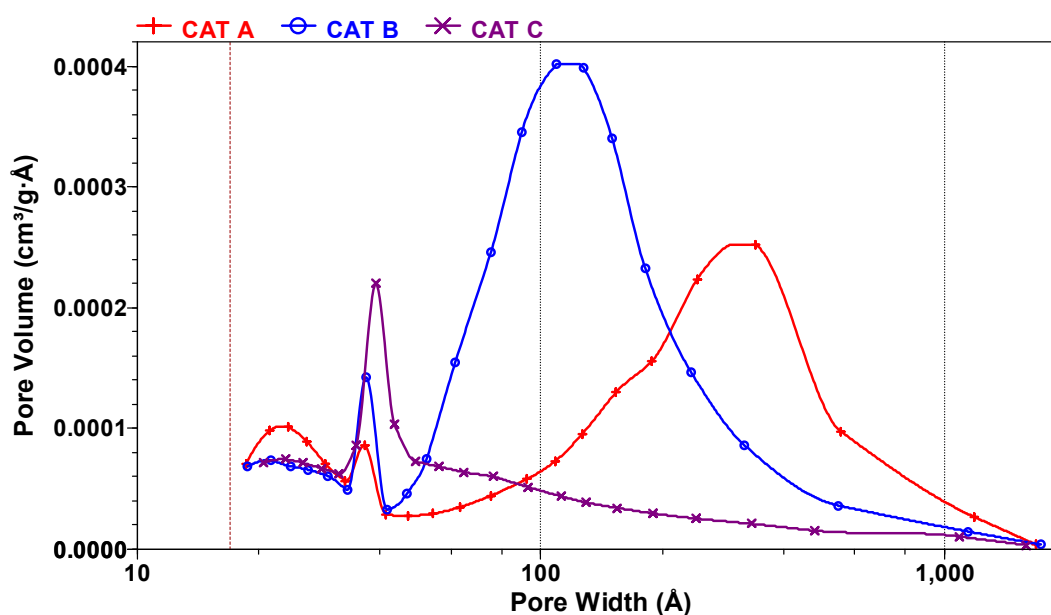


Fig. 3. 77 - Pore distribution of commercial catalysts.

The analyses of H<sub>2</sub> chemisorption performed on the commercial catalysts are show in Tab. 3. 20.

The CAT A is the sample that presents the highest dispersion of the nickel and consequently the lowest nickel particles size (this value is defined apparent because it is calculated from the measured dispersion). The differences may be due to different preparation method and thermal treatment to which the samples were subjected.



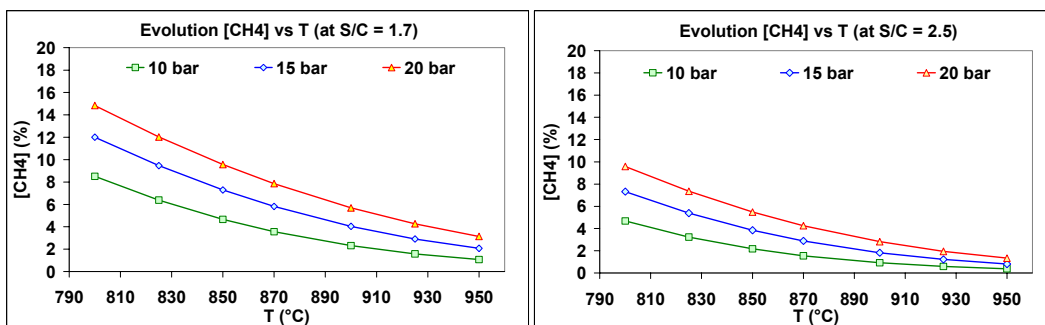


Fig. 3. 78 – Equilibrium methane composition as a function of temperature and pressure.

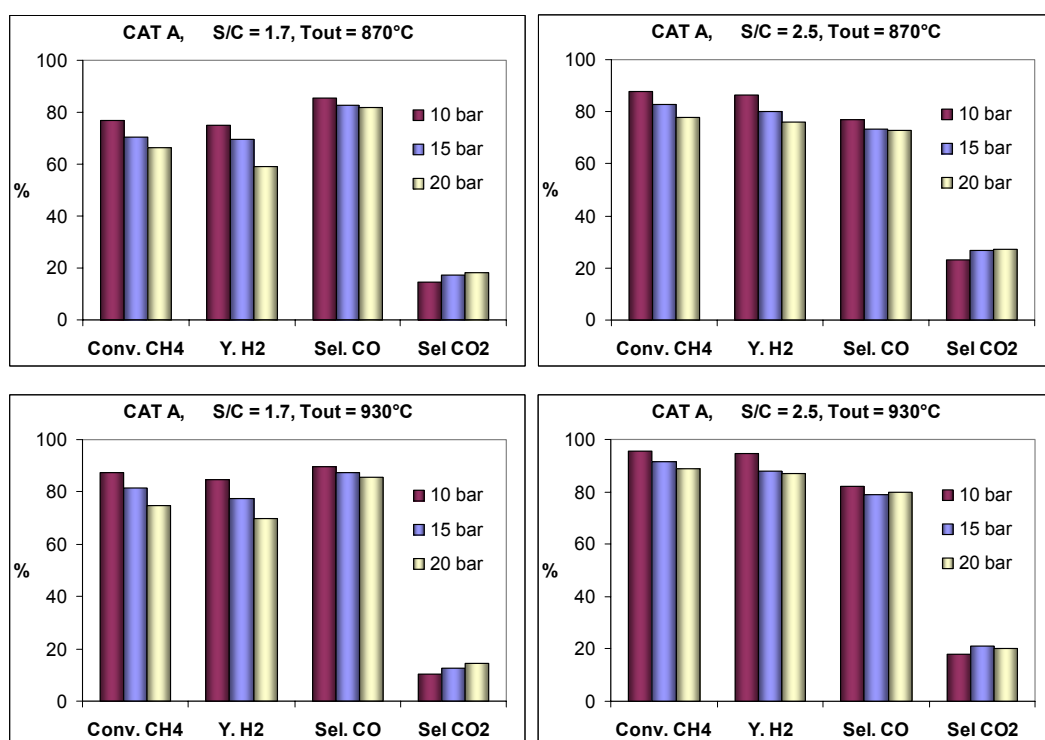
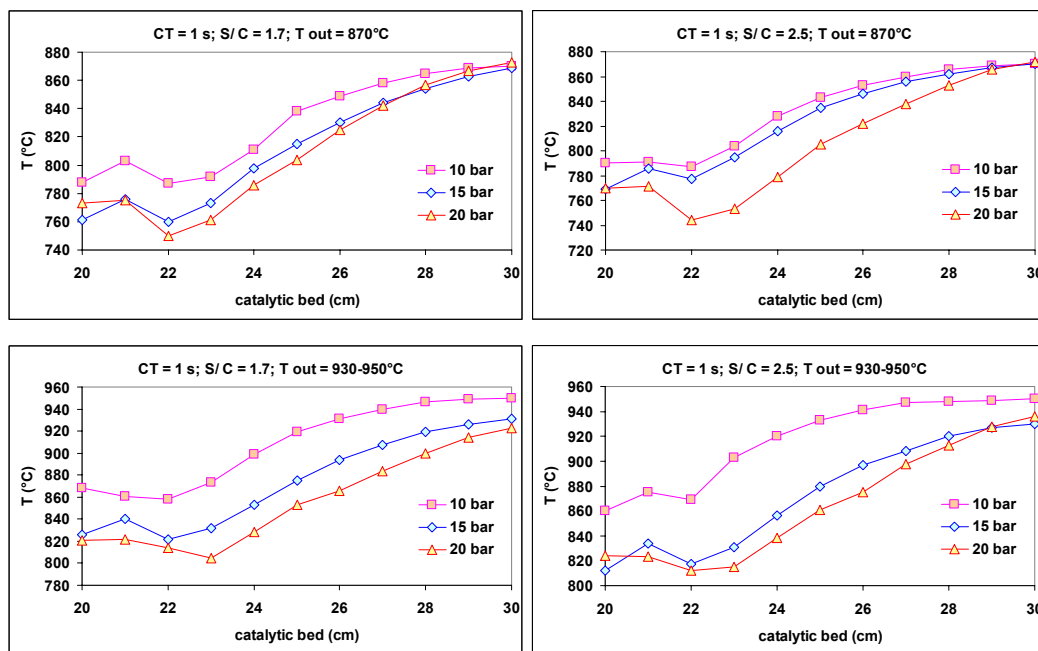


Fig. 3. 79 - Comparison among the activity of CAT A at different pressure.

A comparison among the axial thermal profile of the catalytic bed for the CAT A sample at different pressure is shown in Fig. 3. 80. It is possible to observe that increasing the pressure the  $\Delta T$  increases, leading to lower temperature in the catalytic bed, this will affect the catalytic performances.

Furthermore, the heat flow rate required to maintain the same conversion, changes significantly and may control the catalyst temperature and therefore the reaction rate.



**Fig. 3. 80 - Comparison among the axial thermal profiles of CAT A at different pressure.**

Increasing the S/C ratio, the activity of CAT A was enhanced in terms of methane conversion and hydrogen yields due to the beneficial effect of the increase of water that promotes the steam reforming reaction (Fig. 3. 81). The same effect was observed in all the reaction condition used, both different temperature and pressure. Furthermore, a consistent decrease of CO selectivity (with concomitant CO<sub>2</sub> selectivity increase) is observed, due to the promotion also of the water gas shift reaction that involves the reaction between water and CO ( $\text{CO} + \text{H}_2\text{O} \rightleftharpoons \text{H}_2 + \text{CO}_2$ ). In fact comparing the axial thermal profiles it can be observed that, in all the tests, using the higher S/C ratio, the second part of the catalytic bed reached slightly higher temperature than that observed in the temperature profiles measured with S/C = 1.7, due to the enhanced water gas shift reaction that is a slight exothermic reaction (Fig. 3. 82).

The increase of the temperature favors significantly the steam reforming reaction because it is highly endothermic. On the contrary, the water gas shift is not promoted by the temperature increase and this is reflected in an increase of the CO selectivity. As a consequence the H<sub>2</sub>/CO ratio increase with higher S/C ratio, but decrease increasing the temperature.

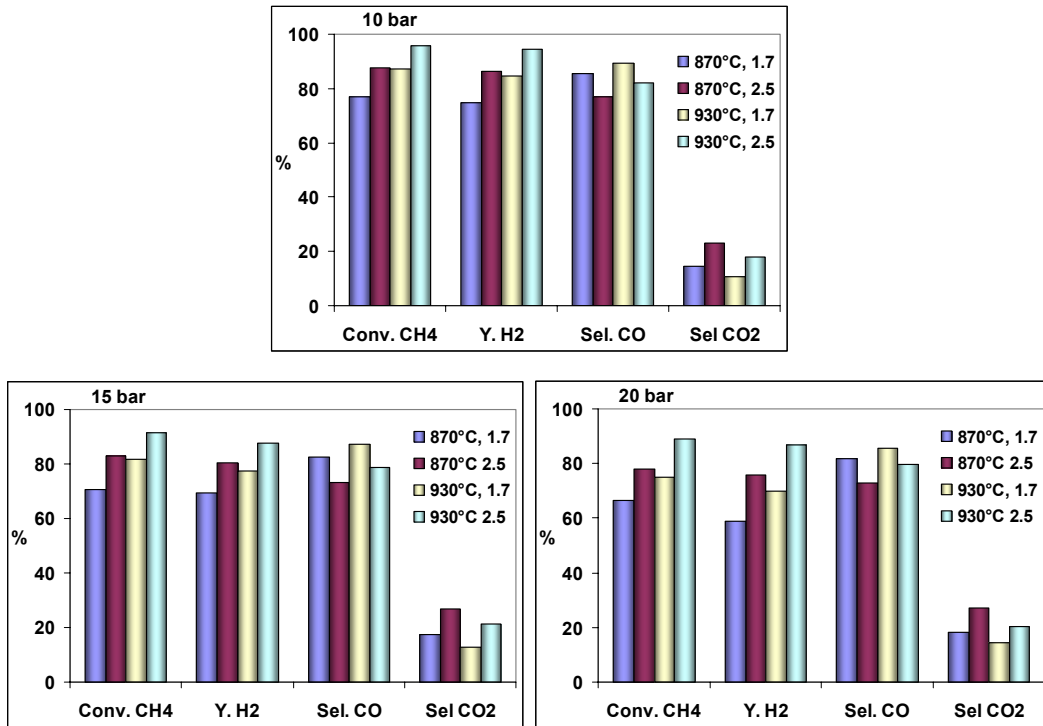


Fig. 3.81 - Comparison among the activity of CAT A at different S/C ratio and temperature.

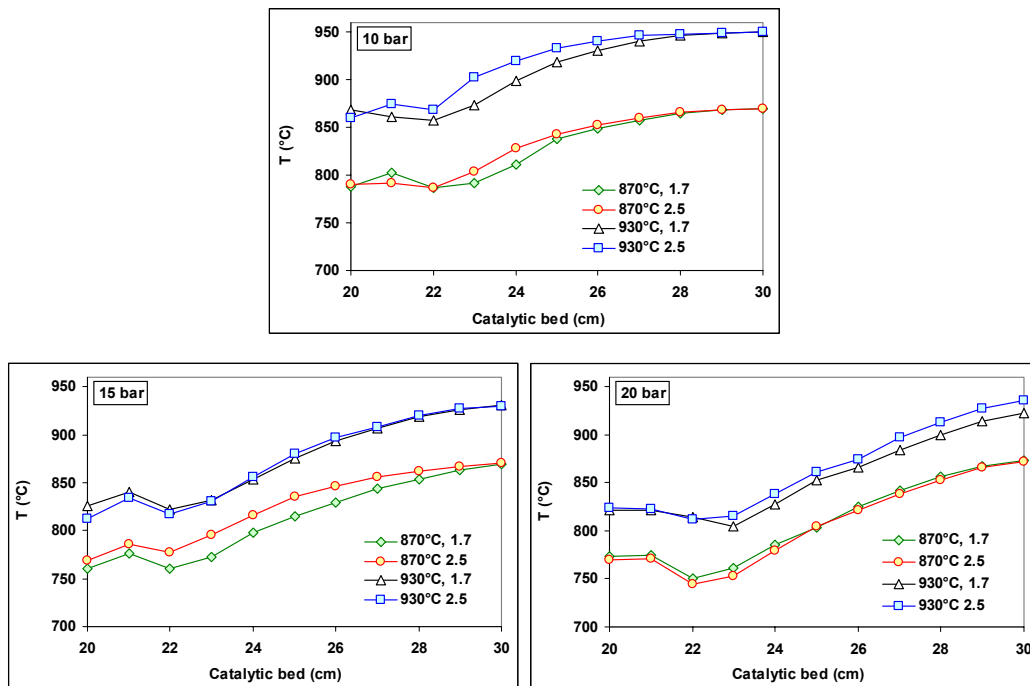


Fig. 3.82 - Comparison among the axial thermal profiles of CAT A at S/C ratio and temperature.

To study the effect of the residence time, the tests were carried out using 12 ml of catalyst with particle dimension of 14-20 mesh. In these tests the oven temperature were set to obtain an outlet temperature of 870°C. The tests were carried out at different contact time: 4, 2, 1.1 and 0.83 s (Tab. 3. 21).

	<b>P = 20 bar CT = 4 s S/C = 1.7 T<sub>oven</sub> = 920°C</b>	<b>P = 20 bar CT = 2 s S/C = 1.7 T<sub>oven</sub> = 932°C</b>	<b>P = 20 bar CT = 1.1 s S/C = 1.7 T<sub>oven</sub> = 970°C</b>	<b>P = 20 bar CT = 0.83 s S/C = 1.7 T<sub>oven</sub> = 1000°C</b>
<b>CH<sub>4</sub> (%)</b>	9.8	10.8	11.2	10.6
<b>H<sub>2</sub> (%)</b>	69.1	67.4	66.5	66.3
<b>CO (%)</b>	15.5	16.8	17.7	18.8
<b>CO<sub>2</sub> (%)</b>	5.7	4.9	4.6	4.2
<b>H<sub>2</sub>/CO</b>	4.5	4.0	3.8	3.5
<b>Conv. CH<sub>4</sub> (%)</b>	68.4	66.8	66.6	68.5
<b>Yield H<sub>2</sub> (%)</b>	68.2	64.3	61.9	62.0
<b>Sel. CO (%)</b>	73.1	77.4	79.4	81.7
<b>Sel. CO<sub>2</sub> (%)</b>	26.9	22.6	20.6	18.3
<b>T<sub>out</sub> (°C)</b>	871	871	871	860
<b>T<sub>in</sub>(°C)</b>	807	795	797	810
<b>T<sub>min</sub> (°C)</b>	768	731	707	694
<b>DT = T<sub>out</sub> - T<sub>min</sub> (°C)</b>	103	140	164	166
<b>DT = T<sub>in</sub> - T<sub>min</sub> (°C)</b>	39	64	90	116
<b>Dry Syngas flow rate (NI/h)</b>	67	95	221	286

**Tab. 3. 21 – Composition of the dry syn gas and catalytic results of the Cat A (T<sub>out</sub> = 870°C, 20 bar, S/C = 1.7, V<sub>cat</sub> = 12 ml (14-20 mesh), different CT).**

Decreasing the contact time from 4 to 0.83 s, the methane conversion does not change significantly (Fig. 3. 83), while the axial thermal profile are quite different (Fig. 3. 84): the temperature of the zone filled with inert material (0-18 cm) can be related to the oven temperature and to the gas flow rate. In fact, in the zone 0-7 cm, the higher oven temperature set for the tests at lower CT increases the inlet temperature of the profile, while from 7 to 18 cm the higher flow rate of the tests

at lower contact time causes a slightly lower temperature. However, the catalytic bed inlet temperatures are around 800°C, in a range of 15°C. In the first zone of the catalytic bed, the decrease of the contact time causes a higher  $\Delta T$ , with a shift of the minimum toward the center of the bed. The axial thermal profile of the second part of the catalytic bed shows lower T for lower CT, even if the oven temperatures are higher.

Only the test at 4 s reaches a flat thermal profile at the end of the catalytic bed. The composition obtained in the test carried out at 4 s corresponds to the thermodynamic equilibrium calculated at a temperature only 20°C lower than that measured at the outlet.

The slightly difference in the methane conversion are probably due to the opposite trend of axial and radial profiles. In fact, decreasing the contact time, the axial mean temperature decrease, but the higher oven temperature, necessary to maintain the same outlet temperature, may causes a higher radial  $\Delta T$ . In fact, the outlet temperature is measured and maintained constant at the radial center of the bed.

This is evident considering the WGS reaction: this reaction is favored at lower temperature, thus looking at the axial thermal profile it should be favored because of the decrease of the temperature with the contact time. On the contrary, decreasing the contact time, the  $H_2/CO$  ratio decreases, indicating a higher contribution of the water gas shift to the process. This can be explained only with a higher radial average temperature that affects significantly the composition of the syngas.

All the commercial samples (data not shown) present the same trend decreasing the contact time (from 4 s to 0.83): the differences in methane conversion were low. Summarizing the results it was observed that the axial thermal profiles were quite different: the inlet temperatures were similar, but in the first zone of the catalytic bed higher  $\Delta T$  were observed at lower CT, with a shift of the minimum toward the center of the bed. In the second part of the bed the temperature was lower for lower CT, even if the oven temperatures were higher. Only in the test at 4 s it was reached a flat trend at the end of the catalytic bed. The slightly difference in the methane conversion are probably due to the opposite trend of axial and radial profiles and the decrease of  $H_2/CO$  ratio is due to the fact that at the end of the bed the radial average temperature is higher than that observed in the middle of the bed and the WGSR is not favored.

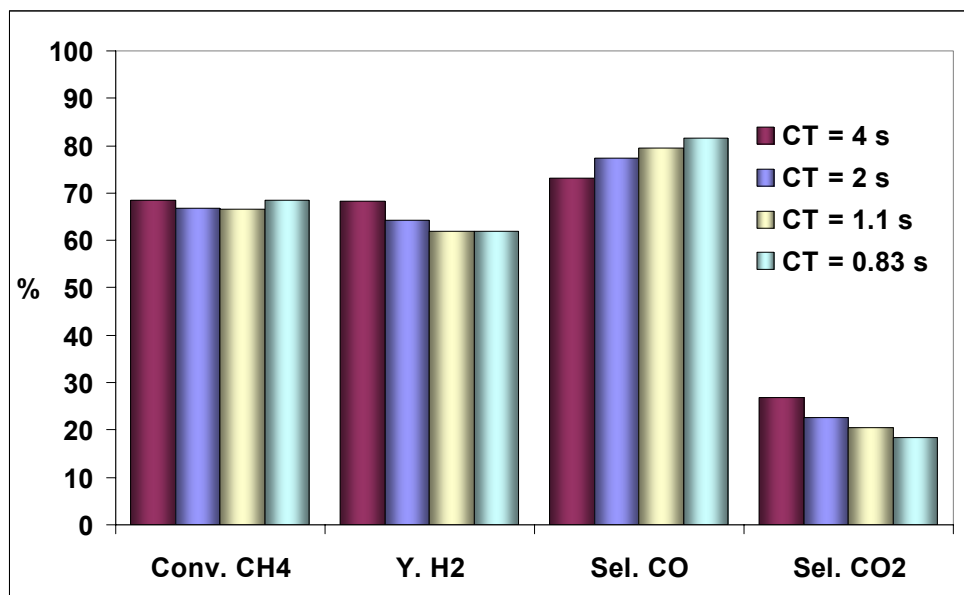


Fig. 3.83 - Comparison of the performances of the CAT A ( $T_{\text{out}} = 870^{\circ}\text{C}$ , 20 bar, S/C = 1.7,  $V_{\text{cat}} = 12$  ml, 14-20 mesh, different CT).

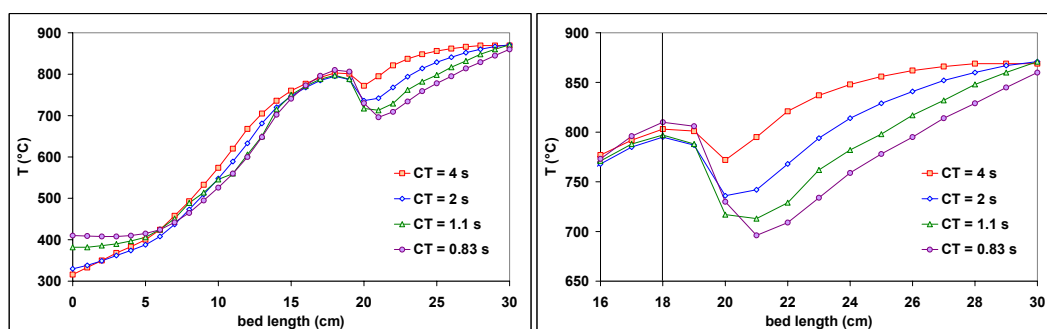


Fig. 3.84 – Axial thermal profile during reaction of the CAT A in the different reaction conditions ( $T_{\text{out}} = 870^{\circ}\text{C}$ , 20 bar, S/C = 1.7,  $V_{\text{cat}} = 12$  ml, 14-20 mesh, different CT).

Finally, to investigate the effect of the reaction parameters in the laboratory scale, the amount of catalyst load was studied. The tests were carried out with 6, 10 and 12 ml of catalysts, all with particle dimension of 14-20 mesh, that correspond to 6, 10 and 12 cm of height of the catalyst bed. The tests reaction conditions were  $P = 20$  bar,  $CT = 1$  s,  $S/C = 1.7$  and the outlet temperature was maintained constant at  $870^{\circ}\text{C}$ .

Increasing the volume of catalyst the methane conversion increases (Fig. 3.85), probably because the different height of catalytic bed leads to a significant different temperature profile. In particular, the CO/CO<sub>2</sub> selectivities are dependent

of the length of the second part of the bed (after the minimum in temperature) where the contribution of the water gas shift is significant. Indeed, the differences in the axial thermal profiles are evident in Fig. 3. 86. In the zone filled with inert material, until the beginning of the catalytic bed, the differences are due to the different reactant mixture fed to have the same reaction conditions (in particular the feed for the catalyst bed of 12 ml is double than that of the 6ml test), while the oven set temperature are not so different:

$$V_{\text{cat}} = 6 \text{ ml} \Rightarrow T_{\text{oven}} = 916^{\circ}\text{C}$$

$$V_{\text{cat}} = 10 \text{ ml} \Rightarrow T_{\text{oven}} = 918^{\circ}\text{C}$$

$$V_{\text{cat}} = 12 \text{ ml} \Rightarrow T_{\text{oven}} = 926^{\circ}\text{C}$$

The temperature decrease in the first part of the catalytic bed, due to the reforming reaction, is related to the absolute amount of reactant feed and to the inlet temperature, indeed it increases increasing the length of the catalytic bed due to higher amount of  $\text{CH}_4/\text{H}_2\text{O}$  mixture. Furthermore, it can be also observed that increasing the catalytic bed length the inlet temperature is lower due to the position of the bed in the reactor, which moves towards the beginning of the oven.

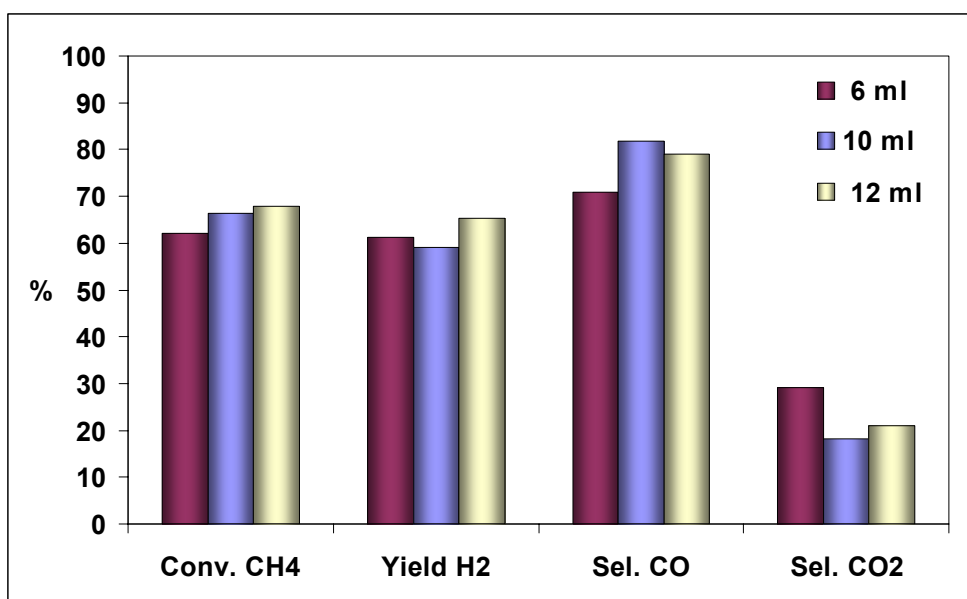


Fig. 3. 85 - Comparison of the performances of the CAT A using different  $V_{\text{cat}}$  ( $T_{\text{out}} = 870^{\circ}\text{C}$ , 20 bar, S/C = 1.7, dp = 14-20 mesh, CT = 1 s).

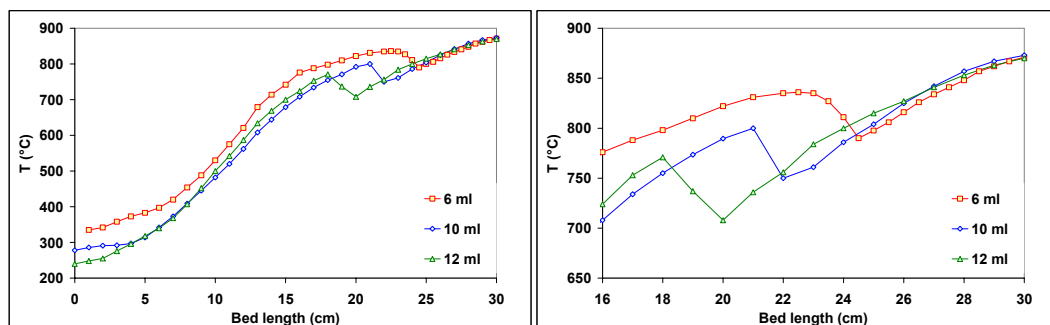


Fig. 3. 86 - Comparison of the axial thermal profiles of the CAT A using different  $V_{cat}$  ( $T_{out} = 870^{\circ}\text{C}$ , 20 bar, S/C = 1.7,  $d_p = 14\text{-}20$  mesh, CT = 1 s).

### 3.2.3. Activity of commercial catalysts

The three commercial catalysts CAT A (13 % Ni/MgAl<sub>2</sub>O<sub>4</sub>) CAT B (18 % Ni / CaAl<sub>4</sub>O<sub>7</sub>) and CAT C (14 % Ni/CaAl<sub>12</sub>O<sub>19</sub>) were tested and compared in the different reaction conditions.

The reaction conditions that were maintained constant in all the tests were:

- the pressure  $P = 20$  bar
- the S/C ratio  $S/C = 1.7$  mol/mol
- the catalyst volume  $V_{cat} = 12$  ml
- the pellets dimension  $d_p = 14\text{-}20$  mesh

For all the samples, the tests, carried out loading 12 ml of samples, correspond to a different weight for each sample, due to their different density:

CAT A 12 ml = 12.9 g

CAT B 12 ml = 12.6 g

CAT C 12 ml = 10.3 g

The 14-20 mesh pellets (1.410-0.841 mm) of the commercial samples were obtained by crashing the pre-formed tablets in smaller ones.

The varied reaction parameters were:

- contact time CT = 4, 2, 1.1 and 0.83 s,
- oven temperature  $T_{oven} = 950$  and  $800^{\circ}\text{C}$ .

The contact times were varied (4, 2, 1.1 and 0.83 s) at a constant outlet temperature ( $870^{\circ}\text{C}$ ) to compare the catalyst performances of the samples with the goal to discriminate among them. The differences in the methane conversion

of the samples are low, whatever the contact time is. However, for all the different contact times the catalysts that presents the higher activity is the CAT A, while the samples that has the worst performances is the CAT B (Fig. 3. 87). The axial thermal profile measured during the catalytic tests are very similar for the different samples (Fig. 3. 87).

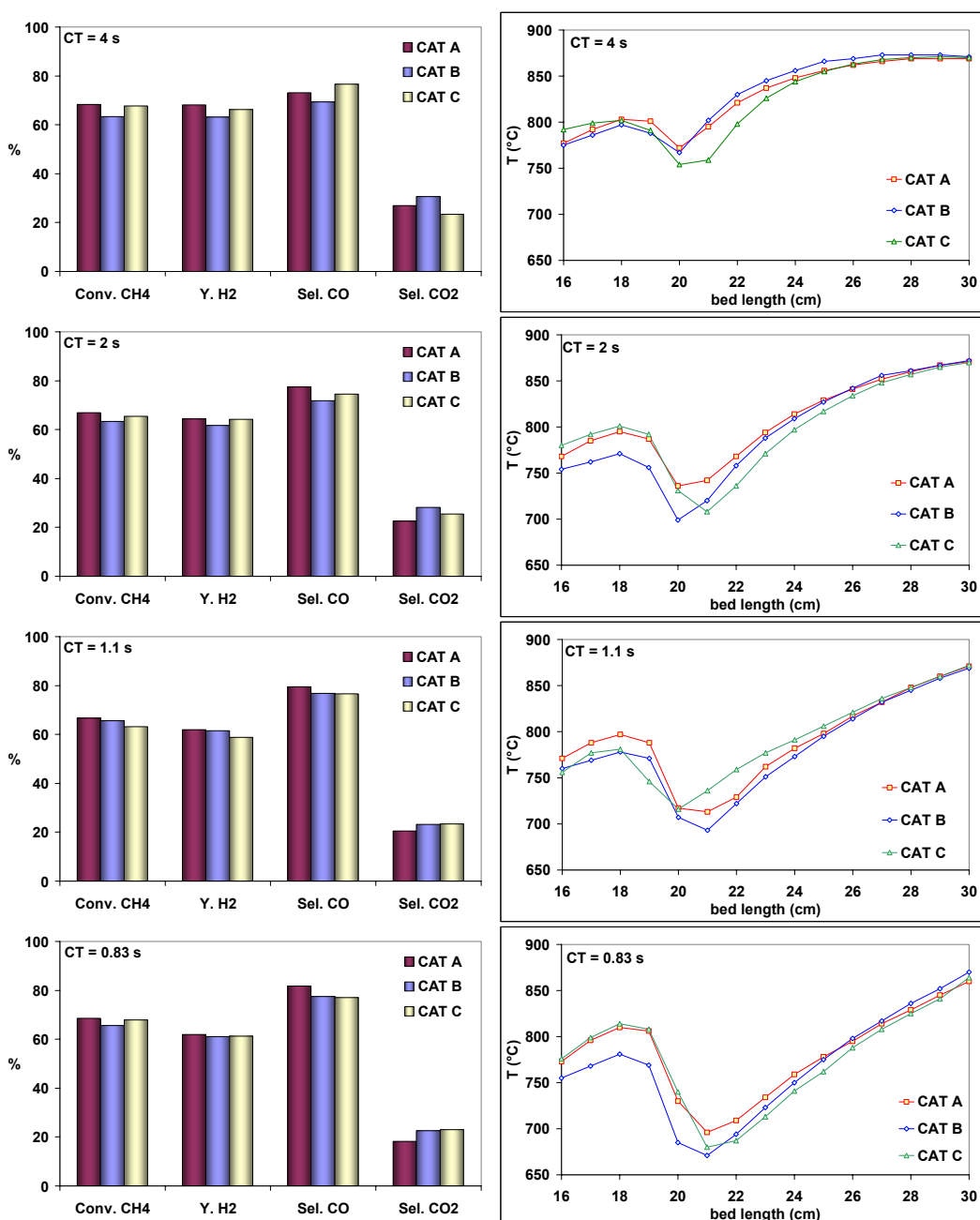


Fig. 3. 87 - Comparison of the performances and of the axial thermal profiles of the CAT A, B and C using different CT ( $T_{out} = 870^{\circ}\text{C}$ , 20 bar,  $S/C = 1.7$ ,  $V_{cat} = 12$  ml and  $dp = 14\text{-}20$  mesh).

The tests carried out at constant oven temperature were performed to compare the catalytic performances of the samples at the same power consumption, to verify the behavior in this condition, and to verify if differences among the catalysts can be evidenced. The tests were carried out at 4, 2 and 1.1 s.

In all the tests the differences among the samples are lower than in the tests carried out maintaining constant the outlet temperature at 870°C (Fig. 3. 88). The test that presents higher differences is the one carried out at 1.1 s.

In these tests, maintaining constant the oven temperature, the sample that present the higher performances is the CAT C (14 % Ni/CaAl<sub>12</sub>O<sub>19</sub>), even if the difference from the activity of CAT A are very small. Also in these tests, the CAT B (18 % Ni/CaAl<sub>4</sub>O<sub>7</sub>) reaches the worst activity.

For what concern the axial thermal profiles, the difference observed among the samples are very low.

In particular, in the first part of the catalytic bed, before the minimum of temperature, some differences are evident in the inlet temperature.

The CAT C presents slightly higher inlet temperature, followed by the CAT A and CAT B. The  $\Delta T$  (differences between the inlet and minimum temperatures) are about the same for all the catalysts, confirming the very similar activity that involve similar heat require. The higher inlet temperature corresponds to the higher activity. On the contrary, in the second part of the catalytic bed, after the minimum, the axial profiles are very similar each other due to the same heat supplied to the reaction.

Indeed, the slightly higher activity of CAT C than the other commercial catalysts, in particular than CAT A (the best catalyst of constant outlet temperature) may be related to the slightly higher temperature profile of all the catalytic bed reached during operation.

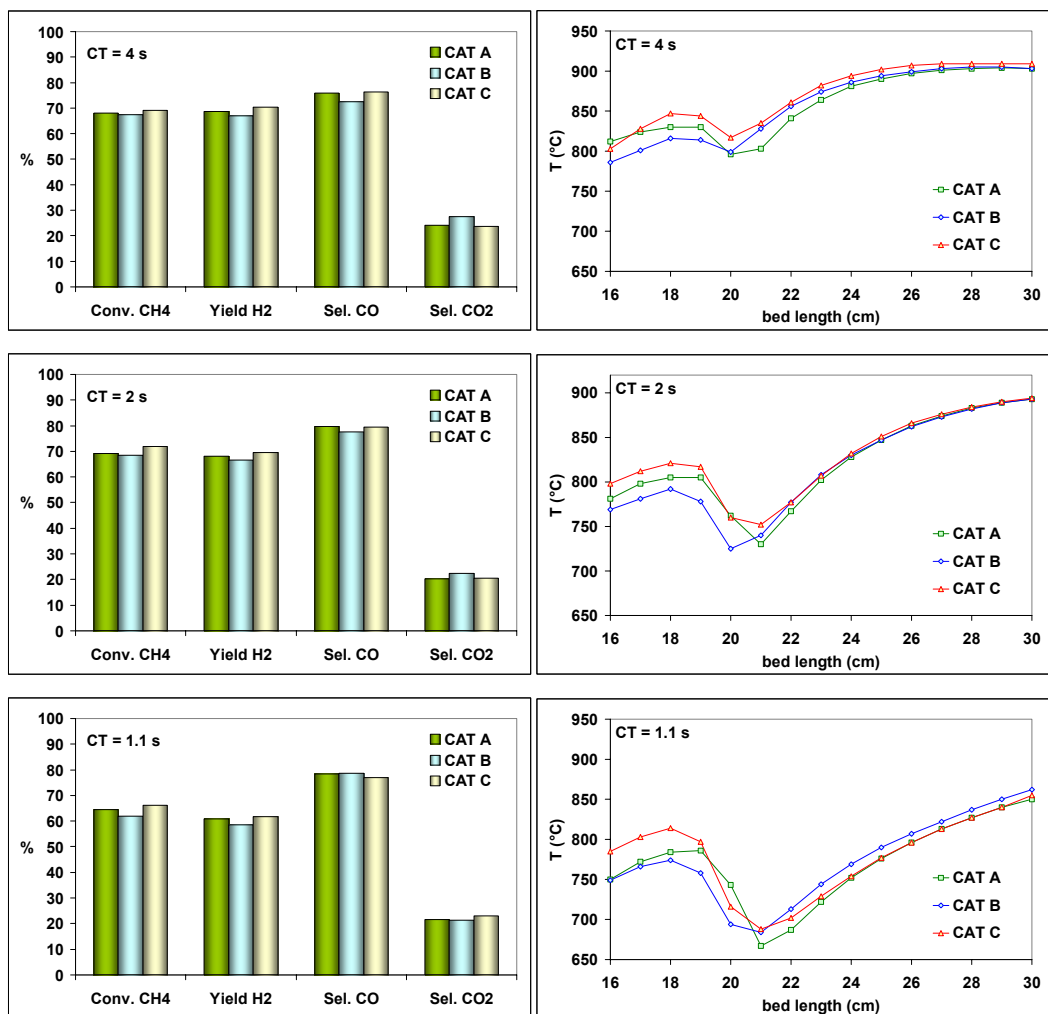


**Fig. 3.88 - Comparison of the performances and of the axial thermal profiles of the CAT A, B and C using different CT ( $T_{\text{oven}} = 950^{\circ}\text{C}$ , 20 bar,  $S/C = 1.7$ ,  $V_{\text{cat}} = 12$  ml and  $d_p = 14\text{-}20$  mesh).**

Finally the commercial catalysts were compared in tests at low temperature that were carried out with constant  $T_{\text{oven}}$  ( $800^{\circ}\text{C}$ ) to compare the catalytic performances of the different samples far from the thermodynamic equilibrium. These tests were carried out to try to emphasize the difference among the catalysts. These tests were carried out at contact time of 4 and 2 s.

The activities at this temperature were low, in accordance with expectation.

The differences between the two different contact times were low (like in the case of the tests at higher temperature). This may be due to the small differences of the outlet temperatures, which means higher oven temperature for the low CT tests.

For what concern the thermal profiles the trends were very similar in the two cases (CT = 4 and 2 s), but the higher feed flow rate for the test at 2 s causes the general lower temperature.

Also in this case, in both tests with different residence time, the differences among the sample activities are very low (Fig. 3. 89). The best performances are obtained, again, by the CAT C sample. Using such low temperature, the CAT B does not present lower performances with respect to the other two commercial sample (the difference are very small).

The axial thermal profiles are slightly different only in the first part of the catalytic bed, where the CAT C still presents the higher inlet temperature, while the second part of the catalytic bed are practically the same for all the catalysts.

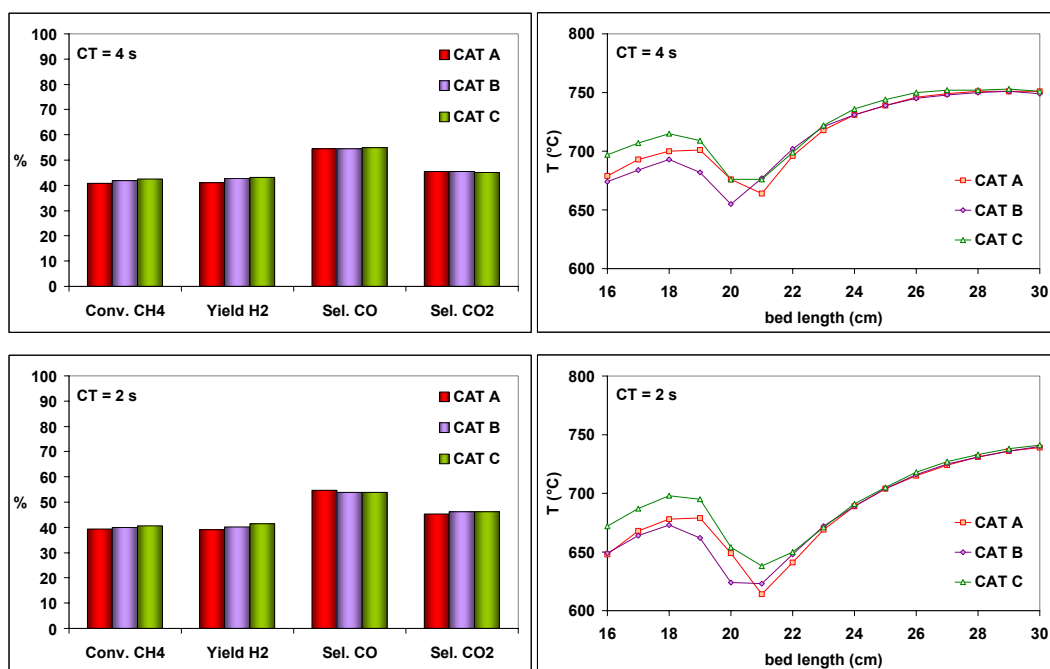


Fig. 3. 89 - Comparison of the performances and of the axial thermal profiles of the CAT A, B and C using different CT ( $T_{\text{oven}} = 800^{\circ}\text{C}$ , 20 bar, S/C = 1.7,  $V_{\text{cat}} = 12$  ml and  $dp = 14\text{-}20$  mesh).

### 3.2.4. Characterization of used commercial catalysts

After the steam reforming catalytic tests, the commercial catalysts were characterized by XRD, porosimetry and  $H_2$  chemisorption analyses in order to evaluate structure modification and deactivation occurred on the samples due to the reactions conditions.

The XRD analyses carried out on the used samples shows only the reduction of the nickel from  $NiO$  to  $Ni^0$ . No sintering of the support or carbon species formation were observed after laboratory catalytic tests by XRD (Fig. 3. 90, Fig. 3. 91 and Fig. 3. 92).

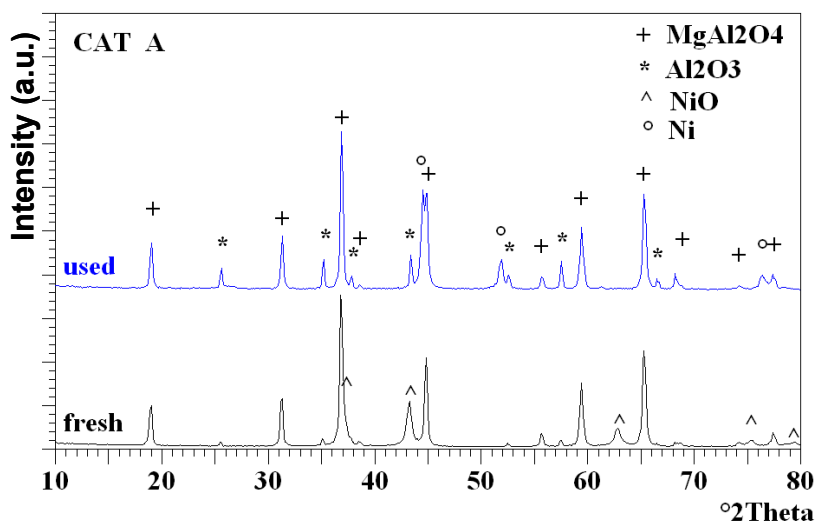


Fig. 3. 90 - Comparison of XRD patterns of fresh and used CAT A (13 %  $Ni/MgAl_2O_4$ ).

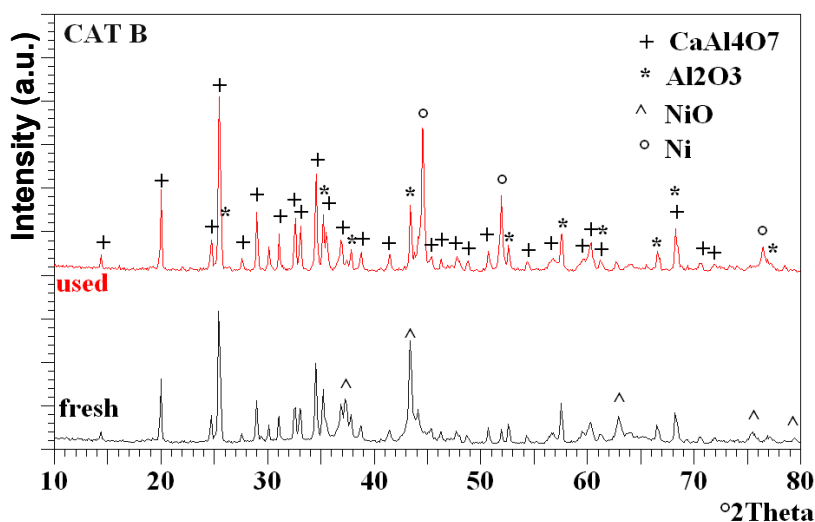


Fig. 3. 91 - Comparison of XRD patterns of fresh and used CAT B (18 %  $Ni/CaAl_4O_7$ ).

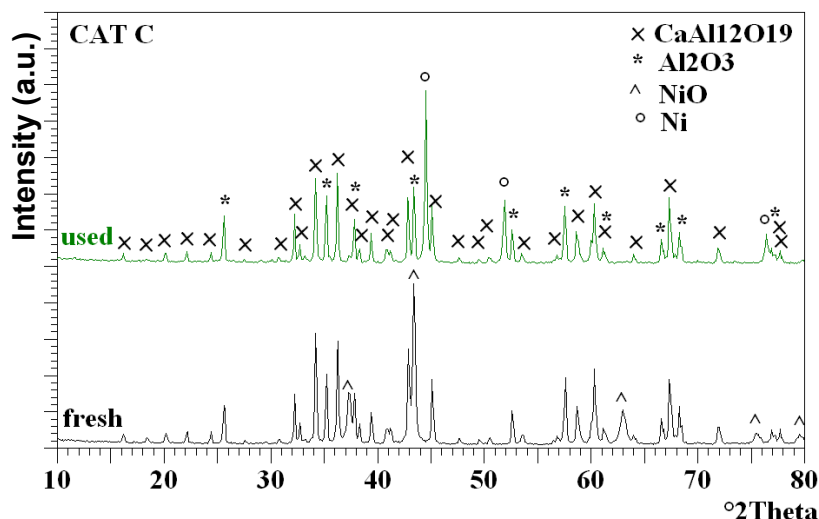


Fig. 3. 92 - Comparison of XRD patterns of fresh and used CAT C (14 % Ni/CaAl<sub>12</sub>O<sub>19</sub>).

The surface areas, measured after the steam reforming tests, present significant decrease with respect those of the fresh samples (Tab. 3. 22). In particular the higher decrease was observed for the CAT B (18 % Ni/CaAl<sub>4</sub>O<sub>7</sub>), its fresh sample had the highest value (~ 23 m<sup>2</sup>/g), while the used one presents a surface area of 2 m<sup>2</sup>/g. The CAT A (13 % Ni/MgAl<sub>2</sub>O<sub>4</sub>) shows the lower textural modification, maintaining a surface area of 8 m<sup>2</sup>/g, the half of initial value, while also the CAT C presents a surface area that is 1/3 of that it had before the catalytic tests.

Beside the decrease of surface area, all the samples, but in particular CAT B and CAT C, present a remarkable decrease of pore volume (Fig. 3. 93). Moreover, CAT A shows a decrease of the micro- and meso-porosity associated to a shift at higher pores width that may be related to the occlusion of the pores by Ni particles.

The CAT B, besides a decrease of surface area of more than ten times, shows, in practice, a total loss of the mesoporosity, especially at pore width greater than 40 Å.

Also the CAT C, that before tests presented the lowest surface area and pore volume, with a maximum of pore width around 39 Å (smaller than the other commercial catalysts), after reaction losses completely the mesoporosity. The sintering was not observed in the XRD patterns of used samples, these lost of surface area and pore volume may be attributed to occlusion of the pores by

same sintering of the support by big nickel particles and maybe by carbonaceous deposits formed during reaction.

		CAT A	CAT B	CAT C
Single Point Surface Area (m <sup>2</sup> /g)	Fresh	18.58	22.19	9.04
	Used	7.88	1.85	2.70
BET Surface Area (m <sup>2</sup> /g)	Fresh	19.10	22.85	9.15
	Used	8.13	2.00	2.91
BJH desorption cumulative volume of pores (m <sup>3</sup> /g)	Fresh	0.161980	0,115330	0.040404
	Used	0.122370	0.022063	0.02171
BLH desorption maximums pore widths (Å)	Fresh	23, 37, 315	37, 118	39
	Used	22, 520	18, 38	18, 37
BJH desorption average pore width (4V/A) (Å)	Fresh	316	188	196
	Used	542	448	348

Tab. 3. 22 – Comparison of surface area values and pores volume and width, before and after reaction of the commercial catalysts.

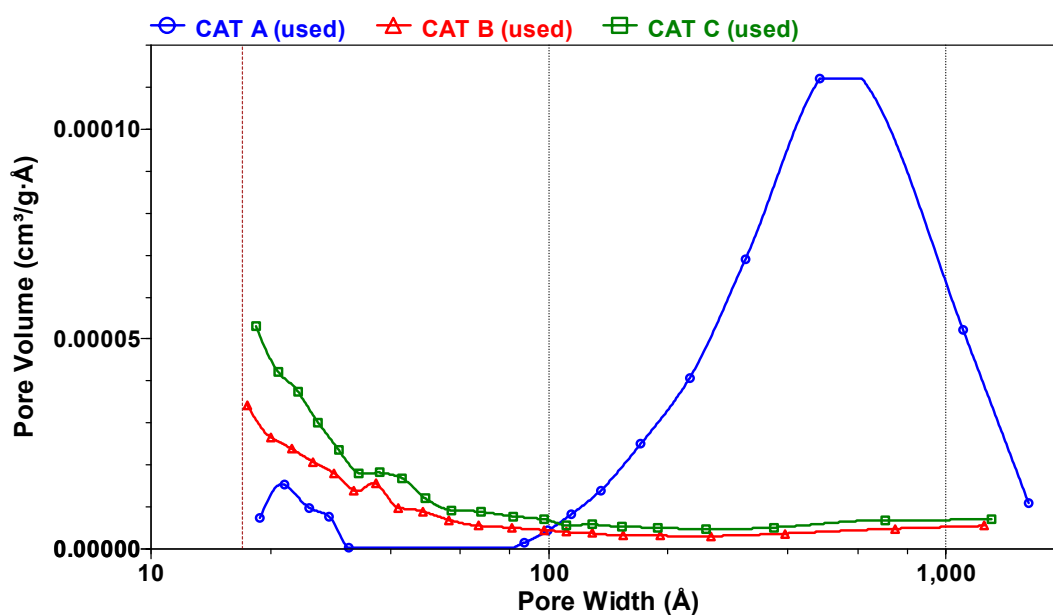


Fig. 3. 93 – Pore distribution of the used commercial samples.

The metallic nickel dispersions of the commercial catalysts, which were not high before reaction, further decrease after reaction (Tab. 3. 23). The highest decrease in nickel dispersion and metallic surface area has been observed for the CAT A. However, CAT A is the sample that maintain the highest surface area and that, apparently, had the smallest nickel particle size before activity tests, indeed, also after catalytic tests it is the samples that has the higher dispersion and, probably this is why this catalyst showed the better catalytic performances (considering the same temperature profile). CAT A is the sample that showed the lowest deactivation in terms of textural properties, even if the nickel sintering is important.

For what concern the CAT C, after the reaction, it presents a dispersion and metallic surface area very similar to those of CAT A, so, it can be deduced that for this reason the activities observed for this two catalysts were so similar. CAT C is the samples that showed the lowest deactivation in terms of Ni sintering.

Opposite trend was observed for CAT B, which deactivated significantly, both surface area and nickel dispersion remarkably decrease with time-on-stream and, in fact, this is reflected in the worst catalytic activity.

		Ni	Ni Dispersion	MSAm	Apparent crystallite size
		<i>wt %</i>	<i>%</i>	<i>m<sup>2</sup>/g metal</i>	<i>nm</i>
CAT A	Fresh	13	4.8	32.0	21
	Used	13	0.22	1.5	460
CAT B	Fresh	18	1.50	9.8	69
	Used	18	0.12	0.8	869
CAT C	Fresh	14	0.66	4.4	154
	Used	14	0.19	1.2	541

**Tab. 3. 23 – Comparison of the H<sub>2</sub> chemisorption results on fresh and used commercial catalyst (MSAm = metallic surface area).**

### 3.3. Catalyst obtained from hydrotalcite (HT) type precursor

The catalyst obtained from hydrotalcite type precursor, after the study carried out for the partial oxidation of methane reaction, chosen to be tested in the steam reforming process is  $\text{Rh}_{0.15}\text{Ni}_8\text{Mg}_{60}\text{Al}_{31.85}$ .

The XRD pattern of the hydrotalcite type precursor shows the typical reflections of this kind of compounds containing silicates as interlayer anions (Fig. 3. 94).

After calcination at 900°C for 12 h, the sample presents mainly the reflections of the forsterite type phase ( $\text{Mg}_2\text{SiO}_4$ ) and minor phases such as MgO, in which Ni and Rh are soluted, and a spinel defective phase (Fig. 3. 95).

For what concern the textural properties of the catalyst obtained from hydrotalcite precursor, it maintain high surface area (93.5  $\text{m}^2/\text{g}$ ) also after calcination at 900°C for 12 h. The sample presents good pore volume and a monomodal distribution of the pore width around 100 Å (Tab. 3. 24 and Fig. 3. 96).

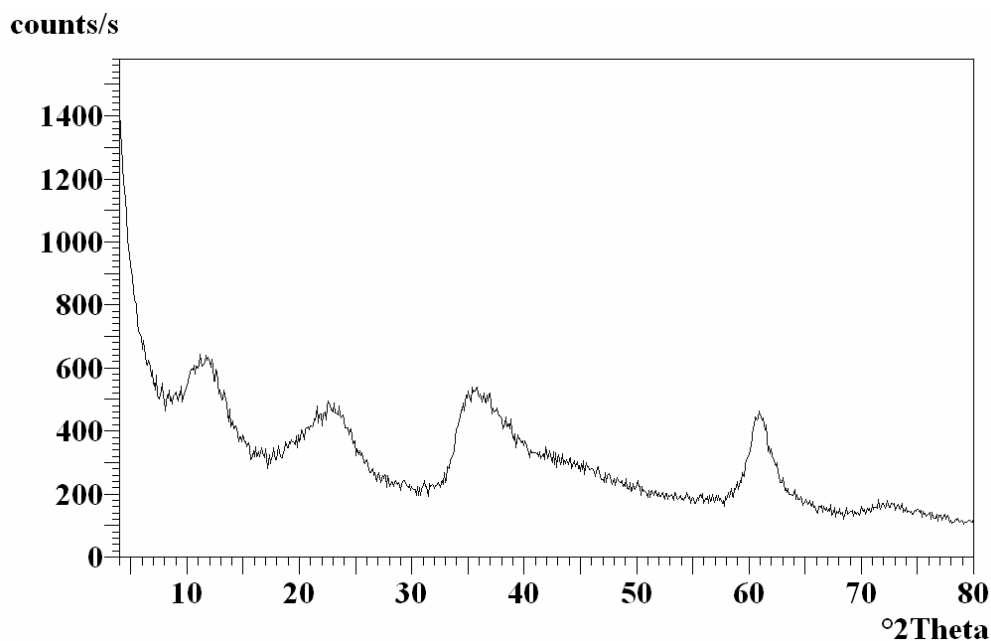


Fig. 3. 94 – XRD pattern of the hydrotalcite type precursor of the catalyst ex-HT  $\text{Rh}_{0.15}\text{Ni}_8\text{Mg}_{60}\text{Al}_{31.85}$ .

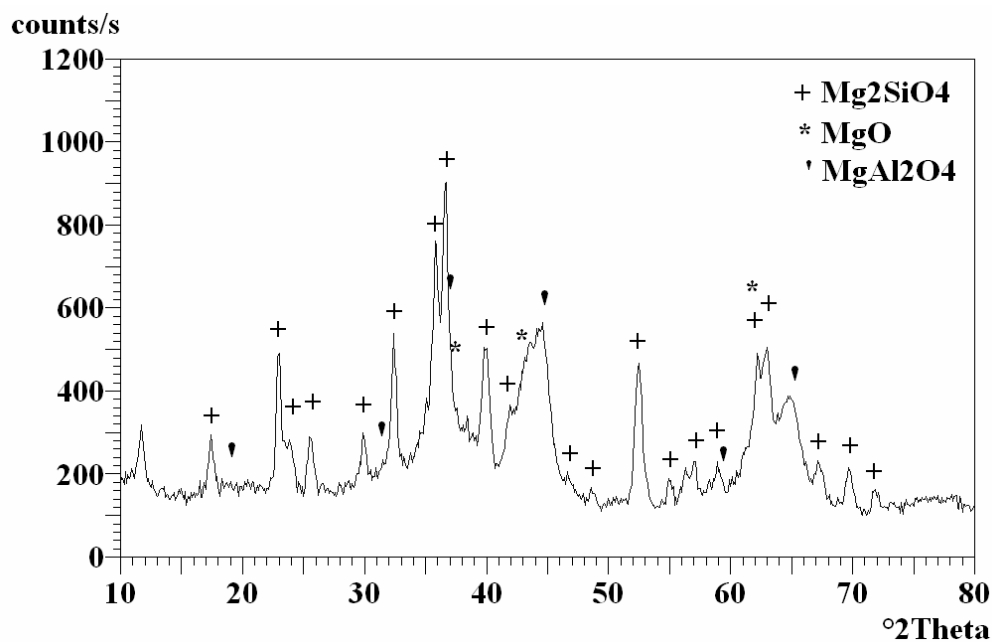


Fig. 3. 95 - XRD pattern of the catalyst ex-HT Rh<sub>0.15</sub>Ni<sub>8</sub>Mg<sub>60</sub>Al<sub>31.85</sub>, calcined at 900°C for 12 h.

EX-HT SILICATE Rh <sub>0.15</sub> Ni <sub>8</sub> Mg <sub>60</sub> Al <sub>31.85</sub>		
Single Point Surface Area	m <sup>2</sup> g <sup>-1</sup>	91.50
BET Surface Area	m <sup>2</sup> g <sup>-1</sup>	93.54
t-plot micropore area	m <sup>2</sup> g <sup>-1</sup>	12.11
t-plot micropore volume	cm <sup>3</sup> g <sup>-1</sup>	0.005109
BJH desorption cumulative volume of pores	cm <sup>3</sup> g <sup>-1</sup>	0.413405
BJH desorption maximums pore widths	Å	100
BJH desorption average pore width (4V/A)	Å	131

Tab. 3. 24 –Surface area values and pores volume and width of the catalyst ex-HT Rh<sub>0.15</sub>Ni<sub>8</sub>Mg<sub>60</sub>Al<sub>31.85</sub>, calcined at 900°C for 12 h.

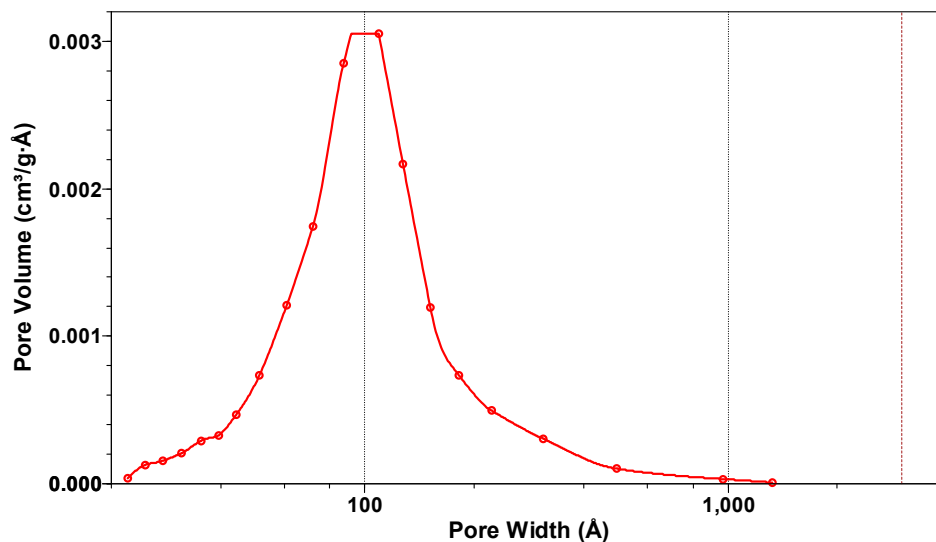


Fig. 3. 96 – Pore distribution of the catalyst ex-HT  $\text{Rh}_{0.15}\text{Ni}_8\text{Mg}_{60}\text{Al}_{31.85}$ , calcined at  $900^\circ\text{C}$  for 12 h.

The fresh sample was subjected to TPR analysis to evaluate the right temperature for the in situ activation to carry out before catalytic tests (Fig. 3. 97). It was observed that the active nickel is reduced in two steps, at  $370^\circ\text{C}$  and  $770^\circ\text{C}$ , the first step correspond to nickel oxide present as solid solution with magnesium in  $(\text{Mg}/\text{Ni})\text{O}$  type phase, while the second step can be related to Ni inserted in the spinel and/or forsterite structures, more difficult to be extracted. Most likely the Rh content is so low (0.26 wt %) that cannot be detected by this method, anyway it compromises the reduction of nickel by decreasing the temperature at which Ni is reduced.

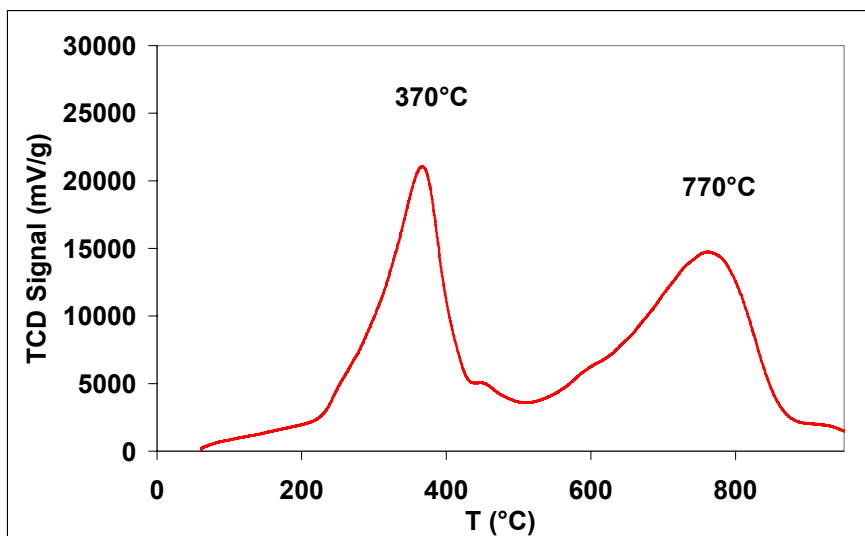


Fig. 3. 97 – Temperature programmed analysis carried out on the catalyst ex-HT Rh<sub>0.15</sub>Ni<sub>8</sub>Mg<sub>60</sub>Al<sub>31.85</sub>, calcined at 900°C for 12 h.

This sample contains 7.95 wt % of Ni and 0.26 wt % of Rh (calculated on the base of the formulation). By H<sub>2</sub> chemisorption analysis, the metal dispersion was calculated (4.75 %) and it is associated with a relative high metallic surface area. Indeed it was calculated that it approximately corresponds to metal particle relatively small (21 nm), good starting point for a steam reforming catalyst.

EX-HT SILICATE Rh <sub>0.15</sub> Ni <sub>8</sub> Mg <sub>60</sub> Al <sub>31.85</sub>		
Ni	wt %	7.95
Rh	wt %	0.26
Metal Dispersion	%	4.75
MSAm	m <sup>2</sup> /g metal	31.3
Apparent crystallite size	nm	21

Tab. 3. 25 –H<sub>2</sub> chemisorption results on catalyst ex-HT Rh<sub>0.15</sub>Ni<sub>8</sub>Mg<sub>60</sub>Al<sub>31.85</sub>, calcined at 900°C for 12 h (MSAm = metallic surface area).

The SMR catalytic tests were performed on the Ex-HT silicates  $\text{Rh}_{0.15}\text{Ni}_8\text{Mg}_{60}\text{Al}_{31.85}$  (Ex-HT sil) using the same reaction conditions of the commercial catalysts.

The SMR tests were performed using 12 ml of catalyst (14-20 mesh). In first tests the oven temperature were set to obtain an outlet T of 870°C. The tests were carried out at the different contact time: 4, 2, 1.1 and 0.83 s.

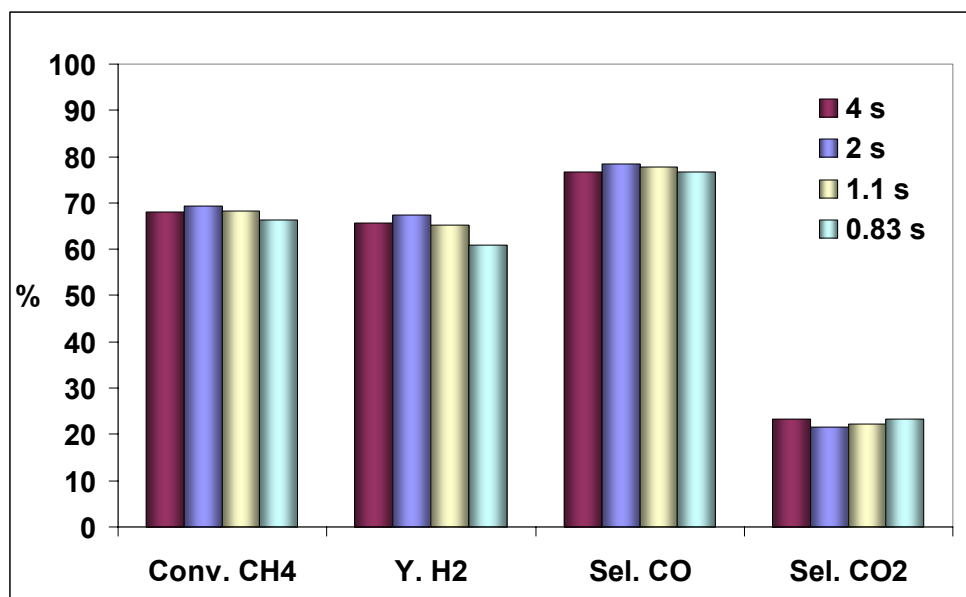


Fig. 3. 98 - Comparison of the performances of the catalyst ex-HT  $\text{Rh}_{0.15}\text{Ni}_8\text{Mg}_{60}\text{Al}_{31.85}$  using different CT ( $T_{\text{out}} = 870^\circ\text{C}$ , 20 bar, S/C = 1.7,  $V_{\text{cat}} = 12$  ml and dp = 14-20 mesh).

In all the reaction conditions, the trend of the results was quite stable. Decreasing the contact time from 4 s to 0.83, the methane conversion does not change significantly (Fig. 3. 98), while the axial thermal profile are quite different (Fig. 3. 99). The temperature of the zone filled with inert material (0-18 cm) can be related to the oven temperature and to the gas flow rate. In fact, in the zone 0-7 cm, the higher oven temperature set increases the inlet temperature of the reactor, while from 7 to 18 cm the higher flow rate of the tests at lower contact time causes a slightly lower temperature. However, the inlet temperatures are around 820-835°C, in a range of 15°C. In the first zone of the catalytic bed, the decrease of the contact time causes a higher  $\Delta T$ , with a shift of the minimum toward the center of the bed. The axial thermal profiles of the second part of the bed show lower T for lower CT, even if the oven temperatures are higher.

The differences in the methane conversions are probably due to a combined effect of the radial and axial profiles and to the decrease of the contact time.

Decreasing the contact time, the axial mean temperature decrease, but the higher oven temperature, necessary to maintain the same outlet temperature, may causes a higher radial  $\Delta T$ . For this reason the methane conversion are not different decreasing the contact time from 4 to 0.83 s.

Comparing the activity of this catalyst with that of the commercial catalyst CAT A (13 % Ni/MgAl<sub>2</sub>O<sub>4</sub>) it can be observed that the sample obtained from hydrotalcite type precursor shows similar or slightly better performances than the commercial sample.

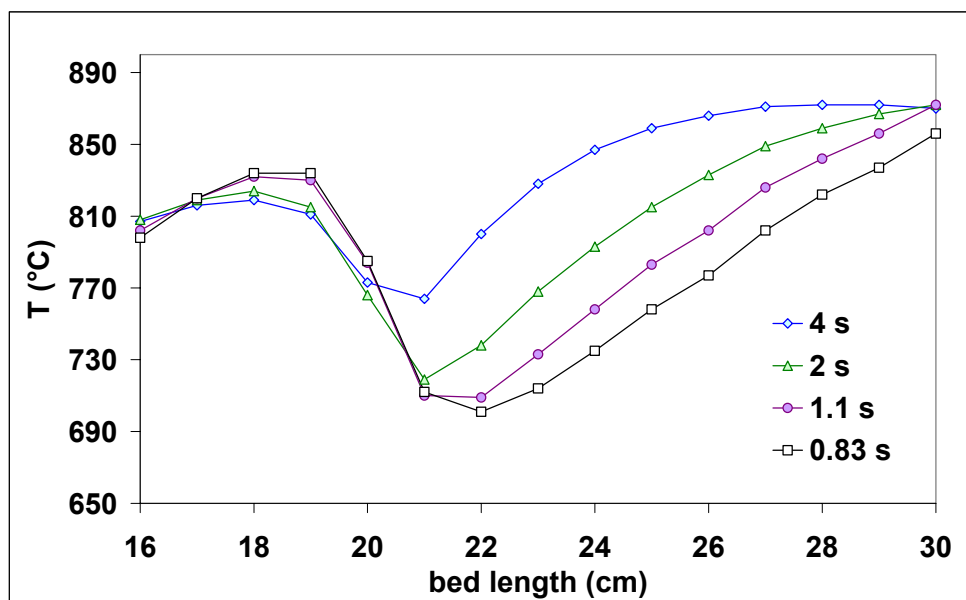


Fig. 3. 99 – Comparison of the axial thermal profiles of the catalyst ex-HT Rh<sub>0.15</sub>Ni<sub>8</sub>Mg<sub>60</sub>Al<sub>31.85</sub> using different CT ( $T_{out} = 870^{\circ}\text{C}$ , 20 bar, S/C = 1.7,  $V_{cat} = 12$  ml and  $d_p = 14\text{-}20$  mesh).

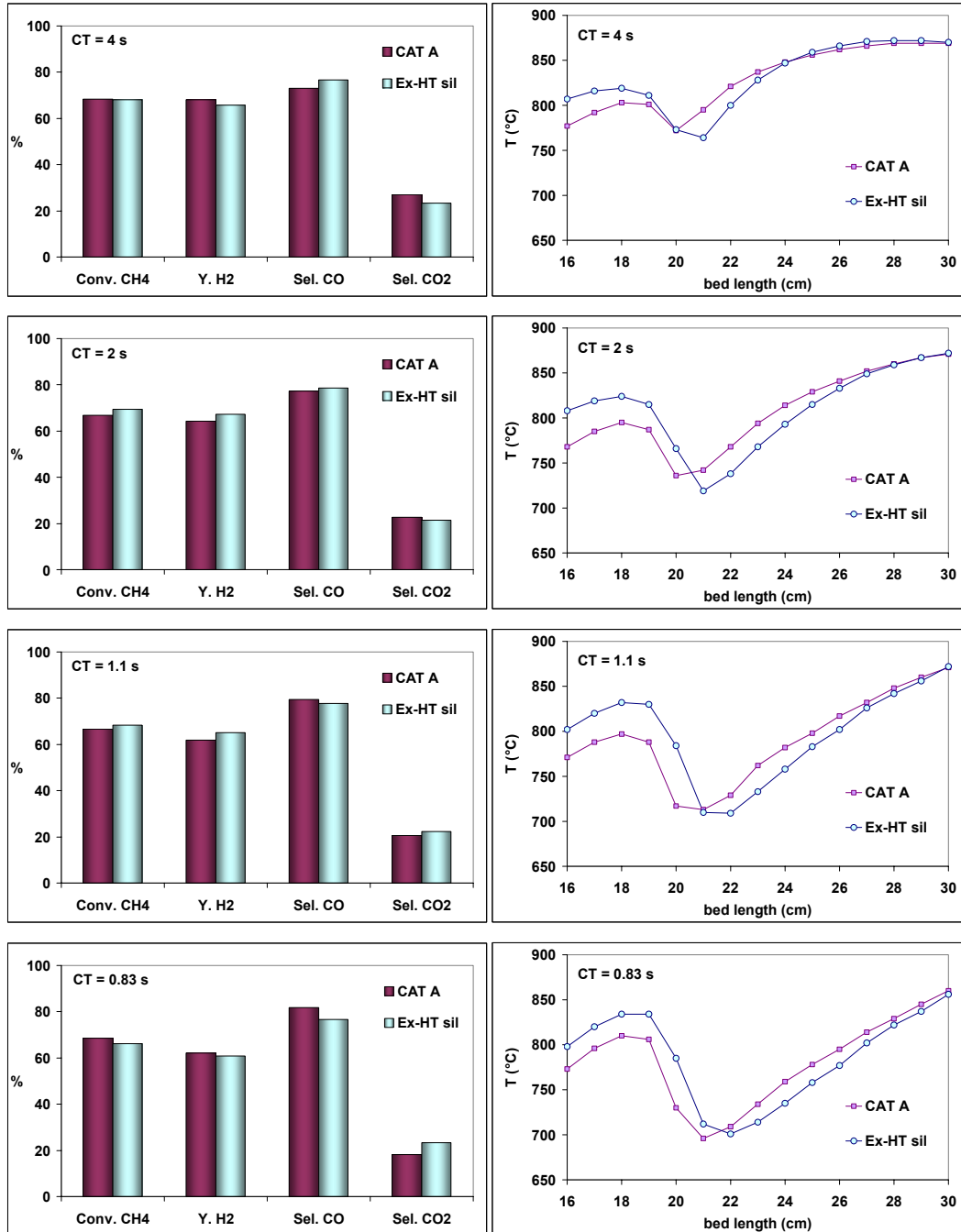


Fig. 3. 100 –Comparison between the activity and the axial thermal profiles of the catalyst ex-HT  $\text{Rh}_{0.15}\text{Ni}_8\text{Mg}_{60}\text{Al}_{31.85}$  and the CAT A (13 % Ni/MgAl<sub>2</sub>O<sub>4</sub>) using different CT ( $T_{\text{out}} = 870^\circ\text{C}$ , 20 bar, S/C = 1.7,  $V_{\text{cat}} = 12$  ml and  $d_p = 14$ -20 mesh).

The ex-HT Rh<sub>0.15</sub>Ni<sub>8</sub>Mg<sub>60</sub>Al<sub>31.85</sub> containing silicates catalyst was investigated also in terms of stability versus partial pressure of steam.

The tests of stability vs H<sub>2</sub>O were performed both in larger excess of water (S/C = 2.5, 3 and 4 mol/mol) and in slight excess of H<sub>2</sub>O (S/C = 1.4 and 1.1 mol/mol).

The tests with higher S/C were carried out to check the stability of the sample (with silicates) in a steam atmosphere (hydrothermal conditions). In fact, it is known that materials containing silica (SiO<sub>2</sub>) form unstable species in presence of water. Therefore, even if it is known that forsterite support has a much higher stability than silica, due to the isolation of the SiO<sub>4</sub><sup>-</sup> species surrounded by Mg<sup>2+</sup>, it is important to study the hydrothermal stability in the SR environmental, also because, it is known that water can modify the structure of catalysts obtained from hydrotalcite containing carbonates (memory effect, reconstruction of the original hydrotalcite structure, rearrangement of the mixed oxide structure).

The tests at lower S/C were carried out in order to check the stability of the catalyst and to determine the S/C limit for the soot formation.

The tests at high steam S/C were carried out on the Ex-HT sil catalysts in the following reaction conditions:

- P = 20 bar
- Tout = 870°C
- Vcat = 6 ml
- Dp = 14-20 mesh
- S/C = 2.5, 3 and 4 mol/mol
- CT = 4, 2 and 1.1 s.

Increasing the S/C ratio the methane conversion increases as the CO<sub>2</sub> selectivity, as expected by the increase of the water that favors both steam reforming and water gas shift reaction (Fig. 3. 101).

The small changes in the axial thermal profile (that regard in particular the ΔT) is produced by the increasing of the amount of converted methane that produces a higher endothermic effect (Fig. 3. 102).

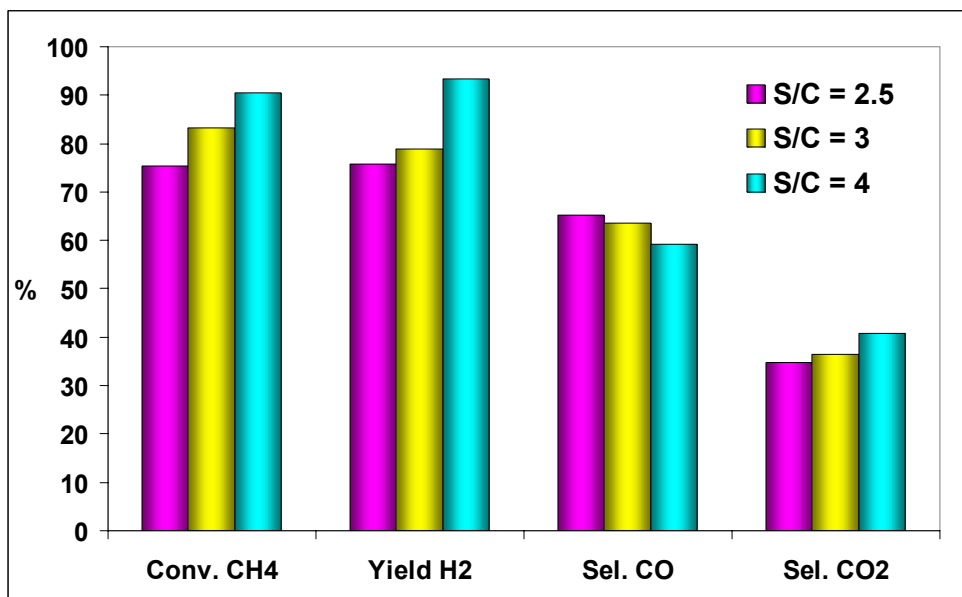


Fig. 3. 101 – Comparison among the activities of ex-HT  $\text{Rh}_{0.15}\text{Ni}_8\text{Mg}_{60}\text{Al}_{31.85}$  tested at different S/C (P = 20 bar, T<sub>out</sub> = 870°C, CT = 4 s, V<sub>cat</sub> = 6ml, D<sub>p</sub> = 14-20 mesh).

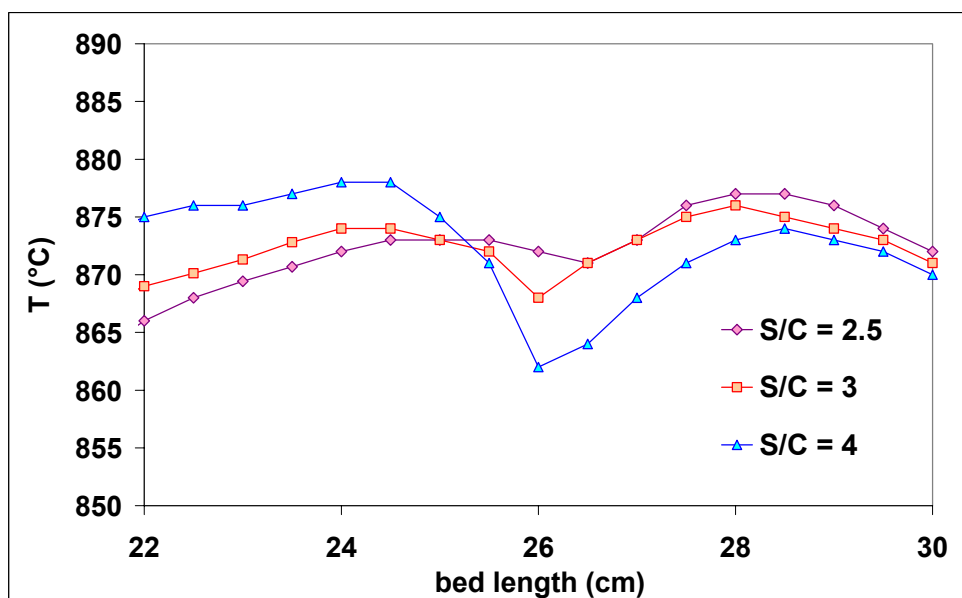


Fig. 3. 102 - Comparison among the axial thermal profiles of ex-HT  $\text{Rh}_{0.15}\text{Ni}_8\text{Mg}_{60}\text{Al}_{31.85}$  tested at different S/C (P = 20 bar, T<sub>out</sub> = 870°C, CT = 4 s, V<sub>cat</sub> = 6ml, D<sub>p</sub> = 14-20 mesh).

The ex-HT Rh<sub>0.15</sub>Ni<sub>8</sub>Mg<sub>60</sub>Al<sub>31.85</sub> was tested for three days in drastic reaction condition (S/C = 4 and CT = 4 s) to enhance the catalyst-water contact during reaction. The results of activity as a function of time-on-stream are reported in Fig. 3. 103 and show very constant trend related to a high stability. The methane conversion is high and very constant. The inlet (877-878°C), the outlet (870°C) and the minimum temperatures (856-858°C, the minimum was observed between 26 and 26.5 cm) do not change during the time-on-stream test (Fig. 3. 104). This confirms the high stability of this catalyst at higher water content.

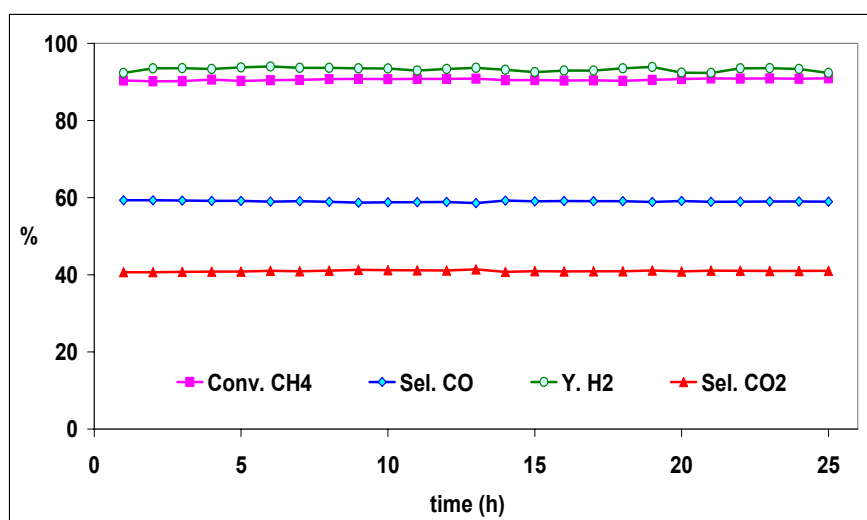


Fig. 3. 103 - Time-on-stream of ex-HT Rh<sub>0.15</sub>Ni<sub>8</sub>Mg<sub>60</sub>Al<sub>31.85</sub> (tested for 3 days) at S/C = 4 (P = 20 bar, T<sub>out</sub> = 870°C, CT = 4 s, V<sub>cat</sub> = 6ml, D<sub>p</sub> = 14-20 mesh).

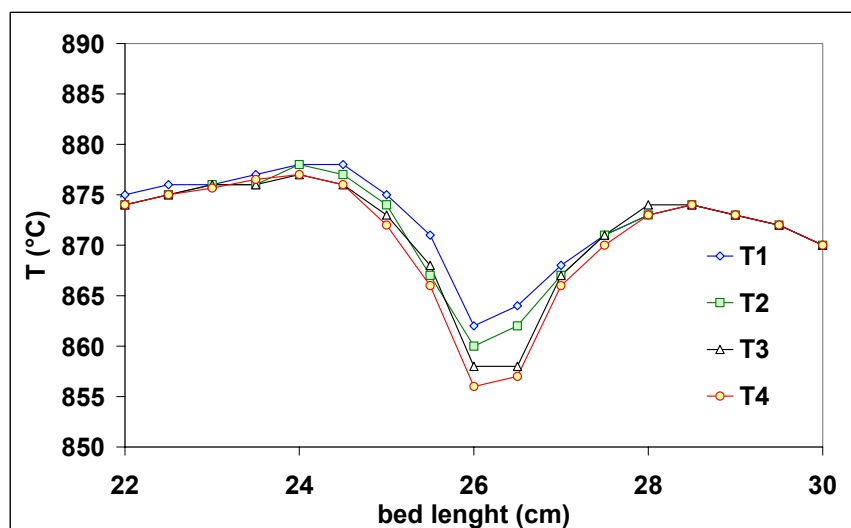


Fig. 3. 104 - Axial thermal profiles during time-on-stream of ex-HT Rh<sub>0.15</sub>Ni<sub>8</sub>Mg<sub>60</sub>Al<sub>31.85</sub> (tested for 3 days) at S/C = 4 (P = 20 bar, T<sub>out</sub> = 870°C, CT = 4 s, V<sub>cat</sub> = 6ml, D<sub>p</sub> = 14-20 mesh).

The tests at low S/C ratio were carried out in order to check the stability of the ex-HT  $\text{Rh}_{0.15}\text{Ni}_8\text{Mg}_{60}\text{Al}_{31.85}$  catalyst in conditions in which the soot formation is favored. For this purpose, tests at S/C 1.4 and 1.1 were carried out ( $P = 20$  bar,  $T_{\text{out}} = 870^\circ\text{C}$ ,  $V_{\text{cat}} = 12$  ml or 6 ml,  $D_p = 14\text{-}20$  mesh,  $CT = 4, 2$  or  $1.1$  s).

Decreasing the S/C ratio to 1.4 mol/mol, a lower activity of the sample is observed than that of the tests at higher S/C (Tab. 3. 26). However, the effect of the decreased contact time is the same of that found for higher S/C ratio.

The C balance does not show any carbon loss attributable to carbon formation in the catalytic bed, notwithstanding the reaction conditions favor the carbon formation.

	<b>P = 20 bar CT = 4 s S/C = 1.4 <math>T_{\text{oven}} = 916^\circ\text{C}</math></b>	<b>P = 20 bar CT = 2 s S/C = 1.4 <math>T_{\text{oven}} = 936^\circ\text{C}</math></b>	<b>P = 20 bar CT = 1.1 s S/C = 1.4 <math>T_{\text{oven}} = 990^\circ\text{C}</math></b>
<b>CH<sub>4</sub> (%)</b>	13.3	12.3	11.5
<b>H<sub>2</sub> (%)</b>	65.9	66.3	65.9
<b>CO (%)</b>	16.2	17.4	18.8
<b>CO<sub>2</sub> (%)</b>	4.6	4.1	3.8
<b>H<sub>2</sub>/CO</b>	4.07	3.81	3.51
<b>CO/CO<sub>2</sub></b>	3.52	4.24	4.95
<b>Conv. CH<sub>4</sub> (%)</b>	61.0	63.6	66.3
<b>Yield H<sub>2</sub> (%)</b>	60.0	61.5	61.0
<b>Sel. CO (%)</b>	77.9	80.9	83.2
<b>Sel. CO<sub>2</sub> (%)</b>	22.1	19.1	16.8
<b>T<sub>out</sub> (°C)</b>	871	870	870
<b>T<sub>in</sub> (°C)</b>	808	806	818
<b>T<sub>min</sub> (°C)</b>	758	710	699
<b>DT = T<sub>out</sub> - T<sub>min</sub> (°C)</b>	113	160	171
<b>DT = T<sub>in</sub> - T<sub>min</sub> (°C)</b>	50	96	119
<b>Dry Syngas flow rate (NI/h)</b>	68	138	241
<b>% C balance (in/out)</b>	98.8	98.2	100.5
<b>% H balance (in/out)</b>	102.1	102.7	106.3
<b>% O balance (in/out)</b>	104.8	104.2	101.8

Tab. 3. 26 - Catalytic results of the catalyst ex-HT  $\text{Rh}_{0.15}\text{Ni}_8\text{Mg}_{60}\text{Al}_{31.85}$  at S/C = 1.4 and different CT ( $V_{\text{cat}} = 12$  ml, 14-20 mesh).

Very high stability was observed during each test for 8 h and no soot formation is detected in the condensed water. Nevertheless, a time-on-stream test was carried out for three days using a CT = 1.1 s. The activity was very stable during the three days of time-on-stream, maintaining the same values of methane conversion and syngas selectivity for all the duration of the tests (Fig. 3. 105). No significant differences were observed in the different axial thermal profiles measured at the beginning and at the end of the tests. Only a slightly decrease of the temperature in the second part of the bed (after the minimum of temperature) was observed.

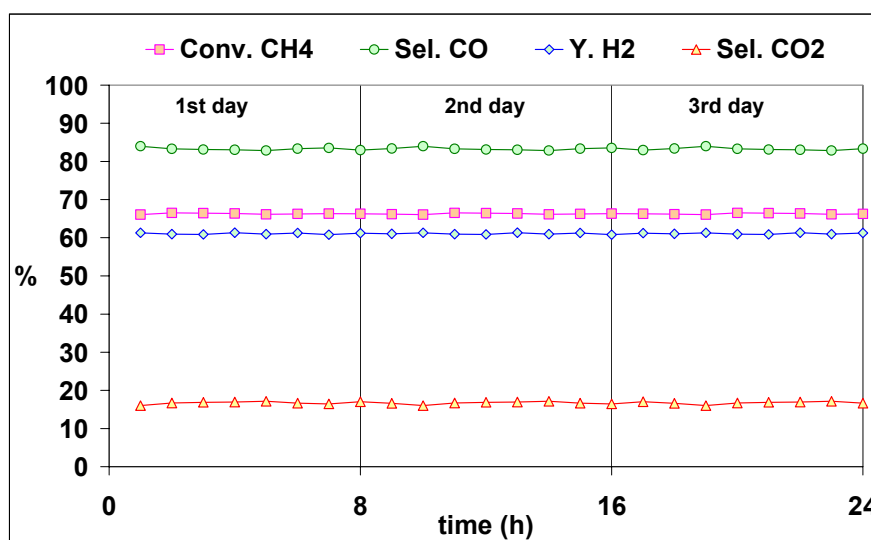


Fig. 3. 105 - Activity of ex-HT Rh<sub>0.15</sub>Ni<sub>8</sub>Mg<sub>60</sub>Al<sub>31.85</sub> with time-on-stream (S/C = 1.4, P = 20 bar, V<sub>cat</sub> = 12 ml, CT = 1.1 s).

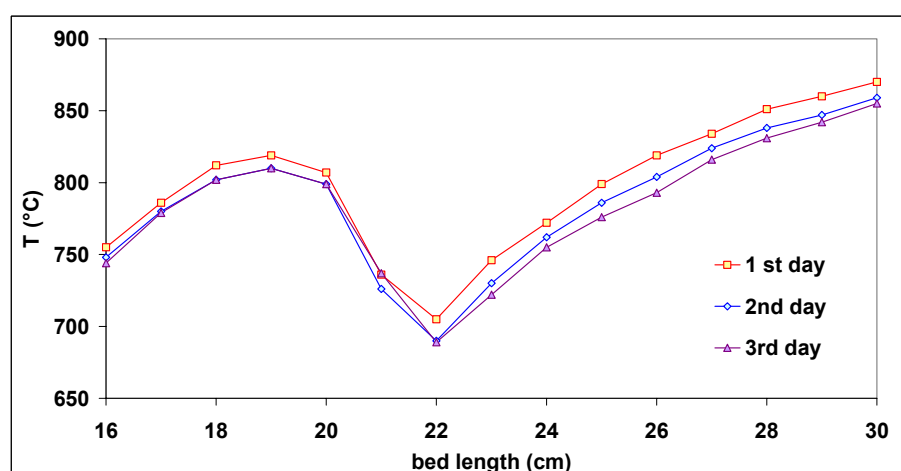


Fig. 3. 106 – Axial thermal profiles of ex-HT Rh<sub>0.15</sub>Ni<sub>8</sub>Mg<sub>60</sub>Al<sub>31.85</sub> with time-on-stream (S/C = 1.4, P = 20 bar, V<sub>cat</sub> = 12 ml, CT = 1.1 s).

Finally a 40 h (5 days) time-on-stream test was carried out on a new load of sample (ex-HT  $\text{Rh}_{0.15}\text{Ni}_8\text{Mg}_{60}\text{Al}_{31.85}$ ) in further drastic condition ( $\text{S/C} = 1.1$  mol/mol, only slightly higher than stoichiometric value). The goal was to stress the catalyst in conditions that favor carbon formation. The reaction conditions were:  $\text{S/C} = 1.1$  mol/mol,  $P = 20$  bar,  $T_{\text{out}} = 870^\circ\text{C}$ ,  $V_{\text{cat}} = 6$  ml,  $d_p = 14\text{-}20$  mesh, and  $\text{CT} = 4$  s.

The low S/C ratio and the high contact time was chosen to enhance the contact of such higher methane concentration on the catalyst, i.e. to maximize the C concentration adsorbed on the Ni particles. The activity of the ex-HT  $\text{Rh}_{0.15}\text{Ni}_8\text{Mg}_{60}\text{Al}_{31.85}$  catalyst as a function of time-on-stream is shown in the Fig. 3. 107.

The methane conversion decreases during the first and the second day from 58.7% to 54.5%. After this initial deactivation, the  $\text{CH}_4$  conversion was stable around 55.7 % for the following three days. The axial thermal profile does not change significantly for the whole duration of the test (Fig. 3. 108).

The C balance is around 97-99% and does not suggest the formation of significant amount of carbon on the catalyst.

However, after this reaction condition, unloading the reactor part of the catalyst was found as powder, indicating pellets crush due to structural modification (carbon formation or silicon carbide formation).

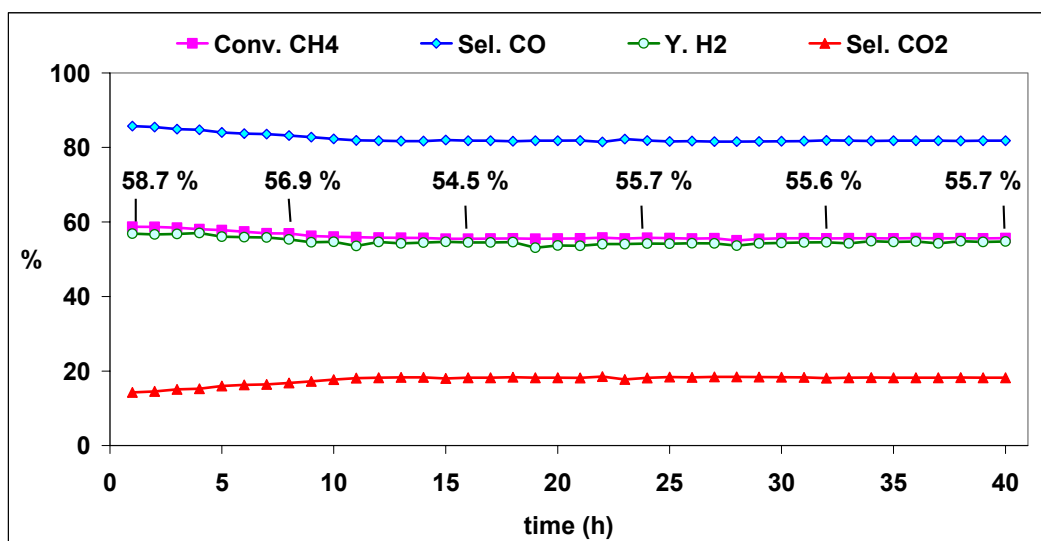


Fig. 3. 107 - Activity of ex-HT  $\text{Rh}_{0.15}\text{Ni}_8\text{Mg}_{60}\text{Al}_{31.85}$  with time on stream ( $\text{S/C} = 1.1$ ,  $P = 20$  bar,  $V_{\text{cat}} = 6$  ml,  $\text{CT} = 4$  s).

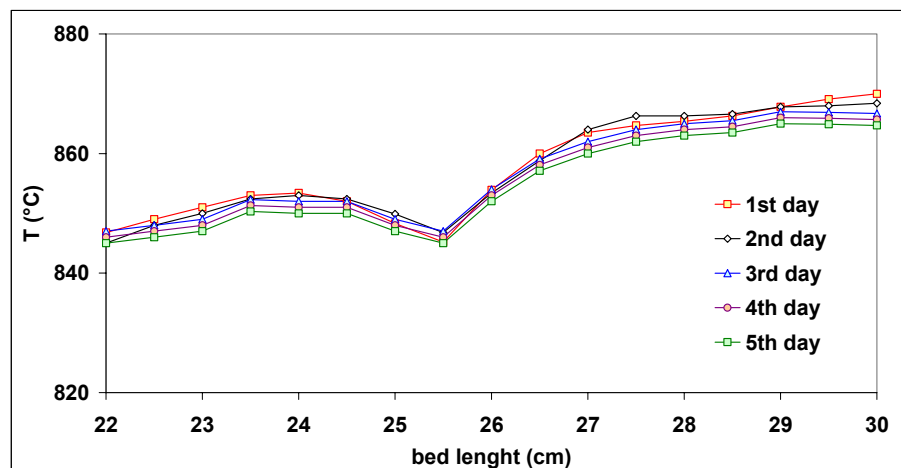


Fig. 3. 108 – Axial thermal profiles of ex-HT Rh<sub>0.15</sub>Ni<sub>8</sub>Mg<sub>60</sub>Al<sub>31.85</sub> with time on stream (S/C = 1.1, P = 20 bar, V<sub>cat</sub> = 6 ml, CT = 4 s).

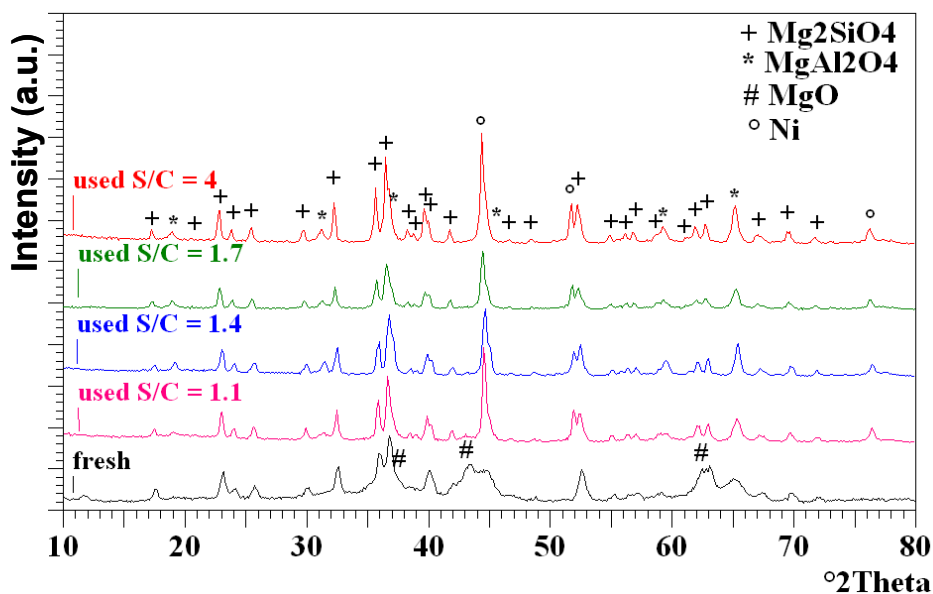


Fig. 3. 109 – Comparison of the XRD patterns of the fresh and used ex-HT Rh<sub>0.15</sub>Ni<sub>8</sub>Mg<sub>60</sub>Al<sub>31.85</sub> tested at different S/C ratio.

The XRD patterns of the ex-HT Rh<sub>0.15</sub>Ni<sub>8</sub>Mg<sub>60</sub>Al<sub>31.85</sub> tested at different S/C ratio are reported in the Fig. 3. 109. With respect to the fresh sample the SMR used catalyst shows the disappearance of the MgO phase and the formation of a well defined spinel phase (MgAl<sub>2</sub>O<sub>4</sub>) that was present only as defective phase in the fresh sample (the reflection at 45 and 65°2θ are present, while the other are not present). In addition, metallic Ni phase is present in the used samples. This structural change does not occur after the catalytic partial oxidation of methane.

Furthermore, the forsterite type phase ( $\text{Mg}_2\text{SiO}_4$ ) remains about constant before and after the SMR catalytic tests.

The Ni crystal size was calculated from XRD patterns, only for the reflection  $d_{220}$  ( $76.37^\circ 2\theta$ ), because the reflection at  $44^\circ 2\theta$  is completely overlapped to a reflection of the spinel phase and that at  $52^\circ 2\theta$  is partially overlapped to one of the  $\text{Mg}_2\text{SiO}_4$  phase. No significant differences were observed in the dimension of the free Ni crystal size (Tab. 3. 27).

S/C ratio	Ni crystal size (nm) [ $d_{220}$ ]
1.1	30
1.4	31
1.7	28
4	28

**Tab. 3. 27 - Ni crystal size of the ex-HT  $\text{Rh}_{0.15}\text{Ni}_8\text{Mg}_{60}\text{Al}_{31.85}$  sample used at different CT, calculated by XRD patterns.**

The used samples, after the tests carried out at different S/C ratio, present significant lower surface area than the fresh sample. This is in accordance to the phase modification observed with the XRD analysis. In addition, it was observed that the surface area and the pore volume decrease increasing the S/C ratio, indicating that greater amount of water influences negatively the catalyst structure, even if the activity was enhanced and high stability with time-on-stream was observed (Tab. 3. 28).

The used sample that present the highest surface area and pore volume was that tested with S/C = 1.1 mol/mol. The sample tested at S/C = 1.4 shows the lowest surface area, probably caused by the higher stress to which it was subjected due to longer catalytic tests. However, the smaller porosity is still present in the samples used at S/C 1.4 showing a similar pore distribution of that tested at S/C = 1.7. On the contrary, the samples tested at S/C = 4, even if shows comparable surface area, losses all the porosity below 100 Å (Fig. 3. 110).

EX-HT SILICATE Rh <sub>0.15</sub> Ni <sub>8</sub> Mg <sub>60</sub> Al <sub>31.85</sub>		Fresh	Used S/C = 1.1	Used S/C = 1.4	Used S/C = 1.7	Used S/C = 4
Single Point Surface Area	m <sup>2</sup> g <sup>-1</sup>	91.50	26.99	8.60	16.53	11.33
BET Surface Area	m <sup>2</sup> g <sup>-1</sup>	93.54	27.60	8.72	16.93	11.56
t-plot micropore area	m <sup>2</sup> g <sup>-1</sup>	12.11	4.00	2.05	2.52	2.41
t-plot micropore volume	cm <sup>3</sup> g <sup>-1</sup>	0.005109	0.001694	0.000912	0.001049	0.001037
BJH desorption cumulative volume of pores	cm <sup>3</sup> g <sup>-1</sup>	0.413405	0.363862	0.132106	0.235775	0.203764
BJH desorption maximums pore widths	Å	100	294	24, 35, 438-1100	26, 551- 1058	20, 25, 495-1050
BJH desorption average pore width (4V/A)	Å	131	421	564	538	613

Tab. 3. 28 –Surface area values and pores volume and width of the catalyst ex-HT Rh<sub>0.15</sub>Ni<sub>8</sub>Mg<sub>60</sub>Al<sub>31.85</sub>, used at different S/C ratio.

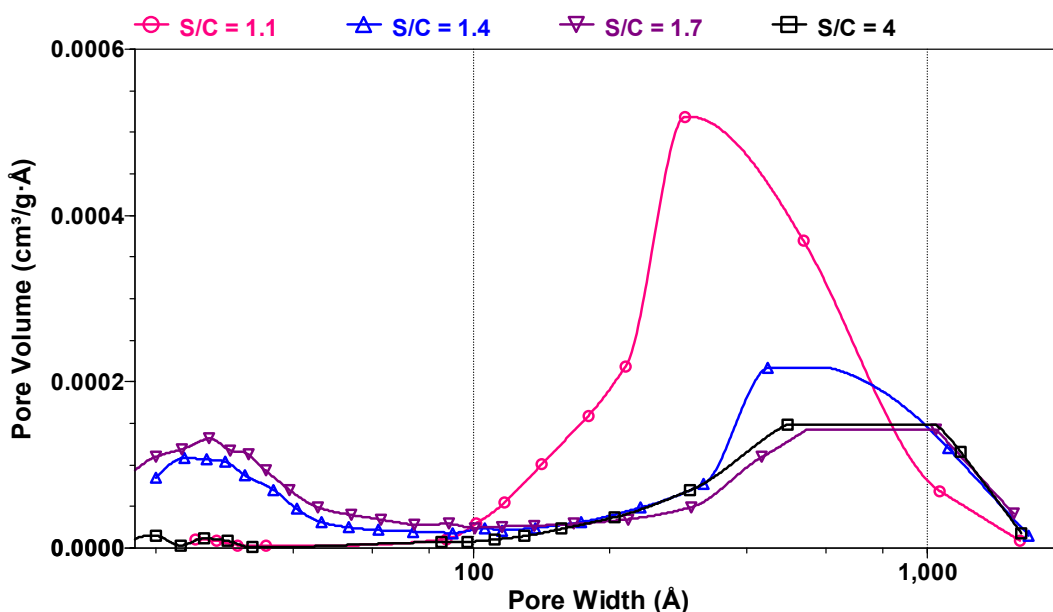


Fig. 3. 110 – Pore distribution of the catalyst ex-HT Rh<sub>0.15</sub>Ni<sub>8</sub>Mg<sub>60</sub>Al<sub>31.85</sub>, used at different S/C ratio.

TPO/quadrupole mass spectroscopy analyses were carried out on the used ex-HT  $\text{Rh}_{0.15}\text{Ni}_8\text{Mg}_{60}\text{Al}_{31.85}$  samples ( $\text{S/C} = 1.1, 1.4$  and  $4$  mol/mol), in order to evaluate the type and the relative amount of carbon species deposited on the surface of the catalysts (Fig. 3. 111).

The samples tested at  $\text{S/C} = 4$  and  $1.4$  show about the same amount of  $\text{CO}_2$  formed at the same temperature ( $310\text{-}330^\circ\text{C}$ ,  $420\text{-}415^\circ\text{C}$  and  $600\text{-}610^\circ\text{C}$ ). The similarity of the two results indicates that the carbon formed on the catalyst tested in the two reaction conditions is the same. This may indicate that some carbon is formed or adsorbed/desorbed anyway on the sample.

For what concern the sample used at very low  $\text{S/C}$  ratio (i.e.  $1.1$ ) the amount of  $\text{CO}_2$  formed during TPO is higher than that formed for the previous samples, indicating that in this reaction condition the formation of carbon was strongly enhanced. In particular atomic carbon ( $\text{C}_\alpha$ ) oxidized at  $340^\circ\text{C}$  produces a  $\text{CO}_2$  peak similar to the previous samples, while it was observed a peak of  $\text{CO}_2$  ten times larger than that observed in other tests that may be due to oxidation of polymeric, amorphous films or filaments ( $\text{C}_\beta$  or  $\text{C}_{\text{C}_V}$ ) of carbonaceous species ( $T = 490^\circ\text{C}$ )<sup>118, 119, 120, 121, 122, 123</sup>.

This catalyst has shown interesting activity and stability and will be compared with the commercial catalyst.

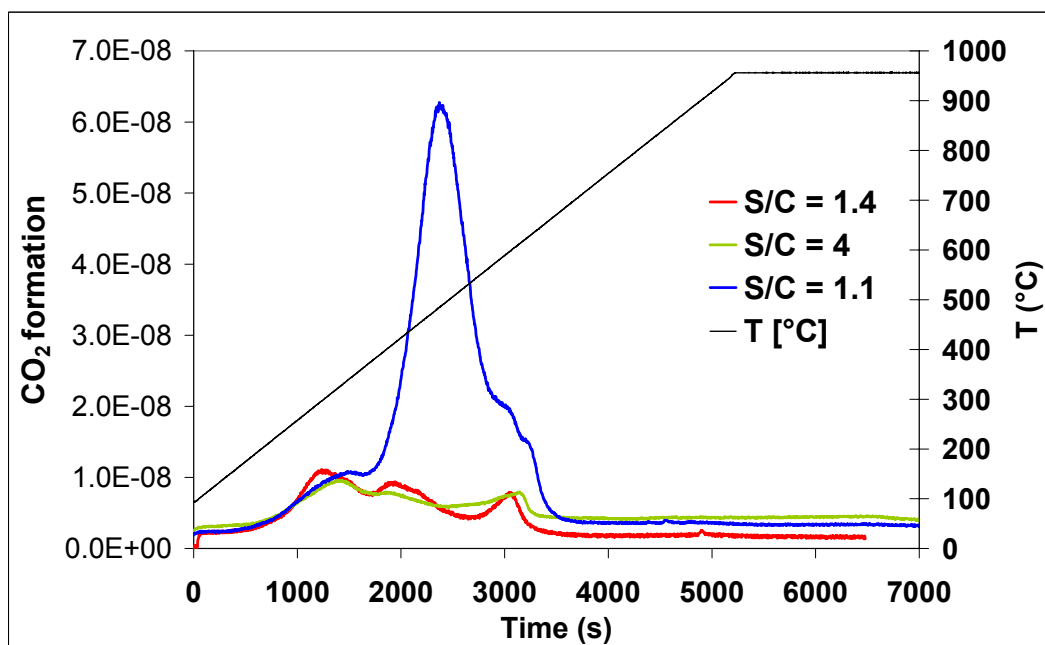


Fig. 3. 111 - Comparison of the  $\text{CO}_2$  formation observed during TPO analysis of the ex-HT  $\text{Rh}_{0.15}\text{Ni}_8\text{Mg}_{60}\text{Al}_{31.85}$  samples tested at different  $\text{S/C}$  ( $1.1, 1.4$  and  $4$ ).

### 3.4. Catalyst obtained from perovskite (PVK)

The perovskite catalyst La<sub>0.8</sub>Ce<sub>0.2</sub>Fe<sub>0.7</sub>Ni<sub>0.25</sub>Rh<sub>0.05</sub>, previously tested in the partial oxidation of methane with good results, was synthesized again and tested also in the steam reforming reaction. The X ray diffraction analysis performed on the new sample, after calcination at 900°C for 12 h, shows the same pattern of the previous one (Fig. 3. 112). The surface area is about 5 m<sup>2</sup>/g and the pore volume is low (Tab. 3. 29).

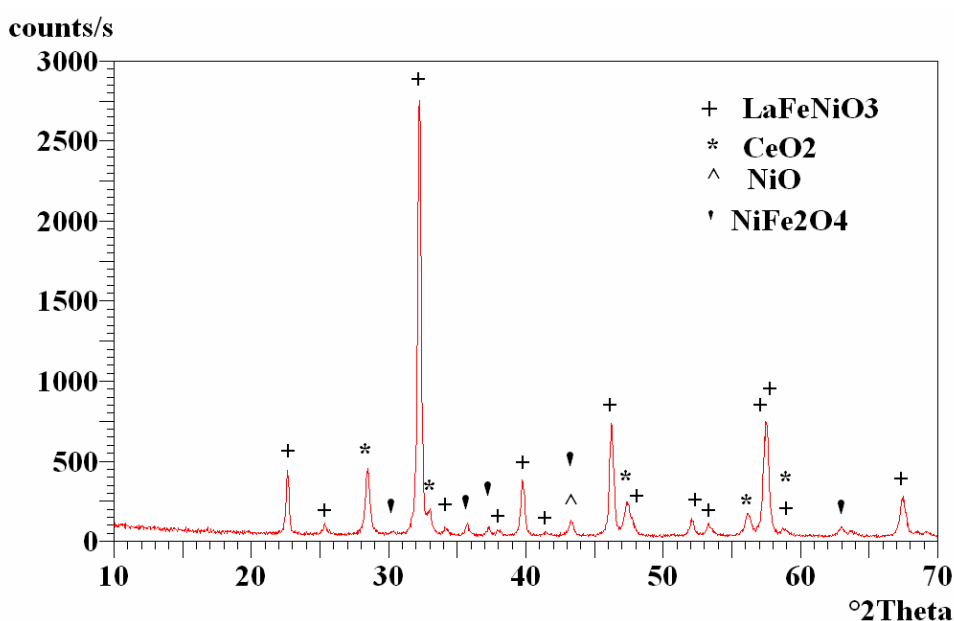


Fig. 3. 112 – XRD patterns of fresh PVK catalyst: La<sub>0.8</sub>Ce<sub>0.2</sub>Fe<sub>0.7</sub>Ni<sub>0.25</sub>Rh<sub>0.05</sub>.

PVK: La <sub>0.8</sub> Ce <sub>0.2</sub> Fe <sub>0.7</sub> Ni <sub>0.25</sub> Rh <sub>0.05</sub> .		
Single Point Surface Area	m <sup>2</sup> g <sup>-1</sup>	4.59
BET Surface Area	m <sup>2</sup> g <sup>-1</sup>	4.67
t-plot micropore area	m <sup>2</sup> g <sup>-1</sup>	0.9298
t-plot micropore volume	cm <sup>3</sup> g <sup>-1</sup>	0.000405
BJH desorption cumulative volume of pores	cm <sup>3</sup> g <sup>-1</sup>	0.083918
BJH desorption maximums pore widths	Å	24, 106, 800
BJH desorption average pore width (4V/A)	Å	736

Tab. 3. 29 –Surface area values and pores volume and width of the fresh PVK catalyst: La<sub>0.8</sub>Ce<sub>0.2</sub>Fe<sub>0.7</sub>Ni<sub>0.25</sub>Rh<sub>0.05</sub>, calcined at 900°C for 12 h.

The distribution of the pore width is mainly in the zone around 24 Å and between 600 and 1000 Å (Fig. 3. 113).

The temperature programmed reduction analysis (TPR, Fig. 3. 114) shows different reduction steps occurring in the catalyst (293, 450, 490 and 575°C). The different reduction temperatures confirm that the nickel is present not only as free NiO (peak at 293°C), but it is also inserted in the perovskite type structure and in NiFe<sub>2</sub>O<sub>4</sub> phase. The nickel inserted in the perovskite and in the spinel type phases is reduced at higher temperature due to the strong interaction with the support bulk structure.

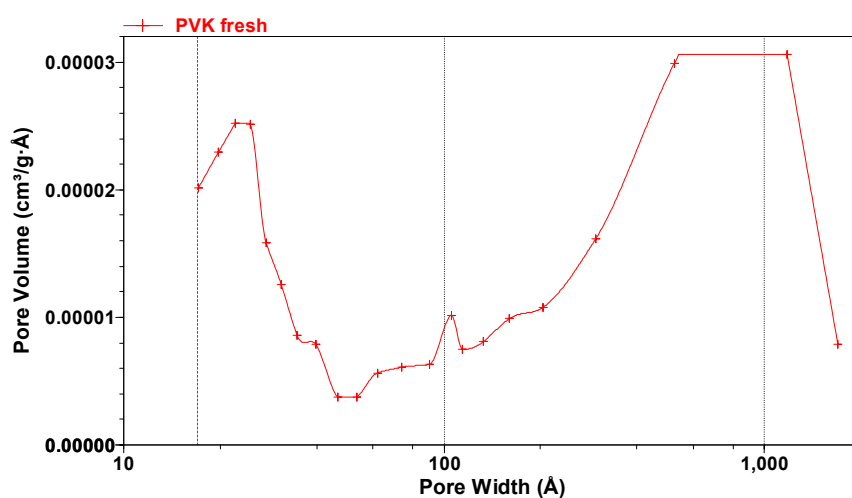


Fig. 3. 113 – Pore distribution of the fresh PVK catalyst: La<sub>0.8</sub>Ce<sub>0.2</sub>Fe<sub>0.7</sub>Ni<sub>0.25</sub>Rh<sub>0.05</sub>, calcined at 900°C for 12 h.

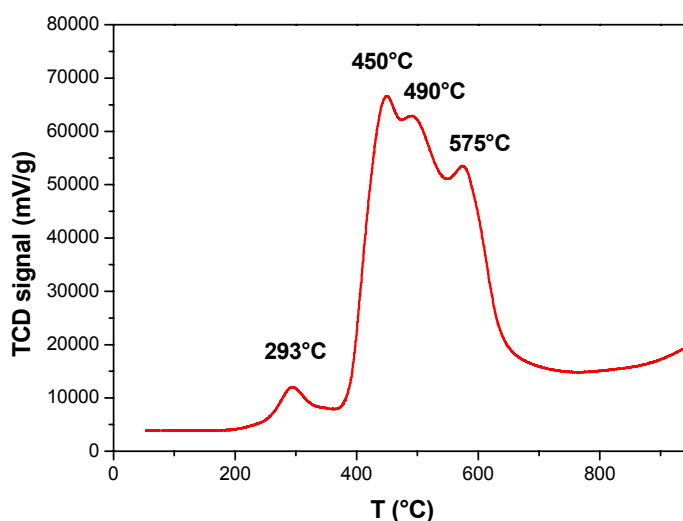
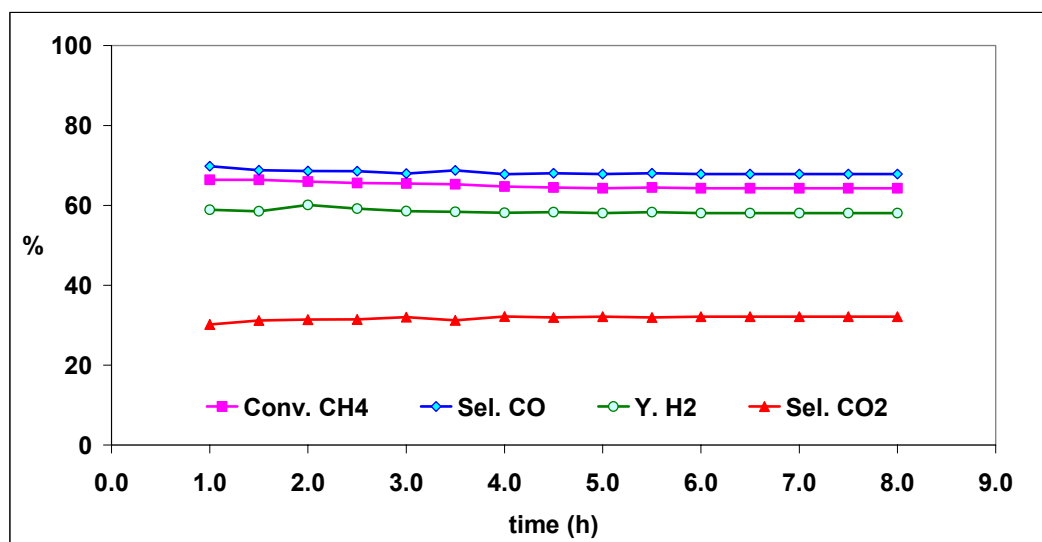


Fig. 3. 114 – TPR of the fresh PVK La<sub>0.8</sub>Ce<sub>0.2</sub>Fe<sub>0.7</sub>Ni<sub>0.25</sub>Rh<sub>0.05</sub> catalyst.

The catalyst has been tested in the steam reforming reaction loading 6 ml of catalyst ( $P = 20$  bar,  $S/C = 1.7$ ,  $T_{out} = 870^{\circ}\text{C}$ ,  $V_{cat} = 6$  ml) and different contact time:  $CT = 4, 2$  and  $1$  s. The sample shows good stability with time-on-stream during the 8 h of reaction carried out for each test, in the Fig. 3. 115 the trend of the test carried out at contact time of 4 s is shown, but also with 2 and 1 s the results were constant.



**Fig. 3. 115 – Activity with time-on-stream of the PVK  $\text{La}_{0.8}\text{Ce}_{0.2}\text{Fe}_{0.7}\text{Ni}_{0.25}\text{Rh}_{0.05}$  catalyst ( $P = 20$  bar,  $S/C = 1.7$ ,  $T_{out} = 870^{\circ}\text{C}$ ,  $V_{cat} = 6$  ml,  $CT = 4$  s)**

Comparing the results of the different tests, carried out changing the contact time (Fig. 3. 116), it can be observed that decreasing from 4s ( $T_{oven} = 920^{\circ}\text{C}$ ) to 2 s ( $T_{oven} = 926^{\circ}\text{C}$ ) the methane conversion and H<sub>2</sub> yield decrease, while the CO selectivity increase. Further decrease of the contact time to 1 s ( $T_{oven} = 964^{\circ}\text{C}$ ) caused higher methane conversion and again higher CO selectivity. This behavior can be explained analyzing both the effect of the axial and radial thermal profiles. In the cases at higher contact time (4 and 2 s), the oven temperature set for maintain the outlet temperature at  $870^{\circ}\text{C}$  are similar ( $920$  and  $926^{\circ}\text{C}$ ). The axial temperature of the catalytic bed, especially after the minimum, decrease with the contact time due to higher feed converted (i.e. higher endothermicity associated with the conversion of higher amount of methane), but the inlet temperatures are similar and very likely also the radial thermal profiles are not significantly different. On the contrary, the test carried out at 1 s required high heat to maintain the same outlet temperature and the radial profile strongly

influences the activity, causing a higher average temperature than that observed in the middle of the bed due to the highest temperature of the skin of the reactor. In addition the inlet temperature results higher.

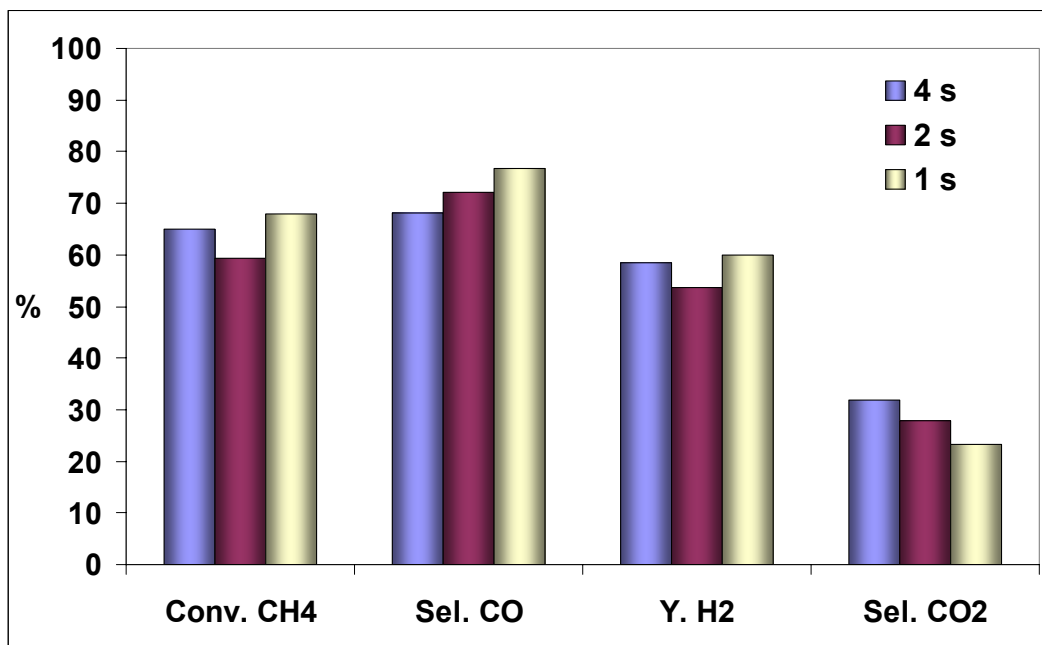


Fig. 3. 116 – Comparison of the results of the PVK  $\text{La}_{0.8}\text{Ce}_{0.2}\text{Fe}_{0.7}\text{Ni}_{0.25}\text{Rh}_{0.05}$  catalyst at different CT (P = 20 bar, S/C = 1.7, T<sub>out</sub> = 870°C, V<sub>cat</sub> = 6 ml, CT = 4, 2 and 1 s)

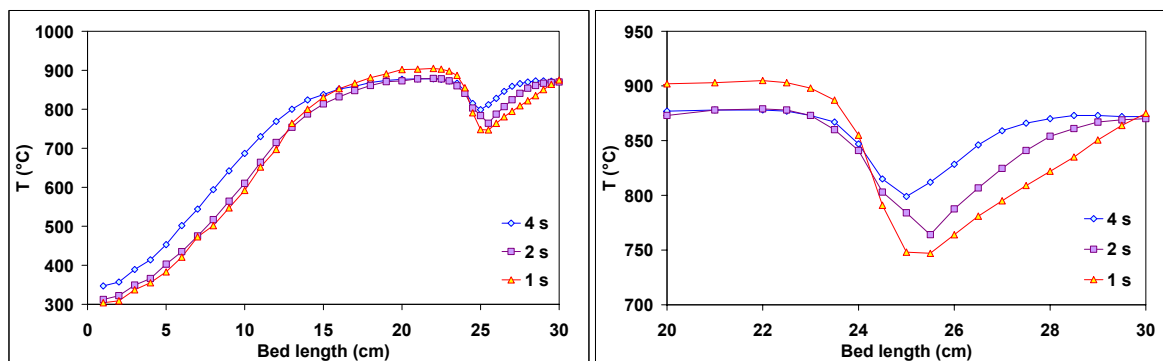


Fig. 3. 117 – Comparison of the axial thermal profiles of the PVK  $\text{La}_{0.8}\text{Ce}_{0.2}\text{Fe}_{0.7}\text{Ni}_{0.25}\text{Rh}_{0.05}$  catalyst at different CT (P = 20 bar, S/C = 1.7, T<sub>out</sub> = 870°C, V<sub>cat</sub> = 6 ml, CT = 4, 2 and 1 s)

The sample used in the steam reforming shows, as the sample tested in the catalytic partial oxidation, the perovskite type phase with a comparable crystallinity of the fresh sample, and moreover a partial reduction of the CeO<sub>2</sub> to Ce<sub>7</sub>O<sub>12</sub>. The nickel is reduced, both NiO and spinel NiFe<sub>2</sub>O<sub>4</sub> phases disappear,

while a Ni-Fe intermetallic phase is formed (instead of metallic nickel), probably due to more drastic reaction condition of the SR than the CPO.

Furthermore, the surface area and the pore volume that were already quite low for the fresh sample, decrease after the reaction (Tab. 3. 30), with particularly loss of the bigger pores between 600 and 1200 Å (Fig. 3. 119).

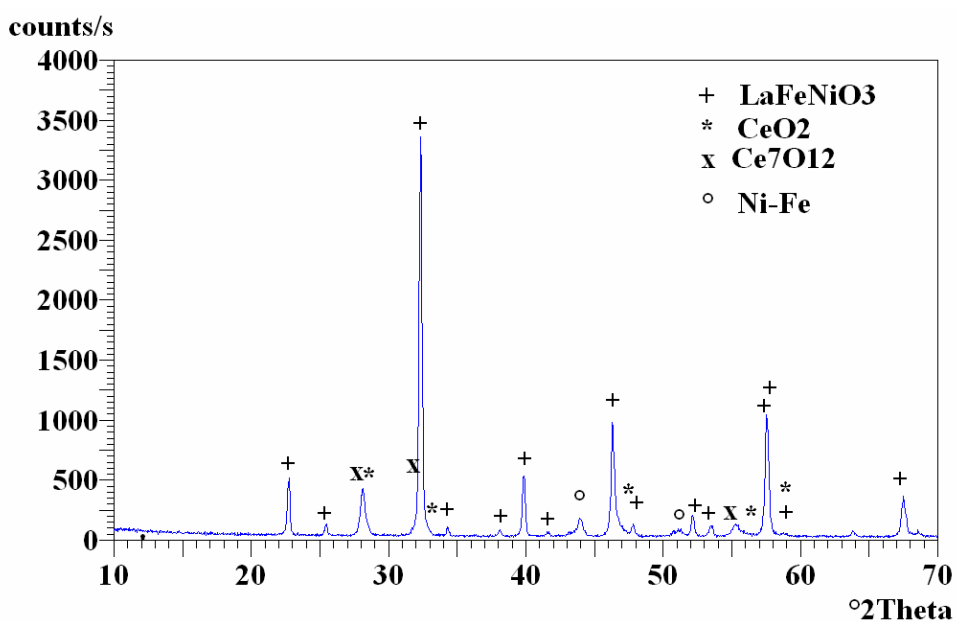


Fig. 3. 118 - XRD patterns of used PVK catalyst:  $\text{La}_{0.8}\text{Ce}_{0.2}\text{Fe}_{0.7}\text{Ni}_{0.25}\text{Rh}_{0.05}$ .

PVK: $\text{La}_{0.8}\text{Ce}_{0.2}\text{Fe}_{0.7}\text{Ni}_{0.25}\text{Rh}_{0.05}$ .			
Single Point Surface Area	$\text{m}^2\text{g}^{-1}$	4.59	2.04
BET Surface Area	$\text{m}^2\text{g}^{-1}$	4.67	2.14
t-plot micropore area	$\text{m}^2\text{g}^{-1}$	0.9298	0
t-plot micropore volume	$\text{cm}^3\text{g}^{-1}$	0.000405	0
BJH desorption cumulative volume of pores	$\text{cm}^3\text{g}^{-1}$	0.083918	0.017145
BJH desorption maximums pore widths	Å	24, 106, 800	32
BJH desorption average pore width (4V/A)	Å	736	342

Tab. 3. 30 –Surface area values and pores volume and width of the used PVK catalyst:  $\text{La}_{0.8}\text{Ce}_{0.2}\text{Fe}_{0.7}\text{Ni}_{0.25}\text{Rh}_{0.05}$ .

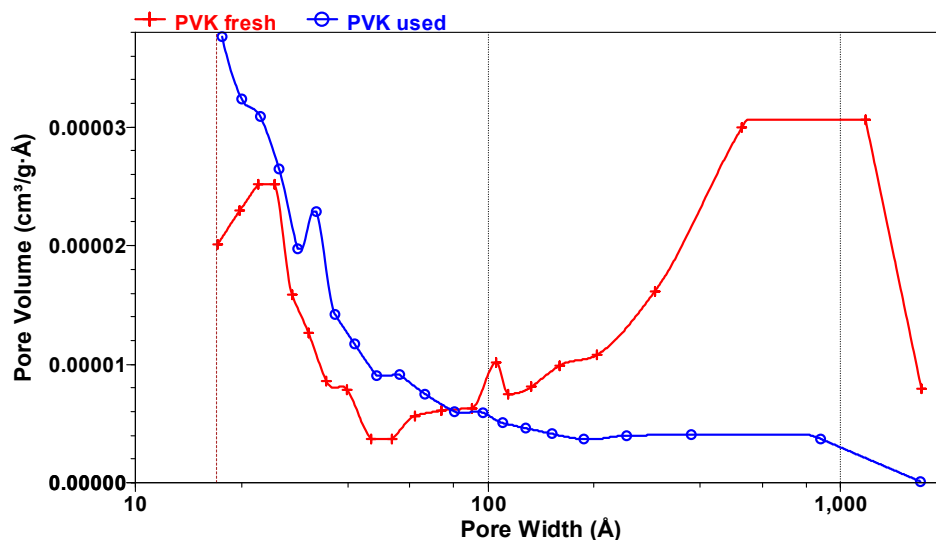


Fig. 3. 119 - Pore distribution of the used PVK catalyst:  $\text{La}_{0.8}\text{Ce}_{0.2}\text{Fe}_{0.7}\text{Ni}_{0.25}\text{Rh}_{0.05}$ .

The used sample was subjected to TPO/mass quadrupole analysis in order to evaluate the amount and the type of carbon deposited on the surface of the catalyst during reaction (Fig. 3. 120). The result shows that some carbon dioxide is formed at 250 and 350°C. The amount is slightly higher than that formed by catalyst obtained from hydrotalcite type precursor (Fig. 3. 111) tested in the same reaction conditions, and it is probably atomic carbon formed by methane dissociation, due to the low temperature of  $\text{CO}_2$  formation.

Also this catalyst presented in the laboratory tests interesting activity and stability and will be compared to the commercial catalyst.

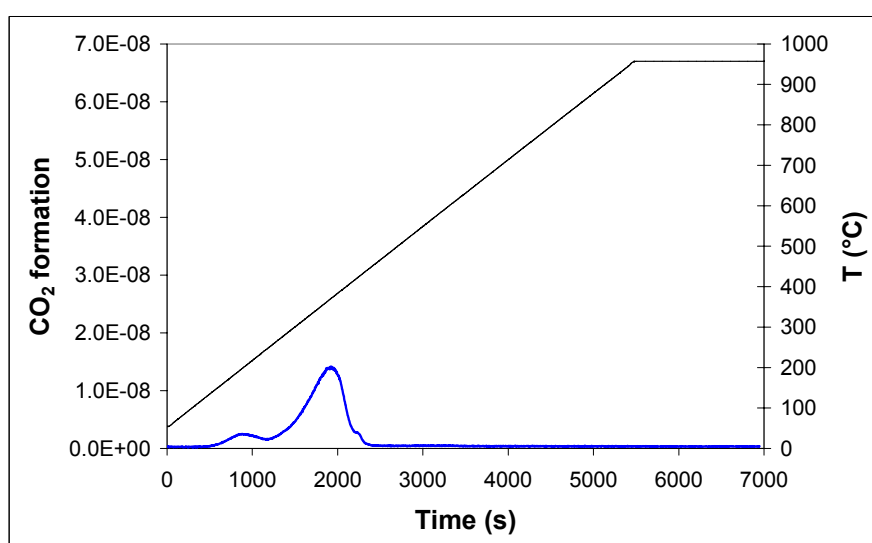


Fig. 3. 120 –  $\text{CO}_2$  formation during TPO analysis.

### 3.5. Comparison among ex-HT sil, PKV and commercial catalysts

The activity of the two catalysts prepared in our laboratory, i.e. the one obtained from hydrotalcite type precursor (ex-HT silicates Rh<sub>0.15</sub>Ni<sub>8</sub>Mg<sub>60</sub>Al<sub>31.85</sub>, 7.95 wt % Ni and 0.26 wt % Rh) and the perovskite type catalyst (La<sub>0.8</sub>Ce<sub>0.2</sub>Fe<sub>0.7</sub>Ni<sub>0.25</sub>Rh<sub>0.05</sub>, 6 wt % Ni and 2 wt % Rh) were compared to the commercial catalyst CAT A (13 wt % Ni/MgAl<sub>2</sub>O<sub>4</sub>).

The reaction conditions of the comparison reported in the Fig. 3. 121 are:

P = 20 bar,

T<sub>out</sub> = 870°C,

S/C = 1.7 mol/mol,

CT = 4, 2 and 1 s,

V<sub>cat</sub> = 6 ml

D<sub>p</sub> = 14-20 mesh.

The ex-HT silicate catalyst presents similar performances with respect to the commercial catalyst at CT = 4 s but better results decreasing the residence time.

The perovskite sample shows lower activity using higher contact time (4 and 2 s), but comparable results are observed decreasing the contact times.

Furthermore, it is interesting to note that in the tests carried out at higher CT, in which the feed flow and the average temperature are lower, the ex-HT sample shows slightly lower water gas shift activity than the commercial sample.

Indeed, the two type of bulk catalysts studied in this work (ex-HT and PVK) in which the active metals (Ni and/or Rh) are stabilized inside oxidic matrix, appear promising as catalysts for the hydrogen production, either in the CPO or SMR processes. It was found that both the non-supported materials have good activity, comparable to that of commercial catalysts, having higher nickel content, and stable results with time-on-stream.

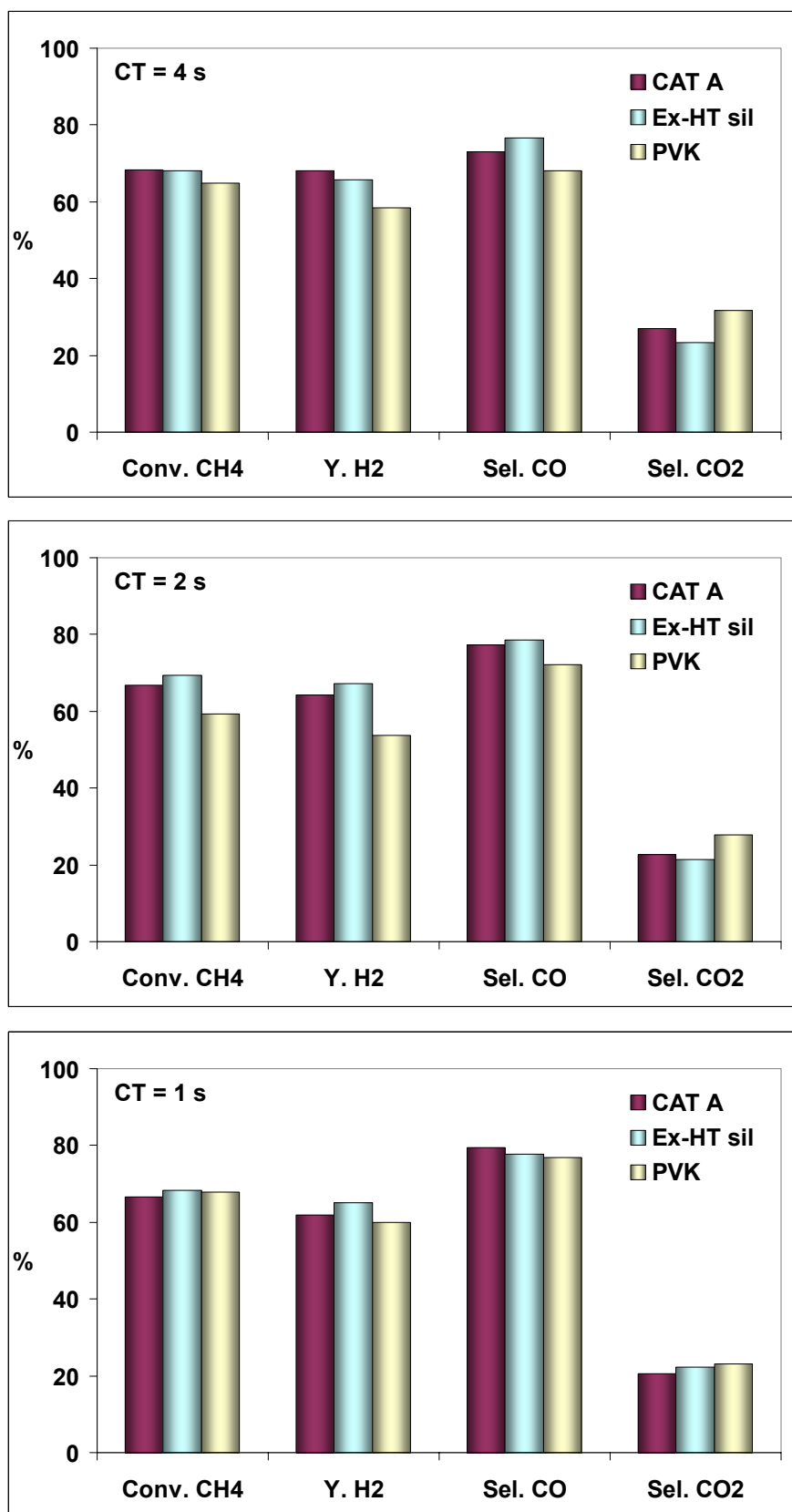


Fig. 3. 121 – Comparison of the activity of Ex-HT sil  $\text{Rh}_{0.15}\text{Ni}_8\text{Mg}_{60}\text{Al}_{31.85}$ , PVK  $\text{La}_{0.8}\text{Ce}_{0.2}\text{Fe}_{0.7}\text{Ni}_{0.25}\text{Rh}_{0.05}$  and commercial CAT A (13 % Ni/ $\text{MgAl}_2\text{O}_4$ ) catalysts.

### **3.6. Structured catalysts: support with high thermal conductivity**

Due to severe reaction conditions of the steam reforming, such as high temperature, pressure and hydrogen content, industrial plants register problems linked to materials: tube resistance to high temperatures, catalyst deactivation and diffusion limitation through the catalyst. In particular, the temperature in the tube may range from 600°C to 950°C because high heat fluxes are necessary, due to the high endothermicity of the reaction. In these conditions, the temperature difference between the external- and inner-tube wall can be higher than 60°C for a thickness of 15 mm: due to this strong stress, the tube may crack during operation. The catalyst deactivation increases this problem, since higher temperatures are required to achieve the same results. Reaction rate is strongly affected by the heat transfer of the ceramic pellets, and the residence time is necessarily high (2-4 s).

To avoid all these problems, a catalyst support having high thermal conductivity could be used. This kind of support can increase the heat transfer radially and along the bed, thus making it possible to operate at lower residence times, while smoothing the thermal profile both inside the reactor tube and at the interface between the tube wall and catalyst.

Silicon carbide (SiC) and metallic foam (FeCrAlY) supported catalysts were prepared and tested in order to study differently shaped supported catalysts (pellets and foams) characterized by high thermal conductivity, such as ceramic carbide, metal gauze and alloy.

#### **3.6.1. Ni/SiC catalysts**

Silicon carbide exhibits a high thermal conductivity and mechanical strength, a low specific weight, and chemical stability: these features make it a promising candidate as a catalyst support in place of the traditional insulator supports (Al<sub>2</sub>O<sub>3</sub>, MgAl<sub>2</sub>O<sub>4</sub>) either in several highly endothermic or exothermic reactions or in aggressive reaction media<sup>124, 125</sup>. Indeed, silicon carbide has been chosen as a support for steam methane reforming (SMR) because its good conductive properties that may improve the temperature profile. In fact it can decrease the high ΔT caused by the high endothermicity of the reaction and, at the same time,

increase the heat transfer from external furnace, reactor wall and catalyst particles.

10 wt % Ni was deposited on the SiC support by incipient wetness impregnation. The sample was calcined at different temperatures (500, 700 and 900°C) in order to study both the chemical-physical properties and the interaction between the support and active phases. The sample calcined at 700°C was tested in a SMR laboratory plant under different operative conditions, in order to evaluate the activity and stability with time-on-stream.

The catalysts (10 wt % Ni/SiC) were prepared by incipient wetness impregnation using  $\text{Ni}(\text{NO}_3)_2$  as nickel precursor and pellets of SiC (0.84 - 1.41 mm) as support by grinding cylinder on 8-14 mesh sieves. The SiC cylinders (type  $\beta$ -SiC) were produced by SICAT France. Three samples were prepared and calcined at 500 and 700°C for 2 h, and at 900°C for 12 h.

The samples of Ni/SiC catalyst calcined at three different temperatures (500, 700 and 900°C) showed only SiC and NiO phases (Fig. 3. 122). It can be observed that the sample calcined at 900°C showed an amorphous band between 20-30°2 $\theta$ , attributable to  $\text{SiO}_2$  formation during the thermal treatment at that high temperature. Furthermore, the XRD and the BET results showed that the calcination temperature does not affect significantly the NiO crystal size (20-30 nm) nor the surface area values of the support (18-22 m<sup>2</sup>/g), which did not show any significant change even after impregnation and thermal treatment.

After reduction at 800°C for 2 h, the sample calcined at 900°C showed the presence of metallic Ni together with a  $\text{Ni}_2\text{Si}$  phase; while the samples calcined at lower temperatures (500 and 700°C) showed the  $\text{Ni}_2\text{Si}$  phase only (Fig. 3. 123). The presence of this phase may be due to the direct reaction between metallic Ni (formed at 500°C) and SiC, a reaction that is thermally activated over 600°C, while  $\text{Ni}_2\text{Si}$  is stable up to 950°C<sup>126, 127, 128</sup>.

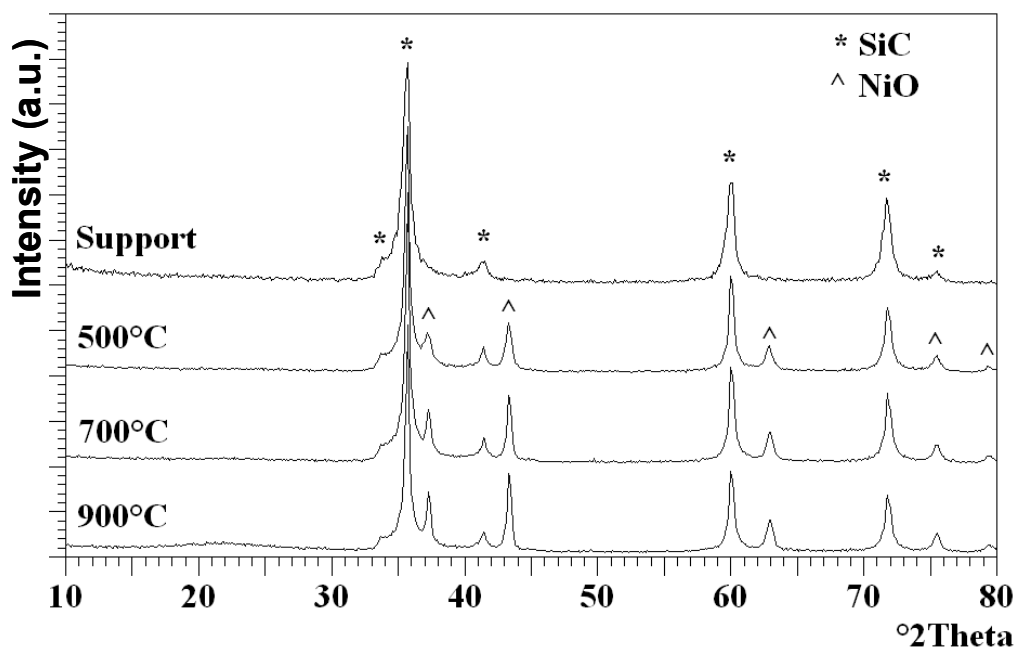


Fig. 3. 122 – XRD patterns of SiC support and of 10 % Ni /SiC calcined at 500°C, 700°C and 900°C.

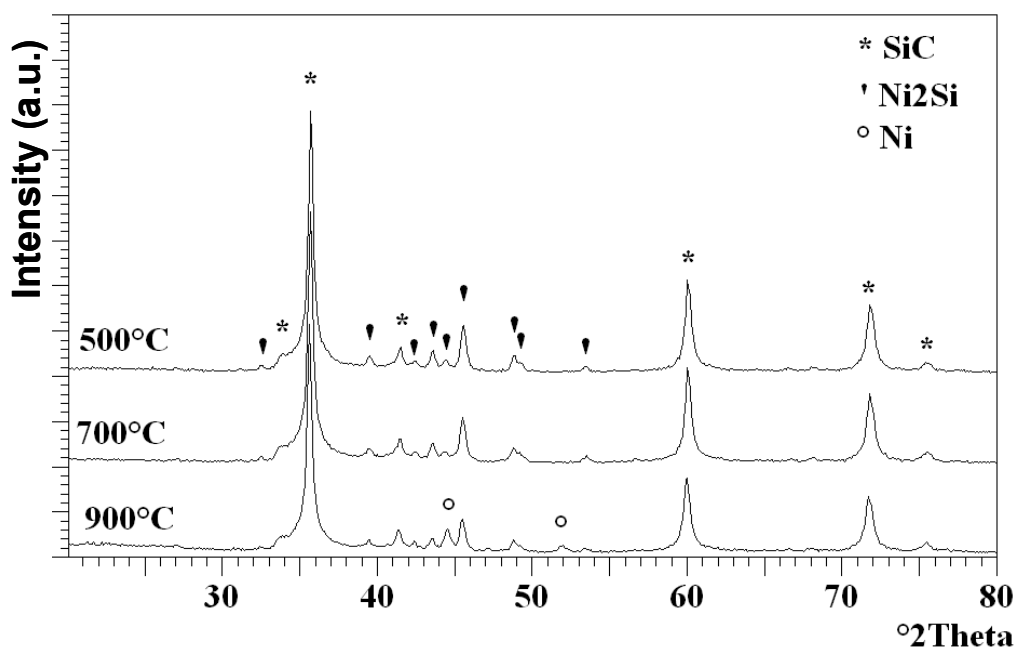


Fig. 3. 123 – XRD patterns of reduced samples (previously calcined at 500°C, 700°C, and 900°C).

Considering that  $\text{Ni}_2\text{Si}$  is predominant in the reduced samples which were previously calcined at 500 and 700°C, it is possible to state that in the sample calcined at 900°C, in which the formation of  $\text{SiO}_2$  was observed, the  $\text{Ni}_2\text{Si}$  formation was inhibited by the  $\text{SiO}_2$  layer, because the latter prevented the contact between SiC and metallic Ni, partly passivating the surface of the support.

TPR analyses (Fig. 3. 124) carried out on the support did not show any reduction peaks. For Ni samples, a main reduction peak at 400 - 450°C with a shoulder at 500 - 550°C was clearly visible. These peaks correspond to the NiO reduction, differently interacting with the support.

The oxidation analysis carried out on the support showed an oxidation shoulder starting at 750°C and related to the superficial oxidation of SiC. The oxidation increased at 850 - 900°C due to bulk SiC oxidation. As for Ni samples, the oxidation of the Ni occurred at 500 - 600°C. Moreover, TPO analyses showed a further oxidation peak centered at 750°C, before the support oxidation. This peak may be attributed to the oxidation of  $\text{Ni}_2\text{Si}$  phase obtained by TPR at 950°C, which partially decomposes  $\text{Ni}_2\text{Si}$  forming  $\text{Ni}^0$ .

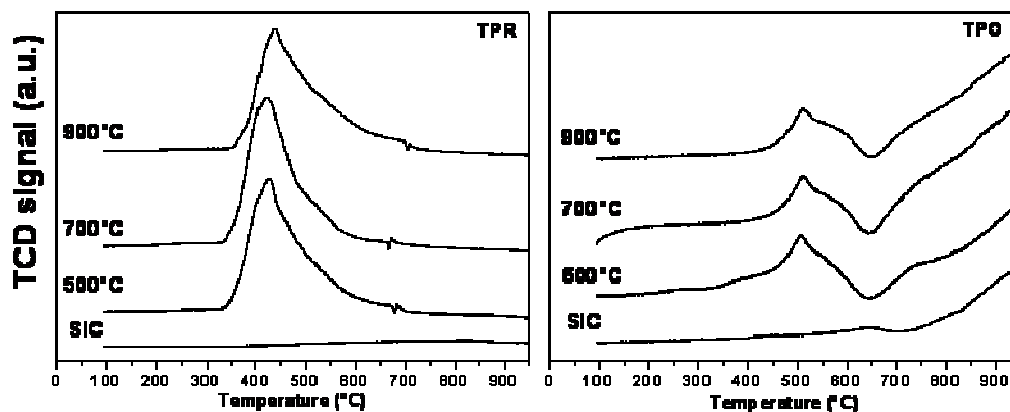


Fig. 3. 124 - Temperature programmed reduction (TPR) and oxidation (TPO) analyses carried out on SiC support and on 10 % Ni /SiC calcined at 500°C, 700°C and 900°C.

Catalytic activity in SMR reaction was carried out for the 10 wt % Ni/SiC sample while maintaining the outlet temperature of the catalytic bed constant at 870°C or 960°C by varying the oven set temperature. The methane conversion and the

syngas selectivity are in agreement with the thermodynamic equilibrium prediction calculated by changing both the S/C ratio and the outlet temperature. In terms of catalyst stability, tests at 870°C show very constant values in the syngas composition during the time-on-stream (Fig. 3. 125). At 960°C the composition of the syngas is still stable but the oxygen balance (in/out) starts to go above 100%, probably due to the formation of SiO<sub>2</sub>. This is also confirmed by the TPO analysis where at 950°C the oxygen uptake becomes significant, therefore showing a limit in the process temperature of the catalyst.

T <sub>out</sub>	870°C	870°C	960°C	960°C
S/C	1.7	2.5	1.7	2.5
P	10 bar	10 bar	10 bar	10 bar
Conv. CH <sub>4</sub>	79.0	79.4	81.7	95.9
Yield H <sub>2</sub>	77.5	78.6	79.9	94.8
Sel. CO	76.3	72.4	85.2	68.8
Sel. CO <sub>2</sub>	23.7	27.6	14.8	31.2

Tab. 3. 31 - Catalytic results of the 10 wt % Ni / SiC calcined at 700°C (CT = 1.1 s).

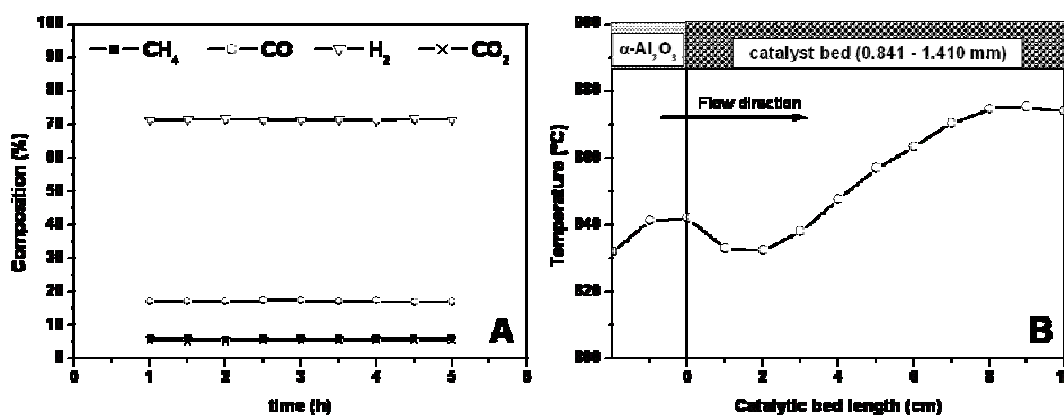


Fig. 3. 125 - Dry syngas composition (A) and axial thermal profile (B) measured during steam reforming reaction on 10 % Ni/SiC calcined at 700°C (P 10 bar; CT 1.1 s; S/C 1.7 mol/mol).

On the other hand, an interesting feature is the  $\Delta T$  between oven temperature and outlet temperature ( $\sim 10^\circ\text{C}$ ), which is an indication of a smoothed axial profile, whereas for commercial catalysts tested in the same conditions a larger difference was observed. This behavior makes it possible to work with a lower oven temperature, thus overcoming some of the problems related with commercial catalysts.

After catalytic tests, the used sample presents a slight decrease in surface area with respect to the fresh catalyst (fresh sample:  $20\text{ m}^2/\text{g}$ , used sample:  $17\text{ m}^2/\text{g}$ ); while the XRD analysis reveals the presence of metallic Ni as the predominant phase instead of  $\text{Ni}_2\text{Si}$  which is present in the reduced sample, probably due to the higher temperature reached by the sample in the reactor at which  $\text{Ni}_2\text{Si}$  is unfavored ( $960^\circ\text{C}$ ) (Fig. 3. 126). In fact, the reduced sample, previously calcined at  $900^\circ\text{C}$ , showed metallic Ni besides the  $\text{Ni}_2\text{Si}$  phase. In the used sample, the presence of the  $\text{SiO}_2$  amorphous phase is much more evident with a broad band between  $15\text{-}30^\circ 2\theta$ . It is probably formed by the reaction with water occurring at very high temperature and during the tests at  $960^\circ\text{C}$ . Indeed, the limit of this type of catalyst has been registered in high temperature tests ( $> 960^\circ\text{C}$ ) due to SiC oxidation to  $\text{SiO}_2$ , with a corresponding decrease in the surface area.

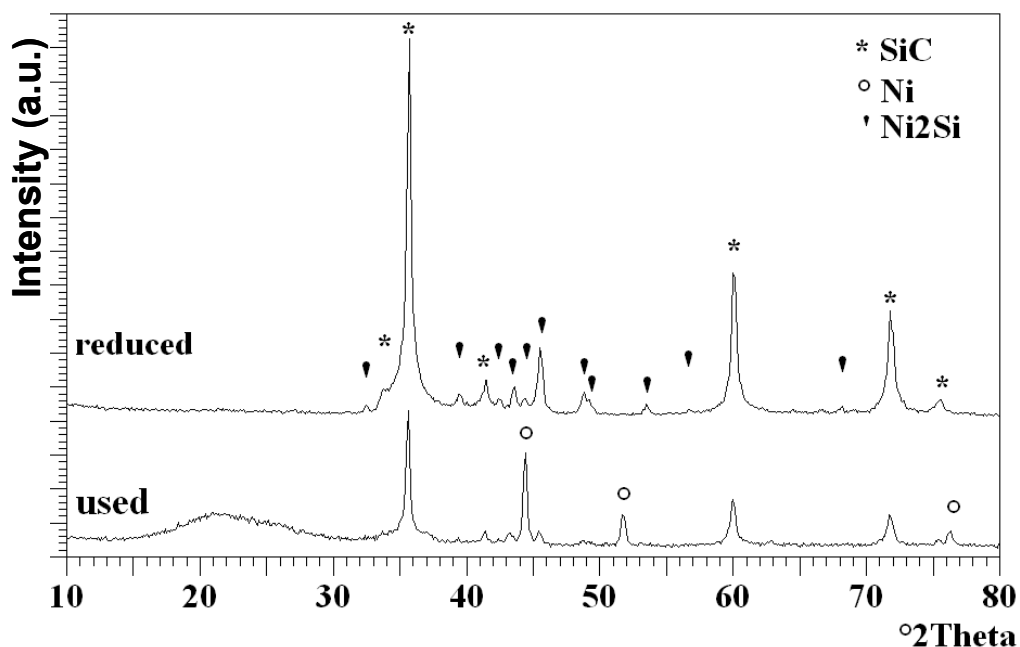


Fig. 3. 126 – Comparison of the XRD patterns of the reduced and used samples (10 % Ni/SiC calcined at  $700^\circ\text{C}$ ).

### 3.6.2. Electrochemical deposition of hydrotalcite type precursors on metallic foams

The conductivity of metallic foams is high and they can be used as support if a method able to deposit the active phase on them can be developed. The method developed in this thesis is based on electrochemical deposition (ECD) and was first applied on electrodes production. Electrodes modified with clays have been extensively studied by E. Scavetta and D. Tonelli (Analytical group of University of Bologna) due to the excellent ion exchange capabilities that such materials display. In particular, electrodes modified with anionic clays, especially layered double hydroxides (LDHs), also called hydrotalcite like compounds (HTlcs) were developed.

The electrochemical deposition by the method developed is possible on materials having good conductivity properties. It is carried out at room temperature using a single compartment, three electrode cell (Fig. 3. 127). Electrode potentials are measured with respect to an aqueous saturated calomel electrode (SCE; i.e. reference electrode [R.E.]). A Pt wire is used as the counter electrode (C.E.) and the working electrode (W.E) is the conductive material which can be covered with the HTlcs. The cyclic voltammetry (CV) curves are recorded using a CH Instrument Mod. 660 C controlled by a personal computer via CH Instrument software.

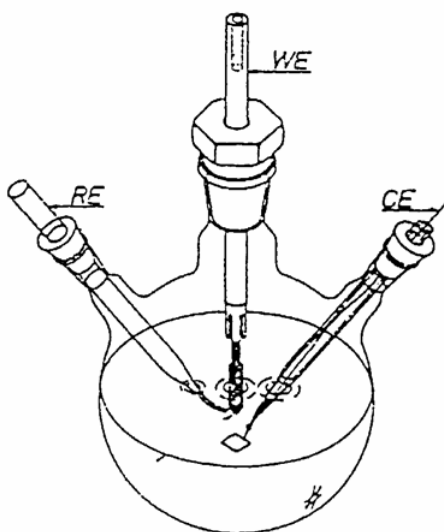


Fig. 3. 127 - Scheme of the three electrode cell.

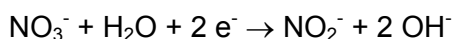
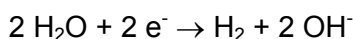
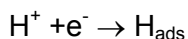
The Ni/Al-NO<sub>3</sub> HT are electro-synthesized starting from freshly prepared solutions of nickel and aluminum nitrate. The solution, from which the hydrotalcite-like phase was prepared was introduced in the three electrode cell. It contains 0.0225 M Ni(NO<sub>3</sub>)<sub>2</sub>, 0.075 M Al(NO<sub>3</sub>)<sub>3</sub>, (Ni : Al = 3 : 1) and KNO<sub>3</sub>, 0.3 M, and is prepared with bi-distilled water.

The application of a cathodic potential (E vs SCE) for a fixed time (deposition time) leads to an increase of the pH near the working electrode (W.E.) surface and the precipitation of the hydrotalcite like material Ni/Al-NO<sub>3</sub> is favored just on this surface (support).

The materials used as support for the electro-synthesis are FeCrAlY foam pellets provided by Air Liquide.

The electrosynthesis was carried out at two different deposition times (600 and 1200s) and at two different potentials (E = -0.9 and -1.2 V).

During the electrosynthesis, several reactions leading to the disappearance of H<sup>+</sup> and to the generation of OH<sup>-</sup> take place:



All these reactions contribute to the precipitation of the Ni/Al-NO<sub>3</sub> HT, near and on the electrode surface. The precipitation of Ni(OH)<sub>2</sub> could be a side reaction and can be evidenced even if its electrochemical signal could partly overlap that of Ni/Al-NO<sub>3</sub> HT.

As a preliminary study, four samples were synthesized. The four samples tested in the SMR reaction were deposited by ECD technique on the FeCrAlY pellets using different potential and deposition time:

- Sample 1 ⇒ - 0.9 V for 600 s
- Sample 2 ⇒ -0.9 V for 1800 s (increasing the deposition time)
- Sample 3 ⇒ - 1.2 V for 600 s (decreasing the applied potential)
- Sample 4 ⇒ - 1.2 V for 1000 s (increasing the deposition time and decreasing the applied potential)

The deposition was carried out on six pellets for loading the SMR reactor for 6 cm in height to compare with the commercial catalysts.

The steam reforming tests were carried out with the reaction conditions of P = 20 bar, CT = 4 s, S/C = 1.7, Toven = 900°C.

After electrochemical deposition and drying, the pellets were calcined at 900°C for 12 h, loaded in the SMR reactor and reduced in situ at 900°C for 2 h with a H<sub>2</sub>/N<sub>2</sub> equimolar flow. It was assumed that, after calcination, the phases present on the support are NiO and NiAl<sub>2</sub>O<sub>4</sub>. As previously seen, the spinel phase is reduced at very high temperature, indeed the reduction temperature was set at 900°C.

In Fig. 3. 128 the daily trend of the activity of Sample 1 is represented. The activity was not good and it continuously decreased from the beginning of the test to the stop of the reaction after 6.5 h. The low value and the significant decrease of the activity, that is an evidence of very poor stability of the catalyst, can be attributable to the low thickness of the layer of active phase deposited on the monolithic metallic pellets. The axial thermal profile measured during reaction was not stable, different profiles of the catalytic bed were observed after 2 h and after 5 h of reaction (Fig. 3. 129), reflecting the instability of the activity.

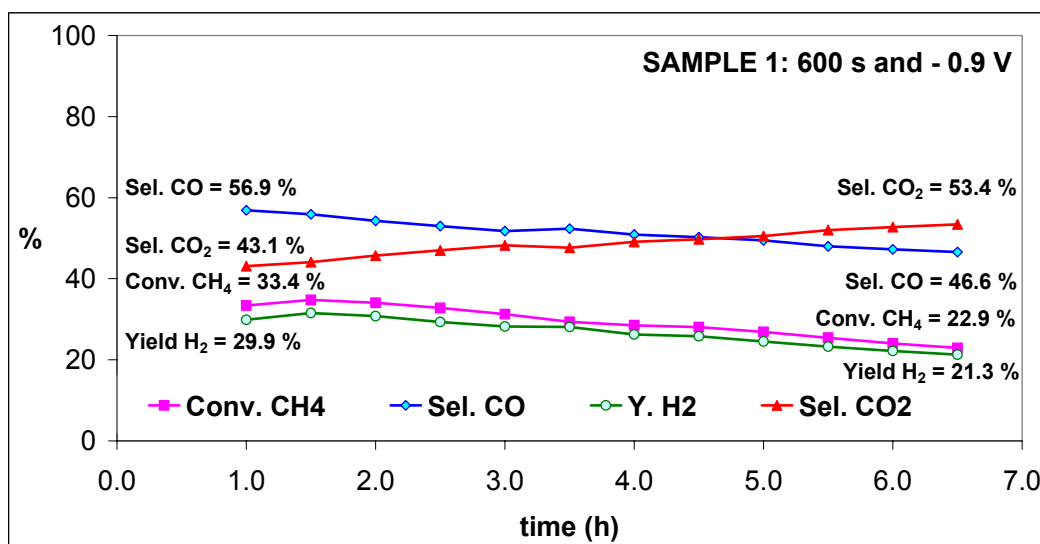


Fig. 3. 128 - Activity of Sample 1 (6 pellets) during 1 day of SMR tests (P = 20 bar, CT = 4 s, S/C = 1.7, Toven = 900°C).

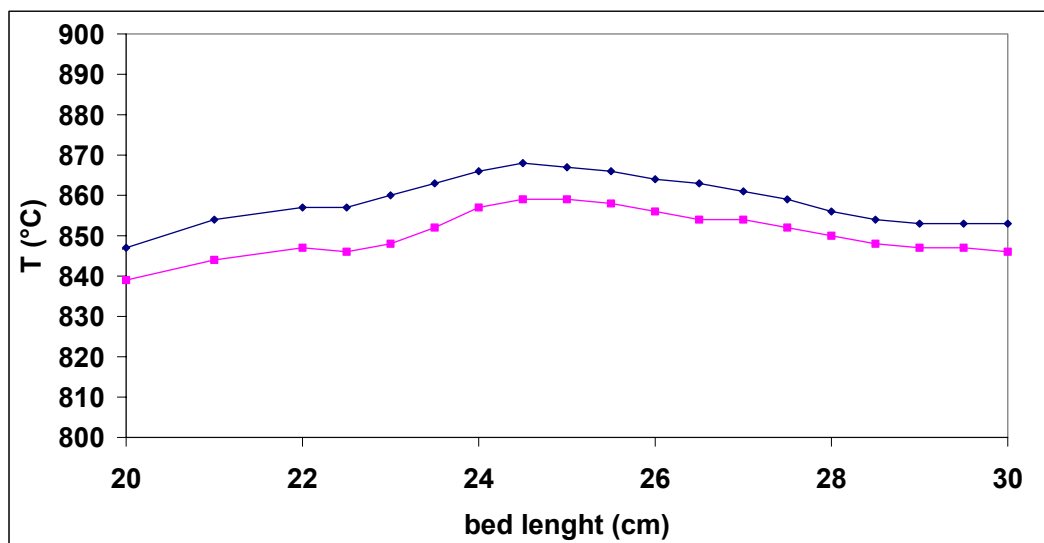


Fig. 3. 129 - Axial thermal profile of the catalytic bed recorded during SMR reaction on the Sample 1 (T1 after 2 h of reaction and T2 after 6 h).

The effect of increasing the thickness and the stability of the layer of the hydrotalcite precursor deposited on the support was studied either by tripling the deposition time (from 600 s to 1800 s, Sample 2) or by changing the applied potential values from -0.9 to -1.2 V and maintaining a deposition time of 600 s (Sample 3).

The results obtained from Sample 2 (- 0.9 V for 1800s) are reported in Fig. 3. 130. In this case, the activity and the stability with time-on-stream are higher than those of the Sample 1 and, even if are still lower than those of commercial samples, it is evident that increasing the deposition time of three times leads to a significant improvement of the performances and in particular of the stability of the conversion and selectivity values. This behavior may be related to the improvement occurred in the deposited HT layer, probably it was obtained a more homogeneous and thick layer.

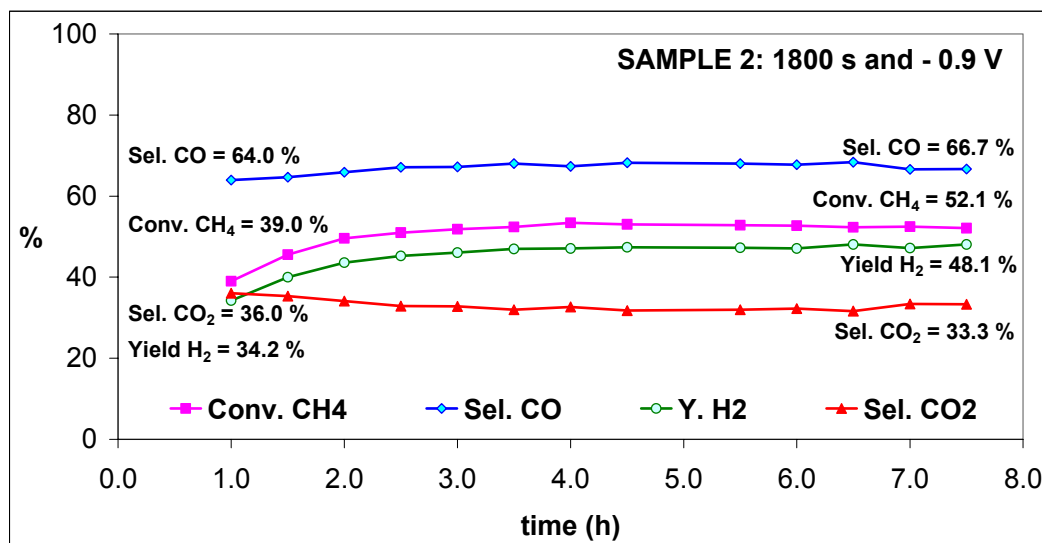


Fig. 3. 130 - Activity of Sample 2 (6 pellets) during 1 day of SMR tests ( $P = 20$  bar,  $CT = 4$  s,  $S/C = 1.7$ ,  $T_{oven} = 900^{\circ}\text{C}$ ).

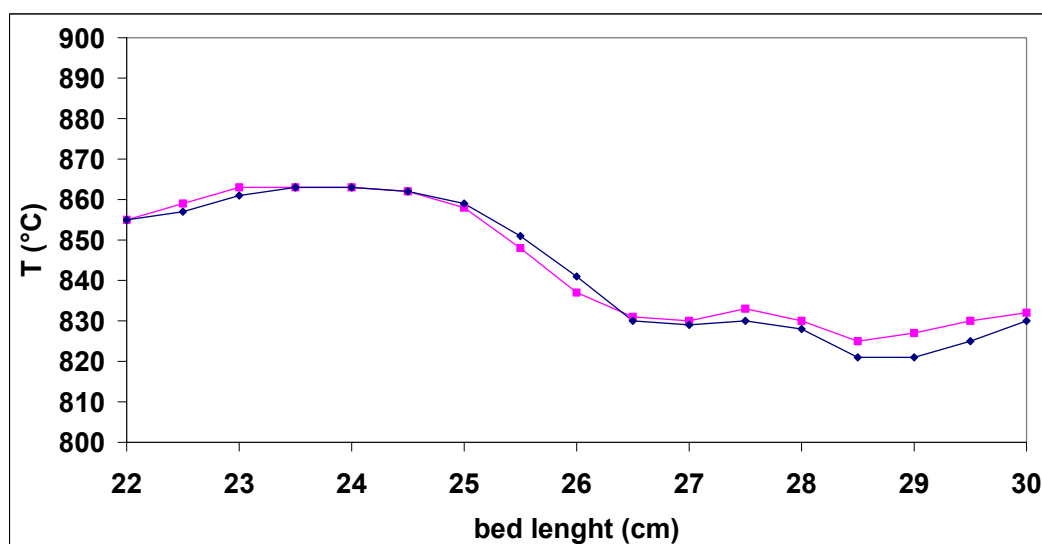


Fig. 3. 131 - Axial thermal profile of the catalytic bed recorded during SMR reaction on the sample 2.

The activity of Sample 3 (deposition time = 600 s / applied potential - 1.2 V) increases with time on stream, probably because the pre-reduction step was carried out in condition not able to reduce the Ni present in the deposited layer. The activity reaches the values obtained with the previous sample with time-on-stream (Fig. 3. 132 and Fig. 3. 133).

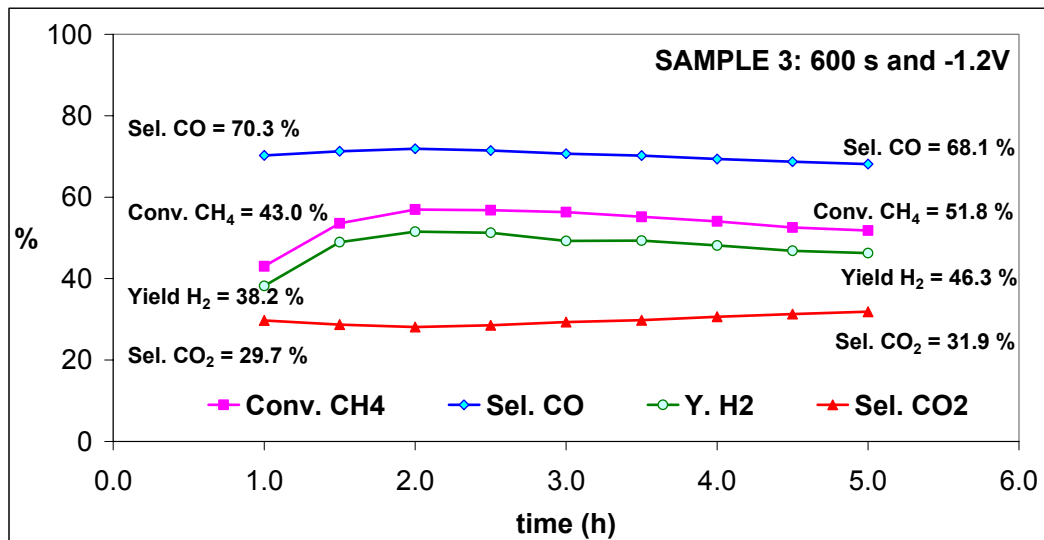


Fig. 3.132 - Activity of Sample 3 (6 pellets) during 1 day of SMR tests ( $P = 20$  bar,  $CT = 4$  s,  $S/C = 1.7$ ,  $T_{oven} = 900^{\circ}\text{C}$ ).

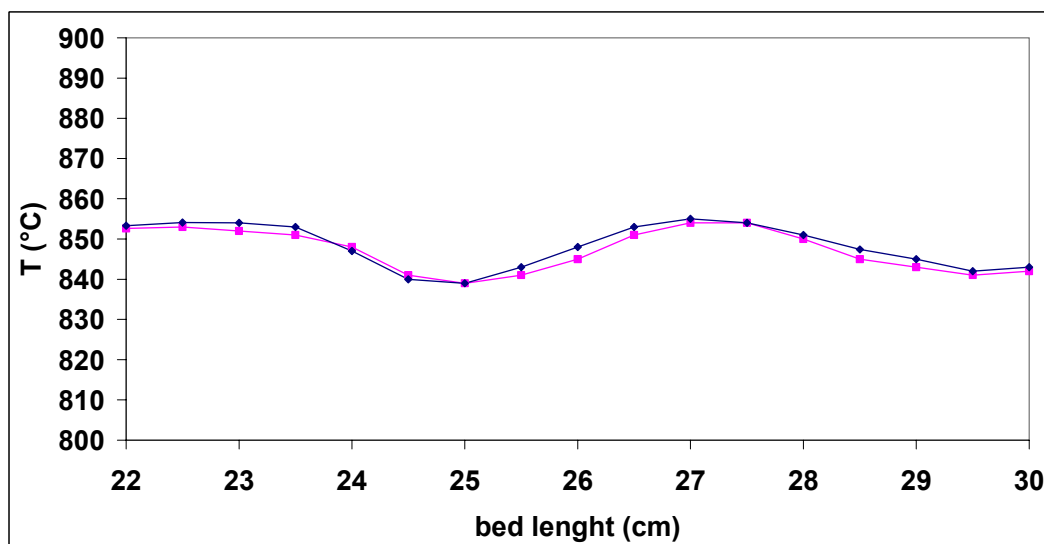


Fig. 3.133 - Axial thermal profile of the catalytic bed recorded during SMR reaction on the Sample 3.

Sample 4, which was prepared both modifying the time of deposition and the applied potential (1000 s and  $-1.2$  V), shows very good performances, similar to those of the commercial catalyst in analogous conditions and also good stability during the 6 h of reaction. In fact, after an increase of the activity in the first hour of time-on-stream, due to completion of activation, the catalytic activity remains constant.

The axial thermal profiles, that showed decreases of temperature (at the beginning of the catalytic bed) of about  $10$ - $20^{\circ}\text{C}$  are a confirmation of good

conductivity of metallic support that improve significantly the heat transfer along the catalytic bed.

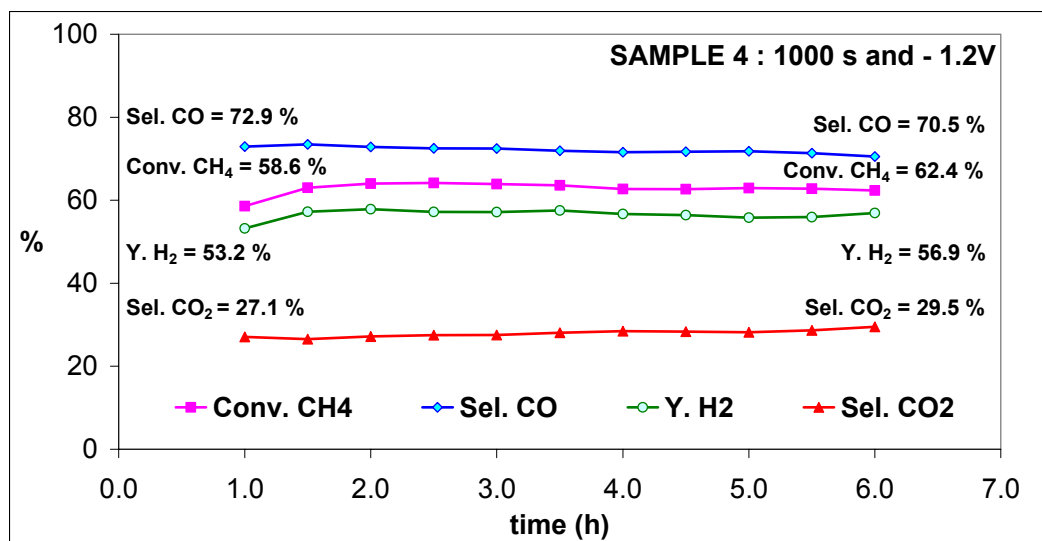


Fig. 3. 134 - Activity of Sample 4 (6 pellets) during 1 day of SMR tests (P = 20 bar, CT = 4 s, S/C = 1.7, T<sub>oven</sub> = 900°C).

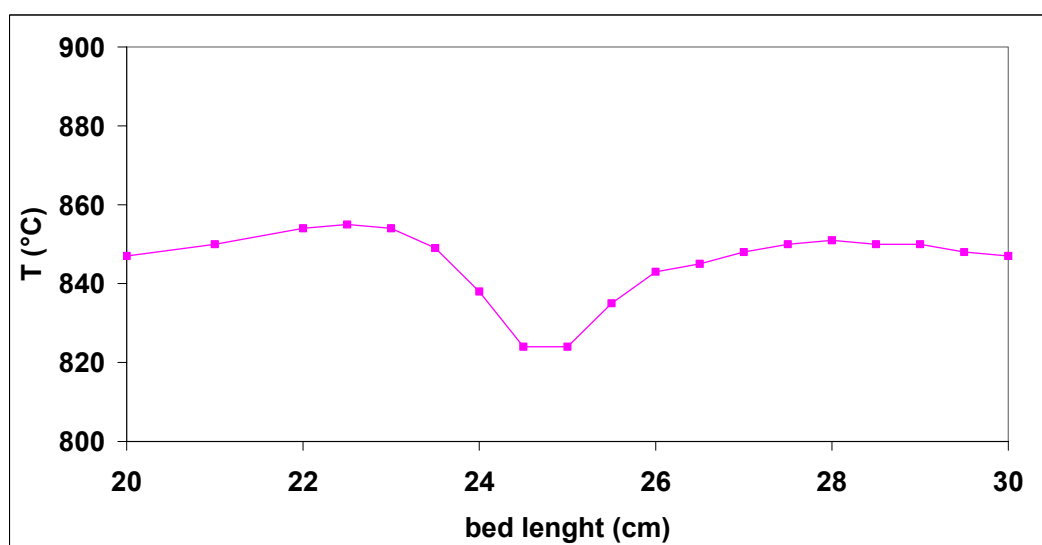


Fig. 3. 135 - Axial thermal profile of the catalytic bed recorded during SMR reaction on the Sample 4.

## CONCLUSIONS

The study of this thesis was focused on the development of new catalysts for the hydrogen production through two different processes, a new one, the catalytic partial oxidation (CPO), and an enhanced well-established process, the steam methane reforming (SMR). Two types of new catalytic materials were examined:

- Bulk catalysts, i.e. non-supported materials, in which the active metals (Ni and/or Rh) are stabilized inside oxidic matrix, obtained from perovskite type compounds (PVK) and from hydrotalcite type precursors (HT);
- Structured catalysts, i.e. catalysts supported on materials having high thermal conductivity (SiC and metallic foams).

The catalyst investigation on the partial oxidation process (CPO) follows a previous work carried out in the laboratory of Department of Industrial Chemistry and Materials of the University of Bologna.

A series of catalysts based on perovskite (PVK) catalysts were carefully studied to determine the best sample formulation in order to enhance the activity, the stability and the reducibility of this type of oxidic structures. The importance of these structures is that they can find important application in  $O^{2-}$  active membrane and therefore can be important to couple good catalyst properties to form layer active membrane.

Firstly, the effect of the insertion of rhodium and its optimal amount in a  $LaFeNiO_3$  perovskite was investigated. The rhodium resulted as a very important element for improving the catalysts activity, especially in reaction conditions that are desirable for an industrial process, probably due to the improved redox properties of the couple Rh/Ni with respect to Ni alone. Furthermore, it is well-known that noble metals are coke-resistant and can give a further beneficial effect, also in this way, to the catalyst performance and life.

Afterwards, the effect of the insertion of low amounts cerium cation was investigated due its redox properties and oxygen storage capacity. It was found

that the cerium stabilize the perovskite structure during reaction, even if there is a limit in the quantity that can be inserted in the PVK with beneficial effects. In addition the catalytic performances were slightly improved in presence of low amount of cerium, thus confirming double beneficial effect given by this metal. Then, the optimal amount of Ni inserted in the structure was studied in order to have the highest activity without excess of this metal. Indeed, an optimal formulation was identified (La<sub>0.8</sub>Ce<sub>0.2</sub>Fe<sub>0.7</sub>Ni<sub>0.25</sub>Rh<sub>0.05</sub>O<sub>3</sub>), and on this sample the effect of the calcination temperature, on the stability of the structure and on the activity was investigated founding that a higher temperature (1100°C instead of 900°C) causes the formation of slightly more crystalline phases, but does not improve the activity nor the structure stability.

A second series of samples was based on hydrotalcite type precursors, containing silicate as interlayer anion, the role of the single active metal (Rh and Ni) was investigated and their synergic effect was observed in samples containing low active phase. It was found that the nickel gives a beneficial contribution to the activity especially at lower temperatures and diluted feeds, while the rhodium presents enhanced performances using more concentrated feed and higher temperature. The sample containing both the active metals, but ½ amounts, presents always improved activity and stability, probably due to a synergic effect established between Rh and Ni. Alloy formation with the high activity cannot be excluded.

Moreover, the bulk matrix composition was studied in order to evaluate the effect of the M<sup>2+</sup>/M<sup>3+</sup> ratio. In systems like Ni/Mg/Al and Rh/Mg/Al, two ratios were examined (65/35 or 80/20). The results show that the 80/20 ratio produces higher catalytic performances because of the active metal is highly distributed in the phases (MgO) where it gives high reducibility and increased stability during reaction conditions.

Furthermore the role of the hydrotalcite type precursors as catalyst matrix or support was investigated studying three different samples, containing the same amount (wt %) of Ni and Rh, but prepared with different methodologies: an ex-HT bulk sample, an impregnated catalyst, using a support obtained from a Ht precursor and a bulk ex-HT catalyst supported on  $\alpha$ -Al<sub>2</sub>O<sub>3</sub>. It was determined the following scale of activity: supported bulk catalyst > bulk catalyst > impregnated catalyst. The better performances of the bulk catalyst supported on  $\alpha$ -Al<sub>2</sub>O<sub>3</sub> may

be attributed to the higher availability and smaller dimensions of the metal particles on the surface, obtained from a more concentrate bulk layer on the alumina support, with respect to the bulk catalyst. The impregnated catalyst showed the lowest activity due to weak interaction between metal particles and support obtained using this technique than that obtained with a bulk catalyst in which the metal are inserted in the structure and strongly connected with the matrix.

In the second part of the work, regarding the steam methane reforming, due to the advanced development of the industrial process, the study was initially focused on the investigation of commercial catalysts, examining the deactivation in industrial conditions, the role of the operating conditions ( $P$ ,  $T$ ,  $CT$ ,  $S/C$ ,  $V_{cat}$  and  $D_p$ ) and the activity of different type of catalysts.

The industrial spent samples, unloaded from different vertical section of catalytic tubes coming from two steam reforming plants showed increased deactivation phenomena going down through the tube. In particular, lower surface area, loss of pores, bigger nickel crystal size and lower activity were observed. Moreover, the presence of low active  $NiAl_2O_4$  was confirmed. Nevertheless, carbonaceous species cannot be individuated, due to switching off conditions of the plant carried out with air or steam, that caused the elimination of possible carbon/coke deposits on the surface.

Subsequently, the effect of the operation parameters in the steam reforming laboratory plant were examined on a commercial catalyst constituted of 13 wt %  $Ni/MgAl_2O_4$ . It was found that the reaction is close to the equilibrium and follows its changes with the reaction parameters, thus:

- An increase of pressure ( $P$ , from 10 to 15 and 20 bar) is unfavorable for the steam reforming reaction, while does not interfere with the water gas shift contribution.
- An increase of the feed molar ratio ( $S/C = H_2O/CH_4$ , from 1.7 to 2.5 mol/mol) leads to a improvement of both steam reforming and water gas shift reactions, with an increase of the  $H_2/CO$  obtained ratio.
- An increase of the temperature profile (tests carried out maintaining constant the outlet temperature at 870 and 930°C) strongly favors the steam reforming reaction that is highly endothermic.

Furthermore, it is important to note that:

- A decrease of the contact time (CT = 4, 2, 1.1 and 0.83 s) leads to a decrease of the activity. However, the observation was influenced by the radial profile (not measured) because the tests were carried out at constant  $T_{out}$ , thus the oven set temperature were increased and there was a contrary effect of axial/radial profiles. The real average temperature of the catalytic bed increases due to higher heat supplied that improve the activity at low CT.
- An increase of catalyst bed volume leads to an improvement of activity, due to an increases of the surface through which the heat flux can be delivered giving flat trend of temperature at the end of the bed.

Three different commercial catalysts (13 wt % Ni/MgAl<sub>2</sub>O<sub>4</sub>, 18 wt % Ni su CaAl<sub>4</sub>O<sub>7</sub>, 14 wt % Ni su CaAl<sub>12</sub>O<sub>19</sub>) were characterized, tested in the steam reforming process and compared. It was shown that in operative conditions, similar to those used in industrial condition and not, the performances of the three samples are very similar, probably due to high nickel content, over dimensioned with respect to the reaction needs. However, the catalyst 13 wt % Ni/MgAl<sub>2</sub>O<sub>4</sub>, seem to be the best, due to lower modification occurring during reaction (higher surface area, lower nickel particle dimensions and indeed lower sintering). In addition, also the 14 wt % Ni su CaAl<sub>12</sub>O<sub>19</sub> catalyst may be a good choice for industrial plant.

The bulk catalysts (PVK and HT) investigated in the catalytic partial oxidation of methane, an ex-HT silicates Rh<sub>0.15</sub>Ni<sub>8</sub>Mg<sub>60</sub>Al<sub>31.85</sub> and PVK La<sub>0.8</sub>Ce<sub>0.2</sub>Fe<sub>0.7</sub>Ni<sub>0.25</sub>Rh<sub>0.05</sub>O<sub>3</sub>, were prepared and tested in the steam reforming reaction giving very good results in terms of activity (comparable to that of commercial catalysts) and of stability with time-on-stream. In particular the ex-HT sample tested either at high S/C (2.5, 3 and 4 mol/mol) or low S/C (1.7, 1.4 and 1.1 mol/mol) showed constant results and low structure modification, especially low metal sintering. The carbon species deposited on the surface of the ex-HT silicates were observed and there are not significant differences among the used samples until S/C = 1.4 mol/mol. Only the sample used with S/C = 1.1 mol/mol showed an increase of amount of carbonaceous deposits.

Moreover, innovative materials for structured catalysts, SiC and metallic foam as supports, were analyzed because their high thermal conductivity, in order to try to overcome problems linked to heat transfer.

The samples obtained by impregnation of Ni on SiC pellets showed interesting characterization due reaction between nickel and support (with the formation during reduction of a Ni<sub>2</sub>Si intermetallic phase) that may be avoided calcining the support at 900°C, because at this temperature a silica layer is formed and isolates the Ni from the SiC support. However, a limitation is observed at high temperature (> 960°C) due to formation of large amount of silica. This may be avoided protecting the support by a oxidic layer (maybe alumina) from the contact with oxidizing species.

Finally, a new method based on electrochemical deposition (ECD) was developed to prepare innovative catalysts. ECD was used to deposits hydrotalcite precursors on FeCrAlY metallic foams pellets. This was a preliminary study, in which the time of deposition and the applied potential were investigated in order to cover, with an uniform active layer of HT precursors, the metallic foam. In the steam reforming reaction, good activity was reached. Each of the four samples, prepared by decreasing the potential and increasing the deposition time, increases the activity and the stability of the samples, and the last one (1000 s and -1.2 V) shows the best performances comparable with those of the commercial catalysts. This method, still not optimized, is very promising for industrial catalyst production, due to very simple preparation procedure.

## REFERENCES

- [1] M. Wietschel, U. Hasenauer, A. de Groot, *Energy Policy*, **34** (2006) 1284
- [2] J. R. Rostrup-Nielsen, *Catal. Rev.*, **46** (2004) 247
- [3] C. W. Forsberg, *Int. J. Hydrogen Energy*, **32** (2007) 431
- [4] B.D. Solomon, A. Banerjee, *Energy Policy*, **34** (2006) 781
- [5] B.van Ruijven, D. P. van Vuuren, B. de Vries, *Int. J. Hydrogen Energy*, Article in press available on line (2007)
- [6] A. Hellman, K. Honkala, I.N. Remediakis, Á. Logadóttir, A. Carlsson, S. Dahl, C.H. Christensen and J.K. Nørskov, *Surf. Sci.*, **600** (2006) 4264
- [7] M. V. Twigg, "Catalyst Handbook", 2nd ed., Wolf Publishing Ltd (1989)
- [8] Z. Yang, W. Guo, J. Lin, D. Liao, *Chin. J. Catal.*, **27** (2006) 378
- [9] C. Liang, Z. Wei, Q. Xin, C. Lin, *Appl. Cat. A*, **208** (2001) 193
- [10] S. M. Yunusov, E. S. Kalyuzhnaya, B. L. Moroz, A. S. Ivanova, T. V. Reshetenko, L. B. Avdeeva, V. A. Likholobov, V. B. Shur, *J. Molec. Catal. A*, **219** (2004) 149
- [11] P. Seetharamulu, V. Siva Kumar, A. H. Padmasri, B. David Raju, K. S. Rama Rao, *J. Molec Catal. A*, **263** (2006) 253
- [12] Q. Xu, J. Lin, J. Li, X. Fu, Z. Yang, W. Guo, D. Liao, *J. Molec. Catal. A*, **259** (2006) 218
- [13] Z. Kirova-Yordanova, *Energy*, **29** (2004) 2373
- [14] D. R. Parisi, M. A. Laborde, *Chem. Eng. J.*, **104** (2004) 35
- [15] X. Liu, G.Q. Lu, Z. Yan, J. Beltramini, *Ind. Eng. Chem. Res.*, **42** (2003) 6518
- [16] M. Stöcker, *Microporous and Mesoporous Materials*, **29** (1999) 3

- [17] F. J. Keil, *Microporous and Mesoporous Materials*, **29** (1999) 49
- [18] T. V. Choudary, D. W. Goodman, *J. Molec. Catal. A*, **163** (2000) 9
- [19] S. Lee, A. Sardesai, *Topics in Catalysis*, **32** (2005) 197
- [20] Y. Guo, W. Meyer-Zaika, M. Muhler, S. Vukojevic, M. Epple, *Eur. J. Inorg. Chem.*, (2006) 4774
- [21] Nakamura, T. Fujitani, T. Uchijima, J. Nakamura, *Surf. Sci.*, **400** (1998) 387
- [22] M. Saito, K. Murata, *Catal. Surveys from Asia*, **8** (2004) 285
- [23] G. A. Mills, *Fuel*, **73** (1994) 1243
- [24] T. A. Semelsberger, R. L. Borup, H. L. Greene, *J. Power Sources*, **156** (2006) 497
- [25] G. R. Moradi, S. Nosrati, F. Yaripor, *Catal. Comm.*, **8** (2007) 598
- [26] J. Fei, X. Tang, Z. Huo, H. Lou, X. Zheng, *Catal. Comm.*, **7** (2006) 827
- [27] K. Sun, W. Lu, F. Qiu, S. Liu, X. Xu, *Appl. Cat. A*, **252** (2003) 243
- [28] V.U.S. Rao, G.J. Stiegel, G.J. Cinquegrane, R.D. Srivastava, *Fuel Processing Technology*, **30** (1992) 83
- [29] J. van de Loosdrecht, Ph.D. thesis, Utrecht University, The Netherlands (1995).
- [30] S. Morselli, Ph.D. thesis, Scuola Normale superiore di Pisa, Italy (2001)
- [31] M. E. Dry, *The Fischer-Tropsch Process-Commercial aspects*, Elsevier Science Publishers, (1990), 183
- [32] H. Schulz, *App. Catal. A*, **186** (1999) 3
- [33] C. H. Bartholomew, *Stud, Surf. Sci and Catal.*, "New Trends in CO Activation", **64**, Chp. 5, 158
- [34] R. L. Espinoza, A. P. Steynberg, P. Jager, A. C. Voslao, *App. Catal. A*, **186** (1999) 13
- [35] C. Song, *Catal. Today*, **77** (2002) 17
- [36] M. Krumpelt, T. R. Krause, J. D. Carter, J. P. Kopasz, S. Ahmed, *Catal. Today*, **77** (2002) 3

- [37] P. Ferreira-Aparicio, M. J. Benito, J. L. Sanz, *Catalysis Reviews*, **47** (2005) 491
- [38] J. R. Rustrup-Nielsen, *Catal. Today*, **63** (2000) 159
- [39] J. N. Armor, *Appl. Cat. A*, **176** (1999) 159
- [40] J. N. Armor, *Catalysis letters*, **101** (2005) 131
- [41] M. A. Peña, J. P. Gómez, J. L. G. Fierro, *Appl. Cat. A*, **144** (1996) 7
- [42] J. R. Rustrup-Nielsen, *Stud. Surf. Sci. Catal. "Natural gas conversion VII"*, **147** (2004) 121
- [43] A. E. Lutz, R. W. Bradshaw, J. O. Keller, D. E. Witmer, *Int. J. Hydrogen Energy*, **28** (2003) 159
- [44] K. Jarosch, T. El Solh, H. I. de Lasa, *Chem. Eng. Sci.*, **57** (2002) 3439
- [45] J. Wei, E. Iglesia, *J. Catal.*, **224** (2004) 370
- [46] J. Wei, E. Iglesia, *J. Catal.*, **225** (2004) 116
- [47] D. Chen, E. Bjorgum, R. Lodeng, K. O. Christensen, A. Holmen, *Stud. Surf. Sci. Catal. - "Natural gas conversion VII"*, **147** (2004) 139
- [48] Y. Matsumura, T. Nakamori, *Appl. Catal. A.*, **258** (2004) 107
- [49] Alstrup, B. S. Clausen, C. Olsen, R.H.H. Smits, J.R. Rustrup-Nielsen, *Stud. Surf. Sci. Catal. - "Natural gas conversion V"*, **119** (1998) 5
- [50] K. Takehira, T. Shishido, M. Kondo, *J. Catal.*, **207** (2002) 307
- [51] A. I. Tsyganok, T. Tsunoda, S. Hamakawa, K. Suzuki, K. Takehira, T. Hayakawa, *J. Catal.*, **213** (2003) 191
- [52] K. Takehira, T. Shishido, D. Shouro, K. Murakami, M. Honda, T. Kawabata, K. Takaki, *App. Catal. A*, **279** (2005) 41
- [53] T. Ohi, T. Miyata, D. Li, T. Shishido, T. Kawabata, T. Sano, K. Takehira, *Appl. Catal. A*, **308** (2006) 194
- [54] A. Fonseca, E. M. Assaf, *J. Power Sources*, **142** (2005) 154
- [55] M. Sturzenegger, L. D'Souza, R. P. W. J. Struis, S. Stucki, *Fuel*, **85** (2006) 1599

- [56] H. Provendier, C. Petit, C. Estournès, S. Libs, A. Kiennemann, *Appl. Catal. A*, **180** (2000) 163
- [57] E. L. Foletto, R. W. Alves, S. L. Jahn, *J. Power Sources*, **161** (2006) 531
- [58] N. Keghouche, S. Chettibi, F. Latrèche, M.M. Bettahar, J. Belloni, J.L. Marignier, *Radiation Physics and Chemistry*, **74** (2005) 185
- [59] O. Yamazaki, K. Tomishige, K. Fujimoto, *Appl. Catal. A*, **136** (1996) 49
- [60] K. Tomishige, Y. Chen, O. Yamazaki, Y. Himeno, Y. Koganezawa and K. Fujimoto, *Stud. Surf. Sci. Catal. - "Natural gas conversion V"*, **119** (1998) 861
- [61] N. P. Siswana, D. L. Trimm, N. W. Cant, *Stud. Surf. Sci. Catal. - "Natural gas conversion V"*, **119** (1998) 789
- [62] W. Dong, H. Roh, K. Jun, S. Park, Y. Oh, *Appl. Catal. A*, **226** (2002) 63
- [63] Y. Oh, H. Roh, K. Jun, Y. Baek, *Intern. J. Hydrogen Energy*, **28** (2003) 1387
- [64] H. Roh, K. Jun, S. Park, *Appl. Catal. A*, **251** (2003) 275
- [65] Q. Zhang, Y. Li, B. Xu, *Catal. Tod.*, **98** (2004) 601
- [66] T. Borowiecki, A. Denis, W. Gac, R. Dziembaj, Z. Piwowarska, M. Drozdek, *Appl. Catal. A*, **274** (2004) 259
- [67] R. Takahashi, S. Sato, T. Sodesawa, M. Yoshida, S. Tomiyama, *Appl. Catal. A*, **273** (2004) 211
- [68] K. Urasaki, Y. Sekine, S. Kawabe, E. Kikuchi, M. Matsukata, *Appl. Catal. A*, **286** (2005) 23
- [69] J. S. B. Wang, Y. L. Tai, W. P. Dow, T. J. Huang; *Appl. Catal. A*, **218** (2001) 69
- [70] J. B: Wang, L. E. Kuo, T. J. Huang, *Appl. Cata. A*, **249** (2003) 93
- [71] J. B: Wang, S.Z. Hsiao, T. J. Huang, *Appl. Cata. A*, **246** (2003) 197
- [72] A. L. Sauvet, J. T. S. Irvine, *Solid State Ionics*, **167** (2004) 1
- [73] Y. Wang, Y.H. Chin, R.T. Rozmiarek, B.R. Johnson, Y. Gao, J. Watson, A.Y.L. Tonkovich, D.P. Vander Wiel, *Catal. Tod.*, **98** (2004) 575

- [74] A. Ishihara, E. W. Qian, I. N. Finahari, I. P. Sutrisna, T. Kabe, *Fuel*, **84** (2005) 1462-1468
- [75] R. Craciun, W. Daniell, H. Knözinger, *App. Catal. A*, **230** (2002) 153
- [76] J.R. Rostrup-Nielsen, *Catal. Tod.*, **37** (1997) 225
- [77] C. H. Bartholomew, *Appl. Catal. A*, **212** (2001) 17
- [78] C. H. Bartholomew, *Catal. Rev. – Sci. Eng.*, **24** (1982) 67
- [79] J. N. Armor, D. J. Martenak, *Appl. Catal. A*, **206** (2001) 231
- [80] D. L. Trimm, *Catal. Tod.*, **37** (1997) 233
- [81] J. R. Rostrup-Nielsen, *Stud. Surf. Sci. Catal. - "Natural gas conversion II"*, **81** (1994) 25
- [82] J. R. Rostrup-Nielsen, *J. Catal.*, **85** (1984) 31
- [83] J. Sehested, J. A. P: Gelten, I.N. Remediakis, H. Bengaard, J. K. Norskov, *J. Catal.* **223** (2004) 432
- [84] J. Sehested, A. Carlson, T. V. W. Janssens, P. L Hansen, A. K. Datye, *J. Catal.* **197** (2001) 200
- [85] C. T Campbell, S. C Parker, D. E. Starr, *Science*, **298** (2002) 811
- [86] J. Sehested, *J. Catal.*, **217** (2003) 417
- [87] Y. H. Hu, E. Ruckenstein, *Adv. Catal.*, **48** (2004) 297
- [88] V. R. Choudhary, A. M. Rajput, B. Prabhakar, *Catal. Lett.*, **15** (1992) 363
- [89] V. R. Choudhary, A. M. Rajput, B. Prabhakar, *J. Catal.*, **139** (1993) 326
- [90] V. R. Choudhary, A. M. Rajput, V. H. Rane, *Catal. Lett.*, **16** (1992) 269
- [91] V. R. Choudhary, A. M. Rajput, V. H. Rane, *J. Phys. Chem.*, **96** (1992) 8686
- [92] V. R. Choudhary, S. D. Sansare, A. S Mamman, *Appl. Catal. A*, **90** (1992) L1
- [93] Y.H. Hu, E. Ruckenstein, *Ind. Eng. Chem. Res.*, **37** (1998) 2333
- [94] F. Basile, G. Fornasari, F. Trifiro, A. Vaccari, *Catal. Tod.*, **64** (2001) 21
- [95] G. R. Gavalas, C. Phichitcul, G. E. Voecks, *J. Catal.*, **88** (1984) 54

- [96] D. A. Hickman, L. D. Schmidt, *J. Catal.*, **138** (1992) 267
- [97] M. Reyniers, C. R. H. de Smet, P. G. Menon, G. B. Marin, *Cattech.*, **6** (2002) 140
- [98] A. P. E. York, T. Xiao, M. L. H. Green, *Topics in Catalysis*, **22** (2003) 345
- [99] K. Takehira, *Catalysis Surveys from Japan*, **6** (2002) 19
- [100] H. Provendier, C. Petit, C. Estournes, S. Libs and A. Kiennemann, *Appl. Catal. A*, **180** (1999) 163.
- [101] F. Basile, P. Del Gallo, G. Fornasari, D. Gary, A. Vaccari, **EP 1419814** (2004) [JP 2004167485; US 20040127351]
- [102] F. Trifiro`, A. Vaccari, in: J.L. Atwood, J.E.D. Davies, D.D. MacNicol, F. Vögtle (Eds.), *Comprehensive Supramolecular Chemistry*, Pergamon Press, Oxford, **7** (1996), Chapter 8, 251.
- [103] F. Basile, L. Basini, M. D'Amore, G. Fornasari, A. Guarinoni, D. Matteuzzi, G. Del Piero, F. Trifiro`, A. Vaccari, *J. Catal.*, **173** (1998) 247
- [104] F. Basile, G. Fornasari, E. Poluzzi, A. Vaccari, *Appl. Clay Sci.*, **13** (1998) 329
- [105] F. Basile, G. Fornasari, V. Rosetti, F. Trifirò, A. Vaccari, *Catal. Tod.*, **91-92** (2004) 293
- [106] S. Albertazzi, P. Arpentinier, F. Basile, G. Fornasari, D. Gary, A. Vaccari, **WO 03099436** (2003) [EP 1511566 (2005)]
- [107] P. Arpentinier, F. Basile, P. Del Gallo, G. Fornasari, D. Gary, V. Rosetti, A. Vaccari, *Catal. Tod.*, **99** (2005) 99
- [108] P. Arpentinier, F. Basile, P. del Gallo, G. Fornasari, D. Gary, V. Rosetti and A. Vaccari, *Catal. Tod.*, **117** (2006) 462
- [109] Basile, Basini, D'Amore, Fornasari, Guarinoni, Matteuzzi, Del Piero, Trifirò and Vaccari, *J. Catal.*, **173** (1998) 247
- [110] Villa, Cristiani, Groppi, Lietti, Forzatti, Corsaro and Rossini, *J. Molec. Catal.A*, **204-205** (2003) 637
- [111] Hou, Yokota, Tanaka and Yashima, *Appl.Catal. A*, **253** (2003) 381

- [112] Villacampa, Royo, Romeo, Montpya, Del Angel and Monzon, *Appl. Catal. A*, **252** (2003) 363
- [113] Hyun-Seong Roh, Ki-Won Jun and sang-Eon Park, *App. Catal. A*, **251** (2003) 275
- [114] Vos, Poels and Bliiek, *J. Catal.*, **198** (2001) 77
- [115] Teixeira and Giudici, *Chem. Eng. Sci.*, **54** (1999) 3609
- [116] Dewaele and Froment, *J. Catal.*, **184** (1999) 499
- [117] C. Li and Y. Chen, *Thermochem. Acta*, **256** (1995) 457
- [118] H.M. Swaan, V.C.H. Kroll, G.A. Martin, C. Mirodatos, *Catal. Tod.* **21** (1994) 571
- [119] M.A. Goula, A. A. Lemonidou, A.M. Efstathiou, *J. of Catal.* **161** (1996) 626
- [120] A. Shamsi, C.D. Johnson, *Catal. Tod.*, **84** (2003) 17
- [121] C.H. Bartolomew, *Catal. Rev. – Sci. Eng.*, **24** (1982) 67
- [122] W.K. Jozwiak, M. Nowosielska, J. Rynkowski, *Appl.Catal. A: Gen.* **280** (2005) 233
- [123] M. Wisniewski, A. Boreave, P. Gelin, *Catal. Comm.* **6** (2005) 596
- [124] P. Leroi, B. Madani, C. Pham-Huu, M. J. Ledoux, S. Savin-Poncet, J. L. Bousquet, *Catal. Today*, **91-92** (2004) 53-58
- [125] W-Z. Sun, G-Q. Jin, X-Y. Guo, *Catal. Comm.*, **6** (2005) 135-139
- [126] R. Roccaforte, F.la Via, V. Ranieri, P. Musumeci, L. Calcagno, G. G. Condorelli, *Appl. Phys A.*, **77** (2003) 727-833
- [127] K.W. Richter, K. Chandrasekaran, H. Ipser, *Intermetallics*, **12** (2004) 545-554
- [128] Y. Du, J. C. Schuster, *Metall. Mater. Trans. A*, **30A** (1999) 2409-2418

## **ACKNOWLEDGEMENTS**

I would like to thank **AIR LIQUIDE** for the financial support and a special thank to **DANIEL GARY** and **PASCAL DEL GALLO**, for their personal contribution to the work carried inside this collaboration.

I would like to thank **PROF. VACCARI**, who gives me the opportunity of doing this PhD and his esteem, **PROF. FORNASARI** for his moral support, availability and for his patient assistance in every occasion. Then, I would like to thank **DOTT. BASILE**, who supervises my work and me, during these years.

Furthermore, I want to thank all the people working in the Department of Industrial Chemistry and Materials.

Finally, a heartfelt thankyou to everyone helps me in my work, especially the students (**FEDERICO**, **GIUSEPPE**, **ROBERTA**, **LEONARDO**, **ALESSANDRO**, **ROCCO**, **MICHELE**, **RINALDO** and **IRENE**) and **PATRICIA** and **SIMONE**.